

Examination Committee: Prof. dr. ir. Paul Van Der Meeren
Chairman
Department of Applied Analytical and Physical Chemistry
Ghent University, Belgium

Prof. dr. ir. Jeriffa De Clercq
Department of Industrial Technology and Construction
Ghent University, Belgium

Prof. dr. ir. Ulf Jeppsson
Department of Biomedical Engineering
Lund University, Sweden

Prof. dr. ir. Julien Laurent
Laboratoire des Sciences de l'Ingénieur, de l'Informatique
et de l'Imagerie
University of Strasbourg, France

Prof. dr. ir. Stijn Van Hulle
Department of Industrial Biological Sciences
Ghent University, Belgium

Promotor: Prof. dr. ir. Ingmar Nopens
Department of Mathematical Modelling, Statistics
and Bioinformatics
Ghent University, Belgium

Dean: Prof. dr. ir. Guido Van Huylenbroeck

Rector: Prof. dr. Anne De Paepe

ir. Elena Torfs

Different settling regimes in
secondary settling tanks:
experimental process analysis,
model development and calibration

Thesis submitted in fulfillment of the requirements for the degree of

Doctor (PhD) in Applied Biological Sciences:
Environmental Technology

Academic year 2015-2016

Dutch translation of the title:

Verschillende bezinkingsregimes in nabezinktanks: experimentele procesanalyse, model ontwikkeling en kalibratie.

Please refer to this work as follows:

Elena Torfs (2015). Different settling regimes in secondary settling tanks: experimental process analysis, model development and calibration, PhD Thesis, Ghent University, Belgium.

ISBN 978-90-5989-821-9

The author and the promoters give the authorisation to consult and to copy parts of this work for personal use only. Every other use is subject to the copyright laws. Permission to reproduce any material contained in this work should be obtained from the author.

Acknowledgments

Het begon allemaal, in een niet zo ver verleden op een unief hier niet zo ver vandaan... Een doctoraat bij BIOMATH, de start van een geweldig avontuur waarbij ik zowel mijn passie voor het modelleren als voor het lesgeven heb ontdekt. Ondertussen kijk ik terug op zes mooie jaren met dit doctoraat als kers op de taart. Ik ben zoveel mensen oneindig dankbaar voor hun steun in het tot stand komen van dit werk. Dit dankwoord kan jullie onmogelijk voldoende eer aandoen maar ik wil toch graag een aantal mensen in de verf zetten.

In de eerste plaats, mijn promotor Ingmar, voor je visie, je wijdse plannen en aanstekelijke enthousiasme. Je wist mij als geen ander te motiveren, je gaf me de kans om mijn eigen weg te zoeken, het vertrouwen om deze weg te bewandelen en de vrijheid om af en toe een zijweggetje in te slaan. Bedankt ook om mij in te leiden in de wonderde wereld van de wetenschappelijke congressen: van de biergartens in Berlijn tot de nachtelijke spelletjes pool in Surfer's Paradise, brainstormen vanaf de koffie bij de allereerste presentaties tot aan de laatste pint 's avonds. Ik heb steeds enorm genoten van je gezelschap.

Although this PhD knows only one official promotor, from time to time it felt like I had two more. Stefan and Raimund, this work would not have been the same without your help. My sincere thanks for your patience in explaining all the fundamental concepts, your eagle eye in reading and rereading (and rereading) large parts of this work, the amazing hospitality (I will never forget the pisco-workshop!) but above all your enthusiasm and support.

Many thanks as well to Florent and Julien for the nice collaboration, the fruitful discussions and the memorable evening at the famous christmas market in Strasbourg.

Moreover, I had the privilege to work with several master thesis students: Sophie, Pieter, Faezeh, Veerle, who have each in their own way contributed to this work.

Mijn geweldige collega's verdienen zeker een plaatsje in dit dankwoord. Jullie maakten de (zeldzame) lastige dagen draaglijk en de leuke dagen ronduit fantastisch! Een aantal personen wil ik hier graag expliciet bedanken. Stijn, voor je ongeëvenaarde Stijn-zijn (en dat is een compliment!). Wim, voor alle hilarische momenten: in een boom, 's avonds op café, samen op de fiets, tijdens onze jam-sessies,... Thanks for standing by me ;-). Séverine, mijn jarenlange bureaugenootje, voor de vele babbels en

de praktische en mentale steun bij het schrijven en indienen van mijn doctoraat. Pieter, voor je humor, je wijze raad en om mij steeds op de hoogte te houden van het reilen en zeilen binnen de vakgroep (zelfs nu je er niet meer werkt). Tinne, voor je eerlijkheid, je directheid, je oprechtheid, kortom om altijd je ongezouten mening te geven (en ook dat is een compliment). Wouter, om steeds paraat te staan als klankbord en de zwempartijtjes bij het kriecken van de dag. *Giacomo, for all your patience and help with the ADCP-measurements*. Mijn partner in crime, settler babe Sophie, voor alle hulp tijdens de laatste loodjes en ook gewoon omdat je zo'n toffe madam bent! Verder ook, Thomas, Katrijn, Youri, Lieven, Ashish, Timothy, Usman, Andres, Niels & Andreia, Chaïm, Daan, Michael en ook alle collega's van Kermit en Biostat voor de vele leuke momenten in de bureau, de koffiekamer, op de gang naar de koffiekamer, tijdens de lunchpauzes, op conferenties, summer walks, biomath weekends, ribbetjesfestijnen,... *You guys are simply awesome!* Tot slot ook een speciale vermelding voor Timpe en Ruth. Jullie stonden steeds paraat om al mijn administratieve vragen te beantwoorden en bij te springen bij praktische zaken. Heel erg bedankt!

Astrid, Janne en Lara: al 15 jaar lang zijn jullie de allerbeste vriendinnen die iemand zich kan wensen. Ik ben ontzettend blij dat ik ook deze mijlpaal met jullie kan delen. Djoene, Coppe, Neleke en DVS: bedankt voor de fijne Ambiorix jaren (ongetwijfeld nog steeds het beste kot van Gent) en de vriendschap die sindsdien alleen sterker geworden is. De milieu-bende: Annelies, Ellens, Astrid, Kim, Cilia, Willem voor de zalige herbronningsweekendjes. Annelies en Ellen, bedankt om alle ups en downs van het doctoraatsleven vanop de eerste rij mee te maken!

Ook mijn geweldige ouders wil ik bedanken om steeds met volle overgave in mij te geloven. Mama, jouw zorgzaamheid en doorzettingsvermogen heb ik steeds als voorbeeld genomen en gaven me de kracht om nooit op te geven. Papa, dankzij jouw wijze raad bij het maken van mijn studiekeuze ben ik gekomen waar ik nu ben. Bovendien voelde je steeds feilloos aan wanneer het tijd was om samen een bolleke te gaan drinken voor een goed vader-dochter gesprek. Mijn zus, broers, schoonzus, schoonbroer en mijn liefste oma voor al jullie liefde en steun. Guy'tje, ik denk nog steeds met veel nostalgie terug aan de vele late night jam sessies op jouw zolderkamer. Tot slot ook 'the boys' voor hun luisterend oor en hun onwankelbaar optimisme!

Tom, met je unieke combinatie van pure ratio en hartverwarmende zachtheid, verdien je een heel boek in plaats van een paragraaf. Bedankt om geen genoeg te nemen met halfslachtige excuusjes maar mij steeds op je kenmerkende subtiele manier aan te sporen om het beste van mezelf te geven. Je begrijpt mij als geen ander en weet elke dag weer een glimlach op mijn gezicht te toveren. Ik kijk al uit naar ons volgende avontuur samen!

Elena
Ghent, September 2015

Contents

Acronyms	XV
Summary	XIX
Samenvatting	XXIII
I Background & objectives	1
1 Background, problem statement and outline	5
1.1 Introduction	5
1.2 Outline	6
2 Literature review	9
2.1 Wastewater treatment	9
2.2 Secondary Settling Tank (SST)	11
2.2.1 Layout of a typical SST	11
2.2.2 Functions of a SST	12
2.3 Settling behaviour of the activated sludge	13
2.3.1 Settling regimes	13
2.3.2 Experimental determination of the settling behaviour	15
2.4 Factors influencing sludge settling behaviour	19
2.4.1 Activated sludge flocculation	19
2.4.2 Hydrodynamics	23
2.5 Modelling of SSTs	24
2.5.1 Overview	24
2.5.2 Mathematical description of the settling behaviour	25
2.5.3 1-D modelling	32
2.5.4 CFD modelling	40
2.5.5 Flocculation models	48
3 Objectives	53
II 1-D modelling for operation and control	55
4 Impact of secondary settling tank models on the development of operation and control strategies for WWTPs	59
4.1 Introduction	59
4.2 Materials and methods	60
4.2.1 Benchmark Simulation Model No. 1	60
4.2.2 Constitutive functions used in the Bürger-Diehl model	62
4.2.3 Case-study: the Eindhoven WWTP	63

4.3	Results and discussion	64
4.3.1	Impact of compression settling on predicted concentration profiles in the Secondary Settling Tank (SST)	64
4.3.2	Impact of compression settling on the performance of the biological reactors	68
4.3.3	Impact of compression settling on the development of control strategies	69
4.3.4	Impact of inlet dispersion on predicted effluent concentrations	73
4.3.5	Practical implications of switching to a more advanced settler model	74
4.4	Conclusions	76
5	Parameter estimation and identifiability analysis of the Bürger-Diehl settler model	79
5.1	Materials and methods	80
5.1.1	Constitutive functions for the Bürger-Diehl model	80
5.1.2	Data collection	80
5.1.3	Parameter estimation	81
5.1.4	Confidence intervals	82
5.1.5	Identifiability of the model parameters	83
5.2	Results and discussion	84
5.2.1	Calibration of the hindered settling velocity	84
5.2.2	Calibration of the sludge compressibility	94
5.3	Conclusions	97
6	Critical analysis of constitutive functions for hindered settling velocity in 1-D settler models	99
6.1	Introduction	99
6.2	Material and methods	101
6.2.1	Experimental data	101
6.2.2	Akaike's Information Criteria (AIC) for model selection	102
6.3	Results and discussion	103
6.3.1	Calibration of hindered settling functions	103
6.3.2	Impact of different hindered settling functions on long-term SBH predictions	106
6.3.3	Impact of different hindered settling functions on velocity profile predictions	107
6.3.4	Identifiability of the power-law functions	110
6.4	Conclusions	111
7	Impact of the flocculation state on settling behaviour: experimental evidence and overview of available modelling frameworks	113
7.1	Introduction	113
7.2	Typical problems when calibrating compression behaviour	114
7.2.1	Calibration of solids stress function	114
7.2.2	Time-variable critical concentration	116
7.3	Experimental data collection	118
7.4	Experimental observations and discussion	119
7.4.1	Impact of variations in shear stress on compression settling	120
7.4.2	In-depth analysis of the settling velocity	121
7.4.3	Overview of available modelling frameworks	123
7.5	Conclusions	124
III	Advanced experimentation and modelling	127
8	Towards improved predictions of effluent suspended solids in wastewater treatment plants by integration of a flocculation model with computational fluid dynamics	131
8.1	Introduction	132
8.2	Materials and methods	134

Contents

8.2.1	The system under study	134
8.2.2	Acoustic Doppler Current Profiler (ADCP) measurement	136
8.3	Integrated model development	138
8.3.1	CFD model	138
8.3.2	Sludge settling velocity	143
8.3.3	Flocculation model	143
8.4	Results and discussion	144
8.4.1	CFD model	145
8.4.2	Integration of a flocculation model	150
8.4.3	Further model development	152
8.5	Conclusions	153
9	A novel methodology for the calibration of discrete settling behaviour of activated sludge	155
9.1	Introduction	155
9.2	Materials and methods	156
9.2.1	Settling column	156
9.2.2	Particle Size Distribution (PSD) measurements	157
9.2.3	Sludge samples	159
9.3	Results and discussion	159
9.3.1	Qualitative measurements of discrete settling behaviour	160
9.3.2	Comparison to effluent quality	163
9.3.3	Quantitative determination of the discrete settling velocity	164
9.4	Conclusions	165
10	Towards mechanistic models for activated sludge flocculation under different conditions based on inverse problems	169
10.1	Introduction	170
10.2	Material and methods	172
10.2.1	Experimental data	172
10.2.2	Inverse problem methodology	174
10.3	Results	177
10.3.1	Experiment 1: 8 meq Ca ²⁺	178
10.3.2	Experiment 2: 16 meq Ca ²⁺	185
10.3.3	Experiment 3: 32 meq Ca ²⁺	188
10.3.4	Summary effect of Ca ²⁺ addition	188
10.3.5	Experiment 4: impact of Dissolved Oxygen (DO)	192
10.3.6	Experiment 5: impact of temperature	193
10.4	Conclusions	195
IV	Conclusions and perspectives	197
11	General discussion and conclusions	201
11.1	Importance of compression settling on operation and control of WWTPs	202
11.2	Model selection and calibration for hindered and compression settling	202
11.3	Development of an integrated flocculation-CFD model to model discrete settling	204
11.4	Extension and calibration of an integrated flocculation-CFD model	204
11.5	General conclusions	205
12	Perspectives and future work	207
	Appendices	217

A Calibration of hindered settling functions based on batch settling data of the Waste Water Treatment Plant (WWTP) of Roeselare	219
B Calibration of hindered settling functions based on batch settling data of the WWTP of Eindhoven	223
Curriculum vitae	227

Acronyms

ADCP Acoustic Doppler Current Profiler.

AIC Akaike's Information Criteria.

AS Activated Sludge.

ASU 1 first Activated Sludge Unit.

BFMC Brute-Force Monte Carlo.

BOD Biological Oxygen Demand.

BSM1 Benchmark Simulation Model No. 1.

CFD Computational Fluid Dynamics.

COD Chemical Oxygen Demand.

DO Dissolved Oxygen.

DSVI Diluted Sludge Volume Index.

EPS Extracellular Polymeric Substances.

ESS Effluent Suspended Solids.

FIM Fisher Information Matrix.

GSA Global Sensitivity Analysis.

HiCS High-rate Contact Stabilisation.

IE Inhabitant Equivalents.

LOT Laser Obscuration Time.

ML Mixed Liquor.

MLSS Mixed Liquor Suspended Solids.

ODE Ordinary Differential Equation.

PBE Population Balance Equation.

PBM Population Balance Model.

PDE Partial Differential Equation.

PSD Particle Size Distribution.

RANS Reynolds-Averaged Navier-Stokes.

RAS Return Activated Sludge.

SBH Sludge Blanket Height.

SBR Sequencing Batch Reactor.

SLR Solids Loading Rate.

SMP Soluble Microbial Products.

SOR Surface Overflow Rate.

SRT Sludge Residence Time.

SS Suspended Solids.

SSE Sum of Squared Errors.

SSP Sludge Settleability Parameter.

SST Secondary Settling Tank.

SSVI_{3.5} Stirred Specific Volume Index at 3.5 gMLSS/l.

SVI Sludge Volume Index.

TN Total Nitrogen.

TP Total Phosphorous.

TSS Total Suspended Solids.

UDF User Defined Function.

UDS User Defined Scalar.

WWTP Waste Water Treatment Plant.

Summary

Water resources in many parts of the world are under increasing pressure due to the continuously rising demand for clean water and the production of large amounts of wastewater. In this respect, a good functioning and cost-effective wastewater treatment system is of crucial importance in order to prevent further pollution and depletion of water resources. The Secondary Settling Tank (SST) has a prominent function in Waste Water Treatment Plants (WWTPs) as it directly affects the effluent quality (being the final step in the treatment) as well as the biomass inventory (through the recycle of the separated micro-organisms to the biological reactor).

The operation and control of SSTs is still an important performance-limiting factor in conventional WWTPs as the exact mechanisms that drive the separation process are not yet fully understood. The performance of a SST is characterised by different regimes of settling behaviour (discrete settling, hindered settling and compression settling) that occur simultaneously at different locations in the SST. Most SST models used to date include only one type of settling (i.e. hindered settling) according to which the sludge will settle as one mass with a velocity depending on its concentration. However, this is a very harsh approximation. In order to improve existing models, the working principle of each different settling regime needs to be investigated. Therefore, this PhD aims to improve existing SST models by developing further insight into the dynamics of each settling regime through experimental analysis and modelling.

A first part of this dissertation focussed on the settling behaviour at the bottom of SSTs where concentrations are typically high and interaction between flocs are known to occur. Under these circumstances, the settling behaviour is characterised by hindered and compression settling. First the impact of accounting for both hindered and compression settling on the formation of the sludge blanket, the final sludge concentration to be recycled, plant sludge inventory and Mixed Liquor Suspended Solids (MLSS) based control actions were illustrated by using the Benchmark Simulation Model No. 1. The numerical results showed that including compression settling allows more realistic predictions of the underflow sludge concentration and the sludge blanket height, which are essential for more accurate wet weather modelling and sludge waste predictions. The choice of secondary settler model clearly has a profound impact on the operation and control of the entire treatment plant. However, including both hindered and compression settling as opposed to only hindered settling complicates the model

calibration. Therefore, a calibration procedure based on well-known batch settling experiments at different initial concentration was applied on the 1-D SST model by Bürger et al. (2011) including both hindered and compression settling. This analysis exposed identifiability issues in the commonly used settling function of Takács et al. (1991) (which tries to capture both discrete and hindered settling). The identifiability issues could be related to the parameter describing the settling behaviour at low concentrations indicating that the settling behaviour at low concentrations requires a separate modelling framework to capture the distinctly different discrete settling dynamics. Moreover, 1-D model simulations with calibrated functions for hindered and compression settling were not able to simultaneously describe all batch curves with a single parameter set. Batch curves for different initial concentrations seemed to require different compression dynamics which is physically not possible. Further investigation into more suitable constitutive functions to describe the different phenomena is thus required.

As a first step towards this, the behaviour of different hindered settling functions was analysed with respect to data of long-term batch settling curves and detailed velocity profiles. The analysis showed that the exponential forms which are most commonly used in traditional SST models do not only account for hindered settling but partly lump compression as well. This makes them unsuitable for advanced 1-D models that explicitly include each phenomenon in a modular way. A power-law function is shown to be more appropriate to describe the hindered settling velocity. However, even with a power-law function the current modelling framework was unable to predict the full settling dynamics indicating that some variability remains that cannot be attributed to variations in concentration alone. In this dissertation a hypothesis is formulated relating this unexplained variability to phenomena such as variations in the flocculation state and segregation of particles during settling. Experimental evidence to support this hypothesis was provided by settling experiments under different flocculation conditions as well as in depth fluctuations in the hindered settling velocity during batch settling. Moreover, a brief overview of possible extensions/alternatives to the current modelling frameworks was presented.

A second part of this PhD focussed on the settling behaviour in the diluted top region of a SST (i.e. the clarification region) where particles undergo a distinctly different settling behaviour characterised by individual particle properties (such as size and density) instead of the concentration. This regime is called discrete settling and will play an important role with respect to the final effluent quality. The aim of this part was to develop a framework which is able to model the settling behaviour at these low concentrations in order to improve predictions of the effluent concentration.

Accurate description of discrete settling requires information on the floc size distribution which in its turn depends on the tank hydrodynamics. A Computational Fluid Dynamics (CFD) model to describe the hydrodynamics of a SST was coupled with

a flocculation model (including both aggregation and breakage of particles). Simulation results showed that the integration of a flocculation model with CFD allows to qualitatively describe the effect of aggregation and break-up and to define specific regions where flocculation is taking place in the SST. Coupling of CFD with flocculation models can serve as a powerful tool to gain knowledge on the processes affecting clarification and hence, the effluent quality in SSTs. However, the practical application of these models requires the selection of a number of specific particle size classes as well as a measurement of the settling velocity for each class. Therefore, a measurement device was developed which allows collecting detailed data of changes in Particle Size Distributions (PSDs) during discrete settling. The results show that the discrete settling behaviour of activated sludge can be described by dividing the sludge in roughly five classes. Moreover, by measuring the evolution in PSD along different depths in the settling device, the discrete settling velocities of the different classes can be quantified. Hence, this measurement device can serve as a first calibration tool for coupled flocculation-CFD models. Next to the number of classes and their settling velocity, calibration of the flocculation model requires further insight in the aggregation/breakage dynamics. The mechanisms driving the aggregation and break-up processes are not yet fully understood and existing kernel structures for collision frequency and efficiency are unable to accurately describe activated sludge flocculation data. Therefore, dynamic PSD data of activated sludge flocculation under different conditions of ionic strength, temperature and dissolved oxygen were analysed with an inverse problem yielding empirical models. Empirical aggregation kernel structures were recovered from the experimental data and implemented in a Population Balance Model (PBM) to model the aggregation process. Furthermore, a methodology was proposed to compare the retrieved kernel with literature kernels in order to identify their flaws. This comparison indicated the need for an aggregation kernel with a fractal dimension that depends on floc size.

Samenvatting

De toenemende consumptie in combinatie met de productie van grote hoeveelheden afvalwater maakt drinkbaar water tot een steeds schaarsere grondstof op vele plaatsen ter wereld. Een optimaal functionerende waterzuiveringsinstallatie zowel met betrekking tot kwaliteit als operationele kosten is dan ook uiterst belangrijk om verdere vervuiling en afname van de huidige watervoorraad in te perken. Een cruciaal proces in de meeste waterzuiveringsinstallaties is de bezinking van de actief slib vlokken in nabezinktanks. Hierbij staan nabezinktanks niet alleen in voor de finale scheiding tussen het gezuiverde water en de actief slib vlokken maar ook voor een constante aanvoer van ingedikt slib naar de bioreactor.

Een goede bedrijfsvoering en controle van nabezinktanks blijft een heikel punt in de werking van waterzuiveringsinstallaties door een gebrek aan kennis over de mechanismen die het scheidingsproces aandrijven. Een typische nabezinktank wordt gekenmerkt door verschillende bezinkingsregimes (discrete bezinking, gehinderde bezinking en compressie bezinking) die allemaal gelijktijdig plaatsvinden op verschillende dieptes in de tank. Populaire modellen voor nabezinktanks vereenvoudigen dit gedrag sterk door slechts één bezinkingsregime (nl. gehinderde bezinking) te beschouwen waarbij het slib bezinkt als één enkele massa met een snelheid die afhankelijk is van de concentratie. Deze aanpak is echter een heel ruwe benadering van de werkelijkheid. Om bestaande modellen te verbeteren, moet het werkingsprincipe van elk bezinkingsregime afzonderlijk worden onderzocht en worden opgenomen in de modelstructuur. Dit doctoraat heeft tot doel om verder inzicht te verwerven in de mechanismen achter ieder bezinkingsregime door middel van zowel experimentele als modelgebaseerde analyse.

Een eerste deel van dit doctoraat concentreert zich op het bezinkingsgedrag onderaan de nabezinktank waar typisch hoge slibconcentraties en dus veel interacties tussen de slibvlokken voorkomen. Onder deze omstandigheden ondergaat het slib gehinderde en compressie bezinking. Het belang van het opnemen van zowel gehinderde als compressiebezinking in modellen voor nabezinktanks werd onderzocht met behulp van het Benchmark Simulation Model No. 1. Zowel het effect op slibdeken hoogte en onderstroom concentratie als het effect op de slibverdeling doorheen het volledige systeem en de hierop gebaseerde controle strategieën werd onderzocht. De simulatieresultaten toonden aan dat met behulp van compressiebezinking meer realistische voorspellingen

van slibdekenhoogte en onderstroomconcentraties worden verkregen wat op zijn beurt dan weer een grote rol speelt voor een goede voorspelling van de spuislib concentratie en meer nauwkeurige simulaties tijdens regenweer. Op deze manier zal de keuze van een goed bezinkingsmodel de werking en controle van de volledige waterzuiveringsinstallatie beïnvloeden.

Het uitbreiden van bezinkingsmodellen met zowel gehinderde bezinking als compressiebezinking zorgt echter voor extra obstakels in het kalibratieproces van deze modellen. Om dit te onderzoeken werd een standaard kalibratie procedure gebaseerd op batch bezinkingstesten bij verschillende initiële concentraties uitgevoerd voor het 1-D bezinkingsmodel van Bürger et al. (2011) waarbij zowel gehinderde bezinking als compressiebezinking in het model werden opgenomen. Tijdens deze analyse kwamen belangrijke identificeerbaarheidsproblemen aan het licht voor de traditionele gehinderde bezinkingsfunctie van Takács et al. (1991) (waarmee zowel gehinderde bezinking als discrete bezinking wordt beschreven). De identificeerbaarheidsproblemen waren te wijten aan de parameter die de bezinkingsnelheid bij lage concentraties beschrijft. Hieruit blijkt dat het bezinkingsgedrag bij lage slib concentraties een eigen modelleeropzet vereist i.p.v. dit gedrag te benaderen door aanpassingen in de gehinderde bezinkingsfunctie. Bovendien toonden de analyses aan dat model simulaties met een gekalibreerde gehinderde en compressie functie niet in staat waren om alle batch data te beschrijven met één enkele parameter set. Batch data voor verschillende initiële concentraties vereisten een verschillend compressiegedrag wat niet strookt met de fysische werkelijkheid. Verder onderzoek naar meer geschikte functies om de verschillende bezinkingsfenomenen te beschrijven is dus noodzakelijk.

Om aan deze nood tegemoet te komen werd eerst en vooral het gedrag van verschillende gehinderde bezinkingsfuncties geanalyseerd t.o.v. langdurige batch bezinkingscurves en gedetailleerde snelheidsprofielen. De analyse toonde aan dat populaire exponentiële functies niet enkel gehinderde bezinking beschrijven maar eveneens een stukje compressiegedrag opnemen in hun structuur. Hierdoor zijn deze functies niet geschikt voor toepassingen in geavanceerde bezinkingsmodellen aangezien deze laatsten tot doel hebben om het exacte mechanisme van elk bezinkingsregime afzonderlijk te beschrijven. Een machtsfunctie bleek hiervoor veel beter geschikt. Zelfs na implementatie van de machtsfunctie was de huidige modelstructuur niet in staat om de volledige bezinkingsdynamiek te voorspellen waaruit bleek dat niet alle variabiliteit in de data kon worden toegeschreven aan veranderingen in concentratie maar er dus nog andere factoren een belangrijke rol spelen. Dit inzicht heeft grote implicaties voor de structuur van bezinkingsmodellen aangezien we hiervoor moeten afstappen van de conventionele aanpak waarbij bezinkingsnelheid enkel aan de slibconcentraties wordt gekoppeld. In deze doctoraatsthesis werd een hypothese naar voren gedragen die de onverklaarde variabiliteit linkt aan variaties in de flocculatietoestand zowel tussen als binnenin slibstalen. Deze hypothese werd gestaafd met behulp van experimentele data van bezinkingsexperimenten bij verschillende flocculatietoestanden en metingen van de bezin-

kingssnelheid over de diepte van een batch reservoir. Daarnaast werd eveneens een kort overzicht gegeven van mogelijke uitbreidingen voor de huidige modelleeropzet.

In een tweede deel van dit doctoraat werd het bezinkingsgedrag in de bovenste regio van nabezinktanks onderzocht. Deze regio is gekenmerkt door zeer lage concentraties waarbij de bezinking van slibvlokken onafhankelijk van de concentratie plaatsvindt maar gestuurd wordt door individuele vlokeigenschappen zoals vloggrootte en dichtheid. Dit regime heet discrete bezinking en draagt in belangrijke mate bij tot de finale effluentkwaliteit. Het doel van dit deel van het doctoraat was dan ook om een model te ontwikkelen waarmee het discreet bezinkingsgedrag van individuele vlokken bij lage concentraties kan worden beschreven.

Aangezien discrete bezinking afhankelijk is van de eigenschappen van individuele vlokken, is informatie over de vloggrootte distributie essentieel om dit gedrag te modelleren. De vloggrootte distributie wordt op zijn beurt sterk beïnvloed door het stromingsprofiel in de nabezinktank vermits hierdoor zones met vlokopbreking en vlok-vorming (aggregatie) ontstaan. De koppeling van een stromingsmodel (CFD) met een flocculatiemodel laat toe om veranderingen in vloggrootte te modelleren. Simulatiere-sultaten toonden aan dat het geïntegreerde flocculatie-CFD model in staat is om het kwalitatieve effect van aggregatie en opbreking te beschrijven en eveneens om specifieke regio's in de tank te definiëren waar deze processen optreden.

Koppeling van stromingsmodellen met flocculatiemodellen vormt met andere woorden een zeer krachtig hulpmiddel in het onderzoek naar factoren die discrete bezinking en hieraan gekoppeld de effluent kwaliteit beïnvloeden. De praktische toepassing van deze modellen vereist echter nog bijkomende kwantitatieve kennis over de benodigde complexiteit van het flocculatiemodel (aantal deeltjesklassen), de exacte bezinkingssnelheden voor iedere deeltjesklasse en de dynamiek waarmee aggregatie en opbreking optreedt binnen elke klasse. Om de complexiteit van het flocculatiemodel en de exacte bezinkingssnelheden voor iedere klasse te bepalen werd een nieuwe meetmethode ontwikkeld waarbij gedetailleerde data van vloggroottedistributies kan gemeten worden tijdens discrete bezinking. Uit de resultaten bleek dat slibvlokken kunnen worden opgedeeld in ruwweg vijf klassen om hun discrete bezinking te beschrijven. Daarenboven kon de discrete bezinkingssnelheid worden afgeleid door de vloggrootte distributies op verschillende hoogten in de bezinkingskolom te vergelijken doorheen de tijd. Verder inzicht in dynamiek waarmee aggregatie optreedt werd bekomen door dynamische data van actief slib flocculatie onder verschillende omstandigheden (temperatuur, zuurstofconcentratie, calcium concentratie) te onderzoeken m.b.v. een inverse methodologie. Hieruit werden empirische aggregatiefuncties afgeleid die vervolgens vergeleken werden met bestaande functies uit de literatuur om zodoende te onderzoeken op welk vlak de bestaande functies falen in het beschrijven van de werkelijkheid. Dit onderzoek wees aan dat het actief slib aggregatieproces gekenmerkt wordt door een variabele fractale dimensie die functie is van de vloggrootte.

PART I

Introduction, literature review and objectives

The first part of this PhD dissertation presents a short introduction to situate the research in the environmental and modelling context (Chapter 1). Subsequently, a literature overview is given providing the reader with the general background and state-of-the-art experimental and modelling techniques in the research domain (Chapter 2). Finally, in Chapter 3 the research objectives for this PhD dissertation are defined.

CHAPTER 1

Background, problem statement and outline

1.1 Introduction

Clean, unpolluted water is a key resource for human health and well-being. Water is also essential for our eco-systems as it provides a natural habitat for many plant and animal species. However, water resources are under increasing pressure in many parts of the world due to the continuously rising demand for clean water and the production of large amounts of wastewater. In this respect, a good functioning and cost-effective wastewater treatment system is of crucial importance in order to prevent further pollution and depletion of water resources.

The activated sludge process is the most widespread process for the biological treatment of domestic and industrial wastewater. This process consists of two consecutive steps: (1) the removal of contaminants by specialised micro-organisms in a bioreactor followed by (2) the separation of the micro-organisms from the effluent in a Secondary Settling Tank (SST). The SST has a crucial function in Waste Water Treatment Plants (WWTPs) as it directly affects the effluent quality (being the final step in the treatment) as well as the biomass inventory (through the recycle of the separated micro-organisms to the biological reactor). As biomass is the driving force for conversion processes and should be present at the desired location for the process to function in an optimal way, secondary clarifier operation will affect the performance of the entire treatment plant.

The operation and control of SSTs is still an important performance-limiting factor in conventional WWTPs as the exact mechanisms that drive the separation process are not yet fully understood. Furthermore, more intense rain events and longer draughts between rain events, caused by climate change, result in WWTPs that are temporarily overloaded both hydraulically and in terms of pollutant load. These peak events have a significant effect on the operation of the SST and thus the system's biomass inventory. In order to safeguard the quality of our water sources, we need to address the impacts

of these new conditions by improving both infrastructure (improving design) and operational strategy and control. Mathematical modelling is a powerful tool to gain insight in how this is best accomplished.

However, past modelling efforts have mainly focussed on modelling the biological processes in the bioreactor and SST models are still greatly oversimplified. The performance of an SST is characterised by different regimes of settling behaviour that occur simultaneously at different locations in the SST. These different settling behaviours each contribute to a separate function of the SST. Most SST models used to date include only one type of settling according to which the sludge will settle as one mass with a velocity depending on its concentration. However, this is a very harsh approximation. In order to improve existing 1-D models, the working principle of each settling regime needs to be investigated separately. At the bottom of SSTs concentrations are typically high and interaction between flocs are known to occur. Under these circumstances, the settling behaviour is characterised by hindered and compression settling which play a key role in the formation of the sludge blanket and the final sludge concentration to be recycled and wasted. In the diluted top region of a SST on the other hand, particles will not interact and settle as individuals at their own velocity depending on individual properties such as size, density,... This regime is called discrete settling and will play an important role with respect to the final effluent quality. This PhD aims to develop further insight into the dynamics of these settling regimes through experimental analysis and modelling.

1.2 Outline

This thesis is structured in four parts as illustrated in Figure 1.1. The first part explains the setting and problem statement for the current work (Chapter 1). Moreover, a thorough literature review (Chapter 2) provides the reader with the necessary background and current state-of-the-art for this PhD dissertation leading to the definition of the research objectives in Chapter 3.

Part II addresses the improvement of existing 1-D models by including both hindered and compression settling. In this respect, Chapter 4 illustrates the importance of compression settling on operation and control of a WWTP during wet weather conditions. The calibration of hindered and compression settling functions from literature based on well-known batch settling tests is described in Chapter 5. This analysis showed that the selection and calibration of valid functions for both hindered and compression settling requires a critical analysis of available functions for each of these processes. Therefore, the behaviour of different hindered settling functions was analysed with respect to data of long-term batch settling curves and detailed velocity profiles (Chapter 6). Finally, in Chapter 7 a hypothesis is formulated regarding the physical explanation behind the remaining variability in the compression phenomenon and experimental evidence is

1.2. Outline

collected to support this hypothesis.

Part III aims to develop a framework to model the discrete settling behaviour in a SST in order to improve predictions of the effluent concentration. In Chapter 8, a flocculation model is successfully integrated with a Computational Fluid Dynamics (CFD) model to build knowledge on the discrete settling dynamics in SSTs. Subsequently, a novel measurement device is developed in Chapter 9 which allows collecting detailed data of changes in Particle Size Distributions (PSDs) during discrete settling and which can be used to calibrate the integrated model. Furthermore, Chapter 10 applies an inverse problem methodology to dynamic PSD data to gain insight into the complex aggregation dynamics described by the flocculation model.

The main conclusions of this PhD dissertation as well as some perspectives for future work are provided in Part IV.

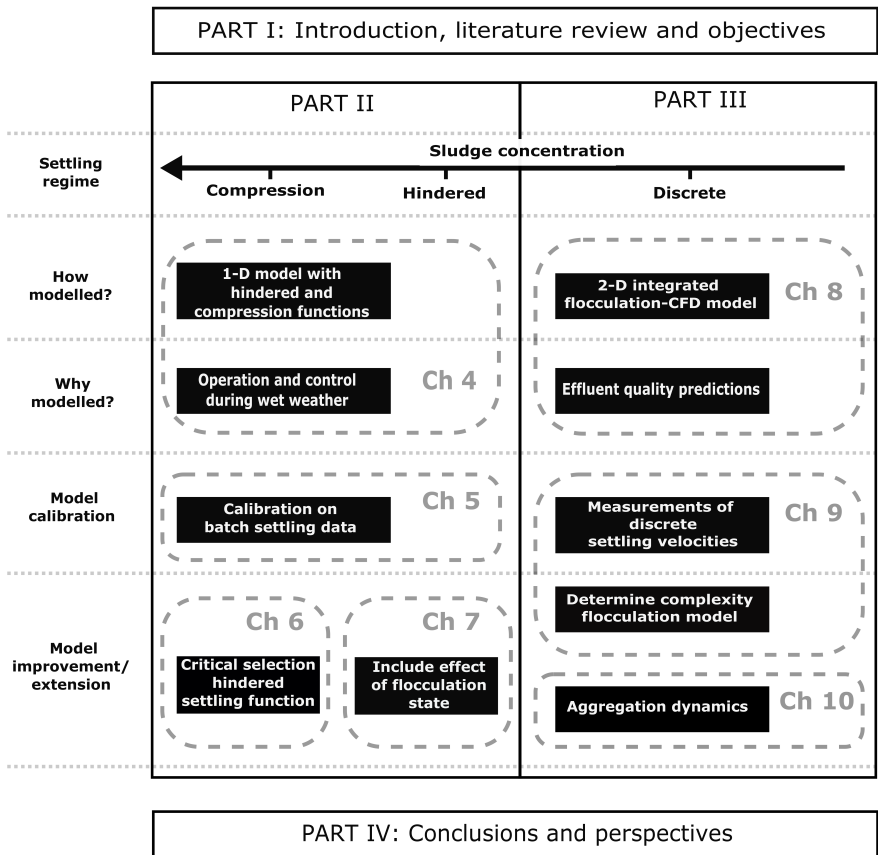


Figure 1.1: Outline of the PhD thesis.

Chapter 1. Background, problem statement and outline

CHAPTER 2

Literature review

2.1 Wastewater treatment

The conventional purification process of municipal wastewater generally consists of three consecutive treatment steps, referred to as primary, secondary and tertiary treatment (Tchobanoglous et al., 2003). A schematic overview of this process is given in Figure 2.1. The primary treatment involves the preliminary removal of coarse material and large particles by means of mechanical operations such as screening, filtration and solids sedimentation. In addition, floating materials (e.g. oils and greases) are skimmed off as a scum.

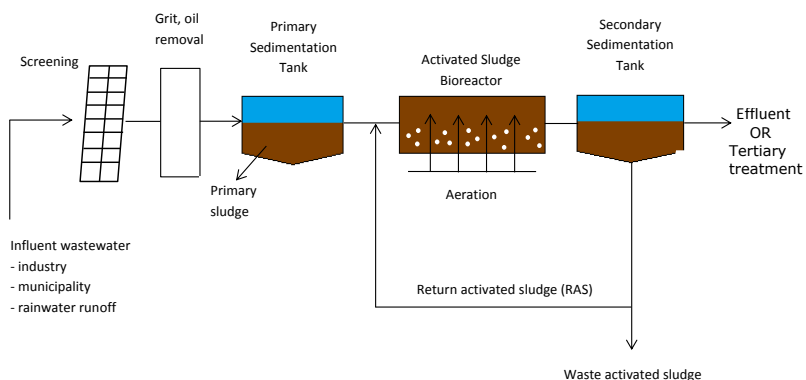


Figure 2.1: Simplified overview of a biological wastewater treatment facility (modified from Nopens (2005)).

During the secondary treatment, organic compounds and nutrients (e.g. phosphorous and nitrogen) are degraded from the wastewater by a variety of micro-organisms and the micro-organisms are separated from the treated water. This treatment is most commonly based on the Activated Sludge (AS) system, which was first introduced in a Sequencing Batch Reactor (SBR) by Ardern and Lockett (1914). The AS system accelerates the natural purification process that occurs in our water systems by overcoming the natural limitation for bioconversion such as limited aeration and limited amount of biomass (Henze et al., 2008).

Nowadays, the application of the AS system typically consists of two main process: (1) a biological process and (2) a solid-liquid separation process. At the start of the biological process, the wastewater is transferred to a bioreactor. Here, it is mixed with a diversified group of micro-organisms, called the activated sludge, which is responsible for the conversion of organic matter and nutrients into biomass. The biomass concentration in the tank is called the Mixed Liquor Suspended Solids (MLSS) concentration. Dissolved Oxygen (DO) levels throughout the bioreactor are controlled by aeration in order to supply the micro-organisms with sufficient oxygen for the aerobic bioconversion of the organic matter as well as creating zones for anoxic or anaerobic degradation of nutrients. From the bioreactor, the Mixed Liquor (ML) is sent to a SST, where the denser solid phase (the activated sludge mass) is separated from the liquid phase (effluent) by gravitational settling (Henze et al., 2008). A large part of the settled sludge is recycled (Return Activated Sludge (RAS)) in order to maintain the desired MLSS concentration in the aeration tank. The remaining part is wasted (Tchobanoglous et al., 2003).

Besides gravitational settling, the wastewater industry increasingly uses membranes to perform the solids-liquid separation. These offer the advantage of a higher effluent quality, a lower space requirement, good disinfection capability and a lower sludge production. However, they are still expensive and additional research is required to deal with operational problems (e.g. membrane fouling) (Judd and Judd, 2011; Le Clech et al., 2006). This work focusses on solids-liquid separation by means of SSTs.

Finally, in the tertiary treatment the objective is to remove residual constituents and to disinfect the effluent in order to destroy pathogens. This additional treatment is sometimes necessary to meet the stringent effluent quality norms and may become increasingly important in future WWTPs. Typical tertiary treatment consists of filtration steps (sand filtration and/or membrane filtration) and disinfection steps (Tchobanoglous et al., 2003).

2.2 Secondary Settling Tank (SST)

2.2.1 Layout of a typical SST

The most commonly used SST configurations are either circular or rectangular tanks. In particular, a circular SST with a central feed system and a radially outward flow of ML to a peripheral effluent weir is one of the most widespread applied configurations (Henze et al., 2008; Tchobanoglous et al., 2003; De Clercq, 2003). An example of such a configuration is given in Figure 2.2 and a schematic representation of half the cross-section in Figure 2.3.

The ML from the biological tank enters the SST through a central inlet structure which may include an energy dissipation well (to reduce high turbulence) and a separate flocculation zone (where the incoming sludge can reflocculate after transport to the SST). Furthermore, the placement of baffles in the system prevents the short circuiting of the flow between the inlet and effluent overflow thus ensuring a minimal residence time in the tank. Hence, the SST provides quiescent flow conditions allowing the sludge mass to settle. The thickened sludge blanket formed at the bottom of the tank can be collected in a sludge hopper by means of a tilted tank slope and a rotating scraper system. Alternatively, the thickened sludge can be removed through a suction system. Clean effluent flows over the edge at the top of the tank.



Figure 2.2: Circular secondary settling tank with central feed system and peripheral effluent overflow weir (WWTP of Roeselare, Belgium).

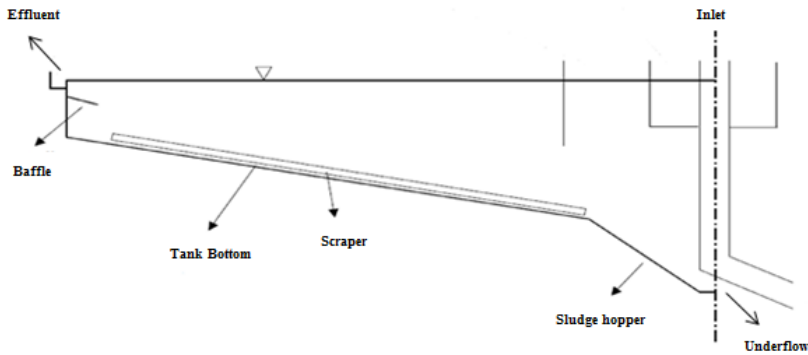


Figure 2.3: Schematic view of a half cross-section of a circular SST.

2.2.2 Functions of a SST

The secondary settling tank has to fulfill three important functions prior to discharge of the treated wastewater to the receiving waters (Ekama et al., 1997).

1. The SST has a **thickening** function to produce a continuous underflow of thickened sludge for return to the aeration tank. It requires the majority of the sludge mass (generally over 98%) that enters the SST to settle at sufficiently high concentrations. Failing to achieve the thickening function, the treatment plant capacity will noticeably decrease because less sludge is recycled to the biological reactor. Furthermore, well compacted solids decrease the costs related to sludge disposal and dewatering processes. The thickening capacity of the SST is controlled by the tank's geometry, the flow rates, the settleability and compactability of the sludge, and the concentration of the solid particles in the biological tank.
2. Secondly, the SST has a **clarification** function. The clarification efficiency depends on the capability to capture the activated sludge particles that enter the SST in the sludge blanket and is consequently a critical aspect in the performance of a WWTP. Failure with respect to clarification behaviour of the SST may result in increased concentrations of Effluent Suspended Solids (ESS). Several factors influence the clarification function including design features, hydraulic disturbances (e.g. short-circuiting or resuspension of sludge particles due to high velocity currents), thickening overloads caused by high sludge blankets, denitrification processes in the SST (Ekama et al., 1997) and the flocculation state and flocculation tendency of the activated sludge. With respect to this last factor it is not only important to produce flocs of sufficient mass to settle in the SST but also to reduce the concentration of small, discrete particles that do not have enough mass to settle in the SST. A more detailed explanation of flocculation behaviour is given in Section 2.4.1.

2.3. Settling behaviour of the activated sludge

3. Finally, the SST also acts as a **sludge storage tank**. Under high hydraulic loading conditions (e.g. periods of heavy rainfall) the SST needs to store sludge without causing an increase in ESS concentration. Wet weather events are extremely stressing conditions in treatment plants due to an increased Solids Loading Rate (SLR) and Surface Overflow Rate (SOR). Under these conditions, sludge will be moved from the aeration tank to the SST. In order to prevent loss of sludge, the SST needs to be able to store this extra sludge. The storage function is mainly ensured by a proper design of the SST.

Failure of the SST in one of these functions leads to excessive loss of Suspended Solids (SS) over the effluent weir. The increase in SS content of the effluent will affect the effluent quality in terms of Biological Oxygen Demand (BOD), Chemical Oxygen Demand (COD), Total Nitrogen (TN) and Total Phosphorous (TP) concentrations (Ekama et al., 1997). In addition, it could affect the behaviour of the biological process by uncontrolled decrease of MLSS and hence the sludge age to values below that required for proper plant performance. Therefore, the SST is regarded as a vital component of every biological treatment.

2.3 Settling behaviour of the activated sludge

2.3.1 Settling regimes

The settling behaviour of AS varies among different regions in the SST and is governed by the **sludge concentration** and its **flocculation tendency**. Based on the latter two factors, the settling behaviour can be classified in four settling regimes (Figure 2.4): discrete non-flocculent settling (Class I), discrete flocculent settling (Class II), zone settling or hindered settling (Class III) and compressive settling (Class IV). These regimes occur simultaneously at different locations in a SST.

At low concentrations (below 600-700 mg/l, dependent on the settleability of the sludge (Mancell-Egala et al., 2012)), the particles are completely dispersed, there is no physical contact between them and the concentration is typically too diluted for particles to sense each other. Each particle settles at its own characteristic terminal velocity which depends on individual particle properties such as shape, size, porosity and density. This regime is called **discrete non-flocculent settling**.

However, AS with a proper biological make-up has a natural tendency to flocculate even at low concentrations (Ekama et al., 1997). Through subsequent processes of collision and cohesion larger flocs are formed during settling. These alterations in size and shape of the flocs cause their settling velocity to change over time but they will still settle as individual flocs. This regime is called **discrete flocculent settling**.

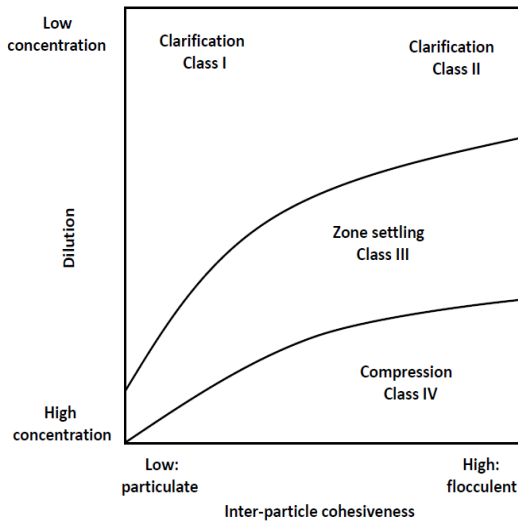


Figure 2.4: Settling regimes (Ekama et al., 1997)

The two discrete settling regimes are also known as **clarification**, because they occur in the clarification zone of a SST. Both settling regimes are of crucial importance to the performance of the SST as clarifier because it concerns particles that settle poorly, remain in the supernatant and are eventually carried over the effluent weir causing increased ESS concentrations.

The transition from discrete settling to **hindered settling** occurs if the solid concentration in the tank exceeds a threshold concentration where the particles no longer settle independently of one another. As can be seen from Figure 2.4, this threshold concentration depends on the flocculation state of the sludge. Each particle is hindered by the other particles and the inter-particle forces are sufficiently strong to drag each particle along at the same velocity, irrespective of size and density. In other words, particles settle collectively, as a zone and therefore this regime is also called **zone settling**. In this regime, a distinct interface between the clear supernatant and the subsiding flocs is formed.

When the solids concentration further increases above a certain critical concentration (5-10 g/l), the settling behaviour changes to **compressive settling**. The exact transition concentration depends on the settleability of the sludge (De Clercq et al., 2008). At these elevated concentrations, the flocs come into physical contact with one another and are subjected to compaction due to the weight of overlying particles. The mechanical contact subjects the flocs to an additional force due to a compressive stress which thickens the sludge and pushes the water in an upward direction. The settling velocity will be much lower than in the hindered settling regime.

2.3. Settling behaviour of the activated sludge

2.3.2 Experimental determination of the settling behaviour

To evaluate the performance of a SST, it is essential to quantify the settling behaviour in these different regimes. Batch settling experiments are an interesting information source in this respect since they eliminate the hydraulic influences of in- and outgoing flows on the settling behaviour. Therefore, several methods aim to determine the settling characteristics of the activated sludge by measuring certain properties during settling in a batch reservoir.

Batch settling experiments

Batch settling curves can be recorded by measuring the height of the suspension/liquid interface (i.e. the Sludge Blanket Height (SBH)) at several time instants during a batch settling experiment.

In a batch settling curve, four different phases occur which are explained in more detail in this section. Each phase marks a change in the settling behaviour at the suspension/liquid interface. Figure 2.5 shows the evolution of the SBH in time during a batch settling experiment with indication of the four phases. However, the settling behaviour is not only changing at the suspension/liquid interface but throughout the depth of the batch settling reservoir. Almost immediately after start up of the experiment four regions are being formed at increasing depth. The top region (region A) consists of supernatant. Below region A, region B, C and D are formed where respectively zone settling, transition settling and compression settling is taking place (Ekama et al., 1997). Figure 2.6 represents the distribution of these regions at different times during a batch settling experiment. Hence, the phases in a batch settling curve (Figure 2.5) occur as the suspension/liquid interface passes through these different settling regions.

From the beginning of the test up to point (a) the suspension/liquid interface is in the **lag phase**. In this phase, the mixed liquor needs to recover from disturbances due to turbulence caused by the filling of the batch column.

During the **hindered settling phase** or zone settling phase which starts at point (a) and ends at point (b) the interface is located in the hindered settling region (region B). This phase is characterised by a distinct linear descent in the batch curve. An equilibrium between the gravitational forces causing the particles to settle and the hydraulic friction forces resisting this motion results in the same settling velocity for all the particles in the region. If the column is not stirred, then the velocity at which the interface is moving downward is called the *hindered settling velocity* (v_{hs}) at the inlet solids concentration (Ekama et al., 1997).

The transition phase starts (point (b)) when the sludge blanket reaches the transition layer (region C). The transition layer is a layer of constant thickness and is formed by

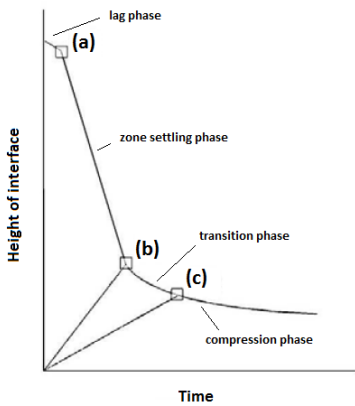


Figure 2.5: Evolution of the sludge blanket height in time with the indication of the four phases (Rushton et al., 2000)

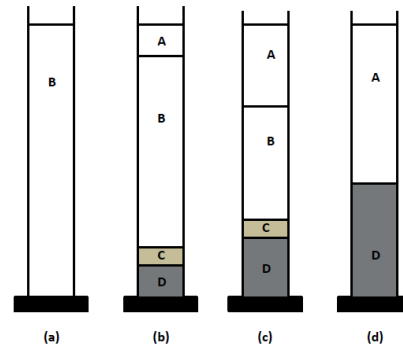


Figure 2.6: Chronological process of a batch settling test (Ekama et al., 1997)

particles coming from the decreasing hindered settling layer and particles coming from the increasing compression layer. Although during this phase the same characteristics exist as in the zone settling regime, the settling velocity decreases due to an increasing concentration gradient with depth. The transition phase ends when the sludge blanket reaches the compression layer.

The last phase starts at point (c) and is called the **compression phase**. The time at which the compression phase starts, called the *compression point*, is difficult to identify. During the compression phase the particles undergo compaction thus creating an increasing **concentration gradient** as well as a decreasing settling velocity.

Recent advances in batch settling experiments

By measuring a batch curve the velocity at which the suspension/liquid interface passes through different settling regions can be investigated. However, the drawback of this method is that it only provides information on the suspension/liquid interface. No information on the settling behaviour inside the sludge blanket nor the build up of the sludge blanket is recorded. Recently, more advanced measurement techniques aiming to provide more detailed information of the sludge settling behaviour over time and depth have been presented (Diehl, 2007; Ramin et al., 2014b; De Clercq et al., 2005; Locatelli et al., 2015).

2.3. Settling behaviour of the activated sludge

Ramin et al. (2014b) extended the standard batch measurement described above with a Solitax[®] Total Suspended Solids (TSS) sensor at the bottom of the batch reservoir. In this way, the evolution of the SBH and the concentration at the bottom of the batch could be recorded simultaneously providing additional information on the thickening behaviour.

Diehl (2007) suggested a new type of batch experiment consisting of two glass columns separated by a moveable plate. Solids can settle in the top column and will accumulate on the plate. When the plate is subsequently pulled aside, the settling behaviour of a concentrated sludge sample on top of clear liquid can be studied. The data collected by this method allow to estimate a larger part of the flux curve.

De Clercq et al. (2005) developed a technique to measure detailed spatio-temporal solids concentrations during a batch test. In this technique Tc-99m Sestamibi, a cationic radioactive tracer, is added to the negatively charged sludge. A gamma camera detects photons emitted by the tracer from which the concentration can be calculated. When the scanner takes an image every 30 seconds, data can be obtained for every height at several time instants providing a detailed concentration profile of the sludge as shown in Figure 2.7. From the concentration profiles the hindered and compression settling phases can be examined in more detail. However, this technique requires specialised equipment and cannot be routinely performed.

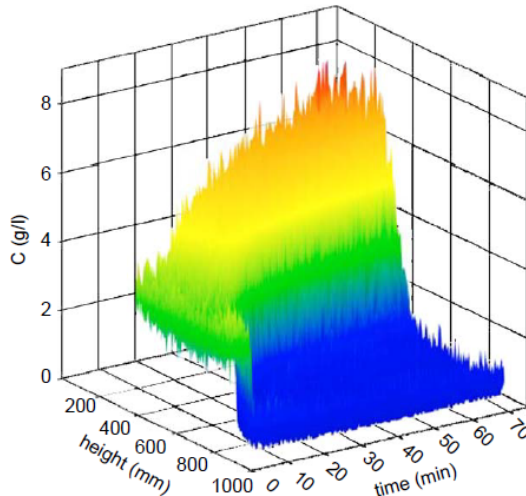


Figure 2.7: Solids concentration profile recorded by means of a radioactive tracer during batch settling at an initial concentration of 3.3 g/l (De Clercq et al., 2005).

In a recent study, Locatelli et al. (2015) developed an experimental procedure to measure settling velocities within the sludge blanket without disturbing it. An ultrasonic

transducer was installed at the top of a batch column to perform vertical measurements. Measurements of the Doppler Effect produced by the displacement of particles on the backscattered ultrasound wave allowed evaluating the settling velocity in depth (Takeda, 1995). This resulted in direct measurements of settling velocity profiles throughout the depth of the sludge blanket (Figure 2.8). Experiments were performed at different initial solids concentrations.

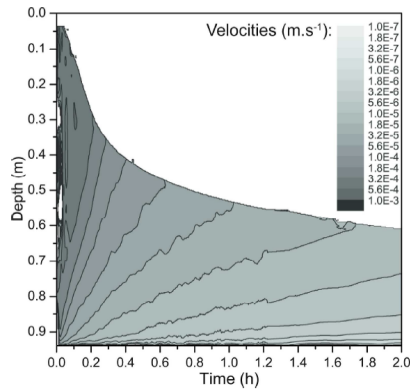


Figure 2.8: Evolution of the settling velocity profile of a sludge sample with an initial concentration of 3.9 g/l during 22 h of batch settling (Locatelli et al., 2015)

Measuring discrete settling

Each of the procedures described above focusses on the settling behaviour inside the sludge blanket in order to obtain information on hindered and compression settling conditions. Neither of these procedures records information on the discrete (flocculent or non-flocculent) settling regime. Generally, the thickening function has been studied and considered more than the clarification function although this function is an equally vital component since it has a profound impact on the ESS concentration. During discrete settling, each particle settles at its own characteristic terminal velocity which depends on individual particle properties such as shape, size, porosity and density. In a typical heterogeneous sludge sample a distribution of particle velocities occurs making velocity measurements more challenging compared to hindered or compression settling which are both concentration driven processes. Some experimental methods to measure settling velocity distributions have been developed.

Chebbo and Gromaire (2009) presented an operating protocol to measure settling velocity distributions in urban drainage (ViCAs). The experimental set-up consisted of an inversed settling column with the column opening at the bottom of the column and a vacuum pump at the top to fill the column with a sludge sample. During the experiment

2.4. Factors influencing sludge settling behaviour

settled particles are collected at the bottom of the column at specific time instances. The mass of particles that have settled during a certain time can then be used to calculate the percentage of particles with a certain settling velocity. This methodology was applied by Bachis et al. (2014) to measure particle size velocity distributions in primary settling tanks.

Ramalingam et al. (2012) applied a novel settling device to measure the discrete settling velocities of AS for pre-defined particle classes. In this methodology a settling column is filled with clear water after which an AS sample from the biological reactor is brought on top of the column and allowed to settle through the clear water. At a predetermined time a well-defined volume is removed at the bottom of the column. The mass in this sample represents the particles that have travelled the length of the column during the specified time. Repeating the experiment at different settling times provides the percentage of particles in each of the pre-defined classes.

Even though each of the techniques above provide a measurement of the velocity distribution they do not provide any information on the underlying property distribution (size, density, porosity,...) that causes the distributed behaviour of the settling velocity. Hribersek et al. (2011) used a similar set-up as Ramalingam et al. (2012). However, instead of collecting the mass of settled particles after a specific settling time, the settling paths of individual particles were tracked with a high-speed camera and linked to the particle size and porosity.

2.4 Factors influencing sludge settling behaviour

The settling behaviour of AS is mostly governed by the **flocculation state** and the **hydrodynamics** of the tank. Therefore, careful consideration of these factors is necessary to design and operate a proper functioning SST (Ekama et al., 1997). These influencing factors are discussed in more detail below.

2.4.1 Activated sludge flocculation

The ability of a SST to act successfully as a clarifier is highly dependent on the potential of the micro-organisms to form a flocculent biomass which settles and compacts well, producing a clear effluent (Das et al., 1993). The aim of the flocculation process is to combine individual flocs into large and dense flocs that settle rapidly and to incorporate discrete particles that normally would not settle alone. In case of failure of the flocculation process or break-up of flocs during the activated sludge process, a fraction of the particles is not incorporated into flocs. They remain in the supernatant of the SST due to lack of sufficient mass and are carried over the effluent weir deteriorating the effluent quality. The sections below discuss the composition of activated sludge flocs and their flocculation mechanisms.

Composition of AS flocs

Activated sludge flocs are aggregates of SS formed through physico-chemical interactions between different micro-organisms, dead cells and particulate organic and inorganic material. A network of Extracellular Polymeric Substances (EPS) holds the different floc constituents together in one structure or floc (Wilén et al., 2003). In addition cation bridging phenomena of multivalent cations (Mg^{2+} , Ca^{2+}) stabilise the flocs and facilitate flocculation (Cousin and Ganczarzyk, 1999). Figure 2.9 gives an image of an AS floc on the left and a schematic representation of the composition on the right.

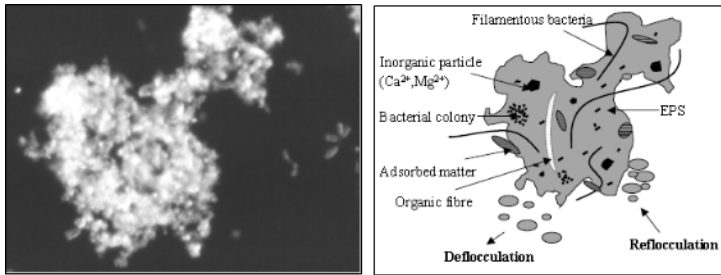


Figure 2.9: Image of an activated sludge floc (left) and its composition (right) (Govoreanu, 2004).

A mixture of different micro-organisms such as bacteria, fungi, protozoa and metazoa is found in AS flocs (Jenkins et al., 1993) due to the availability of a large variety of substrates in wastewaters. With respect to flocculation characteristics micro-organisms can be divided into floc formers and filamentous micro-organisms. If there is a good balance between the two groups, the filamentous micro-organisms will provide a network to which floc formers can attach (backbone structure) resulting in large and strong flocs which are more resistant to shear stresses (Figure 2.10 - center) (Parker et al., 1970; Sezgin et al., 1980). Moreover, the filamentous network can also constitute a filter which removes small particles from the sludge/water mixture producing a clear effluent. It follows that the two main process units of the AS system (bioreactor and SST) are interdependent. A well operating AS system provides proper conditions for the development of a balanced group of micro-organisms which gives rise to large and strong flocs. Failure of the solids-liquid separation process is commonly related to an undesired shift in the microbial composition of the sludge. For example, low DO concentrations necessary in nutrient removal systems to create anaerobic zones can cause an excessive growth of filamentous bacteria resulting in the formation of open, porous flocs with poor settling characteristics. This long standing problem is also referred to as filamentous bulking sludge (Figure 2.10 - left) (Ekama et al., 1997). In contrast, over aeration can lead to poor flocculation and pinpoint flocs formation (Figure 2.10 - right).

2.4. Factors influencing sludge settling behaviour

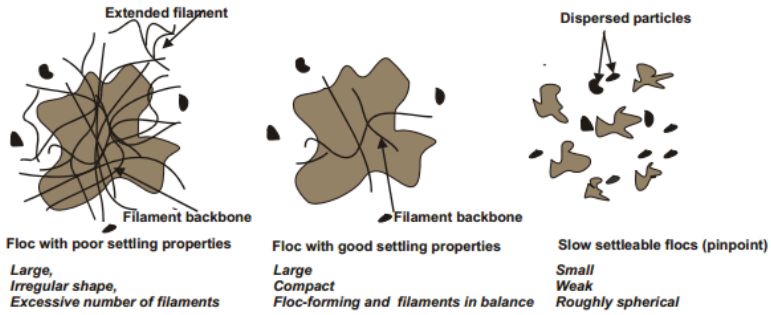


Figure 2.10: Activated sludge floc types which have an influence on solids-liquid separation in secondary clarifiers (Govoreanu, 2004).

Flocculation mechanisms

Due to the heterogeneous nature of biological flocs and their complex structure, both the floc size and the floc morphology can differ considerably in a SST. A broad range of floc sizes may occur, typically varying from a few to thousand μm (Li and Ganczarzyk, 1991). The average final floc sizes and floc size distribution are the result of a dynamic equilibrium state between flocculation and break-up of the microbial aggregates (Lu and Spielman, 1985; Spicer et al., 1996; Mikkelsen, 2001).

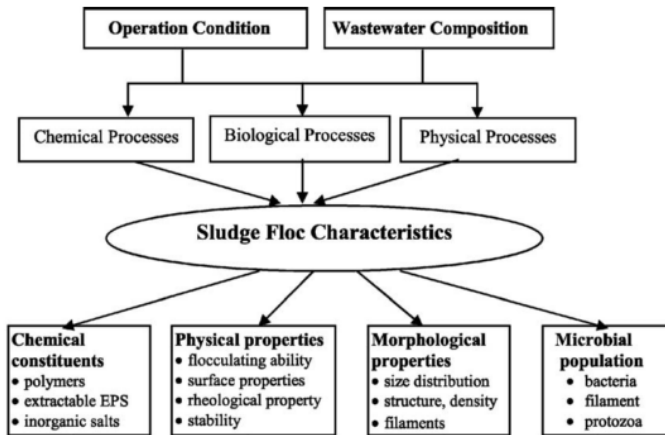


Figure 2.11: Network of physical, chemical and biological factors affecting sludge floc characteristics (modified from Jin et al. (2003)).

Flocculation and breakage of activated sludge in a SST are complex processes and concern biological, physical and chemical phenomena as illustrated in Figure 2.11. More-

over, WWTPs are dynamic systems. Different process parameters change continuously such as temperature, substrate loading, shear forces, sludge age, ionic strength and DO concentration. Due to the complex composition and structure of flocs, alterations in these factors directly or indirectly affect the flocculation process. As a result, the floc size and floc stability may change during settling in a SST (Mikkelsen et al., 1996; Wilén and Nielsen, 2000; Mikkelsen and Nielsen, 2001; Mikkelsen, 2001).

Spicer and Pratsinis (1996b) showed that several phases of floc formation occur before a steady state between flocculation and break-up processes is reached. First, formation of flocs predominates as a result of the coagulation of particles in the presence of polymers. In this way, flocs gain sufficient mass to settle. However, as flocculation persists large flocs with a more open and porous structure are formed. These flocs are less resistant against fragmentation in regions with excessive fluid shear.

Thomas et al. (1999) indicated two discrete steps during the flocculation process: transport and attachment of particles. Obviously, a particle first has to be transported before it can approach other particles in a SST and subsequently collide and attach. This transport step is achieved by local variations in fluid/particle velocities. Three different transport mechanisms exist, each related with a type of aggregation or flocculation step (De Clercq, 2003). Figure 2.12 gives a schematic overview of the particle transport mechanisms.

- **Perikinetic flocculation** is a stochastic process driven by differences in temperature, also known as microflocculation. Particles that follow this transport process approach each other by random Brownian motions (Figure 2.12 - left).
- **Differential settling** is determined by differences in settling velocity between distinct particle sizes (Figure 2.12 - right). Large particles which settle rapidly can collide and incorporate small, slowly settling particles during the settling process. As a result small particles may be removed from the supernatant which otherwise would settle poorly and probably deteriorate the effluent quality.
- **Orthokinetic flocculation**, also called shear-induced flocculation, involves aggregation by imposed velocity gradients due to mixing. When fast moving particles overtake the slower-moving particles in adjacent regions with a lower velocity, they may collide and form a larger floc that settles more rapidly (Figure 2.12 - center). To determine the extent of this flocculation mechanism, information about the hydrodynamics is necessary.

Perikinetic flocculation occurs only when particles are very small ($< 1\mu\text{ m}$). In contrast, flocculation of larger particles ($> 1 - 2\mu\text{ m}$) is dominated by differential settling and orthokinetic flocculation (Tchobanoglous et al., 2003). Whether a transport step is followed by an attachment step depends on several short range forces related with the nature of the surfaces themselves such as electrostatic repulsion, van der Waals or hydrodynamic forces (Thomas et al., 1999).

2.4. Factors influencing sludge settling behaviour

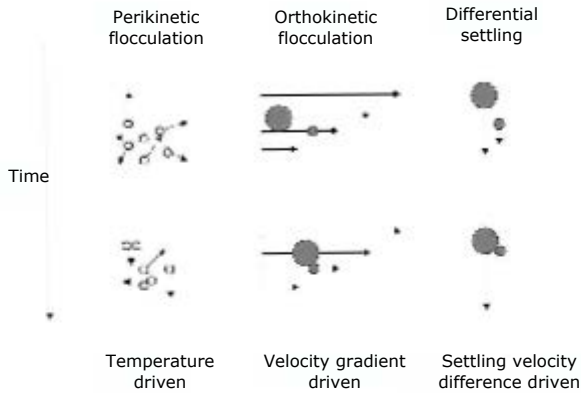


Figure 2.12: The different flocculation mechanisms that induce particle collisions, adapted from Tchobanoglous et al. (2003).

2.4.2 Hydrodynamics

The settling and flocculation processes of the SS in a SST are heavily dependent on the hydrodynamics of the tank. The flow field in the SST is not uniform due to density stratification caused by a concentration difference between the solid loaded influent and the ambient water (Anderson, 1945). If the denser incoming ML leaves the inlet structure, it immediately falls down as a 'density jet' to the sludge blanket. This so-called density current induces a recirculating flow pattern in the clarifier characterised by a strong bottom density current and typically a countercurrent at the water surface. An example of such a flow pattern is shown in Figure 2.13.

Temperature-driven density currents can also occur in a clarifier, but these are not considered here. The multi-layered flow pattern reduces the occurrence of short-circuiting from inlet to outlet. However, the higher velocities in the vicinity of the inlet structure may lead to increased turbulence and hence, resuspension of previously settled solids at the top of sludge blanket (Ekama et al., 1997). The local velocity gradients have a particularly large impact on the aggregation and break-up of flocs.

The use of Computational Fluid Dynamics (CFD) to describe the hydrodynamics in the SST has led to a more comprehensive understanding of the different processes and their interactions in SSTs. These type of models will be discussed in more detail in Section 2.5.4.

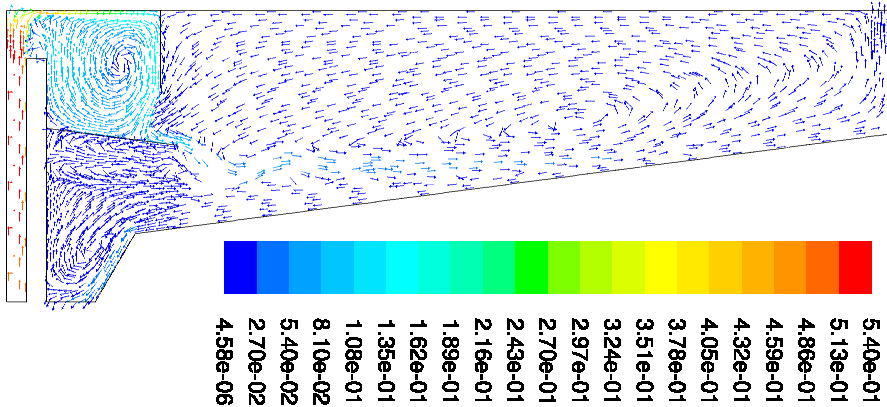


Figure 2.13: Velocity vector field (m/s) of the ML in a SST of the WWTP of Roeselare, Belgium.

2.5 Modelling of SSTs

2.5.1 Overview

The use of mathematical modelling has already proven its theoretical, practical and economical importance in the wastewater industry. Models for SSTs are valuable tools in this respect as they can be used to describe the physical, biological and chemical phenomena occurring in a SST which will in turn influence the performance predictions of the entire WWTP. Ramin et al. (2014a) performed a Global Sensitivity Analysis (GSA) on the Benchmark Simulation Model no. 2 and found that the parameters of SST models provide a significant contribution to the uncertainty of WWTP predictions, particularly for biogas production and effluent quality. Hence, development of appropriate SST models deserves considerable attention. In recent years, the application of SST models has already resulted in an improved understanding of the underlying mechanisms and processes affecting the performance of SSTs. Furthermore, these models can serve as a tool for process optimisation. It is however important to keep in mind that mathematical models only provide an approximation or a simplification of reality.

Several types of settling tank models exist ranging from empirical or **black box** models to more advanced, deterministic or **glass box** models (Ekama et al., 1997). The appropriate model type for a certain problem setting depends on the objective and on the available information sources. Some models serve prediction and/or control purposes and others are developed for understanding of the underlying mechanisms.

The rather simple black box models consist of mathematical relations, statistically fitted to experimental data. Because of their empirical nature, application of the latter models

2.5. Modelling of SSTs

is restricted within the boundaries of calibration. To date, these lumped parameter models are still applied to define the settling behaviour of activated sludge in the tank, such as the simple equations that represent the settling velocity (Section 2.5.2). It is clear that these models only contribute to insights in the very basic mechanisms of the studied process.

In contrast, glass box models are able to predict almost any fluid flow and heat transfer process as a solution of a set of partial differential equations that describes the fundamental physical processes (continuity, momentum, energy, transport of solids and biological reactions) (Zikanov, 2010). As a consequence glass box models are often very complex and computationally demanding. An alternative category of models are the intermediate **grey box** models that combine physical laws with simplified empirical relations to approximate the true behaviour.

In SST modelling several grey box models exist where the amount of physical realism (often linked to the spatial resolution) is defined by the application and objective of the model. The closest approximation to glass box models are 2-D and 3-D CFD models (Section 2.5.4). These models are typically used to build process knowledge and improve the design of secondary settling tanks. Due to the high computational burden, the application of 2-D/3-D models for operation and control is not feasible. Therefore, 1-D models are often used where the flow field and concentration profile are only calculated in the vertical direction of the SST (Section 2.5.3). They may not be able to capture the detailed hydrodynamics created by the internal configurations in the tank but they can easily be combined with models for other unit processes in an integrated WWTP model.

2.5.2 Mathematical description of the settling behaviour

The modelling of SSTs requires a proper mathematical description of the settling behaviour of AS. The development of a general method to characterise the complete settling process is quite challenging due to the co-occurrence of distinct settling regimes. This section provides an overview of research advances to describe the settling behaviour in the different regimes.

Hindered settling velocity

During the hindered settling regime, particles settle as a zone. As discussed in Section 2.3.2 this phase is characterised by a distinct linear descent in a batch settling curve. Hence, the velocity at which the interface is moving downwards during this phase is equal to the hindered settling velocity (v_{hs} or v_{zs}) and can be calculated as the slope of the linear part of the batch settling curve. From Figure 2.14 it can be seen that

these slopes vary for different initial concentrations of the sludge. The hindered settling velocity is thus a function of the sludge concentration with higher concentrations resulting in lower settling velocities.

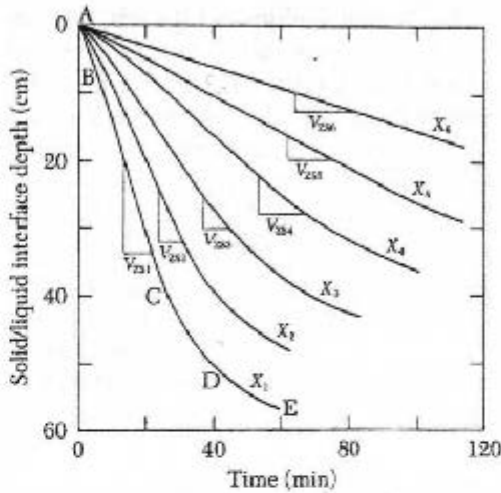


Figure 2.14: Solids-liquid interface as function of time. The slope of the linear part gives the settling velocity in hindered settling conditions, which decreases as concentration (X) increases (Ekama et al., 1997).

Several empirical expressions which describe this inverse relation between the settling velocity (v_{hs}) and the initial solids concentration (X) can be found in literature (Vesilind, 1968; Dick and Young, 1972; Vaerenbergh, 1980; Takács et al., 1991; Cho et al., 1993; Watts et al., 1996; Lakehal and Krebs, 1999). The most commonly used are the functions by Vesilind (1968) and Takács et al. (1991) which are discussed below.

Vesilind (1968) suggested an exponential decreasing function to describe the relation between sludge concentration and v_{hs} (Eq. 2.1). In this equation V_0 represents the maximum settling velocity, X the solids concentration and r_v a model parameter.

$$v_{hs} = V_0 e^{(-r_v X)} \quad (2.1)$$

According to the Vesilind function, the settling velocity continues to increase when the sludge concentration approaches zero ($v_{hs} = V_0$ if $X = 0$). In practice, however, a decrease in settling velocity at low sludge concentrations (<1 g/l) is observed. The hindered settling velocity function of Vesilind (1968) predicts unrealistically high sett-

2.5. Modelling of SSTs

ling velocities in this low concentration range. To capture the decreasing trend at low sludge concentrations Takács et al. (1991) proposed a modified form of the Vesilind function by introducing an additional exponential term and limiting the maximum settling velocity to an arbitrary value $V_{0,\max}$ (Eq.2.2):

$$v_{hs} = \max \left(0, \min \left(V_{0,\max}, V_0 \left(e^{(-r_H \cdot (X - X_{\min}))} - e^{(-r_P \cdot (X - X_{\min}))} \right) \right) \right) \quad (2.2)$$

with X_{\min} the concentration of non-settleable particles (set as a fraction f_{ns}) of the incoming solids concentration), r_H the settling characteristic of the hindered settling zone and r_P the settling characteristic at low solids concentrations. Figure 2.15 illustrates the difference between the functions of Vesilind (1968) and Takács et al. (1991).

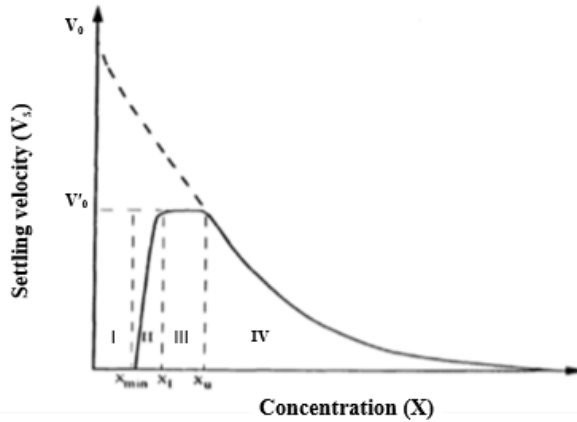


Figure 2.15: Settling velocity model for different sludge concentrations (Takács et al., 1991). Dashed line describes the settling velocity model of Vesilind (1968), solid line describes the function of Takács et al. (1991).

Note that the physical properties of activated sludge flocs and solids-liquid interaction have not been considered in the empirical models of Vesilind and Takács. In general, these functions are very empirical in nature and assume that the settling velocity (v_{hs}) is only a function of the sludge concentration (X) (Vanderhasselt and Vanrolleghem, 2000). In reality settling of flocs depends on a number of factors including particle density, porosity, shape and size and hydrodynamic resistance (drag force) (Patry and Takács, 1992).

Kinnear (2002) attempted to include more fundamental properties such as the densities of dry solids and flocs, viscosity, permeability and specific surface area of primary

particles to represent the settling velocity. However, the calibration of this function requires extensive measurements and simulation results of batch settling curves did not show a significant improvement compared to the empirical function of Vesilind.

Compressive settling velocity

At high solids concentrations previously settled solids will thicken under the weight of overlying particles and undergo compressive settling. Accounting for compressive settling in mathematical descriptions of the settling behaviour has a large influence on the estimation of the SBH and underflow concentration. These latter two parameters are important for control and operation of the clarifier, especially during wet weather conditions.

Compression starts at a certain critical concentration X_{crit} defined as the concentration where particles are in actual physical contact instead of merely in each other's influence sphere. The particles form a compressive network which slows down the settling velocity. The dynamics of the settling velocity in the compression region will thus differ from the dynamics in the hindered settling region (Eq. 2.3). Several mathematical expressions for the settling velocity in the compression region (v_{comp}) have been developed ranging from basic extensions of the hindered settling velocity (Zhang et al., 2006; Stricker et al., 2007) to more fundamentally supported equations (Cacossa and Vaccari, 1994; Kinnear, 2002; De Clercq et al., 2008).

$$v_s = \begin{cases} v_{\text{hs}}(X), & \text{for } 0 \leq X \leq X_{\text{crit}} \\ v_{\text{comp}}(X) & \text{for } X > X_{\text{crit}} \end{cases} \quad (2.3)$$

Zhang et al. (2006) described both hindered and compression settling by the Vesilind function but calibrated a different parameter set (for V_0 and r_V) for each settling regime. Stricker et al. (2007) accounted for compression through the inclusion of additional terms in the settling velocity function of Takács et al. (1991). However, from the momentum balance of the solid component, it is known that compression stress necessarily involves the gradient of the concentration. Therefore, the empirical extensions presented by Zhang et al. (2006) and Stricker et al. (2007) are not able to capture the compression dynamics.

Cacossa and Vaccari (1994) developed a new settling velocity function for v_{comp} where the hindered settling velocity is multiplied by $\left(1 - \frac{\partial X}{\partial z} \frac{1}{K(X)}\right)$, with $K(X)$ an exponential decaying compressibility function and z the height of the settling tank. The hindered settling velocity was calculated by an empirical equation proposed by Tracy (1973) for concentrations higher than the critical concentration. For concentrations

2.5. Modelling of SSTs

lower than a critical concentration they used a linear extension of the empirical equation of Tracy (1973). Kinnear (2002) developed a settling function for v_{comp} based on the continuity and momentum equations for liquid and solids (i.e. water and sludge). However, neither the model of Cacossa and Vaccari (1994) nor the model of Kinnear (2002) gave satisfactory results for the compression phase when applied to a batch settling curve.

Bürger (2000) developed a phenomenological theory of the sedimentation-consolidation process of flocculated suspensions from the mass and linear momentum balances of the solid and liquid components. Based on this work, the total settling velocity can be expressed as

$$v_s = \begin{cases} v_{\text{hs}}(X), & \text{for } 0 \leq X \leq X_{\text{crit}} \\ v_{\text{hs}}(X) \left(1 - \frac{\rho_s \sigma'_e(X)}{X g \Delta \rho} \frac{\partial X}{\partial z} \right), & \text{for } X > X_{\text{crit}} \end{cases} \quad (2.4)$$

with ρ_s the density of the solids, X the concentration of the solids, g the gravitational acceleration and $\Delta \rho$ the density difference between the solids and the liquid. The settling velocity in the compression region consists of the hindered settling velocity v_{hs} and a compressive term that slows down the settling velocity above a certain critical concentration X_{crit} . During the compression phase, the particles form a network that can carry a certain stress, the **effective solids stress** $\sigma_e(X)$. Compression depends on the concentration gradient, the densities of the solid and liquid component and on the derivative of the effective solid stress $\sigma'_e(X)$. It is assumed that $\sigma_e(X)$ is an increasing function of the solids concentration above X_{crit} and that it is zero below it (Bürger et al., 2011; De Clercq et al., 2008).

De Clercq et al. (2008) derived an equation for σ_e from the detailed spatio-temporal concentration measurements performed by De Clercq et al. (2005) described in Section 2.3.2. They found a logarithmic relation between the effective solids stress and the difference between the solids concentration and the critical concentration (Eq. 2.5). In this equation α and β are two parameters that need to be calibrated.

$$\sigma_e(X) = \alpha \ln \left(\frac{X - X_{\text{crit}} + \beta}{\beta} \right) \quad (2.5)$$

Discrete settling velocity

At the top region of a SST characterised by very low concentrations, particles settle typically according to the discrete settling regime. This settling regime is governed both by individual particle properties (e.g. particle size, density and porosity) and solids-water interactions (Vanderhasselt and Vanrolleghem, 2000; Kinnear, 2002). The

three dominant forces acting on the particle are: gravity (F_g), buoyancy (F_b) and drag (F_f). In theory, the terminal settling velocity of a discrete spherical particle falling in a quiescent fluid is given by Stokes' law (Tchobanoglous et al., 2003).

$$v_s = \frac{g}{18} \cdot \frac{(\rho_p - \rho_f)}{\mu} \cdot d^2 \quad (2.6)$$

In this equation ρ_p and ρ_f are the mass densities of respectively the sludge floc and the fluid, d is the particle diameter and μ the dynamic viscosity of the liquid. Sludge particles are however not perfectly spherical, the floc structure is rather irregular and particle porosity also plays an important role. Furthermore, the mass density of the sludge particles is difficult to determine (Kinnear, 2002). In other words, AS flocs cannot be considered as dense particles and therefore the use of Stokes' law to describe the settling velocity is questioned (Jorand et al., 1995).

Practical determination of sludge settling velocities at very low concentration is difficult which makes the development of a reliable method to estimate discrete settling velocities complicated. Therefore, the discrete settling behaviour in AS settling is often described by directly modifying classical hindered settling velocity functions (Takács et al., 1991; Dupont and Dahl, 1995). To date, the Takács settling function is widely accepted and frequently used in design and operation methods, e.g. the solid flux theory (Ekama et al., 1997). Despite the fact that this function predicts more realistic settling velocities at low X than the Vesilind function, it is unfortunately not accurate enough for reliable ESS predictions since it does not capture the true (distributed) settling behaviour. In reality, at lower concentrations no clear relation exists between the settling velocity of particles and the sludge concentrations. Figure 2.16 illustrates that different discrete settling velocities can be measured for different sludge samples and different floc sizes.

An alternative approach in order to improve predictions of the ESS concentration is to take into account the observed distributions in settling velocities (Dupont and Henze, 1992; Lyn et al., 1992; Otterpohl and Freund, 1992; Mazzolani et al., 1998). In this approach, flocs are assigned to different size classes and each class is characterised by its own discrete settling velocity. Since particles of many different sizes occur in the low concentration regions, a limited number of particle size classes is defined together with a representative settling velocity.

Otterpohl and Freund (1992) made a distinction between microflocs and macroflocs. For the macroflocs they multiplied a corrective function with the settling velocity of Vesilind. For the microflocs the settling velocity was set to 0.01 m/h. Measured effluent concentrations were compared with model results over 2 days. The agreement was only good for the first 0.5 days.

2.5. Modelling of SSTs

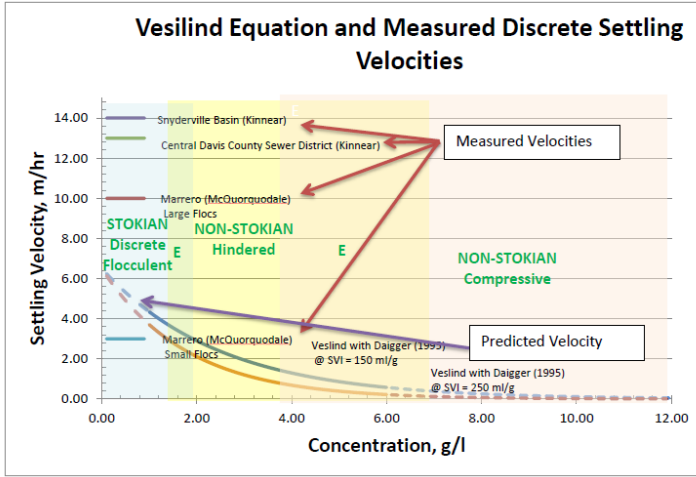


Figure 2.16: Predicted velocities by the Vesilind equation and measured discrete settling velocities to illustrate the sharp discontinuity exhibited in settling velocities when settling type changes, after Kinnear (2002) (Mancell-Egala et al., 2012).

Mazzolani et al. (1998) proposed the following settling model:

$$v_s = f \cdot v_{s,i} + (1 - f) \cdot V_0 \cdot e^{-r_V \cdot (X)} \quad \text{with } f = \begin{cases} 0 & \text{if } X > X_{\max}, \\ 1 & \text{if } X < X_{\min}. \end{cases} \quad (2.7)$$

Here, $v_{s,i}$ is the discrete settling velocity of particle class i , V_0 and r_V are the settling parameters of the Vesilind equation. The partition function f depends on the SS concentration controlled by the parameters X_{\max} and X_{\min} . These represent, respectively, the value above which hindered settling conditions are dominant and the maximum value where discrete settling conditions are present. However, a proper method to determine these latter threshold values is not given by Mazzolani et al. (1998). It is assumed that f is a linear function between the limits X_{\max} and X_{\min} .

During the settling process, the number of particles in a certain class may change due to flocculation and break-up processes. Therefore, accurate description of discrete settling requires information about the dynamics of the particle size distribution. In recent years, numerous studies have aimed to develop a proper mathematical model that can describe the discrete settling velocity more accurately (Griborio, 2004; McCorquodale et al., 2004; Hribersek et al., 2011; Ramalingam et al., 2012). These studies use a combination of hydrodynamic and flocculation models to account for changes in particle size distributions. These models will be discussed in Sections 2.5.4 and 2.5.5.

2.5.3 1-D modelling

Typically, 1-D models are applied for operation and control of SSTs as they can easily be combined with models for other unit processes in an integrated WWTP model due to their relatively low computational demand (Section 2.5.1).

These models are based on the following assumptions:

- the incoming solids of a layer are distributed instantly and uniformly over the cross-sectional area of the layer and
- only vertical movement of solids is considered.

Flux theory

The 1-D modelling of SSTs is based on the flux theory of Kynch (1952). This theory states that the transport of particles is the result of a gravitational settling flux due to the settling of particles and a bulk flux due to bulk movement or convective flow. In Eq. 2.8 the total flux is calculated as the sum of the two fluxes. The first term represents the gravitational settling flux which is uniquely determined by the local solids concentration X and the second term the flux due to bulk movement, where v_c is the vertical bulk velocity.

$$F(X, z, t) = \underbrace{v_s(X) X}_{\text{Settling flux } F_s} + \underbrace{v_c(z, t) X}_{\text{Convective flux } F_c} \quad (2.8)$$

When z is below the inlet, the vertical bulk velocity v_c is downwards and is calculated by $v_{c,u} = \frac{Q_R + Q_W}{A}$, with Q_R the volumetric recycle flow rate, Q_W the volumetric waste flow rate and A the cross-sectional area of the settler. When z is above the inlet, the vertical bulk velocity is upwards and is calculated by $v_{c,o} = \frac{Q_E}{A}$, with Q_E the volumetric effluent flow rate.

Based on the flux theory, the mass balance in the SST can be described by the Partial Differential Equation (PDE) given in Eq. 2.9. In this equation t represents time and z the depth of the SST. The last term of Eq. 2.9 is a source term with Q_f the volumetric feed flow rate, X_f the feed concentration and $\delta(z)$ the Dirac delta function.

$$\frac{\partial X}{\partial t} = -\frac{\partial}{\partial z} F(X, z, t) + \frac{Q_f(t) X_f(t)}{A} \delta(z) \quad (2.9)$$

Layer approach

In WWTP modelling a model for the SST is coupled to models for other unit processes such as the biological reactor. These models typically consist of a set of Ordinary Differential Equations (ODEs). To facilitate the coupling of these models and the numerical solution in typical WWTP modelling software, the PDE describing the SST process is discretised into a set of ODEs which can be handled by standard ODE solvers. To achieve this, the settling tank is divided into horizontal layers with a uniform concentration within each layer. Eq. 2.9 is thus discretised and a mass balance can be performed around each horizontal layer. This approach was first applied by Bryant (1972) and Stenstrom (1976) to model the thickening behaviour in a SST and further extended to include clarification modelling by Vitasovic (1986).

The numerical approximation of the flux $F(X, z, t)$ between two adjacent layers is quite challenging since the flux is a discontinuous function of z (Bürger et al., 2012). Simulating secondary clarifiers thus requires a numerical scheme that deals with this discontinuous function.

Based on the flux theory of Kynch (1952) in combination with the layer approach several 1-D models have been developed in literature. These models differ in their discretisation level, the numerical scheme used to approximate the settling flux between adjacent layers and the processes considered (hindered settling, compression settling, discrete settling, mixing, density currents,...).

Takács settler model

In the model of Takács et al. (1991) the settler is divided in 10 layers of equal thickness. There are five groups of layers present in the model: the top layer, the layers above the feed point, the feed layer, the layers below the feed point and the bottom layer. Each group has its own inputs and outputs which are summarized in Table 2.2.

Table 2.1: Inputs and outputs of the layered settler model (Takács et al., 1991)

Layer	Input			Output	
	Feed	Settling	Bulk liquid flux	Settling	Bulk liquid flux
Top layer	-	-	Up	+	Up
Layers above feed	-	+	Up	+	Up
Feed layer	+	+	-	+	Up-down
Layers below feed	-	+	Down	+	Down
Bottom layer	-	+	Down	-	Down

Note: + = phenomenon considered; - = phenomenon not considered

The model of Takács uses a numerical approximation of the flux $F(X, z, t)$ developed by Stenstrom (1976) and Vitasovic (1986). Stenstrom (1976) proposed a constrained flux which limits the downward flux of solids to that which can be transmitted by the

layer below (Eq. 2.10). Vitasovic (1986) extended this flux function in the clarification zone with a threshold concentration X_T below which the constraint becomes inactive (Eq. 2.11). This extension was necessary to avoid unphysical solution oscillations under certain conditions. The settling velocity v_s in the model of Takács is calculated by the hindered settling function of Takács et al. (1991) provided in Eq. 2.2.

$$F_{s,j} = \min(v_{s,j} X_j, \text{ or } v_{s,j+1} X_{j+1}) \quad (2.10)$$

$$F_{s,j} = \begin{cases} \min(v_{s,j} X_j, \text{ or } v_{s,j+1} X_{j+1}), & \text{if } X_{j+1} > X_T \\ v_{s,j} X_j, & \text{if } X_{j+1} \leq X_T \end{cases} \quad (2.11)$$

In Figure 2.17 the mass balance of each group of layers is summarized (with the flux F_s represented by J_s).

Watts et al. (1996) found that the optimal number of layers in the model of Takács et al. (1991) was 10. When a higher number of layers was used for the discretisation, the model predictions became worse. A coarse 10-layer discretisation introduces significant numerical diffusion between the layers which allows an approximation of the compression and dispersion effects. However, through this approach, the number of layers, N , becomes an important model parameter that changes the model's behaviour instead of only influencing the numerical approximation. This is contradictory to the fact that a numerical solution of a model should converge to the physically correct solution when the discretisation becomes finer.

Advances in 1-D SST modelling

The model of Takács et al. (1991) is used in many simulation programs and performs reasonably well under normal dry weather conditions. However, under situations that diverge from normal operating conditions (e.g. peak flows due to rain events) its predictions lose realism. To obtain proper predictions of underflow and effluent concentrations and SBH under peak flow conditions a more sophisticated model is required.

Several shortcomings that cause the lack of predictive power of the model by Takács et al. (1991) under wet weather conditions have been reported (Jeppsson and Diehl, 1996; Plósz et al., 2011; Bürger et al., 2011; Li and Stenstrom, 2014c,a). First, the numerical flux between two adjacent layers has to be chosen in accordance with the theory for the governing PDE. Jeppsson and Diehl (1996) found that the numerical solutions of Takács' model do not converge to the exact solution of the PDE when the number of layers is increased. One reason is that the numerical flux function of Vitasovic (1986) in the Takács model contains an empirical constant X_T that is not present in the governing PDE. This is in conflict with one of the fundamental principles

2.5. Modelling of SSTs

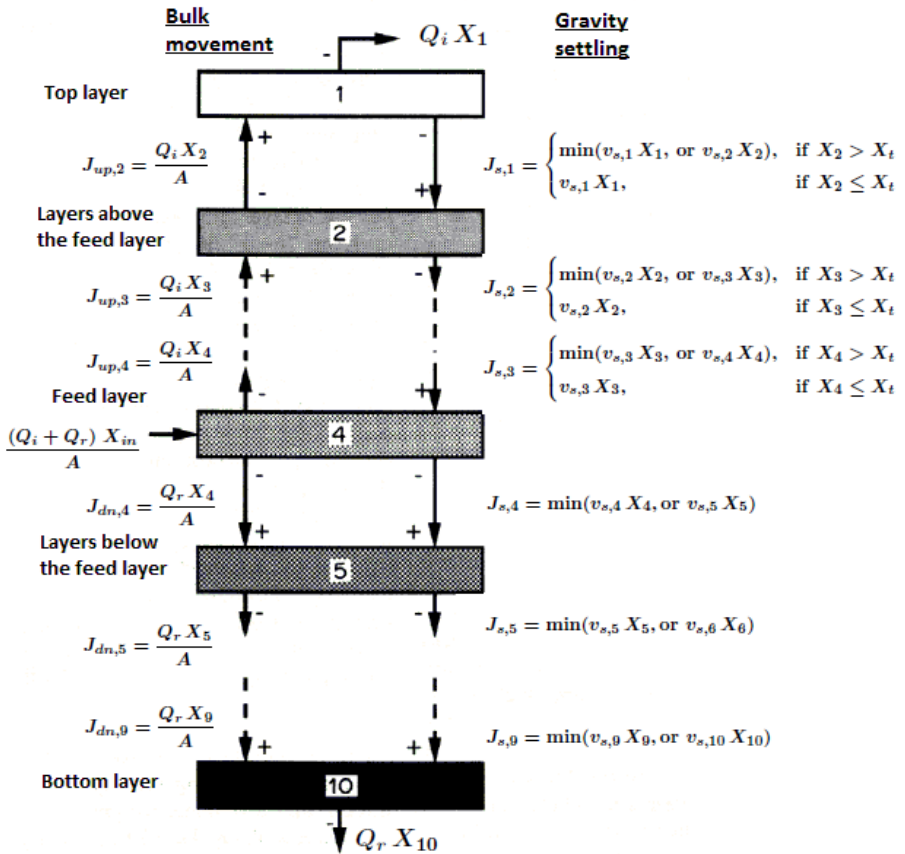


Figure 2.17: Solids balance across each layer (Takács et al., 1991).
The flux F is represented as J in this figure.

for any consistent modelling methodology (Bürger et al., 2011) which states that each model parameter should be present in the governing equations and not be introduced in the numerical method itself.

Bürger et al. (2011) demonstrated that the way the calculation of the flux is incorporated in the model of Takács et al. (1991) gives an unphysical solution under certain conditions. When for example one wants to simulate the filling of a SST to investigate the development of the sludge blanket, the sludge that is introduced in the system will be trapped in the feed layer (Figure 2.18). Indeed, below the feed layer (Eq. 2.10) the downward settling flux is calculated by the minimum flux function of Stenstrom (1976). Hence, when a more concentrated layer is located on top of a layer with a concentration of zero, no sedimentation will occur.

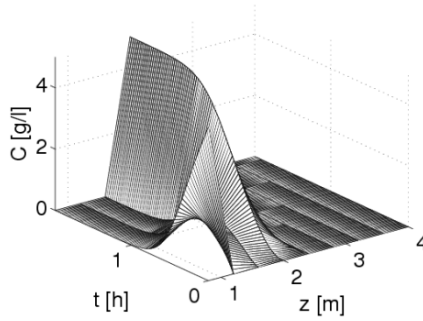


Figure 2.18: Numerical solutions of a batch settling test with sludge on top of clear water with the model of (Takács et al., 1991).

Jeppsson and Diehl (1996) proposed the Godunov scheme (Eq. 2.12) as an alternative for the flux function of Takács. The decisive difference of this method is that it does not make use of an empirical concentration and that it considers all intermediate concentrations between the concentrations of layer j and layer $j + 1$ in the calculation of the flux. The Godunov approach also ensures that the solution of the model converges to the physically correct solution when the number of layers is increased. This scheme has since been used in a number of studies (Diehl and Jeppsson, 1998; Plósz et al., 2007; Bürger et al., 2013) and is mathematically sound (Bürger et al., 2012). Another suitable numerical flux has recently been introduced by Li and Stenstrom (2014b).

$$F_{s,j} = \begin{cases} \min_{X_j \leq X \leq X_{j+1}} v_s(X) X - v_c X, & \text{if } X_j \leq X_{j+1} \\ \max_{X_{j+1} \leq X \leq X_j} v_s(X) X - v_c X, & \text{if } X_j > X_{j+1} \end{cases} \quad (2.12)$$

A second important shortcoming of the model by Takács et al. (1991) is that it only accounts for convective flow and gravity settling. Other phenomena such as compression settling, turbulent diffusivity and dispersion are not included. Takács' model compensates for these missing effects by applying a coarse discretisation (10 layers) which introduces significant numerical dispersion. Although this artificial smoothing produces a more realistic profile, it is not able to describe the true dynamics of a SST causing modellers to make unrealistic calibrations of the settling parameters or even to change the number of layers not realizing that this impacts the numerical dispersion (Plósz et al., 2011). Attempts have been made to handle this shortcoming of Takács' model by accounting for compression through additional terms in the settling flux function (Stricker et al., 2007) or by accounting for inlet dispersion and density currents through the addition of short-circuiting flows (Dupont and Dahl, 1995). Through

2.5. Modelling of SSTs

these approaches the governing PDE still has only first-order derivatives. However, from Fick's law ($J = -D \frac{\partial X}{\partial z}$ with J the diffusion flux and D a diffusion coefficient) (Smith, 2004) and the momentum balance of the solids component (Bürger, 2000), it is known that dispersion and compression necessarily involve also the gradient of the concentration leading to a second-order PDE.

To address this problem 1-D models have been developed which try to explicitly account for dispersion and compression effects by incorporating either a constant or a concentration or overflow-dependent second order term in their PDE ($D \frac{\partial^2 X}{\partial z^2}$, where D is a dispersion coefficient) (Hamilton et al., 1992; Watts et al., 1996; Plósz et al., 2007). By adding this term, the PDE becomes a parabolic differential equation (instead of a hyperbolic differential equation) which will automatically result in a more continuous concentration profile (Zikanov, 2010). For instance, Plósz et al. (2007) showed that by introducing a second-order term dispersion can be modelled as a separate phenomenon and not by numerical dispersion introduced through the discretisation.

The drawback of this approach is that all the previously unmodelled phenomena are lumped into one single term. This is still too coarse to capture the true settling dynamics. In fact, this approach lures inadvertent practitioners into compensating the uncaptured dynamics by either unrealistic calibration of the settling parameters or by introducing an extra parameter in the numerical solution which is not present in the governing PDE (for example the reduction factor η_c in the model by Plósz et al. (2007)). As mentioned before, the latter sharply contrasts with one of the fundamental principles for any consistent modelling methodology (Bürger et al., 2011).

Bürger-Diehl settler model

Recently, a new 1-D model has been presented (Bürger et al., 2011, 2012) which differs from the commonly used model by Takács et al. (1991) in two ways. First, it ensures the solution of the governing PDE by reliable numerical methods. Secondly, it includes extra functionalities in the model structure to obtain a more detailed description of the sludge settling behaviour. This new simulation model, called the Bürger-Diehl model, allows accounting for sediment compressibility and inlet mixing phenomena by extending the PDE from Eq. 2.9 with a compression function (d_{comp}) and a dispersion function (d_{disp}) (Eq. 2.13). These functions can be switched on or off by the user depending on the model study requirements. The decisive difference between this model and many of the models described in the previous section is that the Bürger-Diehl model includes several phenomena in a modular way instead of trying to lump different phenomena in a single parameter or function.

$$\frac{\partial X}{\partial t} = -\frac{\partial}{\partial z} (F(X, z, t)) + \frac{\partial}{\partial z} \left((d_{\text{comp}}(X) + d_{\text{disp}}(z, Q_f(t))) \frac{\partial X}{\partial z} \right) + \frac{Q_f(t)X_f(t)}{A} \delta(z) \quad (2.13)$$

To numerically solve this PDE, it is discretised by dividing the tank into a user-defined number of layers (N). The flux $F(X, z, t)$ is replaced by numerical fluxes containing the Godunov flux. Moreover, a specific implementation of the compression term is needed to ensure that as the number of layers increases, the numerical solution converges to the physically correct solution of the PDE. All implementation details can be found in Bürger et al. (2013). In the Bürger-Diehl model, the number of layers N can thus be set by the user depending on the desired accuracy (i.e. the goal of the modelling exercise) and on the computational time and resources available.

In order to calculate the correct effluent and underflow concentrations, two extra layers are added at the top and bottom of the tank, respectively. There are thus $N + 4$ layers, as indicated in Figure 2.19. It is important to emphasize that the effluent and underflow concentrations are generally not the same as the concentrations in the top and bottom layers within the settler (Jeppsson and Diehl, 1996). This is not taken into account in traditional layer models. The extra layers in the underflow region can be interpreted as the start of the outlet pipe. The underflow concentration X_u can be defined as the concentration in any of these two layers. An overview of the different processes considered over each layer boundary is provided in Table 2.2.

Table 2.2: Processes considered over each layer boundary in the Bürger-Diehl SST model.

	Settling	Compression	Dispersion	Bulk liquid flux
z_{-2}				
\vdots	/	/	/	Up
z_{-1}				
z_0	x	x	/	Up
z_1				
\vdots	x	x	x	Up
\vdots				
z_{j_f-1}				
z_{j_f}				
\vdots	x	x	x	Down
\vdots				
z_{N-1}				
z_N	x	x	/	Down
z_{N+1}				
\vdots	/	/	/	Down
\vdots				
z_{N+2}				

Note: x = phenomenon considered; / = phenomenon not considered

2.5. Modelling of SSTs

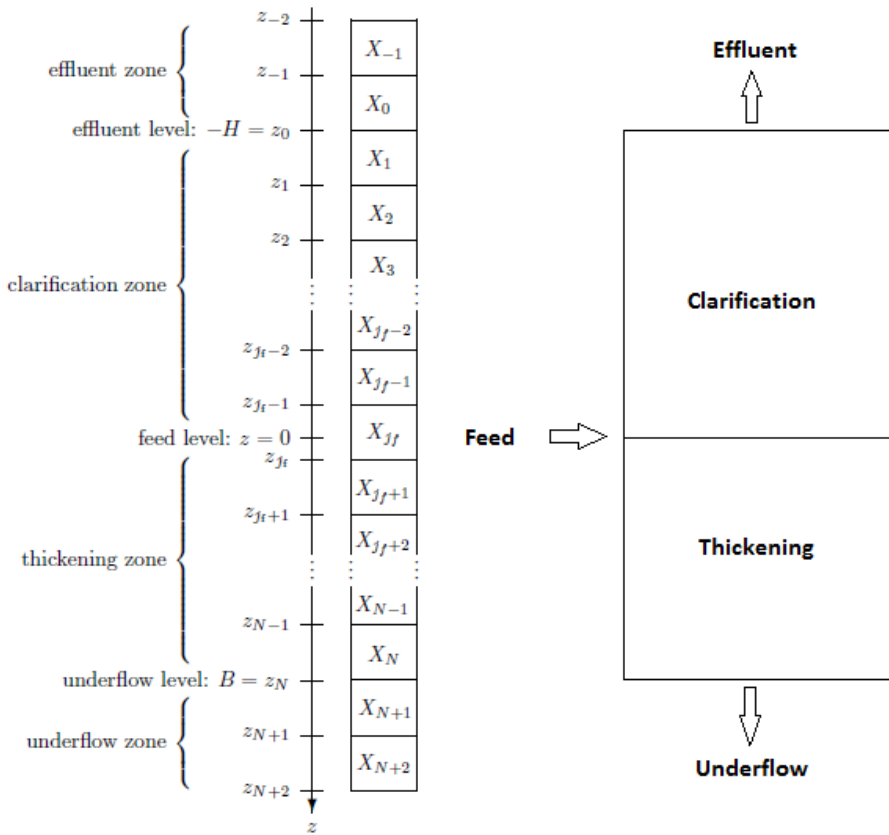


Figure 2.19: Schematic overview of the discretisation of the settler (Bürger et al., 2011).

An important feature of the Bürger-Diehl model is the optional inclusion of compressive settling and flow-rate-dependent inlet mixing phenomena. This is achieved by specific terms for compression and dispersion in the 1-D PDE. The Bürger-Diehl model thus requires three constitutive functions to describe the different phenomena occurring in a SST (hindered settling, compression settling and inlet dispersion). For the hindered settling velocity any available expression from literature (see Section 2.5.2) can be used. The compression function is based on the phenomenological theory presented by Bürger (2000) who derived that compression is a function of the densities of the solid and liquid phases, the constant of gravity and an expression for the solid stress function (σ_e). Hence, the compression function (Eq. 2.14) requires an appropriate function for the solids stress (for example the function of De Clercq et al. (2008) in Eq. 2.5)

$$d_{\text{comp}}(X) = \begin{cases} 0, & \text{for } 0 \leq X \leq X_{\text{crit}} \\ \frac{\rho_s}{g \Delta \rho} v_{\text{hs}}(X) \sigma'_e(X), & \text{for } X > X_{\text{crit}} \end{cases} \quad (2.14)$$

The dispersion function allows to simulate flow-rate-dependent inlet mixing phenomena. Turbulent currents in the settler cause a mixing of lower and higher concentrations of solids. This phenomenon is especially important around the inlet. Therefore, the dispersion function d_{disp} is often set as the product of the fluid velocity and a continuous function of the depth. The continuous function has its maximum at the feed level and is zero some distance away from the inlet (Bürger et al., 2013). This allows modelling a region of higher turbulence around the feed inlet at increased hydraulic loading.

The Bürger-Diehl model is very flexible since the compression and dispersion terms can be switched on or off to meet the user's needs without affecting the solvability of the model. Hence, in its simplest form (no compression and no inlet dispersion), the Bürger-Diehl model reduces to the one by Diehl and Jeppsson (1998) and is a reliable alternative for current models. Moreover, the constitutive functions for hindered settling, compression settling and inlet dispersion in the Bürger-Diehl model can easily be updated or replaced whenever further research provides more insight into these phenomena.

2.5.4 CFD modelling

In recent years, CFD models are gaining popularity as tools to improve insights and/or optimisation of the settling processes in a SST. Their success results from the ability to predict the performance of a settling tank by modelling the internal flow pattern and transport phenomena of solids and solutes in 2-D or 3-D (Wicklein and Samstag, 2009). These models are also applied to perform dynamic simulations of wet weather events and development of wet weather strategies by combining them with whole plant simulators (Griborio et al., 2010). The major disadvantage is their need for high computational capacity.

Governing equations

A CFD model is based on the fundamental conservation laws for mass (continuity equation), energy (first law of thermodynamics) and momentum (Newton's second law) (Zikanov, 2010).

- The **continuity** equation

2.5. Modelling of SSTs

$$\frac{\partial \rho}{\partial t} + \frac{\partial \rho u}{\partial x} + \frac{\partial \rho v}{\partial y} + \frac{\partial \rho w}{\partial z} = 0 \quad (2.15)$$

with u , v and w the components of the velocity vector in resp. the x , y and z directions and ρ the fluid density.

For an incompressible flow, $\frac{\partial \rho}{\partial t} = 0$, the equation is reduced to:

$$\frac{\partial u}{\partial x} + \frac{\partial v}{\partial y} + \frac{\partial w}{\partial z} = 0 \quad (2.16)$$

• The momentum equations

Since the momentum equation is derived from Newton's second law (i.e. mass \times acceleration = force), the momentum equations account for all the body and surface forces applied on a considered fluid parcel. Body forces are external forces acting directly on the fluid parcel such as gravity and are proportional to its mass whereas surface forces result from stresses acting on the sides of the fluid element. It is common practice to highlight the contributions due to the surface forces as separate terms in the momentum equation and to include the effects of body forces as source terms S_M .

The stresses working on a fluid surface are the pressure p and viscous stresses. In **Newtonian fluids** the viscous stresses can be calculated from the rate of deformation with a proportionality factor μ , the (dynamic) viscosity. This yields the **Navier-Stokes equations** (Zikanov, 2010). Eq. 2.17 provides the Navier-Stokes equation in the x -direction for an incompressible fluid. In Eqn. 2.18 and 2.19 the equation for the y and z directions are written in a more concise form.

$$\underbrace{\frac{\partial u}{\partial t} + \frac{\partial u^2}{\partial x} + \frac{\partial(uv)}{\partial y} + \frac{\partial(uw)}{\partial z}}_{\text{Rate of increase of } x\text{-momentum}} = \underbrace{-\frac{1}{\rho} \frac{\partial p}{\partial x}}_{\text{Pressure force}} + \underbrace{\frac{\partial}{\partial x} \left(\nu \frac{\partial u}{\partial x} \right) + \frac{\partial}{\partial y} \left(\nu \frac{\partial u}{\partial y} \right) + \frac{\partial}{\partial z} \left(\nu \frac{\partial u}{\partial z} \right)}_{\text{Viscous forces}} + \underbrace{S_{Mx}}_{\text{Body forces}} \quad (2.17)$$

$$\frac{\partial v}{\partial t} + \text{div}(\mathbf{v}\mathbf{u}) = -\frac{1}{\rho} \frac{\partial p}{\partial y} + \text{div}(\nu \text{grad } v) + S_{My} \quad (2.18)$$

$$\frac{\partial w}{\partial t} + \text{div}(\mathbf{w}\mathbf{u}) = -\frac{1}{\rho} \frac{\partial p}{\partial z} + \text{div}(\nu \text{grad } w) + S_{Mz} \quad (2.19)$$

with $\nu = \mu/\rho$ the kinematic viscosity.

- the **energy equation**

Temperature variations are not considered in this PhD and hence the energy equation is omitted. In other words, only the advection-diffusion processes are taken into account.

The resulting non-linear PDEs often do not have an analytical solution. Hence, a numerical solution or discretisation technique is required to transform the continuous equations in discrete counterparts. This technique requires discretisation in both space and time. In practice, this means that the SST geometry has to be divided into a finite number of grid cells. The governing equations are written for each node of the computational grid. As a result, the flow field over the whole domain is quantified by solving a set of remaining ODEs at each node with proper boundary conditions. The number of grid cells should be large enough to represent the flow pattern in the SST. However, a larger number of cells and hence equations demands longer computational times.

The continuity and Navier-Stokes equations can be combined with additional equations to capture other phenomena such as turbulence, solids settling, flocculation of particles and biological reactions (De Clercq, 2003).

Turbulence modelling

Turbulent flow can be defined as a chaotic and random state of motion in which the velocity and pressure change continuously with time within substantial regions of flow. A turbulent flow develops above a certain critical Reynolds number (approx. 5000). The Reynolds number Re can be calculated based on the characteristic velocity U and length scale L and the kinematic viscosity (Eq. 2.20).

$$Re = \frac{UL}{\nu} \quad (2.20)$$

Despite the low mean flow velocities in a settling tank, the Reynolds number is high enough to cause turbulent flow. The reasons for this are the rather large dimensions of the settling tank and the low viscosity of the liquid mixture. In particular, mixing of the incoming mixed liquor with the flow in the tank causes turbulent flow.

Furthermore, visualisations of turbulent flows reveal rotational flow structures, so-called turbulent eddies, with a wide range of length scales. Parcels of fluid which are initially separated by a long distance can be brought close together by the eddying motions in turbulent flows. As a consequence, heat, mass and momentum are very effectively exchanged. Turbulent flow can be directly modelled by the Navier-Stokes equations. However, this would require a very fine spatial grid since it would have to

2.5. Modelling of SSTs

capture the scale of the smallest turbulent eddies (Kolmogorov length scales) with time steps sufficiently small to resolve the period of the fastest fluctuations. Often in this approach the computational time becomes extremely high.

As an alternative, the Reynolds-Averaged Navier-Stokes (RANS) equations can be used to describe unsteady turbulent flow (Lakehal and Krebs, 1999; De Clercq, 2003; Gribo-rio, 2004). These equations are obtained by decomposing the velocity in a steady mean value U with a fluctuating component $u'(t)$ superimposed on it: $u(t) = U + u'(t)$. This is called the Reynolds decomposition. The Navier-Stokes equations are then averaged out over the turbulent fluctuations in time resulting in laws of motion for mean, time-averaged flow quantities.

However, the RANS equations should somehow account for the influence of the turbulent fluctuations on the mean velocity. Turbulent eddies create recirculating fluid motions that carry momentum and energy into and out of the control volume (Figure 2.20). This momentum exchange causes the faster moving fluid layers to be decelerated and the slower moving layers to be accelerated. Consequently, the fluid layers experience additional turbulent shear stresses, which are known as Reynolds stresses. Hence, by including Reynolds stresses as an additional force in the momentum equations, the RANS account for the influence of turbulence on the mean flow velocity.

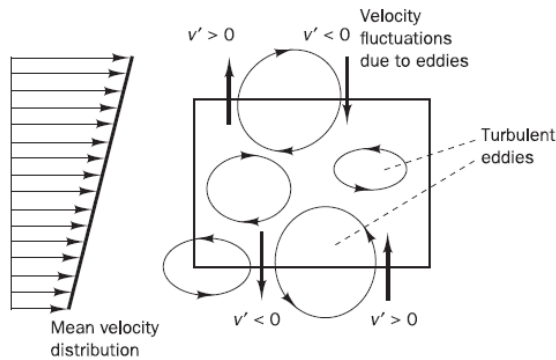


Figure 2.20: Momentum and energy exchange due to turbulent flow (Zikanov, 2010).

The RANS equation for the x -direction can thus be written as follows (y and z -direction can be derived in an analogue way):

$$\frac{\partial U}{\partial t} + \operatorname{div}(U\mathbf{U}) = -\frac{1}{\rho} \frac{\partial P}{\partial x} + \operatorname{div}(\nu \operatorname{grad} U) + \underbrace{\frac{1}{\rho} \left(\frac{\partial (-\rho \overline{u'^2})}{\partial x} + \frac{\partial (-\rho \overline{u'v'})}{\partial y} + \frac{\partial (-\rho \overline{u'w'})}{\partial z} \right)}_{\text{Reynolds stresses}} + S_{My} \quad (2.21)$$

with U and P the mean flow properties. Additional equations are thus required to define the Reynolds stresses since these are unknown and cannot be expressed as a function of the mean velocity and density (Zikanov, 2010).

In SST modelling, rather simple equations based on the eddy viscosity concept are used to evaluate Reynolds stresses. They are based on the presumption that there exists an analogy between the action of viscous stresses and Reynolds stresses on the mean flow. Consequently, similar to the viscous stresses in Eq. 2.17 the Reynolds stresses are modelled proportional to the rate of deformation. The proportionality factor for the Reynolds stresses is called the turbulent eddy viscosity ν_t (Zikanov, 2010). Hence, the kinematic viscosity ν in the Navier-Stokes equations (Eq. 2.17) is replaced by the effective viscosity ν_{eff} in the RANS equations (Eq. 2.22).

$$\frac{\partial U}{\partial t} + \operatorname{div}(U\mathbf{U}) = -\frac{1}{\rho} \frac{\partial P}{\partial x} + \operatorname{div}(\nu_{eff} \operatorname{grad} U) + S_{My} \quad (2.22)$$

The effective viscosity consists of two parts: the molecular viscosity ν and the turbulent viscosity ν_t (Eq. 2.23).

$$\nu_{eff} = \nu + \nu_t \quad (2.23)$$

The value of the parameter ν_t is determined by the state of turbulence. Therefore a turbulence model should be included. Different turbulence models exist among which the k - ϵ model is the most frequently used in SST models (De Clercq, 2003; Rodi, 1980). This model represents a reasonably accurate description of turbulence by linking the turbulent eddy viscosity to the kinetic energy k and the rate of viscous dissipation ϵ (Eq. 2.24).

$$\nu_t = c_\mu \cdot \frac{k^2}{\epsilon} \quad (2.24)$$

2.5. Modelling of SSTs

In this equation, c_μ is an empirical model constant. The quantities of k and ϵ are calculated by means of two coupled semi-empirical transport equations. These equations can be found in Zikanov (2010). As such the turbulence model accounts for the transport rates at which turbulence propagates throughout the settling tank.

Solid transport equation

The settling process is a multiphase problem since AS consist of a liquid phase and a solids phase. It can be modelled as a dispersed phase flow in a **multiphase model** where each phase is governed by its own mass- and momentum equations which are solved simultaneously and coupled by interphase interaction properties (Lakehal, 2002). This approach is quite complex as it requires a thorough understanding of the particle properties and interaction mechanisms involved.

As an alternative, often a **single phase** model is used (De Clercq, 2003). According to this approach, the activated sludge behaves as one single phase, i.e. a homogeneous mixture of water and solids. The solids concentration is then considered as a local property of the mixture and is computed by solving an additional scalar transport equation (Eq. 2.25). When considering multiple particle size classes, separate scalar equations are defined for each size class.

$$\underbrace{\frac{\partial \phi}{\partial t}}_{\text{Rate of increase in } \phi \text{ of fluid element}} + \underbrace{\frac{\partial}{\partial x} \phi u + \frac{\partial}{\partial y} \phi v + \frac{\partial}{\partial z} \phi (w - w_s)}_{\text{Net rate of flow of } \phi \text{ out fluid element}} = \underbrace{\frac{\partial}{\partial x} \left(\frac{\nu_{eff}}{\sigma_s} \frac{\partial \phi}{\partial x} \right) + \frac{\partial}{\partial y} \left(\frac{\nu_{eff}}{\sigma_s} \frac{\partial \phi}{\partial y} \right) + \frac{\partial}{\partial z} \left(\frac{\nu_{eff}}{\sigma_s} \frac{\partial \phi}{\partial z} \right)}_{\text{Rate of increase of } \phi \text{ due to diffusion}} + \underbrace{S_\phi}_{\text{Source term}} \quad (2.25)$$

In Eq. 2.25 ϕ represents the volume fraction of the sludge and $w_s = v_s$ the settling velocity in the direction of gravity. The parameter σ_s is the Schmidt number, which expresses the mass diffusivity in laminar flow conditions and is typically set to a value of 0.7 (Adams and Rodi, 1990). The settling process is thus computed as a mass flux of solids with a settling velocity v_s and is added to the transport term of the scalar equation. The settling velocity can be described by any of the settling velocity functions in Section 2.5.2.

Eq. 2.25 should be solved simultaneously with the continuity and the RANS equations. However, even though the sludge water mixture is considered as one homogeneous phase, the model should still account for the influence of local variations in sludge concentration ϕ on the flow pattern. Indeed, the concentration of solids in the mixture

will influence the local density and viscosity values. Hence, additional equations to calculate the density and viscosity state are required.

The fluid bulk density ρ in the RANS equations is determined as a function of the density of the liquid phase ρ_l , the density of the solid phase ρ_s and the volume fraction of the SS (ϕ).

$$\rho = \frac{\rho_l}{1 - \phi \left(1 - \frac{\rho_l}{\rho_s}\right)} \quad (2.26)$$

The molecular viscosity (ν) in Eq. 2.23 is a property of the sludge-water mixture. This property depends on the sludge rheology, which is defined as its deformation (strain) under influence of shear stresses. The sludge-water mixture cannot be considered as a Newtonian fluid due to particle-particle interactions (Forster, 2002). Consequently, the viscosity of the mixed liquor is not directly proportional to the applied shear rate, but also depends on mixed liquor properties such as the SS concentration (De Clercq, 2003). Different rheological models that describe the relation between the shear stresses (τ) and shear rate ($\dot{\gamma}$) exist (Ratkovich et al., 2013). Examples of rheological models for a non-Newtonian (Herschel-Bulkley model) and a Newtonian fluid are shown in Figure 2.21. The corresponding shear stress vs. shear rate relations are given in Table 2.3.

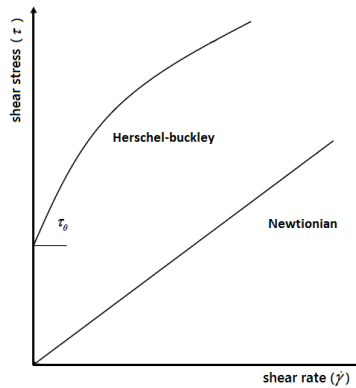


Figure 2.21: Newtonian and non-Newtonian flow behaviours (Herschel-Buckley), modified from De Clercq (2003).

The Herschel-Bulkley model assumes that fluid movement is only initiated when shear stress overcomes a certain critical stress (τ_0). However, De Clercq (2003) investigated the rheology of biological sludge with a sensitive rheometer and demonstrated empirically that a true yield stress does not exist. Instead, the viscosity suddenly becomes extremely high as the shear rate reaches a certain (rather low) value. Therefore, a mo-

2.5. Modelling of SSTs

Table 2.3: Possible shear stress-shear rate relationships

fluid	stress-shear rate relation
Newtonian fluid	$\tau = \mu \dot{\gamma}$
non-Newtonian fluid (Herschel-Bulkley model)	$\tau = \tau_0 + \mu \dot{\gamma}^n$

(with μ , the dynamic viscosity and $\mu = \rho\nu$)

dified form of the Herschel-Bulkley model is proposed:

$$\tau = \left(\frac{\tau_0(X)}{\dot{\gamma}} (1 - e^{-m\dot{\gamma}}) + K(X)\dot{\gamma}^{n-1} \right) \dot{\gamma} \quad (2.27)$$

with the molecular viscosity ($\mu = \tau/\dot{\gamma}$) written as follows:

$$\mu = \frac{\tau_0(X)}{\dot{\gamma}} (1 - e^{-m\dot{\gamma}}) + K(X)\dot{\gamma}^{n-1} \quad (2.28)$$

and m and n two constants. The variables $\tau_0(X)$ and $K(X)$ are both functions of the solids concentration (X) according to Eqn. 2.29 and 2.30 with β_1 , β_2 and β_3 parameters to be calibrated and μ_w the viscosity of water (Lakehal and Krebs, 1999).

$$\tau_0(X) = \beta_1 e^{\beta_2 X} \quad (2.29)$$

$$K(X) = \mu_w + \beta_3 X^2 \quad (2.30)$$

Application of CFD models for SSTs

An important aspect of SST modelling is to find a proper balance between simulation accuracy and computational time. No universal SST model exists due to numerous factors that can all affect the model, such as the inlet position, side water depth and the sludge removal mechanism (Anderson, 1945; Matko et al., 1996). Frequently the simulation times of CFD models for circular settling tanks are significantly reduced by lowering the dimensionality of the model or omitting structures such as the sludge removal system (De Clercq, 2003). The benefits of these simplifications in the model should not affect the desired model accuracy.

The first numerical SST model was presented by Larsen (1977). Even though several assumptions were made in this model, it was accurate enough to indicate both the existence of density currents and their impact on the flow pattern of a rectangular settling tank. After this pioneering work, several SST models have been proposed in literature. Especially during the early and mid-nineties a lot of progress was made in 2-D modelling of circular settling tanks. For example, Devantier and Larock (1986) simulated the stratified turbulent steady 2-D flow in a circular clarifier through incorporation of the rather strong density effect in a SST. Another important contribution was made by Krebs (1991) who investigated the optimal position of the inlet baffle with a 2-D model. Lakehal and Krebs (1999) and Armbruster et al. (2001) examined the importance of a proper rheology function to account for increased viscosity of highly concentrated sludge mixtures by means of dynamic CFD simulations.

Over the last decade, the use of CFD to describe the hydrodynamics in the SST has led to a more comprehensive understanding of the different processes and their interactions in a SST. This knowledge provides the opportunity for optimisation of the settling tank design and retrofitting (De Clercq, 2003). Different studies attempted to find a proper configuration and strategical placement of internal physical features in order to improve the effluent quality and the underflow solids concentration (He et al., 2008; Stamou et al., 2009; Tamayol et al., 2010; Xanthos et al., 2011, 2013). Moreover, as computational power is becoming increasingly available, more advanced CFD simulations become feasible. For example, Patziger et al. (2012) presented a CFD model of a SST coupled to the biological reactor in order to investigate optimal sludge return scenarios. CFD can thus be considered as a powerful tool to gain system knowledge and can be used to avoid tedious and time consuming experiments (Guvonvarch et al., 2015).

2.5.5 Flocculation models

Next to the settling behaviour and the tank's hydrodynamics also the flocculation state of activated sludge plays an important role in the performance of SSTs. Knowledge on the floc size distribution is of crucial importance in the clarification zone where the discrete settling mechanism prevails. Classical models do not account for the interactions between activated sludge particles but simply describe the biomass in a SST by means of a lumped variable such as the sludge concentration (Nopens, 2005). The dynamics of floc size distributions can be described by means of a flocculation model.

Flocculation models should explain two opposing processes: aggregation and break-up. Von Smoluchowski (1917) made a first attempt to model the aggregation process. Later on, models for breakage of particles were added. Several types of flocculation models were proposed ranging from rather simple models such as the model of Parker

2.5. Modelling of SSTs

et al. (1972) which includes only two particle size classes, to more advanced Population Balance Models (PBMs) that consider a broad range of floc size classes (Biggs, 2000; Nopens et al., 2002).

Flocculation model by Parker et al. (1972)

Parker et al. (1972) divided the AS into 2 classes: primary particles and flocs. Based on these two size classes the flocculation kinetics of turbulent mixing are described assuming that break-up and aggregation processes occur simultaneously. The net rate of change of the number of primary particles (n_p) and flocs (n_f) with respect to time is given by the following differential equations:

$$\begin{cases} \frac{dn_p}{dt} = K_b \cdot X \cdot G^m - K_a \cdot X \cdot G \\ \frac{dn_f}{dt} = -K_b \cdot X \cdot G^m + K_a \cdot X \cdot G \end{cases} \quad (2.31)$$

with X the concentration of suspended particles, G the mixing intensity or shear rate and m a parameter. The coefficients K_b and K_a represent the breakage rate and the aggregation rate, respectively.

Population Balance Models

As discussed in Section 2.4.1 aggregation of flocs is the result of two consecutive steps: transport and attachment of particles. Different transport mechanisms exist and the attachment step depends on several short range forces related with the nature of the surfaces themselves. Hence, the model of Parker et al. (1972) gives a very coarse approximation of reality by modelling all these processes with a constant coefficient and dividing the entire floc size interval into only two classes.

PBMs represent a more detailed modelling framework to describe the dynamics of PSDs (Ramkrishna, 2000). The advantage of these type of models compared to the model of Parker et al. (1972) is their ability to describe the whole dynamical distribution of floc sizes influenced by the different flocculation mechanisms and break-up processes.

The governing equation in its most general form is given as

$$\frac{\partial f_1(x, t)}{\partial t} + \frac{\partial}{\partial x} \left(\dot{X}(x, t) f_1(x, t) \right) = h(x, t) \quad (2.32)$$

where x is the distributed property, $f_1(x, t)$ is the number density function, $\dot{X}(x, t)$ is

a continuous growth term and $h(x, t)$ is a reaction term (through discrete events such as aggregation and break-up) (Nopens et al., 2015).

Biggs (2000) developed a population balance model to describe the dynamics of the number density (N_i) in different size classes (i). Since biological growth in a SST occurs on a much longer time scale than aggregation and break-up processes, it can be ignored ($\dot{X}(x, t) = 0$). Only changes in PSD due to discrete aggregation and break-up processes are considered in the reaction term $h(x, t)$. Both aggregation and break-up processes can give rise to birth (source term) and death (sink term) of flocs of a certain size (Eq. 2.33) as illustrated in Figure 2.22.

$$\frac{dN_i}{dt} = \text{Birth}_{\text{aggregation}} - \text{Death}_{\text{aggregation}} + \text{Birth}_{\text{breakage}} - \text{Death}_{\text{breakage}} \quad (2.33)$$

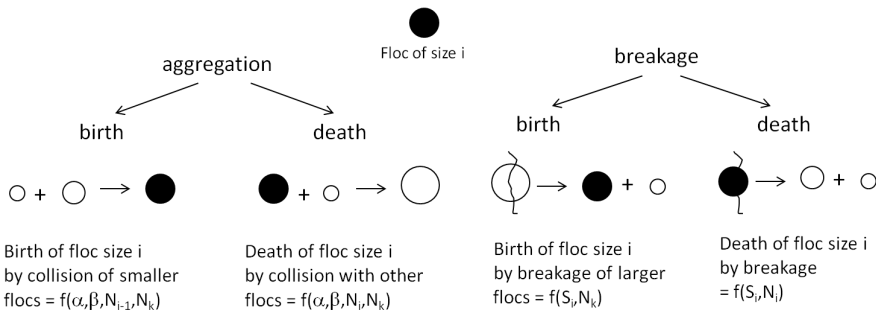


Figure 2.22: Schematic overview of the birth and death concept of aggregation and breakage (Biggs, 2000).

These models require information regarding the frequency of collision between particles (β), the efficiency of these collisions (α) and the breakage rate (S) which are influenced by various factors, such as shear rate, dissolved oxygen, temperature, pH, total suspended solids and sludge age. The mathematical functions used to describe these functions are called kernels but have been proven difficult to determine for AS flocculation (Nopens et al., 2002; Ding et al., 2006).

Coupled flocculation-CFD models

Obviously, mixing plays an essential role in the (de)flocculation process, especially for the introduction of particle-particle interactions (Von Smoluchowski, 1917; Wahlberg et al., 1994). Often the mixing intensity or shear rate, expressed as velocity gradient G is included in the aggregation/breakage rates of a flocculation model. However, these velocity gradients will vary for different locations throughout the SST. A CFD model determines the velocity gradient G on each node of a very fine spatial grid.

2.5. Modelling of SSTs

Thus, coupling of a flocculation model with a CFD model enables quantification of the flocculation rates at each location of the tank.

Griborio and McCorquodale (2006) successfully coupled the flocculation model of Parker et al. (1972) with a single phase CFD model in which three particle size classes were considered: primary particles, small flocs and large flocs. The coupled model was used to improve understanding of the flocculation processes within a center well in a circular SST in order to optimize the geometry of this structure for optimal energy dissipation and AS flocculation. Gong et al. (2011) coupled the model of Parker et al. (1972) with a 3-D CFD model of a rectangular SST to optimise baffle placement. They investigated the dependency of the coefficients K_b and K_a on the shear rate G and the SS concentration in order to incorporate more realism into the flocculation model.

CHAPTER 3

Objectives

From the literature review in Chapter 2 it becomes clear that several experimental methods and modelling frameworks are available to study the different processes (hydrodynamics, flocculation and settling behaviour) in a SST. The available modelling frameworks do not only differ with respect to the processes they include but also in their complexity and application. In this respect, 1-D models are most suited for operation and control (in particularly in combination with other WWTP unit operations) whereas 2-D and 3-D models can be used to build process knowledge which can subsequently aid to improve tank design or existing 1-D models. However, no generally accepted approach to describe the combined effect of the different settling regimes in SSTs is available.

This PhD aims to develop further insight into the different settling dynamics in SSTs by applying different modelling frameworks in combination with experimental analysis. Therefore, a number of objectives are defined which will be addressed in the remaining chapters of this dissertation.

- To investigate under which conditions commonly used models fail to capture the true dynamics in order to assess why and how compression settling becomes important for the operation and control of full-scale WWTPs.
- To select mathematical functions for each of the different settling regimes in a SST based on their ability to describe the underlying process and the feasibility to calibrate their parameters.
- To investigate the impact of tank hydraulics and flocculation on the clarification process through integration of a flocculation model and CFD.
- To calibrate and enhance the integrated flocculation-CFD model based on detailed experimental data of dynamic PSD.

PART II

Towards improved 1-D models for operation and control of SSTs

The second part of this PhD addresses the improvement of existing 1-D models by including both hindered and compression settling. In this respect, Chapter 4 illustrates the importance of compression settling on operation and control of a Waste Water Treatment Plant (WWTP) during wet weather conditions. The calibration of hindered and compression settling functions from literature based on well-known batch settling tests is described in Chapter 5. This analysis showed that the selection and calibration of valid functions for both hindered and compression settling requires a critical analysis of available functions for each of these processes. Therefore, the behaviour of different hindered settling functions is analysed with respect to data of long-term batch settling curves and detailed velocity profiles (Chapter 6). Finally, in Chapter 7 a hypothesis is formulated regarding the physical explanation behind the remaining variability in the compression phenomenon and experimental evidence is collected to support this hypothesis.

CHAPTER 4

Impact of secondary settling tank models on the development of operation and control strategies for WWTPs

Redrafted from: Torfs, E., Maere, T., Bürger, R., Diehl, S., and Nopens, I. (2015c). Impact on sludge inventory and control strategies using the Benchmark Simulation Model no. 1 with the Bürger-Diehl settler model. *Water Sci. Technol.*, 71(10):1524–1535.

Abstract

An improved 1-D model for the secondary clarifier, i.e. the Bürger-Diehl model, was recently presented. In this chapter, the impact of specific features of the Bürger-Diehl model on settler underflow concentration predictions, plant sludge inventory and Mixed Liquor Suspended Solids (MLSS) based control actions is investigated by using the Benchmark Simulation Model No. 1. The numerical results show that by accounting for compression settling, the Bürger-Diehl model allows for more realistic predictions of the underflow sludge concentration and the Sludge Blanket Height (SBH), which are essential for more accurate wet weather modelling and sludge waste predictions. The choice of secondary settler model clearly has a profound impact on the operation and control of the entire treatment plant and it is recommended to use the Bürger-Diehl model as of now in any wastewater treatment plant modelling effort.

4.1 Introduction

The performance of Secondary Settling Tanks (SSTs) significantly affects the effluent quality as well as the biomass inventory (i.e. the biomass distribution in the bioreactor

and clarifier) in a WWTP. As biomass is the driving force for the biokinetic conversion processes, SST operation will affect the performance of the entire treatment plant - both in reality as well as when modelling WWTPs.

A new 1-D model which allows improved and more realistic simulations of secondary clarifiers has recently been presented (Bürger et al., 2011). The decisive difference to traditional layer models is that every detail of the implementation is in accordance with the theory of Partial Differential Equations (PDEs). Furthermore, the Bürger-Diehl model allows accounting for hindered and compressive settling as well as inlet dispersion.

The purpose of this chapter is to evaluate the qualitative effect of the Bürger-Diehl model on the operation and control of a WWTP. Moreover, the impact of specific features of the Bürger-Diehl model on settler underflow concentration predictions, plant sludge inventory, MLSS based control actions and effluent concentration are investigated. The results obtained with the Bürger-Diehl model are compared to the Takács model to illustrate when and why traditional layer models fail to capture the true dynamics of a WWTP and how this can be improved by the specific features of the Bürger-Diehl model. For this purpose simulations are performed with the COST/IWA Benchmark Simulation Model No. 1 (BSM1) (Copp, 2002; Gernaey et al., 2014). Finally, some guidelines for the application of this new settler model in WWTP modelling are also provided.

4.2 Materials and methods

4.2.1 Benchmark Simulation Model No. 1

The BSM1 is a standardised simulation procedure for the design and evaluation of control strategies of conventional WWTPs in terms of effluent quality and operational costs, comprising a detailed description of plant layout, models, inputs and evaluation criteria (Gernaey et al., 2014); see Figure 4.1.

The results shown in this chapter were obtained with the BSM1 with two different settler models (Bürger-Diehl and Takács) in the modelling and simulation platform WEST (<http://www.mikebydhi.com>, mark; Vanhooren et al., 2003). The fourth-order Runge-Kutta numerical integration method with variable time step (RK4ASC) was used for the numerical integration of the ODE system. All simulations were performed with the standard input file for storm weather conditions (i.e. 100 days of steady-state followed by 21 days of dry weather and 7 days of storm weather). The input flow rate (Q_{in}) and the incoming concentrations of readily biodegradable substrate (SS) and ammonium (SNH) during the 7 days of storm weather are shown in Figure 4.2.

4.2. Materials and methods

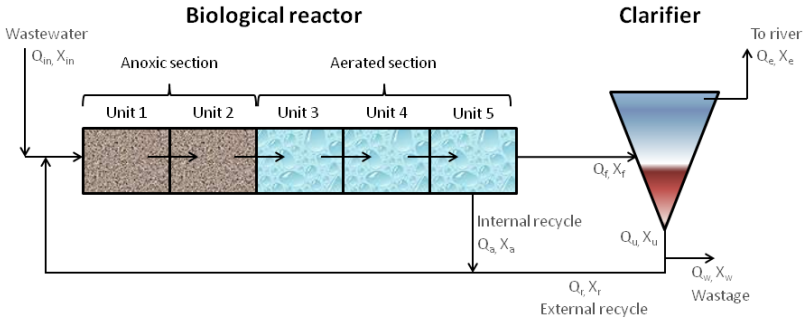


Figure 4.1: General overview of the BSM1 plant.

The incoming flow during storm weather is cut-off at 60,000 m³ due to automatic by-passing.

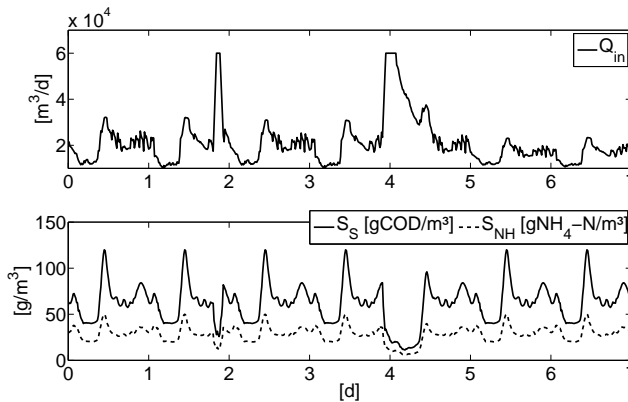


Figure 4.2: Incoming flow rate, soluble substrate concentration and ammonium concentration of the BSM1 model under storm weather conditions.

Furthermore, unless explicitly stated otherwise, all simulations of the Bürger-Diehl model in this chapter have been performed with the same coarse discretisation level as is required for the Takács model (i.e. 10 internal SST layers, 14 layers in total). This choice was made for reasons of comparison. More information on the impact of a finer discretisation is provided at the end of the chapter.

4.2.2 Constitutive functions used in the Bürger-Diehl model

The hindered settling velocity is modelled by the double exponential settling velocity function of Takács as it is the most commonly used in WWTP modelling:

$$v_{hs} = \max \left(0, \min \left(V_{0,\max}, V_0 \left(e^{(-r_H \cdot (X - X_{\min}))} - e^{(-r_P \cdot (X - X_{\min}))} \right) \right) \right) \quad (4.1)$$

with V_0 , $V_{0,\max}$, r_H and r_P as settling parameters and $X_{\min} = f_{ns} \cdot X_{in}$ (with f_{ns} a parameter to quantify the non-settleable fraction and X_{in} the incoming solids concentration).

The compression function is based on the work of De Clercq et al. (2005). Despite accurate measurements of batch tests of activated sludge (De Clercq et al., 2005) and different approaches to solve the inverse problem (De Clercq et al., 2008; Diehl, 2014), it is difficult to obtain an appropriate compression function. The logarithmic function obtained by De Clercq et al. (2008) contains three parameters that are difficult to identify. Here, a function is selected with similar features as the function from De Clercq et al. (2008) but with only two parameters (α and X_{crit}):

$$d_{comp}(X) = \begin{cases} 0 & \text{if } 0 \leq X < X_{crit} \\ \frac{\rho_s \cdot \alpha \cdot v_{hs}(X)}{g \cdot (\rho_s - \rho_f)} & \text{if } X \geq X_{crit} \end{cases} \quad (4.2)$$

with ρ_s and ρ_f the densities of the solids and the fluid respectively and g the constant of gravity. In contrast to the function by De Clercq et al. (2008), this function has an exact primitive which implies a simplified implementation.

The dispersion function d_{disp} is often set as the product of the fluid velocity and a continuous function of the depth. The continuous function has its maximum at the feed level and is zero some distance away from the inlet (Bürger et al., 2013). This allows modelling a region of higher turbulence around the feed inlet at increased hydraulic loading. The following constitutive function was chosen in this chapter:

$$d_{disp} = \begin{cases} \frac{a}{A} \cdot Q_f \cdot \cos^2 \left(\frac{\pi \cdot z}{2 \cdot b \cdot Q_f} \right) & \text{if } |z| < (b \cdot Q_f) \\ 0 & \text{if } |z| \geq (b \cdot Q_f) \end{cases} \quad (4.3)$$

with a and b two dispersion parameters.

Note that it is not the scope of this chapter to propose Eqn. 4.2 and 4.3 as the ultimate approach to model sludge compression or inlet dispersion but merely to illustrate the

4.2. Materials and methods

added value of extending a settler model with these phenomena. Due to the modular structure of the numerical scheme presented by Bürger et al. (2013) each one of these constitutive functions can easily be updated or replaced if future research would lead to further insight into these phenomena. The parameter values used for the different simulations throughout this chapter are summarised in Table 4.1. For the hindered settling function the standard values for BSM1 were used, the compression and dispersion parameters were selected based on the work of resp. De Clercq et al. (2008) and Bürger et al. (2013).

Table 4.1: Parameter values for the different constitutive functions used in this chapter

Parameter	Value
Hindered settling	
V_0 [m/d]	474
$V_{0,max}$ [m/d]	250
r_h [l/g]	0.576
r_p [l/g]	2.86
f_{ns} [-]	0.00228
Compression settling	
X_{crit} [g/l]	5
α [m ² /s ²]	1.2
Inlet dispersion	
a [m]	0.4
b [d/m ²]	3e-5

4.2.3 Case-study: the Eindhoven WWTP

To better understand the added value of the specific features of the Bürger-Diehl model, it is helpful to first consider the behaviour of a full-scale SST under both dry and wet weather conditions. Therefore, online measurements of both underflow concentration (X_{ii}) and SBH during a two-day period of dry weather followed by a two-day storm event at the WWTP of Eindhoven (The Netherlands) are provided in Figure 4.3. The circular SST at this WWTP has a maximum height of 4 m and a central feed inlet. The underflow rate is controlled as a fixed ratio (0.65) of the incoming flow rate.

From these data an important distinction can be made between the operational state and consequent control requirements during respectively dry and wet weather. During dry weather (up to day 2.5), no sludge blanket is detected signifying that under these conditions the settler is oversized and operating at only a fraction of its potential capacity. This is unfortunately the case for many WWTPs worldwide and indicates that during dry weather the system's efficiency could be increased significantly for example

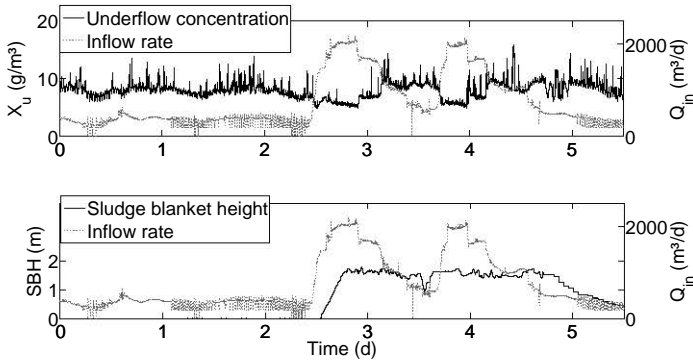


Figure 4.3: On-line measurement data of underflow concentration and SBH during the period of June 1-6, 2013 at the WWTP of Eindhoven (The Netherlands). Two consecutive rain events can be observed after 2.5 days.

by operating the bioreactors at a higher sludge concentration. In contrast, when a storm peak hits the WWTP, a sludge blanket of almost 2 meter is formed and care needs to be taken to avoid the loss of sludge from the system. The underflow concentration on the other hand does not undergo any large variations during the storm event. Only a small dilution effect can be observed. Hence, for this case the main impact of a storm weather event can be found in the SBH variations.

The SBH can thus be a crucial operation and control variable during a storm weather event or when imposing higher solids loads to e.g. operate the bioreactors at a higher sludge concentration even during dry weather conditions (implying higher conversion rates and hence, more flexibility in operation). It is important to develop improved insight (which also implies good quality predictions) to judge as of when process control should focus on keeping sludge in the system and safeguarding effluent quality or on maximising biokinetic conversions.

4.3 Results and discussion

4.3.1 Impact of compression settling on predicted concentration profiles in the SST

To illustrate the effect of compression settling on the SST performance, open-loop simulations (with a fixed underflow rate $Q_u=18,831 \text{ m}^3/\text{d}$) are performed (1) with the model of Takács and (2) with the Bürger-Diehl model with the compression function activated. Inlet dispersion is not considered for these simulations ($d_{disp} = 0$). Fig-

4.3. Results and discussion

ures 4.4 and 4.5 show the differences in SBH and underflow concentration predictions between both models. The SBH is defined as the height of the first layer with a concentration that exceeds the threshold value of 0.9 g/l. This threshold value was selected as it approx. corresponds to the concentration where a clear sludge/water interface is starting to form (i.e. transition between discrete and hindered settling).

An increased flow rate to the SST in the simulations with the Bürger-Diehl model causes the sludge blanket level to rise significantly and results in only a modest increase in the underflow concentration. This contrasts with a very drastic increase in the underflow concentration and a moderate effect on the SBH in the Takács model. By only considering hindered settling, the sludge in the Takács model will settle unrealistically fast resulting in a highly concentrated bottom layer. By including compression, the settling velocity will be slowed down at higher concentrations due to a compressive force. Hence, the inclusion of compression settling creates a dampening effect on the underflow concentration resulting in smaller variations on the underflow but a pronounced increase of the SBH.

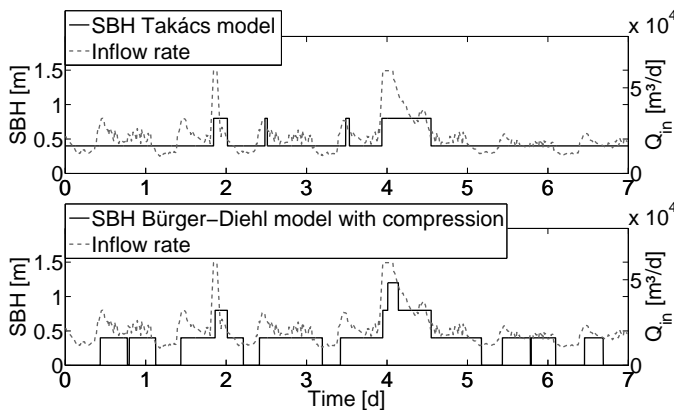


Figure 4.4: Open loop ($Q_u=18,831 \text{ m}^3/\text{d}$) dynamic simulations of the sludge blanket height for the models of Takács and Bürger-Diehl under storm weather conditions.

To compare the behaviour of the models to the measured trends observed in Figure 4.3, closed-loop simulations were performed with $Q_u = 0.65 \cdot Q_{in}$ (operational strategy as in the WWTP of Eindhoven). As the waste flow rate is kept at a constant value of $385 \text{ m}^3/\text{d}$, only the recycle flow rate to the biological reactors is affected. The results are shown in Figures 4.6 and 4.7.

In the case of the Takács model, an increased loading to the clarifier during a storm peak results in a significant dilution of the underflow concentration and only a brief elevation of the sludge blanket. In contrast, the simulations with the Bürger-Diehl model (with compression) predict only a slight dilution effect during the storm peaks. Here, the

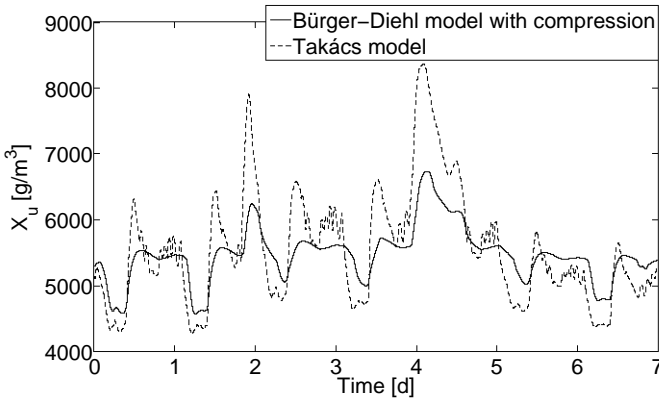


Figure 4.5: Open loop ($Q_u=18,831 \text{ m}^3/\text{d}$) dynamic simulations of the underflow concentration for the models of Takács and Bürger-Diehl under storm weather conditions.

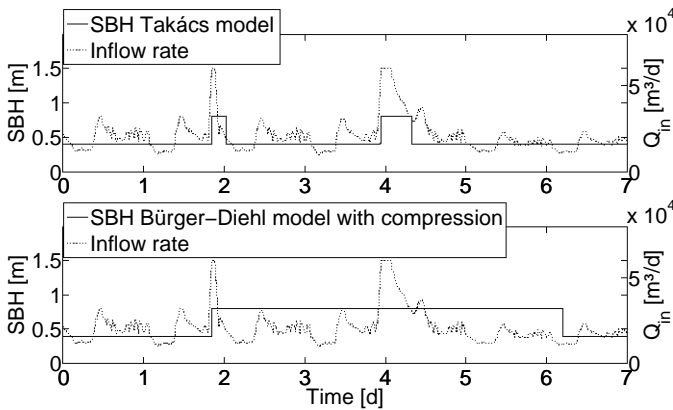


Figure 4.6: Closed loop ($Q_u = 0.65 \cdot Q_{in}$) dynamic simulations of the sludge blanket height for the models of Takács and Bürger-Diehl under storm weather conditions.

elevation in sludge blanket is clearly the dominant effect which corresponds to the observations made in reality (Figure 4.3). It thus becomes evident that by accounting for compressive settling, the dynamics of SBH and underflow concentrations during storm weather can be modelled in a much more realistic way. This will impact the recycle flow as well as sludge wastage (and related operational costs).

To further illustrate the differences in behaviour between the two settler models, the complete concentration profiles for the open loop simulations at times $t=0.1 \text{ d}$ (before the storm event) and $t=4.2 \text{ d}$ (when the maximum flow rate hits the SST) are shown

4.3. Results and discussion

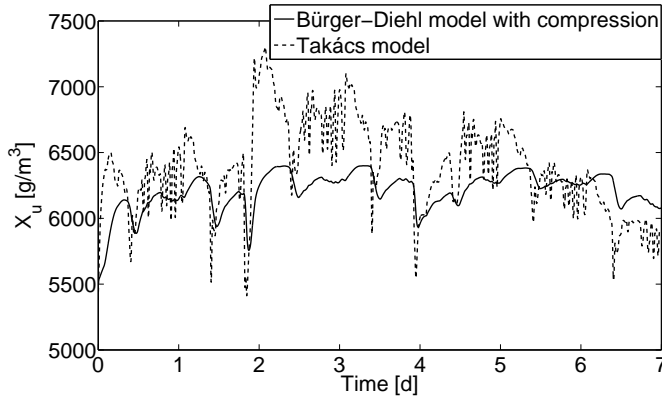


Figure 4.7: Closed loop ($Q_u = 0.65 \cdot Q_{in}$) dynamic simulations of the underflow concentration for the models of Takács and Bürger-Diehl under storm weather conditions.

in Figure 4.8. From these concentration profiles the importance of another feature of the Bürger-Diehl model becomes evident. The inclusion of additional layers at the outlet boundaries does not only allow more realistic predictions of the underflow concentrations but also influences the SBH and the concentration profile inside the sludge blanket.

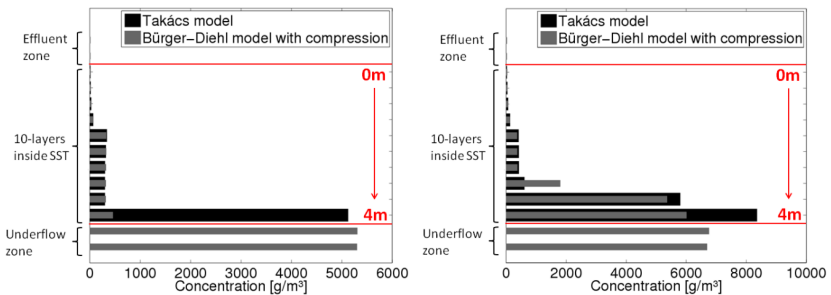


Figure 4.8: Concentration profiles during dry weather ($t=0.1$ d - left) and storm weather ($t=4.2$ d - right) for the two settling models.

As could be seen from Figure 4.4, the SBH in Takács' model never drops below a value of 0.4 m, corresponding to the thickness of the bottom layer. This minimum SBH is inherent to the structure of the Takács model: sludge settles to the bottom of the tank and accumulates in the last layer. (Adding additional layers to reduce the thickness of the bottom layer is not to be done for the Takács model as one changes the numerical dispersion and hence the dispersion of the settler.) Unless the settler would be operated

at extremely dilute circumstances, Takács' model will never be able to predict a sludge blanket of 0 m. However, in a full-scale treatment plant, the absence of a sludge blanket is often encountered during dry weather operation. Consequently, the Takács model predicts a persistent error of 10% of the height of the SST. The reason for this behaviour is the common but erroneous assumptions that the underflow concentration is always equal to the one in the bottom layer. In the Bürger-Diehl model this problem does not occur due to the existence of additional layers below the bottom which represent the underflow region. As both hindered and compression settling occur over the outlet boundary (see Table 2.2), sludge can settle into the underflow layers and the absence of a sludge blanket inside the SST can be modelled. Thus, by explicitly modelling the underflow region as well as extending the settling behaviour with a compression function, a more advanced 1-D model provides more realistic predictions of the SBH behaviour which would allow operating the SST in a more efficient way.

4.3.2 Impact of compression settling on the performance of the biological reactors

The previous section illustrates that sediment compressibility notably influences the SBH and the underflow concentration. Whereas the SBH is mainly important with respect to the performance of the SST, the impact range of the underflow concentration stretches out much further as a large part of the underflow is recycled to the bioreactor. Hence, compression settling will also influence the biosolids concentration in the bioreactors. Figure 4.9 shows the predictions for the MLSS concentration in the first Activated Sludge Unit (ASU 1) for both the Takács model and the Bürger-Diehl model with compression (for an open loop simulation). The latter model increases the predicted effect of a storm peak on the MLSS concentration (i.e. dilution directly after the peak and increased concentration during the recovery phase after a peak event). Due to the dampening effect of compression on X_u , less sludge is instantaneously returned to the bioreactor when a storm hits compared to the Takács model's predictions. This results in less recovery and a more pronounced effect of the storm peak on the bioreactor performance. Thus, traditional settler models, which do not account for compressive settling, might severely underestimate the effect of a storm event due to an underestimation of the biomass dilution effect in the bioreactor and hence instantaneous severely reduced conversion rates. The latter will result in underprediction of potential peaks in the effluent COD and NH_4 . When using such a model for developing mitigation strategies under wet weather, one risks taking insufficient action.

Moreover, the MLSS concentration will directly influence the conversion rates in the biological reactors since these are typically of the form $r = \mu X$, where μ is a growth kinetics function. As an example, the nitrification rate in the first aerated activated sludge unit and the relative differences in predicted nitrification rate between the two models are shown in Figure 4.10. The relative differences are calculated as follows

4.3. Results and discussion

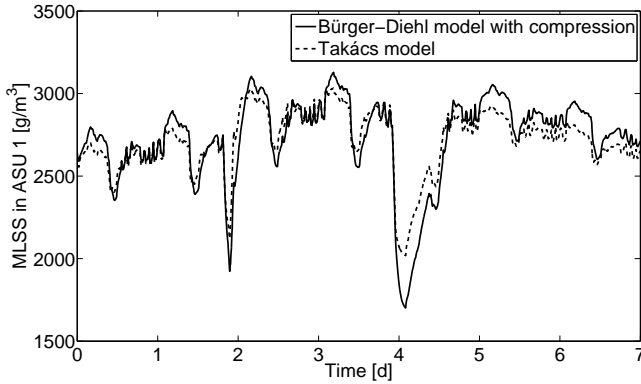


Figure 4.9: Simulated MLSS concentration in the first activated sludge unit for an open-loop simulation.

(with T for Takács, BD for Bürger-Diehl):

$$\text{Relative difference} = \frac{|r_T - r_{BD}|}{r_T} \quad (4.4)$$

From the figure it becomes clear that the effect of compression settling influences the performance of the entire plant. The observed differences in underflow concentration between the models result in a maximal difference of almost 20% for the predicted nitrification rate. Hence, when only hindered settling is considered (as is the case for the traditional layer models), this might 'force' modellers to calibrate kinetic parameters for the wrong reasons. If X is wrongly predicted by the model, the degrees of freedom in μ (e.g. μ_{\max} , affinities, etc.) will be used to obtain the correct value for the total conversion rate r . Figure 4.10 further demonstrates that slight differences in conversion rates already exist during dry weather operation. The relative error also needs significant time (approx. 0.5 days) to reduce to lower values after a storm event.

4.3.3 Impact of compression settling on the development of control strategies

Since the sludge inventory is the driving force behind the performance of a WWTP, a pronounced difference in the predictions of the biomass concentrations will also influence plant-wide control strategies. Therefore, the impact of the two settler models on the implementation of a control strategy that aims to maintain the MLSS concentration in a desired range through manipulation of the underflow rate Q_u is investigated (see Figure 4.1).

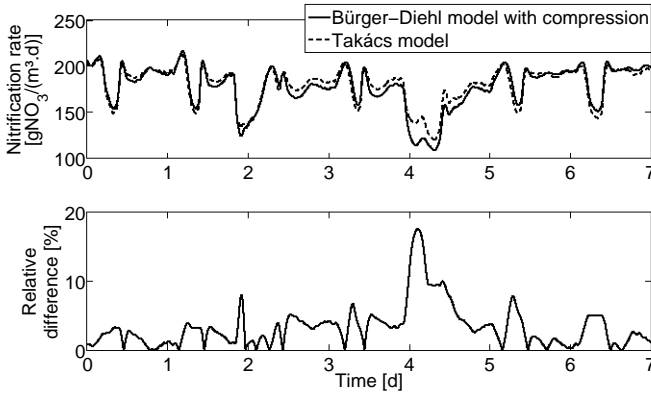


Figure 4.10: Simulated nitrification rate in the 3rd activated sludge unit (1st aerated unit) during storm weather conditions.

As a first step, the very simple control strategy of Figure 4.6 was adopted, ($Q_u = 0.65 \cdot Q_{in}$). This control strategy should reduce the plunge in the MLSS concentration during a storm event since more sludge will be recycled to the biological tanks. However, during highly dilute conditions (which usually occur during storm weather) this control strategy can become insufficient. Therefore the constant-ratio controller is extended with a PI controller which controls the MLSS concentration in ASU 1 at a setpoint of 2800 g/m^3 by adapting the underflow rate. The control strategy is implemented in ASU 1 since this is the first location where disturbances in the incoming flow will be perceived. If the dilution effect is counteracted here, it will also counteract the effect in the downstream bioreactors. The PI controller serves as an auxiliary control strategy and will therefore only become active if the MLSS concentration drops below $2,500 \text{ g/m}^3$. Once the MLSS concentration surpasses an upper threshold ($\text{MLSS} > 2,850 \text{ g/m}^3$), the PI controller is switched off. The limits for manipulation of the underflow rate are set to 0.33 and 1.5 times Q_{in} (Tchobanoglous et al., 2003).

As both settler models predict different concentrations in the underflow of the SST, a similar manipulation in Q_u will lead to different responses in the MLSS concentration. Hence, both models require different tuning of the control parameters. To further understand the nature of each model's requirements, the responses to a step increase in the volumetric underflow rate Q_u are examined. In order to mimic the behaviour under high flow conditions, a step increase in Q_u from $18,831 \text{ m}^3/\text{d}$ to $20,000 \text{ m}^3/\text{d}$ was applied under a constant incoming flow of $30,000 \text{ m}^3/\text{d}$ (and corresponding incoming concentrations selected from the standard BSM1 input file). (Note that investigating the step response during actual storm weather ($60,000 \text{ m}^3/\text{d}$) is not feasible since simulations with a long period of such increased flow conditions would upset the system too much making it no longer representative of realistic operating conditions.) Figure 4.11

4.3. Results and discussion

shows the resulting step responses for both models. On the left-hand side the absolute values of the MLSS concentrations are depicted, on the right-hand side the net step-response values are shown with respect to the steady-state value of each model before the step increase. For both models the MLSS concentration shows an initial steep increase followed by a much slower increase until a new steady state is reached. The initial steep increase can be related to a period where the sludge that is present at the bottom of the clarifier is simply recycled at a higher rate. However, this sludge will not be replenished at the same velocity as it is pumped away causing the underflow concentration to drop and a switch to a second period where the system response slows down until a new steady-state value for the MLSS concentration is reached.

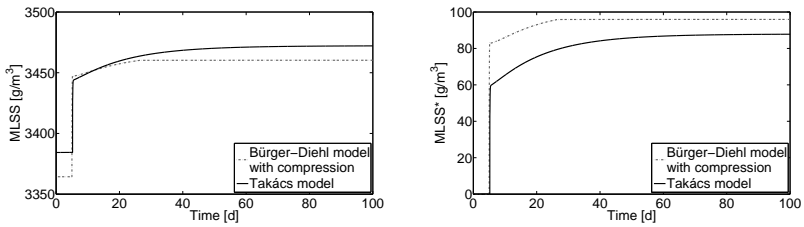


Figure 4.11: Response of the MLSS concentration in the first activated sludge tank to a stepwise variation in the underflow rate from $18,831 \text{ m}^3/\text{d}$ to $20,000 \text{ m}^3/\text{d}$ with a constant incoming flow of $30,000 \text{ m}^3/\text{d}$. MLSS* means the net step response with respect to the initial steady state.

The initial steep increase in MLSS concentration is 30% larger for the Bürger-Diehl model compared to the Takács model. Due to a combined effect of compression settling and the additional layers in the underflow region, more sludge is present in the SST when using the Bürger-Diehl model. Consequently, as more sludge is readily available to be recycled when Q_u increases, it will take somewhat longer before the underflow concentration will be affected and the settling sludge flux to the bottom layers becomes limiting. Due to the underprediction of the SBH in the Takács model during storm weather, the response to the control action will be wrongly predicted which may result in a poorly tuned controller. Hence, developing a control strategy based on Takács' model poses a risk of not producing the desired system behaviour under closed-loop conditions in practice. As the Bürger-Diehl model (which has been shown to predict a more realistic system behaviour) predicts a larger response for the same increase in Q_u , it will require a more conservative tuning of the parameters in the PI controller to ensure a stable system response. Moreover, the control strategy developed for the Bürger-Diehl model requires a higher ratio in the constant-ratio controller. The explanation for this lies in the much lower underflow concentration predicted by the Bürger-Diehl model during storm weather as was illustrated in Fig-

ure 4.5. Figure 4.12 shows the manipulations in underflow concentration and the MLSS concentration when a control action with a constant ratio and a PI controller is tuned and implemented for both models. The control parameters for the Takács model are $K_p=10$ $[(\text{m}^3/\text{d})\cdot(\text{g}/\text{m}^3)^{-1}]$ and $\tau_I=1$ $[\text{g}/\text{m}^3]$ and a constant ratio of 0.65. In the Bürger-Diehl model a constant ratio of 0.75 and a more conservative PI controller with parameter values $K_p=1$ $[(\text{m}^3/\text{d})\cdot(\text{g}/\text{m}^3)^{-1}]$ and $\tau_I=5$ $[\text{g}/\text{m}^3]$ are applied. The large dilution in MLSS concentration that was observed in the open loop simulation results of Figure 4.9 is successfully counteracted by the applied control strategies. Due to the lower PI settings in the Bürger-Diehl model, much lower control actions for the underflow concentration are now applied during the storm event. This will not only influence the recovery period of the MLSS concentration but will also affect the cost calculations in the BSM model.

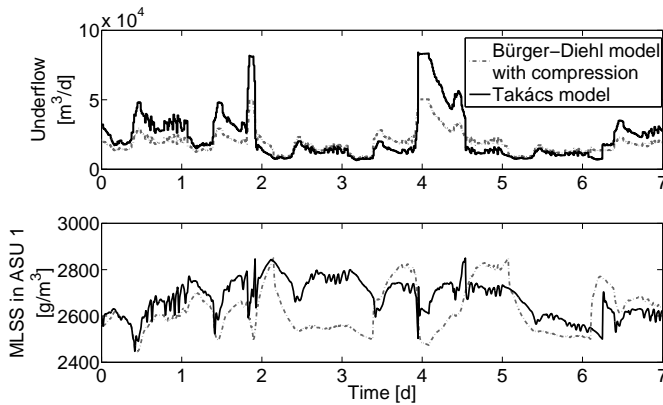


Figure 4.12: Dynamic simulation with the implementation of an MLSS control strategy ($Q_u = 0.65 \cdot Q_{in} + \text{PI controller with } K_p=10$ $[(\text{m}^3/\text{d})\cdot(\text{g}/\text{m}^3)^{-1}]$ and $\tau_I=1$ $[\text{g}/\text{m}^3]$ for Takács and $Q_u = 0.75 \cdot Q_{in} + \text{PI controller with } K_p=1$ $[(\text{m}^3/\text{d})\cdot(\text{g}/\text{m}^3)^{-1}]$ and $\tau_I=5$ $[\text{g}/\text{m}^3]$ for Bürger-Diehl). Manipulations in underflow rate (top) and MLSS concentration in the first activated sludge tank (bottom) under storm weather conditions.

These results show that the choice of settler model can notably influence the evaluation of proposed control schemes. Since a real SST typically undergoes a significant increase in the SBH during storm weather, thereby storing additional sludge in the system, its response to an increase of the underflow rate can be more extreme than would be predicted by the Takács model as the latter underpredicts the elevation of the SBH. Consequently, operating a real SST calls for more conservative control parameters than would be suggested by the Takács model. Hence, switching to more advanced settler models can potentially benefit the development of many future operation and control strategies. Moreover, this would allow for more advanced control strategies to be de-

4.3. Results and discussion

veloped (for example control of the SBH in order to operate the system at higher sludge concentrations).

4.3.4 Impact of inlet dispersion on predicted effluent concentrations

The dispersion term active around the inlet allows modelling a region of higher turbulence around the feed inlet at increased hydraulic loading. The height of the affected region is related to the incoming flow rate. The effluent concentration will thus be influenced by the incoming feed flow and can be calibrated with the dispersion function and not using the settling function's degrees of freedom as is artificially done nowadays. The problem with the latter is that such an action adapts the settling behaviour at all locations (instead of only in a certain region around the feed inlet) and in a similar fashion in time. Moreover, it changes the wrong mechanism as shear is the reason for the upset in the settler, not the settling properties. Including dispersion will therefore improve predictions in the right zone, i.e. the clarification zone and only during times when hydraulic loading is elevated.

Figure 4.13 shows the effluent concentrations predicted by different settling models. The model by Takács et al. (1991) predicts higher effluent concentrations than the Bürger-Diehl model without dispersion. The difference in the effluent concentrations is a result of the different boundary implementations. In the traditional models, a small number of layers is used to produce the desired effect of numerical dispersion. This is, however, an incorrect approach, since the user should be able to choose any N based on the desired accuracy and available simulation time. In the Bürger-Diehl model, physical dispersion is treated as a function that can be calibrated independently of N .

It should be noted that neither of the presented models include discrete settling behaviour (i.e. settling of individual flocs rather than function of X) which is the governing settling mechanism in the clarification zone. Therefore, none of these models will be able to accurately predict effluent concentrations, although dynamic trends can be captured qualitatively. Including discrete settling in a 1-D model remains challenging since settling behaviour at very low concentrations is not dependent on the local sludge concentration but on the flocculation state and the Particle Size Distribution (PSD) of the sludge. Hence, these phenomena and their effects on discrete settling should be included to better predict effluent SS concentrations. This will be further discussed in Part III.

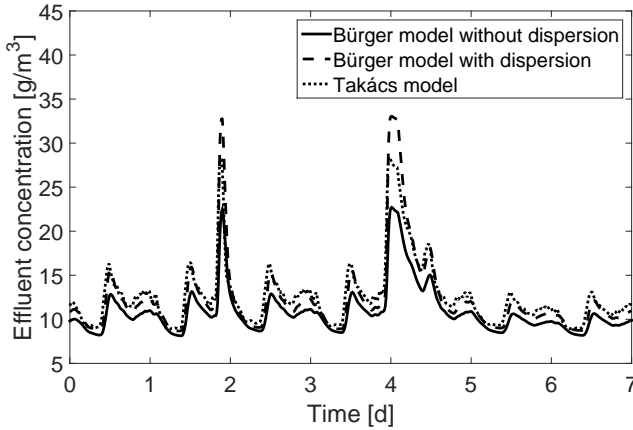


Figure 4.13: Dynamic simulation of the effluent concentration under storm weather conditions.

4.3.5 Practical implications of switching to a more advanced settler model

As the Takács model depends on the numerical dispersion (which is inherent in the model structure) for its simulation results, it should only be used with a 10-layer discretisation (as this approximately mimics dispersion under dry weather). However, Jeppsson and Diehl (1996) demonstrated that a discretisation with 10 layers is too coarse an approximation to capture the detailed dynamic behaviour of the settler. By applying the Godunov scheme for the settling flux and handling the compression term in a mathematically sound way, the Bürger-Diehl model ensures that increasing the number of layers will result in a more accurate approximation of the governing PDE thus producing smaller errors in the underflow concentration. Note that for reasons of comparison, all simulations of the Bürger-Diehl model in this chapter have been performed with the same coarse discretisation level as is required for the Takács model. Their accuracy could easily be improved by a finer discretisation.

To quantify the added value of an increasing number of layers on the model accuracy, simulations at different discretisation levels are compared to a reference simulation with a very fine discretisation (360 layers), which is assumed to be a close approximation of the exact solution. Simulations were performed under both dry and wet weather conditions. The numerical errors in the underflow concentration were quantified by calculating the relative error at each time point t_i as follows:

$$\text{RE}(X_u, t_i) = \frac{|X_{u,360}(t_i) - X_{u,N}(t_i)|}{X_{u,360}(t_i)} \quad (4.5)$$

4.3. Results and discussion

with $X_{u,N}$ the concentration in the underflow, N the discretisation level and $X_{u,360}$ the underflow concentration of the reference simulation with 360 layers.

Calculating the numerical errors of the SBH is less straightforward since the SBH is limited to the layer intervals as determined by the discretisation. Moreover, as the SBH can be zero, the errors are simply quantified as absolute errors:

$$AE(SBH, t_i) = |SBH_{360}(t_i) - SBH_N(t_i)| \quad (4.6)$$

Unlike the underflow error, the error in the effluent concentration will not propagate throughout the system. Furthermore, accurate predictions of effluent concentrations in a 1-D model are currently still troublesome as 1-D models do not include discrete settling behaviour. Therefore the numerical error on the effluent concentration is not shown here.

Figure 4.14 shows the numerical errors in X_u and SBH for simulations with the Bürger-Diehl model with compression. The grey boxes indicate the time-intervals over which the numerical errors were calculated. During dry weather, the errors in the underflow concentration are quite small, even for the 10-layer discretisation. However, during wet weather, when the underflow concentration increases rapidly, the error for the 10-layer discretisation augments up to an average of approximately 10%. By using a 30-layer discretisation this error is reduced to less than 5%. Note that the numerical error will increase if compression settling is not considered since compression somewhat dampens the variations in the underflow concentration.

Also for the SBH a 10-layer discretisation (with a minimum variation of 40 cm) is clearly quite coarse to describe the dynamic behaviour. The numerical error reduces significantly when a 30-layer discretisation is applied.

However, more accurate predictions will inevitably come at a cost of increased simulation time. More layers imply more computations at each time step. Furthermore, the maximum allowed time step of the numerical scheme to ensure a stable and correct solution becomes smaller as the number of layers increases. For explicit fixed-step solvers (such as Euler or RK4) the maximum allowed time step is restricted by the so-called CFL condition, which unfortunately restricts the time step substantially when compression or dispersion is included (details can be found in Bürger et al. (2013)). In recent work Diehl (2014) compared different ODE solvers with respect to their efficiency for the simulation of BSM1 with the Bürger-Diehl model under storm weather conditions. Moreover, they introduced a semi-implicit time-discretisation method for which the simulation time with a 30-layer discretisation was shown to be approximately 7 times faster than a standard explicit solver such as Euler (placing it in the same range of computational effort as a 10-layer simulation with an explicit solver).

These results show that the currently used Takács model can be replaced by the Bürger-

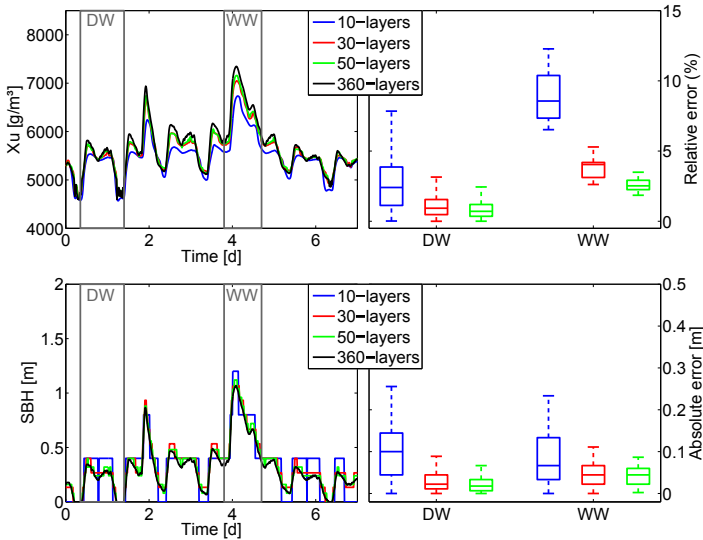


Figure 4.14: Simulated underflow concentrations with corresponding relative numerical errors (top) and simulated sludge blanket heights with corresponding absolute numerical errors (bottom) for different discretisation levels in dry and wet weather conditions (DW and WW).

Diehl model providing a reliable alternative without having to make too many sacrifices with respect to simulation time. Consequently, from the results presented in this section, it is recommended to use a discretisation with at least 30 layers for simulations where the SST is coupled to one or more biological reactors. With a discretisation of 30 layers, the relative errors on the underflow concentration and SBH are reduced significantly while the simulation time is still acceptable. If more detailed simulation results are required from the modelling study or when the settler is modelled as a stand-alone system, the number of layers is recommended to be increased in order to have more accurate predictions.

4.4 Conclusions

In this chapter the impact of the recently proposed Bürger-Diehl settler model on operation and control of a WWTP in comparison to the traditional Takács model is investigated by using the Benchmark Simulation Model No. 1.

- Open- and closed-loop simulations were performed with both settler models during storm weather conditions and the simulated underflow concentration (X_u) and SBH were qualitatively compared to online settler data of the WWTP of

4.4. Conclusions

Eindhoven. It was shown that the Takács model overpredicts the variations in X_u and underpredicts the SBH elevation whereas the Bürger-Diehl model provides more realistic predictions of X_u and SBH behaviour by accounting for compression settling and explicitly modelling the underflow region.

- The impact of the two settler models on the sludge inventory and conversion rates in the bioreactors was investigated as poor predictions of the recycled biomass force modellers to calibrate kinetic parameters for the wrong reasons. A substantial difference of up to 20% for the predicted nitrification rate was observed between the two settler models during storm weather indicating that the choice of settler model influences the simulation results of the entire treatment plant.
- An MLSS-based control strategy was implemented. Simulation results showed that operating a SST calls for more conservative control parameters than would be suggested by the Takács model due to the underprediction of the SBH elevation in this model. In order to improve operation and control of WWTPs, we need to step away from traditional layer models towards more sophisticated models such as the Bürger-Diehl model.
- Simulations were performed with and without inlet dispersion and the impact on the effluent concentration was investigated. By accounting for inlet dispersion an increase in effluent concentration due to high loading rates can be calibrated. Dispersion is thus modelled as a separate constitutive function instead of artificially imposing a desired level of numerical dispersion by fixing the discretisation at a small number of layers. However, accurate prediction of effluent concentrations requires further research into the discrete settling behaviour in the clarification zone. This will be discussed in Part III.
- Although the Bürger-Diehl model is not associated with a fixed number of layers, it was found that a discretisation of the model with 30 layers provides an acceptable trade-off between model accuracy and required simulation time.

Chapter 4. Impact of secondary settling tank models on the development of operation and control strategies for WWTPs

CHAPTER 5

Parameter estimation and identifiability analysis of the Bürger-Diehl settler model

Redrafted from: Torfs, E., Vlasschaert, P., Amerlinck, Y., Diehl, S., Bürger, R., and Nopens, I. (2013b). Towards improved 1-D settler modelling: calibration of the Bürger model and case study. In *Proceedings of 86th Annual Water Environment Federation Technical Exhibition and Conference (WEFTEC)*, Chicago, Illinois, USA, October 5-9.

Abstract

In the previous chapter it was shown that the new 1-D model by Bürger et al. (2011, 2013) allows for more realistic predictions of underflow concentration and SBH by accounting for compression settling. However, the addition of a compression function in this new 1-D model complicates the model calibration. The specific objective of this chapter is to calibrate the Bürger-Diehl model for a full-scale WWTP based on well-known settling velocity tests. The hindered settling velocity functions by Vesilind (1968) and Takács et al. (1991) were calibrated based on the linear slopes of batch settling curves at different concentrations. Both settling velocity functions gave a good fit to the experimental data but identifiability issues were observed for the function of Takács et al. (1991) resulting in very large confidence intervals for its parameters. Subsequently, the calibrated Vesilind settling velocity was implemented in the Bürger-Diehl model and the parameters of the additional compression function were calibrated by fitting the model to the batch settling curves. Also for the parameters of the compression function, identifiability issues were observed. Moreover, 1-D model simulations with calibrated functions for hindered and compression settling were not able to simultaneously describe all batch curves with a single parameter set. Batch curves for different initial concentrations seemed to require different compression dynamics. These results suggest that further investigation into more suitable constitutive functions

is required.

5.1 Materials and methods

5.1.1 Constitutive functions for the Bürger-Diehl model

To describe the hindered settling velocity, the exponential settling function by Vesilind (1968) (Eq. 5.1) and the double exponential settling function by Takács et al. (1991) (Eq. 5.2) are selected as these are most commonly used to date. The original function by Takács et al. (1991) (Eq. 2.2) with five parameters was hereby simplified to include only three parameters: V_0 , r_H and r_P (Eq. 5.2). This can be justified as $V_{0,max}$ and X_{min} present arbitrary parameters to better mimic the settling behaviour in the clarification zone. As the goal of this chapter is to calibrate hindered and compression settling (based on data of sludge blanket heights), including these parameters will unnecessary complicate the calibration process.

$$v_{hs} = v_0 \cdot e^{-r_V \cdot X} \quad (5.1)$$

$$v_{hs} = v_0 \cdot (e^{-r_H \cdot X} - e^{-r_P \cdot X}) \quad (5.2)$$

Compression settling is characterised by Eq. 4.2. Accounting for compressive settling thus requires the calibration of two additional model parameters α and X_{crit} .

Since this study focusses mainly on the calibration of the sludge settling behaviour and not on the hydraulics of the settling tank, inlet dispersion is not considered ($d_{disp}=0$).

5.1.2 Data collection

To calibrate the novel 1-D model data was collected at 3 different WWTPs: the WWTP of Destelbergen (Belgium), the WWTP of Roeselare (Belgium) and the WWTP of Eindhoven (The Netherlands). At each treatment plant sludge samples were collected from the underflow of the SSTs and effluent samples were collected from the overflow weirs.

The settling behaviour of each collected sludge sample was characterised during a series of batch settling experiments. The batch settling experiments were performed in a cylindrical reservoir with a volume of 1.5 L and a diameter of approximately 9 cm. The reservoir was filled with a sludge sample at a certain initial solids concentration after which the position of the suspension/liquid interface was measured after 0, 0.5, 1, 2, 3, 4, 5, 7.5, 10, 15, 20, 30 and 45 min of settling. This methodology is illustrated in

5.1. Materials and methods

Figure 5.1 where the positions of the suspension/liquid interfaces during experiments at different initial concentrations are indicated by the red arrows.



Figure 5.1: Photograph of a batch settling tests indicating the suspension/liquid interface

To investigate the settling behaviour as function of the solids concentration batch settling data need to be collected at different initial solids concentrations. Therefore, a dilution series was made by diluting sludge samples from the underflow of the SST with effluent from the same WWTP. The settling tests were performed with dilutions of respectively 100%, 80%, 60%, 40% and 20% of sludge from the underflow of the SST.

It should be noted that a diameter of 9 cm is quite small for a batch settling reservoir and significant wall effects have been known to occur during settling in such small reservoirs. Consequently, the measured settling behaviour may deviate from the corresponding behaviour in a full-scale SST and estimated parameters should not be extrapolated. However, the estimated parameters can be used to model the data from which they were derived and as such these data serve as valuable information to assess a SST model's ability to describe the dynamics of hindered and compression settling.

5.1.3 Parameter estimation

The optimal parameters for the constitutive functions in the Bürger-Diehl model are determined through the minimisation of an objective function that quantifies the quality of the model's fit to the experimental data. For the calibration exercise in this chapter the Sum of Squared Errors (SSE) calculated by Eq. 5.3 is selected as objective function. In this equation N is the number of data points, y_i the measured value at time i and $\hat{y}_i(\theta)$ the corresponding model prediction for a certain parameter set θ .

$$\text{SSE} = \sum_{i=1}^N (y_i - \hat{y}_i(\theta))^2 \quad (5.3)$$

Finding the optimal parameter set that corresponds to a minimum value for the objective function requires an efficient search of the parameter space. As a highly accurate solution to the optimisation problem is not required (since the data are already subjected to measurement noise), the simple and quick Simplex iteration algorithm was used here (Nelder and Mead, 1965).

5.1.4 Confidence intervals

To check the quality of the parameter estimations, confidence intervals are calculated. The confidence intervals can be determined by using the error covariance matrix $C_H(\hat{\theta})$. However, calculating this matrix requires the inverse of the Hessian of the objective function which can be quite cumbersome to compute. Therefore, the inverse of the Fisher Information Matrix (FIM) is used as an approximation of the error covariance matrix (Donckels, 2009). The FIM can easily be calculated through eq. 5.4 as it only requires a matrix with the measurement errors Q (eq. 5.5) and the local sensitivity functions $\left(\frac{\partial y}{\partial \theta}\right)_i$ at each time instant i for which experimental data is collected.

$$\text{FIM} = \sum_{i=1}^N \left(\frac{\partial y}{\partial \theta}\right)_i^T Q_i \left(\frac{\partial y}{\partial \theta}\right)_i \quad (5.4)$$

$$Q = \begin{bmatrix} \frac{1}{\sigma_1^2} & 0 & 0 & \cdots & 0 \\ 0 & \frac{1}{\sigma_2^2} & 0 & \cdots & 0 \\ 0 & 0 & \ddots & \ddots & \vdots \\ 0 & 0 & 0 & \ddots & \vdots \\ 0 & 0 & 0 & \cdots & \frac{1}{\sigma_N^2} \end{bmatrix} \quad (5.5)$$

The local sensitivity functions are computed by a numerical approximation as described in Eq. 5.6. In this equation y is the model output and θ a model parameter. $\Delta\theta$ can be calculated by $p\theta$, where p is the perturbation factor. Here, a perturbation factor of 10^{-5} is used to ensure an adequate approximation of non-linearities in the model without risking interference of numerical errors.

$$\frac{\partial y(t)}{\partial \theta} = \lim_{\Delta\theta \rightarrow 0} \frac{y(t, \theta + \Delta\theta) - y(t, \theta)}{\Delta\theta} \quad (5.6)$$

5.1. Materials and methods

Finally, the confidence intervals of the estimated parameters can be calculated from the FIM with eq. 5.7, where t_{N-p}^α is the two-tailed t-distribution, with N the number of data points, p the number of estimated parameters, α the significance level and where $\text{FIM}^{-1}(i, i)$ is the element on row i and column i of the inverse of the FIM.

$$\delta_i = \pm t_{N-p}^\alpha \sqrt{\text{FIM}^{-1}(i, i)} \quad (5.7)$$

5.1.5 Identifiability of the model parameters

A Global Sensitivity Analysis (GSA) was applied to investigate the identifiability of the estimated parameters. This GSA was performed with the Brute-Force Monte Carlo (BFMC) method developed by Beven and Binley (1992).

To execute the BFMC method, a large number of simulations are performed each using a different parameter set sampled from an a priori defined parameter space. The latter can be based on expert knowledge, literature findings or previously calculated confidence intervals. Subsequently, the simulations are classified into behavioural and non-behavioural simulations depending on whether or not they provide a satisfactory fit to the experimental data. To facilitate this classification, each simulation is evaluated by an objective function. When the value of the objective function is above an a priori defined threshold value, the simulation is marked as behavioural (Saltelli et al., 2008). The objective function is shown in Eq. 5.8. (Note that this function is closely related to the objective function used for parameter estimation.)

$$\ln |L| = - \sum_{i=1}^N ((\hat{y}_i - y_i) W(i))^2 \quad (5.8)$$

In this equation, L represents the likelihood, N the number of data points, \hat{y} the model outputs, y the measured data and W a vector of weighting factors. The choice of the weighting factors will be explained in the next sections.

The BFMC method is illustrated in Figure 5.2. The left graph shows the different model runs vs. the experimental data. In the right graph the values of the objective function for each run are plotted as a function of the value of (one of) the parameter(s). Behavioural runs are indicated in grey whereas non-behavioural runs are indicated in black. By plotting the values of the likelihood as a function of the parameter values, the identifiability of the model parameters can be investigated. If the objective function shows a clear maximum in a narrow range of parameter values, this parameter has a distinct optimum and is thus identifiable. However, if the behavioural runs are spread over a very broad parameter range, no clear optimum can be found which indicates that the parameter is not identifiable.

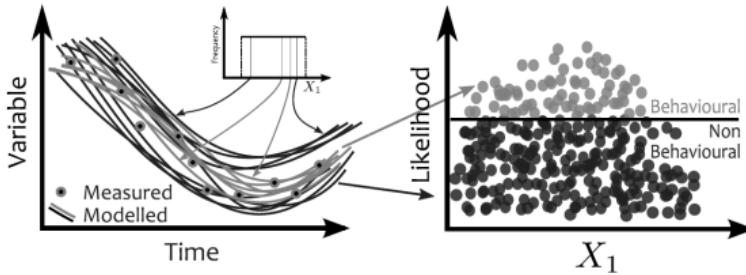


Figure 5.2: Representation of the BFMC-method.

In order to facilitate the interpretation and visualisation of the results, all likelihood values in this chapter are rescaled to obtain values between 0 and 1. Rescaling was done according to the following equation:

$$L_{\text{rescaled}} = \frac{L - L_{\min}}{L_{\max} - L_{\min}} \quad (5.9)$$

5.2 Results and discussion

Only the results for the WWTP of Destelbergen are shown in this chapter. However, all conclusions drawn are valid for each of the cases. The results for the WWTPs of Roeselare and Eindhoven can be found in Appendices A and B.

5.2.1 Calibration of the hindered settling velocity

Determining the hindered settling velocity from batch settling experiments

A number of batch settling experiments are carried out with sludge from the underflow at different dilutions. The sludge concentration of the sample is determined by a Total Suspended Solids (TSS) test according to method 2540 D of Standard Methods (Eaton et al., 1995). During the batch settling tests the height of the suspension/liquid interface is measured at several time instances resulting in a curve with the evolution of the sludge blanket height for each dilution (Figure 5.3).

The hindered settling regime is characterised by an equilibrium between the gravitational forces causing particles to settle and the hydraulic friction forces resisting this motion. Therefore, all particles settle collectively as a zone and the sludge blanket height will show a linear descent. The concentration in the hindered settling region is uniform and equal to the initial solids concentration of the batch. Hence, the slope

5.2. Results and discussion

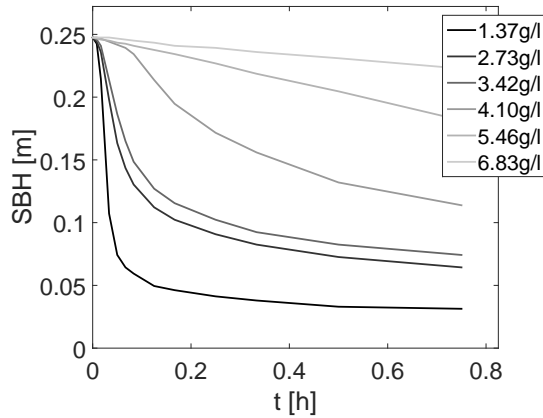


Figure 5.3: Batch settling curves for different initial solids concentrations with sludge from the WWTP of Destelbergen.

of the linear part of a batch settling curve at a certain initial solids concentration corresponds to the hindered settling velocity at this concentration, providing the initial concentration is lower than X_{crit} . (Once the initial concentration is higher than X_{crit} the sludge is already undergoing compression at the start of the experiment making it impossible to have an independent measurement of the hindered settling velocity.) By calculating the slopes of the linear part of the batch curves for different initial concentrations, the hindered settling velocity can be determined as a function of the solids concentration.

The hindered settling velocity for the data in Figure 5.3 was computed in MATLAB[®] by determining the steepest slope between three consecutive datapoints. This procedure is illustrated in Figure 5.4 (left) and the resulting velocities are presented in Figure 5.4 (right) and Table 5.1.

Table 5.1: Measured hindered settling velocities at different initial concentrations

Concentration (g/l)	v_{hs} (m/h)
1.37	4.39
2.73	2.01
3.42	1.53
4.10	0.46
5.46	0.09
6.83	0.05

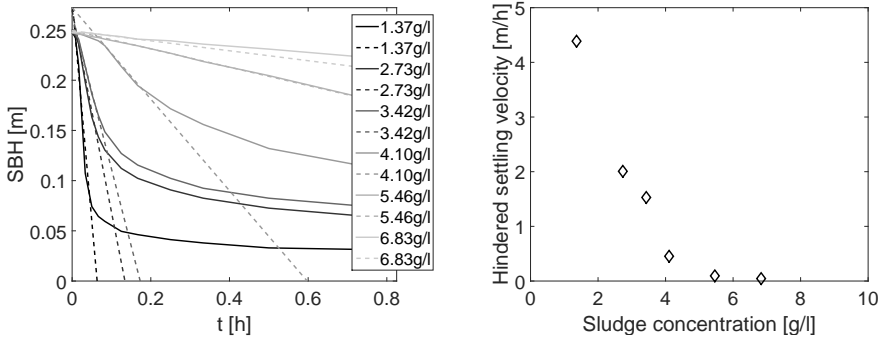


Figure 5.4: Batch settling experiments at different initial solids concentrations with indication of the maximum slope for each curve (left). The maximal slope represents a measurement of the hindered settling velocity (right).

These experiments thus provide direct measurements of the hindered settling velocity which can be used to estimate the parameters of the hindered settling functions by minimising the objective function defined in Eq. 5.3. The results of this parameter estimation will be discussed later on in this chapter.

Calibration by empirical relations based on SSPs

In practice people prefer to avoid the rather time-consuming batch experiments. However, without the batch settling data to provide direct measurements of the hindered settling velocity, they need to rely on empirical relations to obtain values for the hindered settling parameters. Several empirical equations that relate the hindered settling parameters of the function of Vesilind (1968) to simple measurements of Sludge Settleability Parameters (SSPs) have been described in literature (Härtel and Pöpel, 1992; Koopman and Cadee, 1983; Pitman, 1984).

Typical SSPs are the Sludge Volume Index (SVI), Diluted Sludge Volume Index (DSVI) and Stirred Specific Volume Index at 3.5 gMLSS/l (SSVI_{3.5}). The SVI is defined as the volume of 1 g of settled sludge after 30 minutes of settling. DSVI and SSVI_{3.5} are both extensions of the standard SVI-test where the sludge is either diluted to avoid very high sludge concentrations as this may influence the results (DSVI) or a fixed sludge concentration of 3.5 g/l in combination with gentle stirring is applied (SSVI_{3.5}). More information on the measurement procedures can be found in Ekama et al. (1997).

In this section, the validity of these empirical relations to estimate the hindered settling parameters is investigated. Therefore, a single SVI-, DSVI- and SSVI_{3.5} test were performed with sludge from the underflow of the WWTP of Destelbergen. The results are shown in Table 5.2.

5.2. Results and discussion

Table 5.2: Measured SSPs in ml/g for sludge from the WWTP of Destelbergen

Test	SSP (ml/g)
SVI	99
DSVI	83
SSVI _{3.5}	105

The measured SSP values from Table 5.2 were subsequently used to calculate the hindered settling parameters v_0 and r_V according to three different empirical equations from literature (Härtel and Pöpel, 1992; Koopman and Cadee, 1983; Pitman, 1984). The empirical equations and the resulting parameters are given in Table 5.3.

Table 5.3: Estimated values for v_0 (m/h) and r_V (l/g) by empirical relations based on SSPs

Reference	Equations	Parameter values
Härtel and Pöpel (1992)	$v_0 = 17.4 e^{-0.0113 \text{ SVI}}$ $r_V = -0.9834 e^{-0.00581 \text{ SVI}} + 1.043$	$v_0 = 9.647$ $r_V = 0.488$
Koopman and Cadee (1983)	$\ln(v_0) = 2.605 - 0.00365 \text{ DSVI}$ $r_V = 0.249 + 0.002191 \text{ DSVI}$	$v_0 = 9.993$ $r_V = 0.431$
Pitman (1984)	$\frac{v_0}{r_V} = 67.9 e^{-0.016 \text{ SSVI}_{3.5}}$ $r_V = 0.88 - 0.393 \log\left(\frac{v_0}{r_V}\right)$	$v_0 = 5.669$ $r_V = 0.446$

The validity of these empirical relations is examined by simulating the function of Vesilind (1968) with the parameter values predicted by each of the equations from literature. Subsequently, the results are compared to the measured hindered settling velocities (Table 5.1) in Figure 5.5.

Figure 5.5 shows that the function of Vesilind (1968) calibrated using any of the empirical equations is not able to describe the measured data. This could be expected as sludges with a similar SVI may show a different settling behaviour depending on the sludge properties. Moreover, when using the empirical relations, two parameters are estimated based on only one data point. The SSPs thus provide insufficient information to describe the settling behaviour at different sludge concentrations. For these reasons, it can be concluded that the use of empirical relations based on SSPs is not a valid method to estimate the parameters of the settling functions and should be avoided. The parameter values calculated from the empirical relations can however be used as initial values for further parameter estimation.

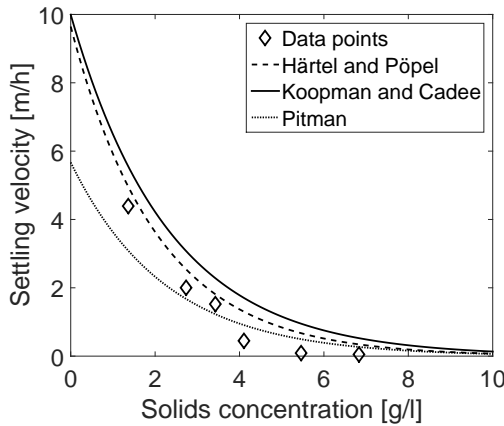


Figure 5.5: Settling velocity as function of the solids concentration. Symbols: measured settling velocities from batch settling tests. Lines: calculated settling velocities by the function of Vesilind (1968) with parameter values based on empirical equations.

Parameter estimation based on batch settling data

As discussed above the hindered settling velocity can be determined from the linear slopes of the batch settling curves resulting in several measurements of hindered settling velocity as a function of sludge concentration. These data points can be used to perform a parameter estimation for the hindered settling velocity functions by Vesilind (1968) and Takács et al. (1991).

Initial parameter estimates for v_0 and r_V/r_H were obtained from the empirical equation of Härtel and Pöpel (1992) (see Table 5.3). The initial value for r_P was set to tenfold the initial value for r_H (Takács et al., 1991). Starting from these initial estimates optimal parameters are found by minimising the SSE between the hindered settling velocities measured from the batch experiments and the velocities predicted by the hindered settling velocity functions (see Section 5.1.3). Confidence intervals were calculated according to the procedure described in Section 5.1.4.

Table 5.4 provides the initial parameter estimates, the optimal parameters after optimisation and the 95% confidence intervals of the estimated parameters. Calculation of the confidence intervals requires knowledge on the measurement errors in order to define the matrix Q (see Eq. 5.5). As the measured sludge blanket heights were determined visually in graduated cylindrical reservoir, their measurement errors depend on the coarseness of the graduation (i.e. 50 ml for the reservoir used). Hence, a measurement error of 20 ml was considered on the measured SBH data. To determine the

5.2. Results and discussion

error on the calculated hindered settling velocities, this error was propagated through the calculation process. By randomly sampling in the interval $[x-20\text{ml } x+20\text{ml}]$ for each data point and calculating the corresponding slopes, a measurement error for the calculated hindered settling velocities is obtained. This measurement error was then used in the matrix Q to calculate confidence intervals on the estimated parameters. The simulation results of both calibrated functions vs. the experimental data points are shown in Figure 5.6.

Table 5.4: Initial values, optimal values and confidence intervals of the estimated parameters of the settling functions

	Initial value	Optimal value	Confidence interval
Vesilind			
v_0 (m/h)	9.647	10.608	± 1.265
r_V (l/g)	0.488	0.634	± 0.038
Takács			
v_0 (m/h)	9.647	82.082	± 11668
r_H (l/g)	0.488	0.989	± 3.316
r_P (l/g)	4.88	1.160	± 3.957

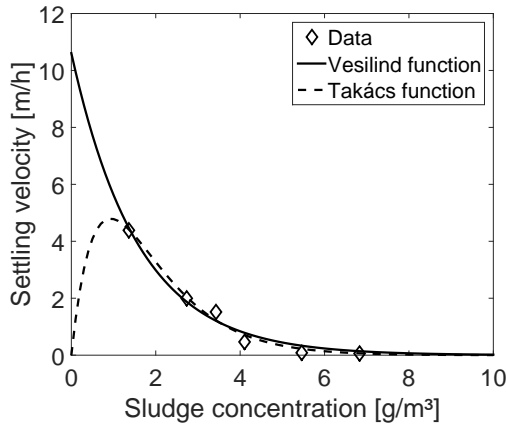


Figure 5.6: Settling velocity as function of the solids concentration. Symbols: measured settling velocities. Lines: calculated settling velocities after calibration of the functions by Vesilind (1968) and Takács et al. (1991).

From Figure 5.6 it can be seen that both hindered settling functions show a good fit to the experimental data. However, some problems with respect to the parameter estimation of the Takács function are observed in Table 5.4. First of all, unrealistically high values are found for the parameter v_0 (representing the maximum settling velocity)

as well as uncommon values for r_P . Values reported in literature are in the order of magnitude of 10 m/h for v_0 and approx. a tenfold of the value of r_H for the parameter r_P (Takács et al., 1991). Moreover, very large confidence intervals are found for the parameters of the function of Takács et al. (1991). These observations indicate that based on the available data, it is not possible to obtain an accurate estimation of the optimal parameters of the settling velocity function by Takács et al. (1991).

The decisive difference between both settling velocity functions is that the function of Takács et al. (1991) requires an additional parameter r_P to be estimated. This additional parameter is introduced to capture the decrease in settling velocity at low sludge concentrations (<1 g/l) which is observed in practice. The hindered settling velocity function of Vesilind (1968) predicts unrealistically high settling velocities in this low concentration range. However, introducing the additional parameter r_P in the hindered settling function is a very artificial way to mimic the settling behaviour at low concentrations. In reality, at lower concentrations the sludge follows a completely different settling regime: discrete (flocculent or non-flocculent) settling. During discrete settling the sludge will no longer settle as a zone and no distinct sludge/water interface is formed making it impossible to record a batch settling curve. Hence, as no data is available in the operating range of the parameter r_P , this parameter cannot be properly estimated based on the available data resulting in the large confidence intervals from Table 5.4.

Global sensitivity analysis of the settling functions

To evaluate the identifiability of the calibrated parameters, a global sensitivity analysis is performed with the BFMC-method (Section 5.1.5). Therefore, the settling velocity functions are evaluated 10,000 times with different parameter sets. The following ranges are defined for the different parameters:

- v_0 (Vesilind)=[0-50] m/h
- v_0 (Takács)=[0-200] m/h
- r_V/r_H =[0-2] l/g
- r_P =[0-20] l/g.

The weighting factors in the likelihood function of Eq. 5.8 were set to 1, except for the 2 highest concentrations. Here, the weighting factors were set to 0.2 since it becomes increasingly difficult to determine the linear part of the batch settling curves at high sludge concentrations (see Figure 5.4).

Figure 5.7 and Figure 5.8 show the evolution of the likelihood value across the parameter ranges for both hindered settling functions. Parameter sets that result in a higher likelihood than the initial parameters (derived from the empirical relation of Härtel

5.2. Results and discussion

and Pöpel (1992)) are classified as behavioural and indicated in grey. Non behavioural runs are indicated in black. For the function of Vesilind (1968) (Figure 5.7), it can be observed that all behavioural runs can be found in a relatively small range of parameter values resulting in one unique parameter set to fit the experimental data. The parameters for the settling function of Vesilind (1968) are thus identifiable.

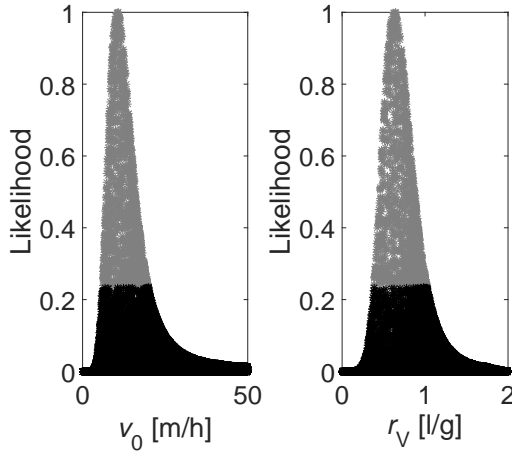


Figure 5.7: Plot of the likelihood as a function of the parameter values for v_0 (left) and r_V (right) of the settling function of Vesilind (1968). Behavioural runs are indicated in grey, non behavioural runs in black.

From Figure 5.8 it can be seen that the optimal values for the parameters of Takács' function are not as clearly defined as was the case for the parameters in the Vesilind function. The parameter r_H shows a clear optimum (similar to r_V) albeit that the behavioural runs are spread over a wider range. For the parameter r_P high likelihood values are found throughout the entire sampling interval indicating that it is not possible to estimate this parameter in a unique way from the available data. Moreover, the identifiability of the parameter v_0 is compromised by the presence of r_P in the parameter estimation exercise as a small fraction of the behavioural runs occurs at very high values of v_0 (Figure 5.9).

The outcome of the BFMC analysis provides further insight into the parameter optimisation problem of the hindered settling velocity. The results in Figure 5.8 confirm that it is not possible to find a unique value for the parameter r_P based on data of batch settling curves. Moreover, including this parameter in the parameter estimation will result in worse predictions for the remaining parameters. A possible solution would be to use a fixed value of r_P when calibrating the hindered settling function of Takács et al. (1991) thus only estimating v_0 and r_H . Calibration of the parameter r_P can then

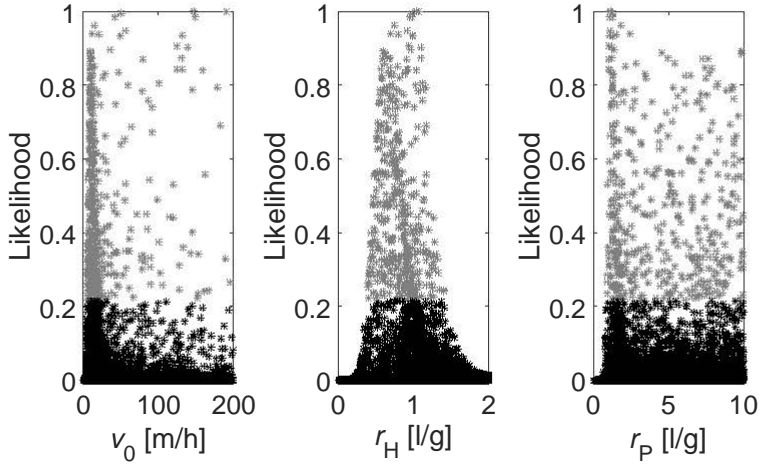


Figure 5.8: Plot of the likelihood value as a function of the parameter values for v_0 , r_H and r_P . Behavioural runs are indicated in grey, non behavioural runs in black.

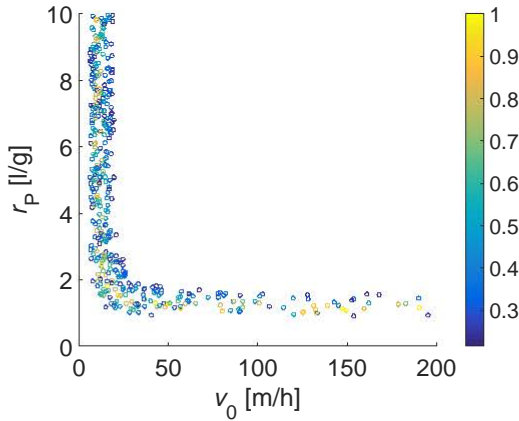


Figure 5.9: Plot of the likelihood values for the different parameter combinations of v_0 and r_P resulting in behavioural runs.

be done at a later stage in the modelling exercise (for example based on data of effluent concentrations). However, this approach poses the risk of altering the settling behaviour in the entire concentration range instead of only at low concentrations. A more rigorous approach would be to step away from the hindered settling function of Takács et al. (1991) that tries to mimic the settling behaviour at low concentrations in an artificial way and to try and capture the true discrete settling regime of the particles

5.2. Results and discussion

at low sludge concentrations in a different expression and collect data to calibrate it. The latter approach requires a completely new framework and will be explored further in Chapter 8.

1-D SST simulation

Once the parameters of the settling velocity function are calibrated, they can be used in a 1-D SST model to simulate the settling behaviour during the batch settling experiments. A model is built in WEST[®] (<http://www.mikebydhi.com>, Denmark) that allows to simultaneously predict batch settling curves at different initial concentrations (Figure ??). Each batch experiment is simulated as a SST with the dimensions of the cylindrical reservoir and an initial concentration corresponding to one of the batch settling tests. Furthermore, the incoming and outgoing fluxes are set to 0. The position of the sludge blanket height is modelled as the first layer where the concentration exceeds 0.9 g/l.

For each SST the Bürger-Diehl model is selected. Due to the aforementioned identifiability issues with the hindered settling function of Takács et al. (1991) and since the settling behaviour in the clarification zone is not of interest when simulating the sludge blanket height, it was chosen to use the settling function of Vesilind (1968) as constitutive function for hindered settling. Compression settling is not considered in these simulations.

Figure 5.10 shows the batch settling data (solid lines) and the corresponding model predictions (dashed lines). The initial steep increase of the SBH (characteristic for hindered settling) is captured well by the model. However, after this initial descent the model underpredicts the SBHs. At low initial solids concentrations this underprediction is small to moderate but the predictions worsen as the initial concentrations increase. As only hindered settling is considered in these simulations, the model overpredicts the settling velocity when sludge starts to thicken causing a severe underprediction of the sludge blanket height at higher sludge concentrations. These results clearly illustrate the need to include compression settling in a 1-D model. The Bürger-Diehl model allows to account for compressive settling as well as hindered settling. However, this requires the calibration of additional parameters for the compression function.

It should be noted that two things were not taken into account in the presented calibration exercise. First, it can be argued that the measured settling curves for initial concentrations of 5.46 g/l and 6.83 g/l are already in the compression phase at the start of the experiment and should thus not be used to estimate the hindered settling parameters. However, when these curves were removed from the parameter estimation exercise the predictions became worse (more explanation on this will be provided in Chapter 6). Second, a clear lag phase is present in the measured settling curve at

4.10 g/l which is not considered in the model. This lag phase can be either removed from the data according to the procedure presented by De Clercq (2006) or explicitly modelled as described in Diehl (2014). However, the conclusions for this chapter do not change if the behaviour in the lag phase is considered.

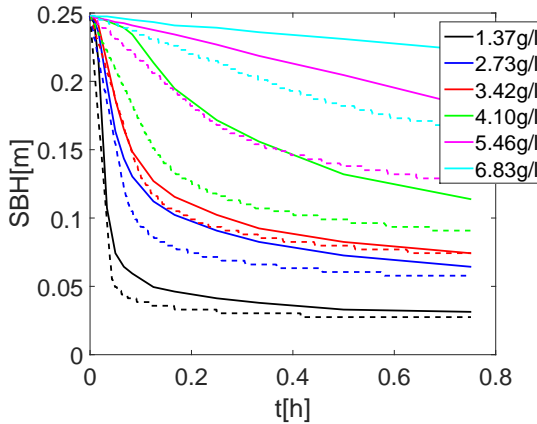


Figure 5.10: Batch settling curves for different initial solids concentrations. Solid lines: measured sludge blanket heights. Dashed lines: sludge blanket heights modelled by the 1-D Bürger-Diehl SST model with the hindered settling functions of Vesilind (1968).

5.2.2 Calibration of the sludge compressibility

The compression term lowers the actual settling velocity at higher concentrations which allows for more realistic predictions of the SBH. This function contains two additional parameters that need to be calibrated: α , an empirical parameter (in m^2/s^2) and X_{crit} , the critical concentration where sludge flocs start to undergo compression (i.e. when they are in physical contact). In contrast to the hindered settling velocity which can be measured directly from the linear slopes of the batch settling curves, no straightforward measurements for compression settling exists. Therefore, the compression function is calibrated by fitting the evolution of the SBHs as predicted by the 1-D model to the full batch settling curves that were recorded during the batch experiments (Figure 5.3).

Given that no a priori knowledge is available on the objective function or the probability of running into local optima, a preliminary screening of the parameter space is performed by means of the BFMC method. This explorative screening provides important information on the identifiability of the parameters, correlations between the parameters and the location of optimal parameter ranges which can then be used in a further optimisation. The following ranges were defined for α and X_{crit} :

5.2. Results and discussion

- α [m^2/s^2]=[0-1.5]
- X_{crit} [g/m^3]=[0-8000]

The BFMC analysis is performed based on 10,000 model runs of the 1-D Bürger-Diehl model with random sampling from the defined parameter ranges. The hindered settling parameters are already calibrated from the procedure described above and are thus kept at a fixed value. Each model run is evaluated by calculating the likelihood function. However, a slight modification was made to the likelihood function of Eq. 5.8. Instead of squaring the errors between the experimental data and the model predictions, the absolute value of the errors was used. As the maximum SBH is only 0.25 m (height of the settling column) the difference between the predicted SBHs and the measured SBHs is always smaller than 1. Squaring these differences would thus reduce the significance of large errors. Figure 5.11 shows the evolution of the modified likelihood values across the parameter ranges for the compression parameters α and X_{crit} . Model runs that provide a better fit to the data than the case with only hindered settling are classified as behavioural.

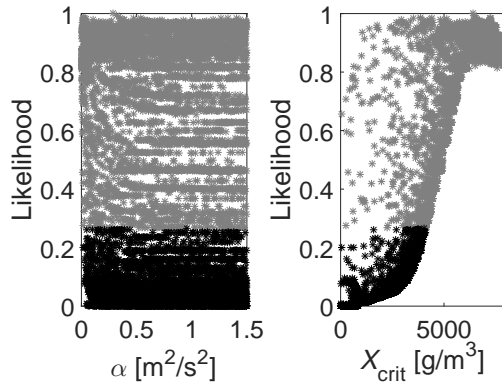


Figure 5.11: Plot of the likelihood in function of the parameter values for α (left) and X_{crit} (right). Behavioural runs are indicated in grey, non behavioural runs in black.

The results of the BFMC-analysis illustrate that behavioural runs are found over a broad range for both parameters. For X_{crit} a clear preference for high parameter values can be observed but some higher likelihood values are also found at low values for X_{crit} . Hence, it is not possible to find a unique optimum for the parameters of the compression function. The reason behind this becomes apparent by visualising the location of the highest likelihood values in the 2-D parameter space (Figure 5.12). A logarithmic trend can be observed indicating a distinct correlation between the parameters. Both the combination of high α and high X_{crit} values as well as the combination of low α and low X_{crit} values provide high likelihood values. Numerous parameter combinations

providing an optimal fit to the data can thus be found signifying that the parameters are not identifiable.

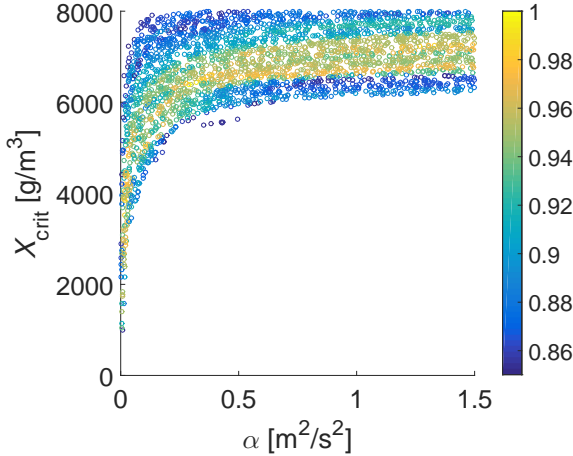


Figure 5.12: Plot of the likelihood in function of different parameter combinations of α and X_{crit} .

The highest value for the likelihood function is found at $\alpha=0.037$ and $X_{crit}=4068$. To investigate the added value of the compression function, simulation results with this parameter set are compared to the experimental data in Figure 5.13.

The 1-D model without compression settling (Figure 5.10) performed reasonably to predict the batch curves at low initial sludge concentrations but severely underpredicted the SBH for higher initial sludge concentrations. Including compression improves predictions at high initial sludge concentrations but at the expense of a lower predictive power for the low initial concentrations. By including compression, elevated SBHs are predicted for all batch settling curves as the settling velocity and consequently the descent of the sludge/water interface is slowed down due to the formation of a compressive network. When considering the simulation results without compression (Figure 5.10) the required elevation of the SBH to match the measured data differs substantially between the batch settling curves suggesting that different amounts of compression are required for different initial solids concentrations. However, as the formation of a compressive network during settling of sludge is a physical phenomenon, the dynamics of this phenomenon should not depend on the initial concentration in the batch column but only be time dependent (i.e. kicking in earlier or later when a certain X_{crit} is reached). Hence, the results in this section demonstrate that the currently selected combination of constitutive functions for hindered settling and compression settling does not succeed in capturing the true settling dynamics. Further investigation into the nature of these constitutive functions is necessary which will be the subject of the next

5.3. Conclusions

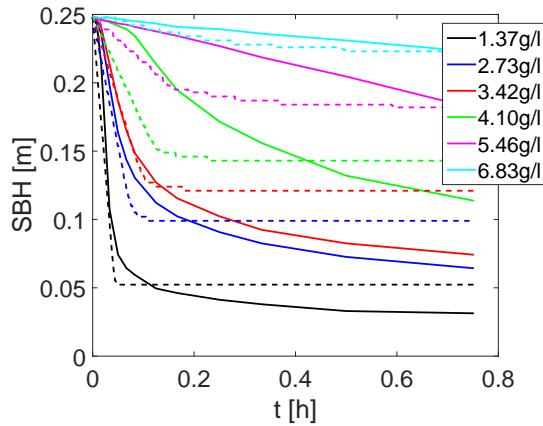


Figure 5.13: Batch settling curves for different initial solids concentrations. Symbols: measured sludge blanket heights. Lines: sludge blanket heights modelled by the 1-D Bürger-Diehl SST model with the hindered settling functions of Vesilind (1968).

chapters.

5.3 Conclusions

The objective of this chapter was to calibrate the 1-D SST model by Bürger et al. (2011, 2013) including a function for hindered settling and a compression function. The identifiability of the calibrated parameters was investigated as well as the model's ability to predict batch settling data.

- The validity of several empirical equations to estimate the parameters of the hindered settling functions by Vesilind (1968) based on simple SSPs was verified. It was found that SSPs provide insufficient information to describe the settling behaviour at different sludge concentrations and that their application to calibrate hindered settling parameters should be avoided.
- The parameters of the commonly used hindered settling function of Vesilind (1968) and Takács et al. (1991) were calibrated based on the linear slopes of batch settling curves at different initial concentrations. Both functions provided a good fit to the experimental data. However, large confidence intervals were found for the parameters of the hindered settling function by Takács et al. (1991).
- The identifiability of the hindered settling parameters was investigated with the BFMC-method. The parameters of the settling velocity function of Vesilind

(1968) were found to be identifiable resulting in a unique optimal set of parameters. The settling velocity function of Takács et al. (1991) is, however, not identifiable. Including an extra term in the hindered settling function to mimic the settling behaviour in the clarification zone reduces the identifiability and reliability of the parameter estimation. Either r_P should be calibrated separately or an alternative approach to model discrete settling at low sludge concentrations should be implemented.

- 1-D model simulations of the batch settling data with the optimised hindered settling function of Vesilind (1968) produced an underestimation of the measured SBH at high initial solids concentrations indicating a clear need to include compression settling in 1-D modelling.
- To calibrate the parameters of the compression function a coarse screening of the parameter space was performed by means of the BFMC-method and the predicted SBHs were compared to the SBH measurements. This revealed clear identifiability issues caused by significant correlation between the parameters.
- 1-D model simulations with an optimal parameter set for the compression function were not able to simultaneously describe all batch curves with a single parameter set. Batch curves for different initial concentrations seemed to require different compression dynamics. These results suggest that the combination of the hindered settling function by Vesilind (1968) and the currently selected compression function is not able to capture the true settling behaviour. Further investigation into more suitable constitutive functions is required.

CHAPTER 6

Critical analysis of constitutive functions for hindered settling velocity in 1-D settler models

Redrafted from: Torfs, E., Balemans, S., Locatelli, F., Bürger, R., Laurent, J., François, P., Diehl, S., and Nopens, I. (2015a). Critical analysis of constitutive functions for hindered settling in 1-D settler models. In *Proceedings of Watermatex2015*, Gold Coast, Australia, June 15-17.

Abstract

Advanced 1-D models for SSTs aim to incorporate more realism by explicitly accounting for several phenomena that influence the settling process. For each of them a valid mathematical expression needs to be selected to obtain a calibrated model that can be used for operation and control. The presented work evaluates different available expressions for hindered settling based on long term batch settling data. The analysis shows that the exponential forms which are most commonly used in traditional SST models not only account for hindered settling but partly lump other phenomena as well. This makes them unsuitable for advanced 1-D models that explicitly include each phenomenon in a modular way. A power-law function is shown to be more appropriate to describe the hindered settling velocity.

6.1 Introduction

The strength of the Bürger-Diehl SST model is twofold. It presents a numerical scheme that is consistent with current PDE-theory to ensure convergence in the solution and it allows the modeller to account for several phenomena (such as hindered settling, sludge compression and inlet dispersion) in a modular way making it very flexible in

its application. However, the latter aspect requires the selection of a set of constitutive functions that are able to describe the dynamics of each of these processes. Eq. 6.1 indicates the different constitutive functions that need to be defined (v_{hs} - hindered settling, d_{comp} - compression settling, d_{disp} - inlet dispersion). Each of these functions can easily be updated or replaced whenever research provides further insight in any of these phenomena. As gravitational settling and compression settling are the governing processes to predict important operating variables such as sludge blanket height and recycle concentration, the selection of constitutive functions for d_{disp} will not be considered here. Note that the compression function in Eq. 6.1 is written in its most general form as all analysis and conclusions in this chapter are made independently of any specific structure for d_{comp} .

$$\begin{aligned}
 \frac{\partial X}{\partial t} = & \\
 & - \frac{\partial}{\partial z} (v_c(t) X) && \text{convective flow} \\
 & - \frac{\partial}{\partial z} (\mathbf{v}_{hs}(\mathbf{X}) X) && \text{gravitational settling} \\
 & + \frac{\partial}{\partial z} \left(\mathbf{d}_{comp}(\mathbf{X}) \frac{\partial X}{\partial z} \right) && \text{compression settling} \\
 & + \frac{\partial}{\partial z} \left(\mathbf{d}_{disp}(\mathbf{z}, \mathbf{Q}_f(t)) \frac{\partial X}{\partial z} \right) && \text{inlet dispersion} \\
 & + \frac{Q_f(t) X_f(t)}{A} \delta(z) && \text{incoming feed flow}
 \end{aligned} \tag{6.1}$$

In the previous chapter it was shown that the combination of the most commonly used hindered settling functions (Vesilind, 1968; Takács et al., 1991) and a compression function based on the work of Bürger (2000) and De Clercq et al. (2008) is not able to accurately predict batch settling data. However, for each of these constitutive functions several alternatives have been presented in literature (Richardson and Zaki, 1954; Vesilind, 1968; Takács et al., 1991; Cho et al., 1993; De Clercq et al., 2008; Diehl, 2014; Ramin et al., 2014b). As hindered settling is active both in the hindered settling regime as well as in the compression regime (with compression settling working as a force against hindered settling), it follows that the hindered settling velocity should be the first function to examine. An inadequate choice for this function can after all impede the selection and calibration process of the remaining functions.

Literature on hindered settling is dominated by exponential and power law functions with the exponential functions being most established in commonly used layer models. However, since hindered settling is the only driving force considered in many of these layer models, the exponential relation may not have been selected for its superiority in describing the phenomenon of hindered settling as such but for its overall performance

6.2. Material and methods

including the ability to partially compensate for missing phenomena. De Clercq et al. (2008) found that an exponential expression for the hindered settling velocity in combination with an expression for compression settling was not able to describe experimental batch settling data whereas a power-law function could. Moving to advanced settler models which try to explicitly account for each phenomenon separately thus requires to re-evaluate available hindered settling functions.

Moreover, a thorough understanding of the different settling regimes requires more detailed data than simple batch settling curves. Hence, this chapter evaluates the validity of different constitutive functions for hindered settling based on detailed data of long-term batch experiments.

6.2 Material and methods

Constitutive functions for hindered settling

Four hindered settling functions are considered in the current analysis: the most commonly used exponential functions of Vesilind (1968) (Eq. 6.2) and Takács et al. (1991) (Eq. 6.3), the power-law function of Cole (1968) (Eq. 6.4) which gave satisfactory results in the work of De Clercq et al. (2008) and finally a power-law function proposed by Diehl (2014) (Eq. 6.5). The latter selected this power-law function based on an extensive study to identify an expression for v_{hs} by solving an inverse problem. In these equations X represents the sludge concentration and V_0 , r_V , r_H , r_P , k , \bar{X} and q are positive parameters to be calibrated.

$$v_{\text{hs}}(X) = V_0 e^{-r_V X} \quad (6.2)$$

$$v_{\text{hs}}(X) = V_0 (e^{-r_H X} - e^{-r_P X}) \quad (6.3)$$

$$v_{\text{hs}}(X) = k X^{-n} \quad (6.4)$$

$$v_{\text{hs}}(X) = \frac{V_0}{1 + \left(\frac{X}{\bar{X}}\right)^q} \quad (6.5)$$

6.2.1 Experimental data

The analysis of these constitutive functions is performed based on two sets of batch settling data. The first dataset was collected by De Clercq et al. (2005) who performed in-depth batch experiments by means of a radio-tracer. These experiments were performed with sludge from the WWTP of Destelbergen (Belgium) at three different initial

concentrations (2.4, 3.23 and 4.3 g/l) resulting in three sets of complete concentration profiles during 6 hours of settling (referred to as Dataset 1).

The second set of data was collected by Locatelli et al. (2015) who applied an ultrasonic velocity profile technique to measure settling velocities within the sludge blanket without disturbing it. The measurements were performed by an ultrasonic transducer which was installed above a settling column to perform vertical measurements of the settling velocity. The ultrasonic velocity profile technique was originally developed by Takeda (1995) who reported the following specifications: a spatial resolution of 0.75 mm, a spatial measurement error of 1.1%, a velocity resolution of 0.75 mm/s and a velocity measurement error of 3.5%, indicating that this methodology provides accurate measurements of the in-depth settling velocity. Locatelli et al. (2015) performed experiments with sludge from the WWTP of Rosheim (France) at 6 different initial concentrations (1.5, 2.7, 3.2, 4.0, 4.6 and 5.6 g/l). As the initial concentration for each experiment is known and the settling velocities are measured, the settling fluxes can be calculated at each time from which changes in concentration can be tracked in order to determine the concentration profile. The experiments thus resulted in 6 sets of complete velocity and concentration profiles during approx. 1 hour of settling (referred to as Dataset 2). Moreover, this dataset was extended with one additional experiment at a concentration of 3.9 g/l where the settling process was monitored during 22 hours of settling.

6.2.2 Akaike's Information Criteria (AIC) for model selection

The performance of the selected constitutive functions with respect to the experimental data can be quantified with a criterium for model selection such as AIC (Burnham and Anderson, 2004). This criterium assesses different model structures taking into consideration their goodness of fit as well as their complexity (Eq. 6.6). Lower values for AIC indicate a better model.

$$AIC = N \log \left(\frac{SSE}{N} \right) + 2p \quad (6.6)$$

In this equation N represents the number of datapoints, p the number of model parameters and SSE the sum of squared errors between the measured and simulated values.

6.3 Results and discussion

6.3.1 Calibration of hindered settling functions

For each dataset the settling parameters of Eqs. 6.2-6.5 were calibrated. Calibration was performed based on the slope of the linear descent of the sludge blankets (Figure 6.1) as described in Chapter 5.

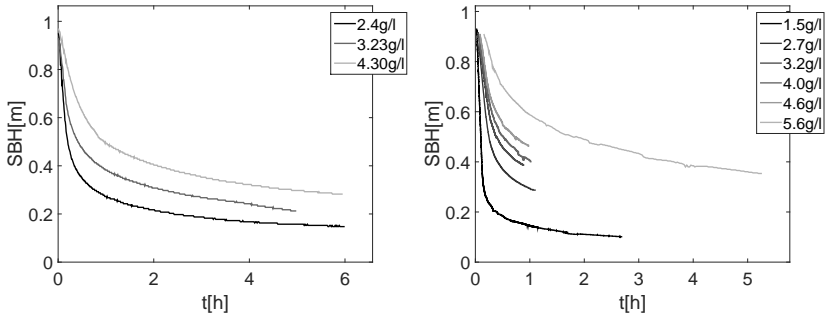


Figure 6.1: Measured SBH data from De Clercq et al. (2005) (left) and Locatelli et al. (2015) (right).

This resulted in three datapoints for the first dataset and 6 datapoints for the second dataset. Subsequently, the parameters for the hindered settling functions were calibrated by solving a least squares problem. The resulting parameter sets and model fits are shown in Table 6.1 and Figure 6.2. In Dataset 1 no confidence intervals could be calculated for the functions of Takács et al. (1991) and Diehl (2014) as for these functions three parameters need to be estimated based on only three datapoints. Hence, the t-test statistic in Eq. 5.7 cannot be calculated. Infinite confidence intervals are found with Dataset 2 for the function of Takács et al. (1991) as the local sensitivity at the measured concentrations is zero for parameter r_P confirming once more that parameter r_P is not identifiable based on hindered settling data.

From Figure 6.2 it can be observed that all four hindered settling functions provide a good fit to the data. The performance of each hindered settling function is quantified with the AIC criterium in Table 6.2 (lowest AIC value for each dataset indicated in bold). Next to the analysis for Dataset 1 and Dataset 2 also the results for the batch settling data from Chapter 5 are included. The power-law functions seem to perform better for the data of Locatelli et al. (2015) whereas the exponential functions perform better for the data of De Clercq et al. (2008) and Chapter 5. In general all four functions produce AIC values in a similar range. Hence, it is difficult to select an optimal constitutive function based on these results.

Table 6.1: Optimal parameter values for the different hindered settling functions.

parameter	Dataset 1	Dataset 2
Vesilind		
V_0 [m/d]	256 ± 81	310 ± 11
r_V [l/g]	0.55 ± 0.09	0.57 ± 0.01
Takács		
V_0 [m/d]	$4.38e5 \pm \text{NaN}$	$310 \pm \infty$
r_H [l/g]	$0.872 \pm \text{NaN}$	$0.573 \pm \infty$
r_P [l/g]	$0.873 \pm \text{NaN}$	$0.025 \pm \infty$
Cole		
k [kg/m ² h]	12.72 ± 4.52	10.11 ± 0.34
n [-]	1.701 ± 0.294	1.423 ± 0.027
Diehl		
V_0 [m/d]	$277 \pm \text{NaN}$	440 ± 165
X [g/l]	$1411 \pm \text{NaN}$	931 ± 0.301
q [-]	$2.0831 \pm \text{NaN}$	1.73 ± 0.112

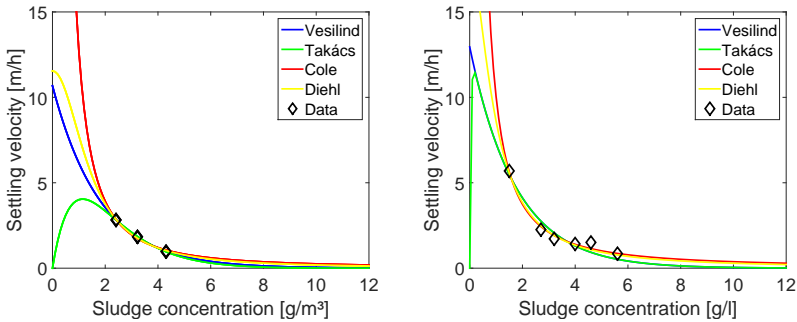


Figure 6.2: Comparison of different hindered settling functions calibrated to measured data of De Clercq et al. (2005) (left) and data of Locatelli et al. (2015) (right).

Table 6.2: Model selection of the different constitutive functions based on Akaike's Information Criterion.

	Vesilind	Takács	Diehl	Cole
Dataset 1	-18.19	-22.55	-10.46	-11.04
Dataset 2	-7.49	-5.49	-11.70	-16.06
Dataset chapter 5	-7.58	-6.92	-6.58	-4.89

6.3. Results and discussion

However, a similar fit to the hindered settling data does not imply similar simulation results when implementing the functions in a 1-D model. Both at low and high concentration ranges (where hindered settling does not occur or cannot be measured separately) differences between the presented functions can influence the predictions of the 1-D model. At low concentrations (<1 g/l) discrete settling prevails (i.e. settling of individual flocs with size as the dominant influence rather than concentration). Including discrete settling in a 1-D model remains challenging and is outside of the scope of this chapter. At concentrations above approx. 6 g/l the differences in predicted settling velocities in Figure 6.2 may seem small, however, from a relative perspective, they are profound. This is illustrated by the more detailed view of the predicted hindered settling velocities at high sludge concentrations in Figure 6.3. In reality, at these higher concentrations hindered settling will be slowed down by the formation of a network of particles that undergo a compressive force. The choice of the hindered settling function in this region will thus be important for the subsequent selection and calibration of a constitutive function for compression.

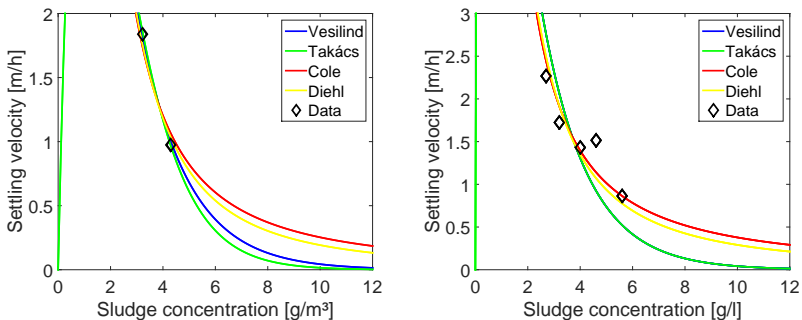


Figure 6.3: Zoom of the predicted hindered settling functions calibrated to measured data of De Clercq et al. (2005) (left) and data of Locatelli et al. (2015) (right) to illustrate differences at high concentrations.

To assess this influence, the hindered settling functions need to be implemented in a 1-D model to see how they perform in predicting SBH data and velocity profiles. One exponential and one power-law function are selected for this further analysis. For the exponential functions, the function of Vesilind is selected due to the identifiability issues observed with the function of Takács in Chapter 5 and Table 6.1. The power-law functions are represented by the function of Diehl. The latter choice was made from an implementation perspective. As can be seen from Figure 6.2 the function of Cole goes to infinity when X approaches 0. Hence, implementing this function in a 1-D model requires an additional settling function for low solids concentrations. The settling behaviour at low concentrations is however not yet fully understood nor can it be properly modelled to date.

6.3.2 Impact of different hindered settling functions on long-term SBH predictions

The hindered settling functions of Vesilind (Eq. 6.2) and Diehl (Eq. 6.5) are implemented in the Bürger-Diehl settler model (discretised with 90 layers) and used to simulate the experimental batch settling data. For the first dataset, the resulting predictions of SBH are provided in Figure 6.4.

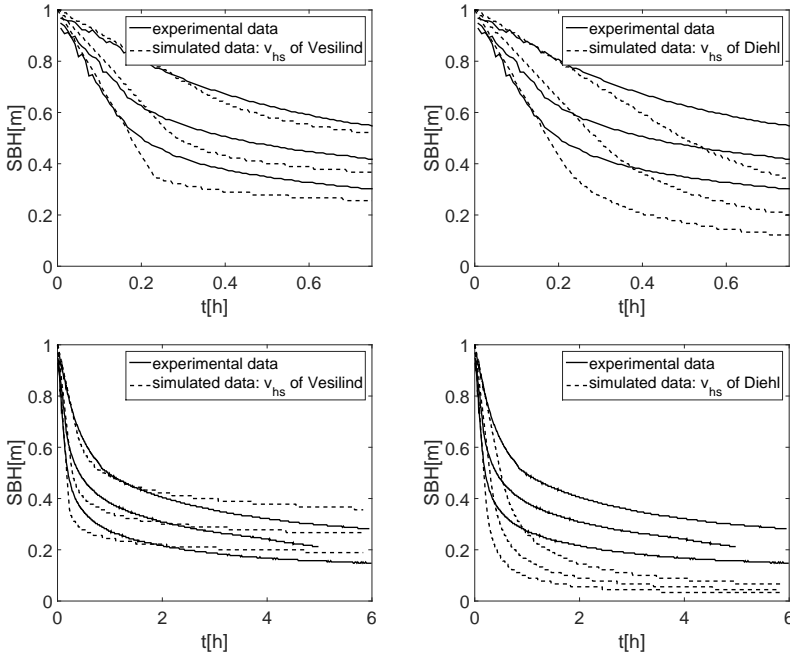


Figure 6.4: Measured SBHs (solid line - from De Clercq et al. (2005)) and predicted SBHs (dashed lines) by the Bürger-Diehl model with only hindered settling. Left: hindered settling function of Vesilind (1968), right: hindered settling function of Diehl (2014). Results during first 45 min of batch settling (top) and 6 hours of settling (bottom).

First, the SBH predictions during the first 45 minutes of settling are investigated (shown at the top of Figure 6.4) as this is the typical duration of batch settling experiments. For both hindered settling functions the 1-D model performs well in predicting the initial linear descent of the sludge blanket but the models underpredict the SBH once the curve of the SBH starts to bend (corresponding to the onset of compression settling). This underprediction is much larger for the hindered settling function of Diehl. From a modelling point of view, the underprediction is as expected. A 1-D model that only accounts for hindered settling will evidently overpredict the settling velocity

6.3. Results and discussion

at high concentrations and thus underpredict the SBH since it disregards the gradual compressibility that the formed particle network undergoes. To include more physical realism a compression function should be added which further slows down the settling velocity at high solids concentrations causing the sludge blanket to descend less rapidly.

However, as the dataset collected by De Clercq et al. (2005) provides data of up to 6 hours of settling these effects can be investigated in more detail. Therefore, the full measurements and simulation results for 6 hours of settling are shown at the bottom of Figure 6.4. These results clearly show that the 1-D model simulations with the exponential function of Vesilind perform much better in describing the overall trend in the experimental data. However, from a physical perspective these predictions do not make any sense. The predictions switch from an underprediction of the SBH (at $t < 2\text{h}$) to an overprediction of the SBH (at $t > 2\text{h}$) whereas we expect the SBH to be underpredicted over the entire experiment since no compression settling is taken into account. Hence, using an exponentially decaying function to describe hindered settling does not only account for hindered settling but already (unintentionally) lumps in some compressive behaviour (by predicting very low values for v_{hs} at high sludge concentrations - see Figure 6.3). Although this results in a model that performs relatively well in predicting the general trends, it will hamper further efforts to include more realism in 1-D models by accounting for other phenomena such as compression. Adding any type of compression function will decrease the settling velocity at higher concentrations and thus increase the predicted SBHs resulting in somewhat better predictions for $t < 2\text{h}$ but much worse predictions at $t > 2\text{h}$. The power-law function suggested by Diehl (2014) does perform as expected from a hindered settling function, i.e. an underprediction of the SBH over the entire time-interval and can thus be combined with a constitutive function for compression settling to obtain a more advanced 1-D model that accounts for both hindered and compression settling. Note that the seemingly small differences in v_{hs} predictions at high concentrations that were observed in Figure 6.2 cause considerable differences in SBH predictions and should not be ignored.

6.3.3 Impact of different hindered settling functions on velocity profile predictions

These findings were further validated on the second dataset by Locatelli et al. (2015) which provided experimental data of the settling velocity as well as the concentrations over the entire depth of the settling column during 22 hours of settling at an initial concentration of 3.9 g/l. The measured velocity and concentration profiles were compared to 1-D simulation results with the hindered settling functions of Vesilind (1968) and Diehl (2014) in the Bürger-Diehl model (discretised with 90 layers). Both experimental measurements and simulation results consist of data in three dimensions (velocity, time and depth). To facilitate the visualisation, the experimental data and the simu-

lation results are presented in two dimensions from two different viewing points in Figure 6.5. The left side of Figure 6.5 shows the evolution of the velocity profile as a function of time and the right side shows the evolution of the sludge blanket height as a function of time. The most important features of the batch profiles are further summarized in Table 6.3.

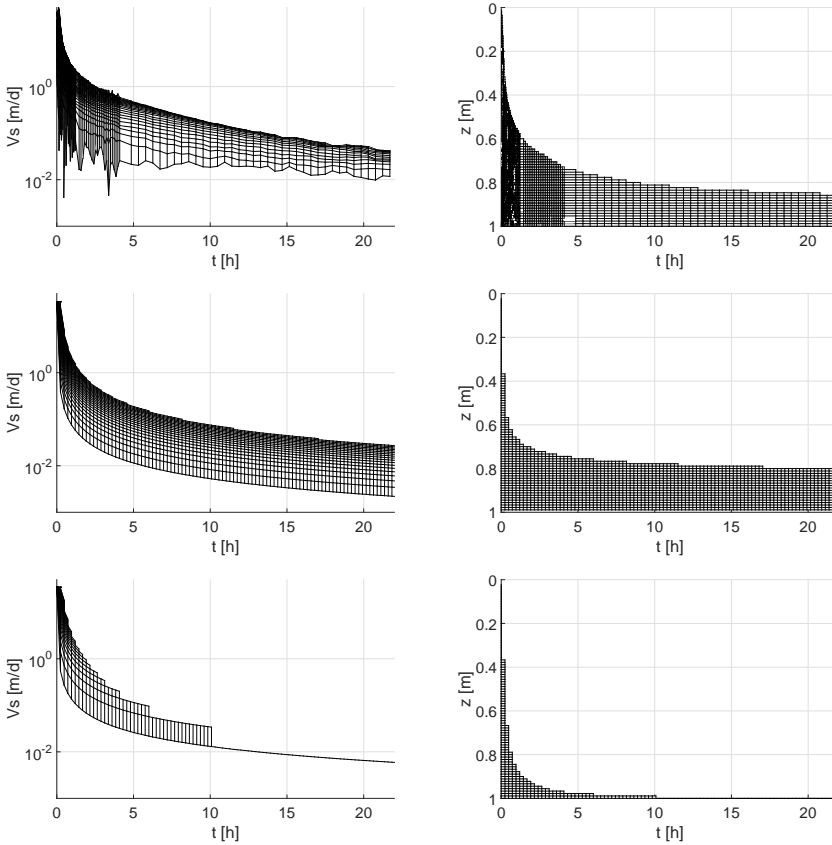


Figure 6.5: Velocity profiles inside the sludge blanket (left) and evolution of the SBH (right) for a batch settling experiment at an initial concentration of 3.9 g/l. Experimental data (top), simulation with the settling velocity of Vesilind (middle) and simulation results with the settling velocity of Diehl (bottom).

First, the simulation results with the commonly used exponential function of Vesilind are evaluated with respect to the experimental data. Comparing the SBHs between the experimental data and the model predictions leads to similar observations as in the previous section. The model with the hindered settling velocity of Vesilind over-

6.3. Results and discussion

Table 6.3: Comparison of important features between the experimental data of Locatelli et al. (2015) and 1-D simulations with the calibrated hindered settling functions of Vesilind and Diehl after 22 hours of settling

	Exp. data	1-D simulations	
	Locatelli et al. (2015)	v_{hs} of Vesilind	v_{hs} of Diehl
SBH [m]	0.15	0.21	0.02
$v_{s,bottom}$ [m/s]	0.0124	0.0022	0.0059
$v_{s,SBH}$ [m/s]	0.0380	0.0027	0.0200
X_{bottom} [g/l]	32.0	21.8	315.6
X_{SBH} [g/l]	9.0	10.5	31.6

predicts the SBH at long settling times (predicted value of 0.21 m vs. a measured value of 0.15 m) indicating that it predicts settling velocities that are too low at higher sludge concentrations. This is further confirmed through the analysis of the velocities and concentration values. Where the 1-D model with the hindered settling velocity of Vesilind predicts a sludge concentration similar to the measured value at the height of the sludge blanket, the predicted velocity is approx. 10 times smaller. At the bottom of the batch reservoir, this effect is even more pronounced with a measured concentration much higher than the predicted concentration even though the measured velocity still exceeds the predicted value. In summary, the prediction of low velocities at high concentrations in the commonly used exponential hindered settling functions hamper the thickening behaviour resulting in underpredictions of the bottom concentration and overpredictions of the SBH making these functions unsuitable to combine with a compression function in advanced 1-D models.

The simulation results with the power-law hindered settling velocity of Diehl (2014) show a remarkably different behaviour. The model predicts a sludge blanket of only two layers thick and an extremely concentrated bottom layer. Intuitively, this may seem strange, however, from a theoretical point of view this behaviour corresponds to what is expected from a hindered settling function. Without the presence of a compressive stress the particles can thicken at will resulting in an integral accumulation of particles in the bottom layer.

If the modelling study requires a very simplified settler model (i.e. only accounting for hindered settling), an exponential settling function is clearly the best choice as it partially lumps other phenomena thus enforcing more realism. However, if these simplified settler models do not suffice for the objective of the modelling study (as is often the case for example in dynamic wet weather simulations in WWTP modelling) these models cannot simply be extended with additional phenomena such as compressive settling. A more advanced settler model that explicitly accounts for each phenomenon should be applied. For the latter models a power-law type function is found more

appropriate in describing the hindered settling behaviour. This can subsequently be extended with a compression function for more accurate predictions of the sludge settling behaviour. The choice of the compression function will be discussed in the next chapter.

6.3.4 Identifiability of the power-law functions

Following the identifiability analysis that was performed for the exponential hindered settling functions in Chapter 5, the parameter identifiability for the power-law functions of Diehl (2014) and Cole (1968) are investigated here. Each hindered settling function was evaluated 10,000 times for different parameter combinations and the likelihood function (Eq. 5.8) was calculated for each simulation. The threshold for behavioural runs was set to a value of 0.8. Figures 6.6 and 6.7 present the results for the power-law functions of Diehl (2014) and Cole (1968), respectively.

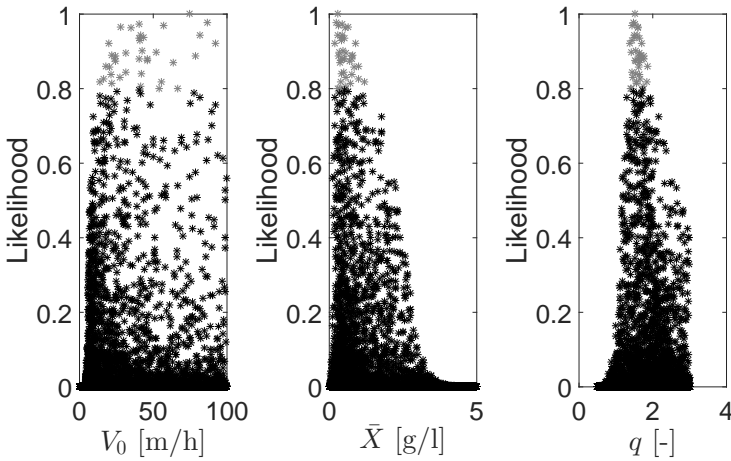


Figure 6.6: Plot of the likelihood value as a function of the parameter values for V_0 , \bar{X} and q of the hindered settling function of Diehl (2014). Behavioural runs are indicated in grey, non behavioural runs in black.

Whereas the parameters \bar{X} and q in the function of Diehl (2014) show a distinct optimum, optimal values for the parameter V_0 are found in a broad interval. Hence, the parameter V_0 is not identifiable based on the available data. The parameter V_0 defines the intersection with the Y-axis (i.e. the maximum value of the settling velocity at a concentration of zero) and will exert its main influence on the settling behaviour at low sludge concentrations (as indicated by the local sensitivity analysis in Figure 6.8). Similarly as for the parameter r_P in the settling function of Takács et al. (1991) identifiability issues arise due to a lack of data in regions of low sludge concentrations. The

6.4. Conclusions

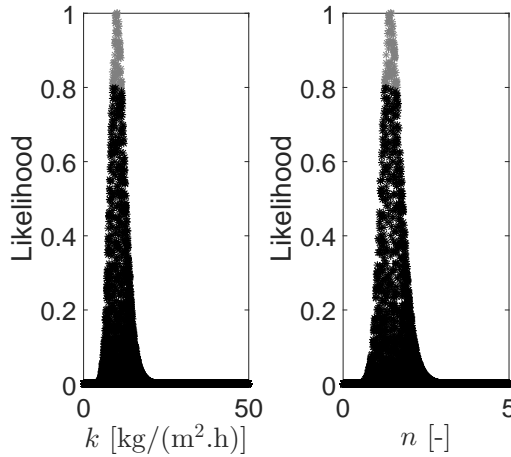


Figure 6.7: Plot of the likelihood as a function of the parameter values for k and n of the hindered settling function of Cole (1968). Behavioural runs are indicated in grey, non behavioural runs in black.

power-law function of Cole (1968) with only two parameters does not show any identifiability issues. However, it is not able to model the settling behaviour at low sludge concentrations as it predicts settling velocities up to infinity in this region. These results demonstrate once more the need to develop a novel approach to model the discrete settling behaviour at low sludge concentrations which will be investigated further in Part III.

6.4 Conclusions

Two types of hindered settling functions were examined. The exponential relations as presented by Vesilind (1968) and Takács et al. (1991) and power-law type functions as presented by Cole (1968) and Diehl (2014). The behaviour of these functions was evaluated based on long-term data of SBHs, concentration profiles and velocity profiles.

- The most commonly used exponential hindered settling functions produce contradictory results when confronted to long term batch data. At long settling times they underestimate the thickening behaviour of sludge resulting in SBH predictions that are too high and bottom concentrations that are too low. This behaviour does not correspond to the concept of hindered settling indicating that they do not only account for hindered settling but partially lump in compression in their model structure as well. One needs to bear in mind that the inclusion

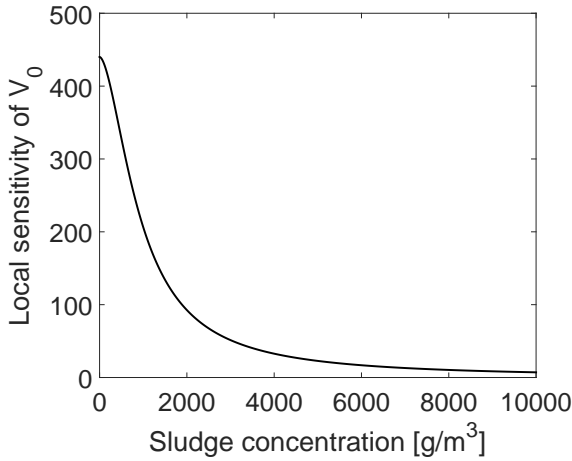


Figure 6.8: Local sensitivity of the settling velocity function of Diehl to the parameter V_0 .

of compression here cannot be further tuned and cannot be disconnected from hindered settling.

- The power-law functions predict lower settling velocities at high sludge concentrations compared to the exponential functions. This results in almost perfect thickening behaviour (represented by extremely high bottom concentrations and a very thin sludge blanket). Hence, these functions perform as expected from a hindered settling function.
- Whereas the exponential functions are clearly the best choice for simplified settler models that only include a hindered settling function, they are not suitable if we want to move towards advanced settler models that aim to explicitly account for several phenomena. For the latter models a power-law type function is shown much more appropriate in describing the hindered settling behaviour. Hence, it is recommended to use a power law function in the further quest to solve the compression part of the settling problem.
- Identifiability issues were observed when estimating the hindered settling parameters that define the settling velocity at low sludge concentrations indicating the need for a novel approach to measure and model discrete settling.

CHAPTER 7

Impact of the flocculation state on settling behaviour: experimental evidence and overview of available modelling frameworks

Redrafted from: Torfs, E., Locatelli, F., Balemans, S., Diehl, S., Bürger, R., François, P., Laurent, J., and Nopens, I. (2015b). Impact of the flocculation state on hindered and compression settling: experimental evidence and overview of available modelling frameworks. In *Proceedings of Watermatex2015*, Gold Coast, Australia, June 15-17.

Abstract

In order to move towards advanced 1-D models for secondary settling a more thorough understanding of compression settling is necessary. The inability of the current modelling frameworks to capture the variability in the compression phenomenon indicates that there is a missing link in the expression describing compressive settling. This can potentially be attributed to phenomena such as variations in the flocculation state and segregation of particles during hindered settling which are not considered in the modelling frameworks. In this chapter evidence is provided to support this hypothesis together with a brief overview of possible extensions/alternatives to the current modelling frameworks allowing to account for a changing flocculation state.

7.1 Introduction

Several studies have shown that only accounting for hindered settling is insufficient to capture the complex settling behaviour of activated sludge (De Clercq et al. (2008); Ramin et al. (2014b), Chapter 4). Therefore, an important aspect when moving to more advanced settler models is the phenomenon of compression, i.e. the resistance

to hindered settling caused by the network of flocculated particles that arises at high concentrations. The compression phenomenon is modelled in the Bürger-Diehl model as shown in Eq. 7.1. (Note that the dispersion term is omitted in this representation.)

$$\frac{\partial X}{\partial t} = -\frac{\partial}{\partial z} F(X, z, t) + \frac{\partial}{\partial z} \underbrace{\frac{v_{hs}(X)\rho_s}{(\rho_s - \rho_f)g} \frac{d\sigma_e(X)}{dX}}_{\substack{\text{Compression function} \\ d_{comp}}} \frac{\partial X}{\partial z} + \frac{Q_f(t)X_f(t)}{A} \delta(z) \quad (7.1)$$

The compressive term is dependent on the densities of the solid ρ_s and liquid component ρ_f , on the derivative of the effective solids stress σ_e and on the hindered settling velocity v_{hs} . The dependency of the compression function on v_{hs} is derived from the mass and linear momentum balances of the solid and liquid components by Bürger (2000) and can be explained intuitively by considering hindered settling as the rate at which the compressive network expands. Whereas Eq. 7.1 finds its origin in established conservation laws and a power-law function was shown to be most suitable to describe hindered settling (Chapter 6) no convincing physically motivated expression for σ_e exists today.

The effective solids stress is considered as a non-decreasing function of X when the concentration exceeds a certain critical concentration X_{crit} at which the solid particles are in permanent contact with each other.

$$\frac{d\sigma_e(X)}{dX} = \begin{cases} 0 & \text{if } X < X_{crit} \\ > 0 & \text{if } X \geq X_{crit} \end{cases} \quad (7.2)$$

This chapter illustrates typical problems associated with the selection and calibration of a solids stress function and provides an experimentally motivated hypothesis as to the nature of these problems.

7.2 Typical problems when calibrating compression behaviour

7.2.1 Calibration of solids stress function

In Chapter 4 a solids stress function was selected based on the work of De Clercq et al. (2008). This function was unable to accurately predict batch settling data in combination with the hindered settling function of Vesilind (1968) or Takács et al. (1991) (see Chapter 5). Through a more detailed analysis of the behaviour of different hindered

7.2. Typical problems when calibrating compression behaviour

settling functions Chapter 6 showed that a power law function (such as the hindered settling function proposed by Diehl (2014)) is more suited to describe hindered settling. Therefore, the ability of the solids stress function from Chapter 4 (Eq. 4.2) combined with the power-law function of Diehl (2014) (Eq. 6.5) to predict compression behaviour is tested here. Both functions are implemented in the Bürger-Diehl model and their potential to predict the batch curve data of Locatelli et al. (2015) is analysed. The parameters of the hindered settling velocity are calibrated based on the slopes of the batch curves (see Chapter 6) and the parameters of the solids stress function are calibrated by directly fitting the Bürger-Diehl model to the batch settling curves. The simulation results with the optimal parameter set are shown in Figure 7.1 (right).

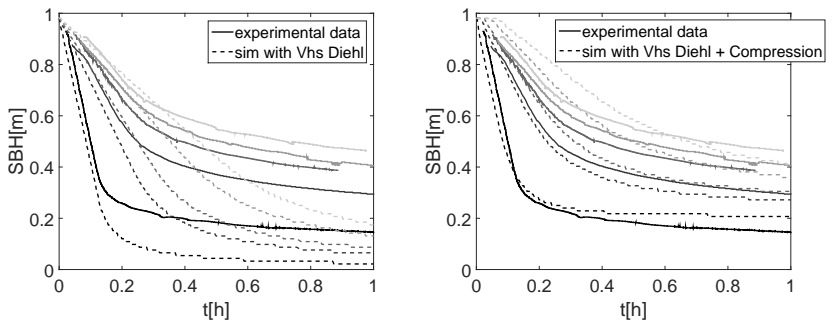


Figure 7.1: Measured SBHs (solid line - from Locatelli et al. (2015)) and predicted SBHs (dashed lines) by the Bürger-Diehl model with a power-law hindered settling function (left) the combination of a power-law hindered settling function and a calibrated compression function (right).

The simulation results show a clear improvement with respect to the simulations where only hindered settling is considered Figure 7.1 (left). However, the model is still not able to capture the behaviour of the complete batch curves. For simulation times up to 20 minutes, the batch curves of the lowest concentrations are predicted quite well but an overprediction of the batch curves at higher concentrations is observed. For longer simulation times all batch curves are underestimated except the curve for the lowest initial concentration which is overestimated. It is impossible to compensate for all these prediction problems through adjustments of the compression parameters only. For example, the overprediction at the high concentrations for $t < 20$ min suggests that the onset of compression (X_{crit}) is set too low. Increasing X_{crit} will worsen the underpredictions at later time instances. The latter indicates a need for more compression and could thus be compensated for by increasing α . However, increasing α will in its turn worsen the overpredictions of the batch curve at the lowest initial concentration. Hence, accurate predictions of all settling curves with a single parameter set are not possible indicating that a phenomenon that occurs in reality is not present in the

model. Moreover, as attempts to improve predictions in some parts of the batch settling curves will worsen predictions in other parts of the experimental data, several parameter combinations will provide similar overall prediction results suggesting a structural identifiability problem. The latter is confirmed by the occurrence of high likelihood values over large parameter ranges as shown in Figure 7.2.

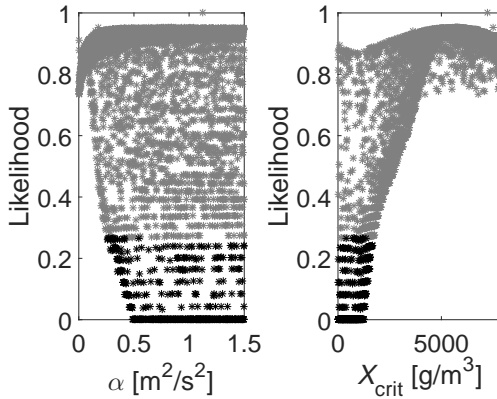


Figure 7.2: Plot of the likelihood in function of the parameter values for α and X_{crit} . Behavioural runs are indicated in grey, non behavioural runs in black.

7.2.2 Time-variable critical concentration

These observations indicate that some variability is still present in the data which is not captured by the current constitutive function for σ_e . In recent years, a number of studies have tried to extract an expression for σ_e from experimental batch settling data by means of inverse modelling (De Clercq et al., 2008; Ramin et al., 2014b; Diehl, 2014). De Clercq et al. (2008) collected detailed in-depth concentration profiles by means of a radiotracer and used these data to derive a logarithmic function for σ_e . Ramin et al. (2014b) collected data of sludge blanket heights and bottom concentrations during batch settling tests at different concentrations and derived an alternative equation for σ_e . However, both authors concluded that the use of a solids stress function that is only depending on X is insufficient to describe the physics of compression. They were able to overcome this problem by introducing a variable critical concentration (X_{crit}). Figure 7.3 shows SBH predictions for simulations with a variable critical concentration obtained by De Clercq et al. (2008) and Ramin et al. (2014b).

De Clercq et al. (2008) deduced from experimental observations that the critical concentration is located just below the discontinuity of the sludge blanket height. Hence, a variable X_{crit} was introduced by tracking this discontinuity throughout the model si-

7.2. Typical problems when calibrating compression behaviour

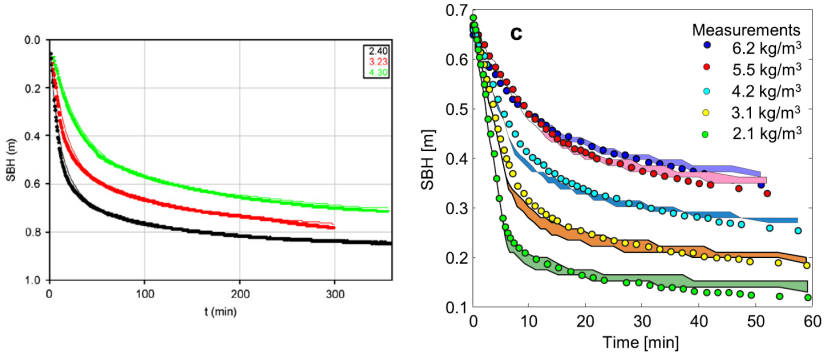


Figure 7.3: SBH predictions with a variable critical concentration obtained by De Clercq et al. (2008) (left) and Ramin et al. (2014b) (right). Experimental data (symbols) vs. simulation results (solid lines). Simulation results for Ramin et al. (2014b) indicate 95% prediction uncertainty.

mulations and setting the critical concentration to the value just below it (thus making X_{crit} vary in time for each experiment). Ramin et al. (2014b) implemented a critical concentration with a value of 0.1 g/l higher than the initial concentration in the batch thus making it vary between different experiments. The reasoning behind the latter is that as long as the sludge undergoes hindered settling the concentration should remain constant. Hence, as soon as the concentration exceeds the initial concentration, a gradient starts to form which indicates the onset of compression. However, during batch settling a concentration gradient will always occur from time $t > 0$ since no sludge can exit the column at the bottom. Hence, the initial formation of a gradient can be a feature of the settling reservoir and does not necessarily correspond to the onset of compression.

However, two problems occur with the approach of a variable X_{crit} . First, looking at the history of Eq. 7.1 we can state that from a physical point of view, the critical concentration should be a constant value for the same type of sludge since it represents the concentration at which particles have permanent contact with one another. The question arises why independent studies find evidence of a variable critical concentration when from a physical point of view we would expect this to be constant. One simple hypothesis could be that the empirical relations that were developed for σ_e are simply insufficient to capture the true behaviour and the variable X_{crit} serves to compensate for this. To test this hypothesis Diehl (2014) performed an extensive study on the concentration profiles collected by De Clercq et al. (2005) to identify expressions for $v_{\text{hs}}(X)$ and $d_{\text{comp}}(X)$ without assuming any a priori information on the functions. It could be concluded that no identification of $d_{\text{comp}}(X)$ was possible and

that the physics of compression cannot be modelled with a solids stress function that is only depending on X . This confirms the findings of De Clercq et al. (2008) and Ramin et al. (2014b) that some time varying phenomenon is occurring that is not captured by the currently used modelling framework.

A second problem with the introduction of a variable X_{crit} is that no physical explanation for the observed variance was found in any of the studies above and the introduced variability on X_{crit} is based on information that is only available in controlled batch experiments. During continuous operation of a full-scale clarifier, no information on the initial concentration is available and the location of the sludge blanket height cannot easily be tracked as predicting this value is actually one of the goals of the modelling exercise. Hence, applying the implementation schemes proposed by De Clercq et al. (2008) and Ramin et al. (2014b) to model full-scale dynamic systems is likely not feasible.

Therefore, the remainder of this chapter aims to investigate the physical or biological phenomenon behind the unexplained variability in the compression behaviour. An important assumption that was made in the derivation of Eq. 7.1 is that the suspended particles are monosized and cannot overtake each other. Hence, variations in the flocculation state and segregation of particles during settling are not included and could potentially explain the nature of the variability in the compression phenomenon.

7.3 Experimental data collection

Three types of experimental data were analysed in order to investigate the impact of the flocculation state of a sample on its compression behaviour. The experiments differ in the scale of the process affecting the flocculation state: microbial make-up (experiment 1), exposure to shear stress prior to settling (experiment 2) and local variations over the depth of a settling reservoir (experiment 3).

For the first type of data, batch settling curves of conventional Activated Sludge (AS) from the WWTP of Destelbergen (Belgium) are compared to settling curves with sludge from a lab-scale High-rate Contact Stabilisation (HiCS) reactor. Figure 7.4 shows a schematic representation of the HiCS system. In the first reactor, called the contactor, the bacteria come into contact with the substrate. The second reactor (the stabiliser) is aerated to stimulate the growth of bacteria. The HiCS system combines a feast-famine regime with very short Sludge Residence Times (SRTs) (≈ 1 day) to select for biomass with high storage rates in order to maximise the energy recuperation (Dionisi et al., 2005; Meerburg et al., 2015). The specific selection for certain microbial species will naturally influence the floc formation process and hence, the settling behaviour.

For the second set of experimental data a sample is collected from the biological reactor

7.4. Experimental observations and discussion

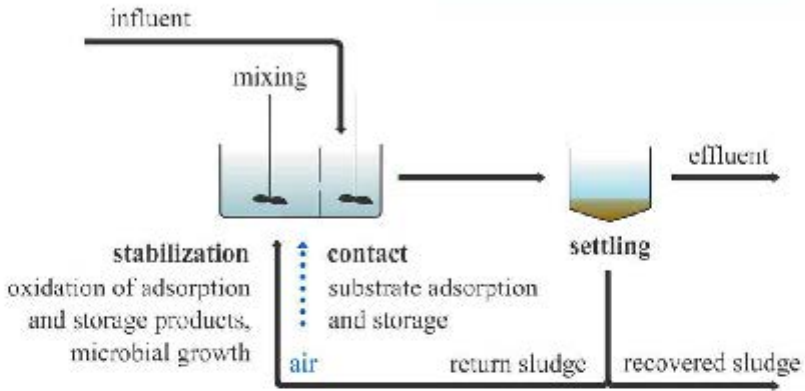


Figure 7.4: Schematic representation of a high-rate contact stabilization system (Meerburg et al., 2015).

at the WWTP of Destelbergen (Belgium) and a number of batch settling tests were conducted in 2 liter columns with a diameter of 9 cm. The evolution of the SBH was monitored during 30 minutes of settling. All tests were performed at the same initial sludge concentration (3.5 g/l) but at a different initial flocculation state. The latter was obtained by applying different amounts of shear (force) to the sample prior to settling. These experiments were performed in parallel with two identical settling columns.

The third dataset consists of the experimental data collected by Locatelli et al. (2014) who developed an experimental procedure to measure settling velocities within the sludge blanket by means of an ultrasonic transducer. These data were introduced in Chapter 6 and provide measurements of the evolution of the settling velocity in both time and depth.

7.4 Experimental observations and discussion

Impact of floc composition on compression settling

Batch settling curves for conventional AS from the WWTP of Destelbergen (Belgium) and sludge from a lab-scale HiCS reactor are shown in Figure 7.5. A significant difference in the settling behaviour of the two systems can be observed. The settling curves of the two highest concentrations of the conventional sludge (5.46 g/l and 6.83 g/l resp.) show very poor settling properties. The absence of an initial linear descent in these

curves signifies that compression is present from the start of the settling experiment. The critical concentration will thus be smaller than 5.46 g/l. For the settling curves of the sludge of the HiCS reactor a clear linear descent is present up to a concentration of 8.5 g/l, indicating that $X_{crit} > 8.4$ g/l. This sizeable difference in compression behaviour can be attributed to the combination of a very short SRT in combination with a feast-famine regime in the HiCS reactor. Such growth conditions are known to have an advantage for floc-formers (Guo et al., 2014) resulting in small, dense flocs with good-settling and compaction properties. (It should be noted that the absence of a filamentous network hampers the ability of the flocs to act as a filter to remove small particles resulting in an increased turbidity of the supernatant.)

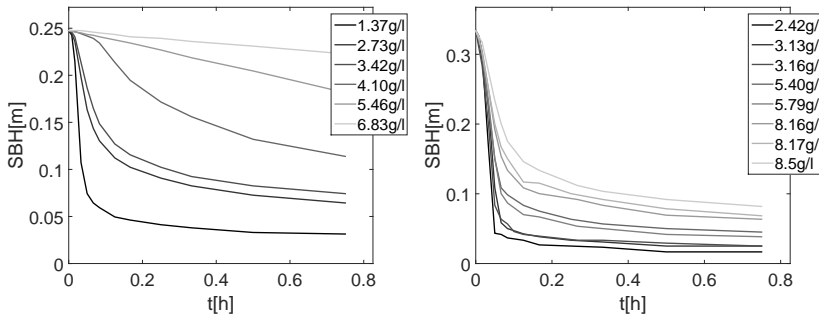


Figure 7.5: Comparison of batch settling curves for conventional AS from the WWTP of Destelbergen (left) and sludge from a lab-scale HiCS-reactor (right).

7.4.1 Impact of variations in shear stress on compression settling

In this experiment a sludge sample from the WWTP of Destelbergen was forced to undergo different amounts of shear stress prior to settling. The results of the batch settling test are presented in Figure 7.6. The experiments were performed on the same day in two parallel settling columns shown resp. in the left and the right side of the figure. The evolution of the sludge blanket height (and thus the settling velocity at the top of the sludge blanket) changes noticeably between the different experiments. Since each of these tests was performed at exactly the same initial concentration the differences in settling behaviour cannot be attributed to variations in concentration but only to variations in the flocculation state. By stirring the sample, loosely bound flocs are broken up into more stable aggregates with better settling properties resulting in a faster decrease in the sludge blanket height. This can be explained by the release of EPS acting like a polymer to increase flocculation (Laurent et al., 2009). (Stirring the sample at high shear rates also resulted in increased supernatant turbidity due to

7.4. Experimental observations and discussion

the formation of colloids. However, modelling the clarification process is outside the scope of this chapter.)

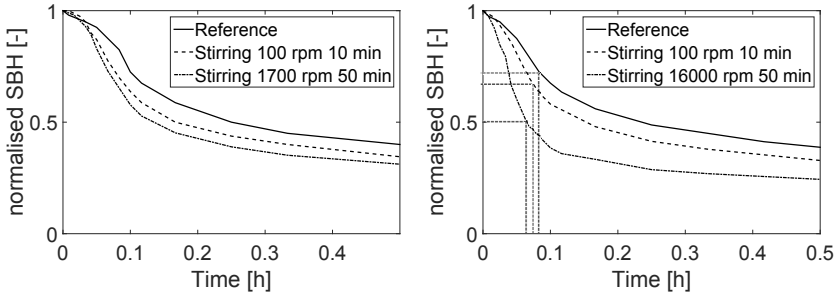


Figure 7.6: Evolution of the sludge blanket height during batch settling experiments at the same initial sludge concentration but a different flocculation state.

Both hindered and compression settling are influenced by these variations in the flocculation state. When mixing is applied prior to settling, steeper slopes can be observed in the linear part of the batch curves indicating an increase in the hindered settling velocity. The impact of the flocculation state with respect to the onset of compression settling is illustrated in Figure 7.6 (right). The horizontal and vertical grey dotted lines indicate the point where the sludge blanket enters the compression zone. Hence, at this point the concentration at the top of the sludge blanket should equal X_{crit} . When shear is applied prior to settling, the sludge water interface reaches the compression zone at an earlier time and more importantly at a much lower sludge blanket height (and thus in a more concentrated state). A more concentrated sludge blanket at the onset of the compression zone thus indicates a higher critical concentration. This confirms that changes in flocculation state can account for variations in the critical concentration. Due to the applied shear, larger, less stable flocs will be reduced to smaller, denser flocs with different packing properties resulting in a sample that can reach higher concentrations before the particles are in permanent contact.

7.4.2 In-depth analysis of the settling velocity

The previous experiments clearly indicated the impact of changes in the flocculation state prior to settling on the compression behaviour. However, they are not able to explain the time-variability observed by De Clercq et al. (2008) within a single batch experiment. Therefore, the settling velocity measurements of Locatelli et al. (2015) are analysed throughout the depth of the settling column in order to provide further insight into this phenomenon.

Figure 7.7 shows two velocity profiles measured by Locatelli et al. (2015) at initial

sludge concentrations of 1.5 g/l and 4.6 g/l. On these profiles, two regions with different settling behaviour can be distinguished. The top of the profiles (above the horizontal grey, dashed lines) corresponds to the hindered settling region and should be characterized by a vertical trend. At the bottom of the profile a downward decreasing trend can be observed corresponding to the compression region.

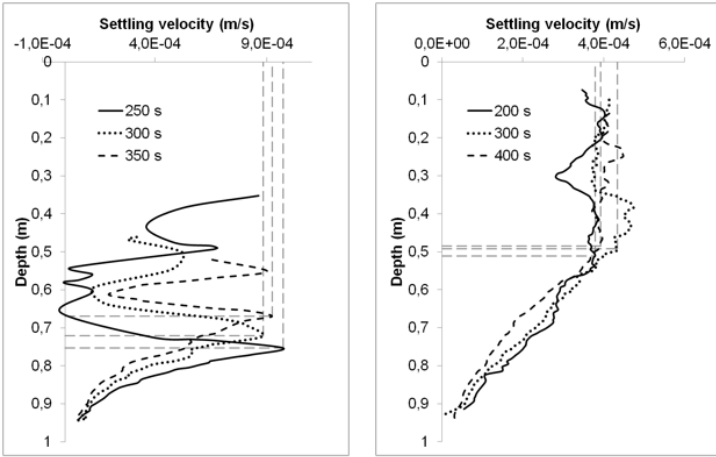


Figure 7.7: Settling velocity profiles recorded with an ultrasonic transducer during batch settling at an initial concentration of 1.5 g/l (left) and 4.6 g/l (right).

In the hindered settling zone the measured velocity profile does not show one fixed velocity but a vertical trend with horizontal fluctuations. Analysis of the velocity profile over time illustrates that these fluctuations are not random but can be tracked throughout the settling process. In these fluctuations, negative velocities can be attributed to particles moving upwards with the water flow whereas high settling velocities can be attributed to particles with very good settling properties. These observations indicate that particles do not settle collectively as a zone as is a common assumption for hindered settling. Moreover, by comparing the two graphs in Figure 7.7, it clearly appears that the magnitude of the velocity fluctuations decreases when the concentration increases. This observation was confirmed by other measurements obtained with different concentrations and quantified by calculating the standard deviation of the derivative of the settling velocity with respect to depth in the hindered settling region (see Table 7.1).

The fact that the observed fluctuations in the hindered settling region are not random suggests that the fluctuations correspond to variations in the internal properties of the sludge blanket, such as heterogeneities in the floc size distribution and that a segregation of particles with different size is occurring in the hindered settling region. This is supported by the decrease in magnitude of the fluctuations with increasing concen-

7.4. Experimental observations and discussion

Time	1.5 g/l	3.2 g/l	4.6 g/l
250 s	1.3e-02	5.2e-03	1.7e-03
300 s	6.0e-03	3.9e-03	1.4e-03
350 s	6.1e-02	2.8e-03	1.2e-03

Table 7.1: Standard deviations of the derivative of the settling velocity with respect to depth in the zone settling region.

tration. Indeed, at higher concentrations the flocs are more densely packed making a distinct segregation of particles more difficult. Local variations in floc size distribution and the segregation of particles over the depth of the hindered settling region may be the reason for the variations in the critical concentration as changes in particle size influence the formation of a compressive network.

7.4.3 Overview of available modelling frameworks

From the experiments above it becomes clear that the flocculation state of a sludge sample prior to settling has a profound influence on its compression settling behaviour and the concentration (X_{crit}) at which the sample starts to form a compressive network. Moreover, segregation of particles during the settling process may cause the critical concentration to vary over time.

Accurate description of this behaviour will therefore require refinement of the currently used modelling framework. Polydispersed systems undergoing break-up and flocculation have already been extensively studied in many chemical engineering applications and different modelling frameworks are available in literature. The available frameworks include very detailed models consisting of a system of n coupled PDEs (with n a chosen number of particle size classes). These models can account for polydisperse sedimentation where particles of different sizes overtake one another or can even be further extended to include reaction terms for flocculation and break-up (i.e. Population Balance Models (PBM)) (Nopens et al., 2015). Such detailed models will of course come at a cost of an increased simulation time as well as additional calibration challenges and are therefore less suitable to be used for operational and control purposes. More simplified models that only introduce one additional PDE have also been developed. Gustavson et al. (2001) introduced a memory function that stores the maximum volume fraction a particle has encountered during sedimentation to describe irreversible changes in permeability. A second example is the work by Betancourt et al. (2014) who developed a model for continuous sedimentation that is able to account for the influence of flocculant dosage on the settling velocity. The authors introduced one additional variable (one additional PDE) which tracks the local flocculation state and allows to have a settling velocity that varies with changes in the flocculation state. Hence, these available modelling frameworks can serve as a starting point for the fur-

ther development of SST models to include additional variability caused by changes in the flocculation state.

7.5 Conclusions

A compression function with constant parameters was shown unable to simulate batch settling curves at different initial concentration with a single parameter set indicating that some unexplained variability remains. The application of a variable critical concentration (corresponding to the onset of compression) is reported in literature. However, no physical explanation for this variability is provided and current implementation strategies are not feasible for dynamic simulations in full-scale SSTs. In this chapter a hypothesis was formulated relating the unexplained variability in the critical concentration to changes in the flocculation state of the sludge. Experimental evidence supporting this hypothesis was presented and an overview of potential model extensions was provided.

- In a first experiment, the compression behaviour of sludges with a different microbial make-up was investigated by comparing batch settling curves of conventional activated sludge to sludge from a HiCS reactor (operated to specifically select for floc-forming species resulting in small, dense flocs). Significant differences with respect to the onset of compression were observed with a critical concentration smaller than 5.46 g/l for conventional sludge and larger than 8.5 g/l for the sludge from the HiCS reactor. Hence, changes in the flocculation state caused by differences in the microbial make-up of the sludge flocs greatly influence the dynamics of compression.
- A second experiment examined the settling behaviour of sludge samples with identical concentrations but different flocculation states (obtained by applying different amounts of shear (force) prior to settling). Applying shear to a sludge sample resulted in distinctly different hindered settling velocities. Moreover, a more concentrated sludge blanket at the onset of the compression (i.e. a higher critical concentration) could be observed. Changes in the flocculation state can thus provide an important contribution to variations in the critical concentration as they will alter the rate at which the compressive network expands as well as the packing properties of the network.
- Finally, settling velocity measurements (Locatelli et al., 2015) were analysed throughout the depth of a settling column. Measurements in the hindered settling zone showed a broad range of settling velocities indicating that different particles are settling at different velocities. These results suggest that the common definition of hindered settling which states that particles settle collectively as a zone, is not valid for activated sludge. Instead, segregation of particles is

7.5. Conclusions

occurring resulting in local variations in floc size distribution. As changes in particle size influence the formation of a compressive network, segregation of particles could explain the occurrence of a time-varying critical concentration. Further analysis of these type of detailed velocity data can significantly improve the understanding of activated sludge settling behaviour.

- In order to accurately predict the settling behaviour of AS, a model should include information on the flocculation state of the sludge. Polydispersed systems undergoing break-up and flocculation have already been extensively studied in many chemical engineering applications. Different modelling frameworks which differ in the level of detail are available in literature. The applicability of these models to activated sludge should be tested.

Chapter 7. Impact of the flocculation state on settling behaviour: experimental evidence and overview of available modelling frameworks

PART III

Towards improved predictions of effluent concentrations in Wastewater Treatment Plants

The third part of this PhD aims to develop a framework which is able to model the discrete settling behaviour in a Secondary Settling Tank (SST) in order to improve predictions of the effluent concentration. In Chapter 8 a flocculation model is successfully integrated with a Computational Fluid Dynamics (CFD) model to build knowledge on the discrete settling dynamics in SSTs. Subsequently, a novel measurement device is developed in Chapter 9 which allows collecting detailed data of changes in Particle Size Distributions (PSDs) during discrete settling and which can be used to calibrate the integrated model. Furthermore, Chapter 10 applies an inverse problem methodology to dynamic PSD data to gain insight into the complex aggregation dynamics described by the flocculation model.

CHAPTER 8

Towards improved predictions of effluent suspended solids in wastewater treatment plants by integration of a flocculation model with computational fluid dynamics

Redrafted from:

Torfs, E., Vesvikar, M., and Nopens, I. (2013a). Improved Predictions of Effluent Suspended Solids in wastewater treatment plants by integration of a PBM with Computational Fluid Dynamics. In *Proceedings of the 5th Population Balance Modelling Conference*, Bangalore, India, September 11-13.

Balemans, S. (2014). Towards improved secondary settling tanks by means of computational fluid dynamics. Master's thesis, Dept. of Mathematical Modelling, Statistics and Bioinformatics, Ghent University, Ghent, Belgium.

Abstract

In the clarification region of SSTs settling is characterised by the size, shape and density of each individual floc instead of their concentration. This is called discrete settling. Accurate description of this settling behaviour requires information on the floc size distribution which in its turn depends on the tank hydrodynamics.

A CFD model to describe the hydrodynamics of a SST was coupled with the flocculation model by Parker et al. (1972) which divides the particles into primary particles and flocs and includes both aggregation and breakage of particles. Simulation results show that the integration of a flocculation model with CFD allows to qualitatively describe

the effect of aggregation and break-up and to define specific regions where flocculation is taking place in the SST. Moreover, through the integrated model it becomes possible to describe the discrete settling behaviour of particles in regions with low sludge concentrations, allowing for more detailed simulations of the effluent concentration under various conditions.

8.1 Introduction

Classical settling models relate the settling velocity to the sludge concentration. However, this relation will only be valid if the concentration of the flocs exceeds a certain threshold where the (in)direct inter-particle forces become sufficiently strong to drag each particle along at the same velocity irrespective of size or density (i.e. hindered settling). At lower concentrations, as can be found in the upper region of a SST, concentrations are too dilute for particles to sense each other and the settling velocity will depend on the size and density of each individual floc. Each particle will thus settle at its own characteristic velocity independent of the concentration. This regime is called discrete settling (Ekama et al., 1997). Moreover, Chapter 7 provided evidence of particle segregation during hindered settling which may induce additional variability in the hindered settling and compression behaviour. Hence, also at higher sludge concentrations, the approach to relate sludge settling only to concentration may be questioned. However, this chapter will focus on settling in the clarification zone.

The clarification region of a SST is of particular interest since particles that settle poorly here, will not make it into the sludge blanket and be carried over the overflow weir deteriorating the effluent quality. As the settling velocity in this region depends on the individual floc properties, detailed information on the PSD is required to accurately describe the clarification process. The dynamics of the PSD can be tracked by a flocculation model which describes changes in PSD due to aggregation and break-up processes. Several types of flocculation models exist to date and have been applied to activated sludge flocculation. These range from rather simple models including only primary particles and flocs (Parker et al., 1972) to more advanced Population Balance Models (PBMs) that include a wide range of floc size classes (Biggs and Lant, 2002; Nopens et al., 2005, 2015).

The aggregation and breakage dynamics governing the PSD are not constant but depend on the local velocity gradients and thus on the hydrodynamics in the SST. The use of CFD to describe the hydrodynamics has already severely improved the understanding of some phenomena (He et al., 2008; Stamou et al., 2009; Tamayol et al., 2010; Xanthos et al., 2011, 2013) which has led to new designs of inlet structures and more knowledge-based location and dimensions of baffles. However, in order to thoroughly understand the complex performance of SSTs both hydrodynamics and flocculation need to be addressed in an integrated way in order to capture all phenomena.

8.1. Introduction

Some studies have already aimed at integrating these different processes in order to improve the understanding of the SST performance. Griborio and McCorquodale (2006) combined a CFD model with a flocculation model to investigate the optimum design of a center well in SSTs. This chapter aims at integrating a flocculation model with a CFD model as a first step towards simulating the discrete settling behaviour in order to obtain improved predictions of the Effluent Suspended Solids (ESS) concentration. A schematic overview of the envisioned modelling framework is provided in Figure 8.1. Local velocity gradients are modelled in a CFD model and fed to a flocculation model in order to track changes in PSDs throughout the SST. This is the focus of the current chapter. In a future step, each floc size class in the integrated model can be characterised by its own settling velocity allowing to describe the discrete settling behaviour in the clarification zone with more rigour. The latter step requires further refinement and calibration of the integrated model which will be the topics of Chapters 9 and 10.

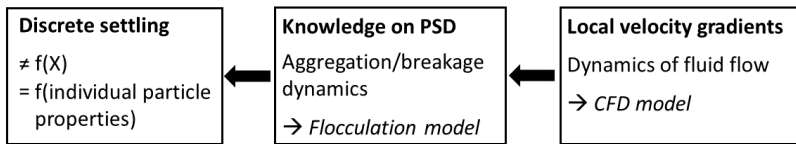


Figure 8.1: Schematic overview of processes affecting discrete settling and modelling frameworks to account for them.

The downside of such integrated flocculation-CFD models is the high computational demand making them unsuitable for real-time applications in operation and control of clarifiers. They can, however, be used as a tool to build process knowledge by studying the impact of different operational and design conditions on the ESS concentration. The detailed knowledge provided by these type of models will aid in improving existing 1-D models. Laurent et al. (2014) developed a protocol to use CFD as a supportive tool to develop improved models for operation and control (so called next generation simple WWT models). The conceptual protocol is shown in Figure 8.2. This methodology can also be applied to SST models where integrated flocculation-CFD models are applied to build system knowledge. This is envisioned in the current chapter.

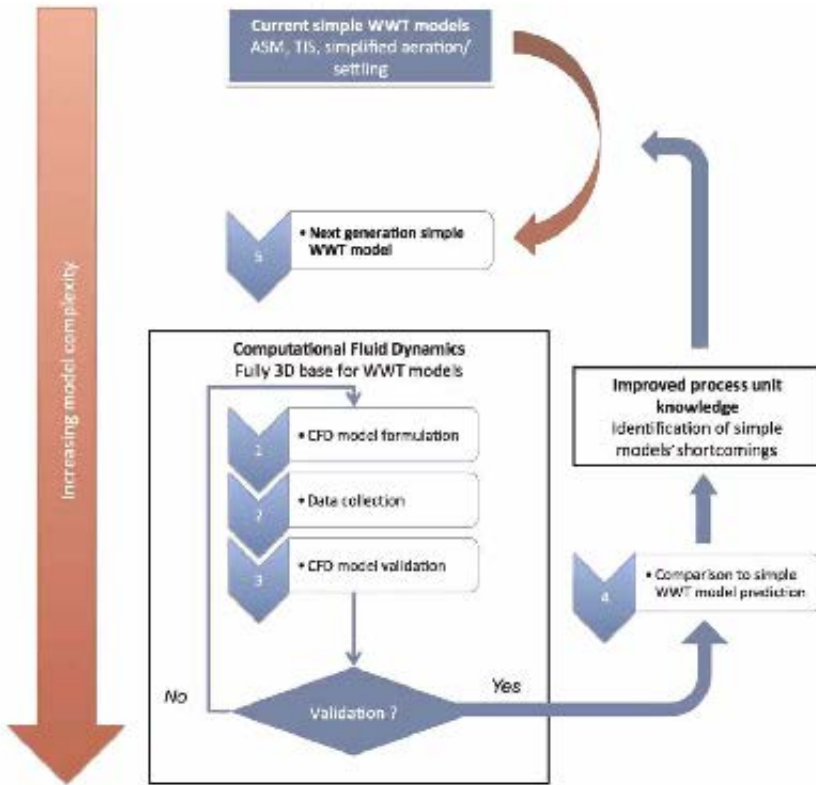


Figure 8.2: Conceptual protocol for the potential use of CFD as a supportive tool for WWT process modelling (Laurent et al., 2014).

8.2 Materials and methods

8.2.1 The system under study

The SST under study is a part of the Waste Water Treatment Plant (WWTP) of Roeselare (Aquafin, Belgium). The WWTP of Roeselare has a total biological capacity of 73,600 Inhabitant Equivalents (IE). The incoming domestic (87%) and industrial wastewaters (13%) undergo a preliminary treatment by means of mechanical operations (screens) and primary settling after which the biological treatment takes place in two parallel aeration tanks. The Mixed Liquor (ML) from both aeration tanks is collected in a central pit and distributed equally over four circular SSTs (\varnothing 32m) with a volume of approximately 2,000 m³. A schematic overview of the treatment plant is given in Figure 8.3.

8.2. Materials and methods

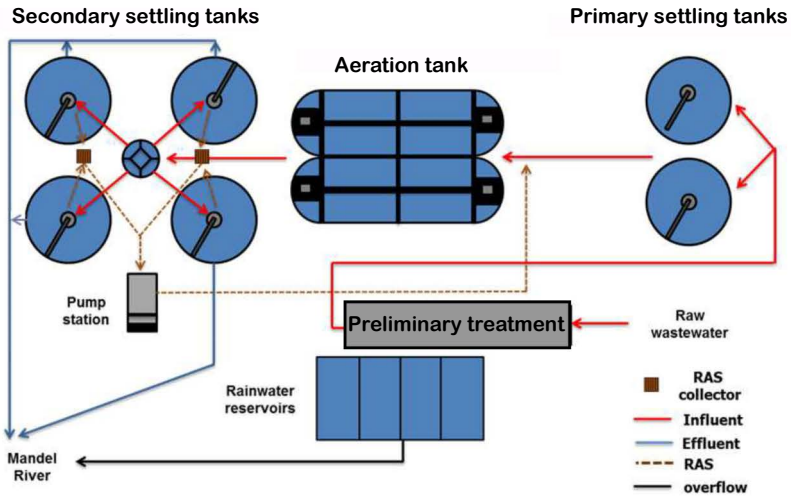


Figure 8.3: Overview of biological wastewater treatment plant of Roeselare

The system under study in this chapter consists of the upper right SST in Figure 8.3. The SST receives the ML through four inlets in the central feed structure. The inlet structure includes a flocculation well and a reflection baffle. The depth of the SSTs varies from 4 m in the centre to 2 m at the outside wall. The flow is directed radially outward to the peripheral effluent weir and the overflowing water is discharged into the Mandel river, a tributary of the Leie. The concentrated Return Activated Sludge (RAS) at the bottom of each tank is guided to the central sludge hopper by the tilted tank bottom slope and a rotating scraper mechanism. In Figure 8.4, the geometry of the complete SST as well as a schematic of the inlet structure is provided.

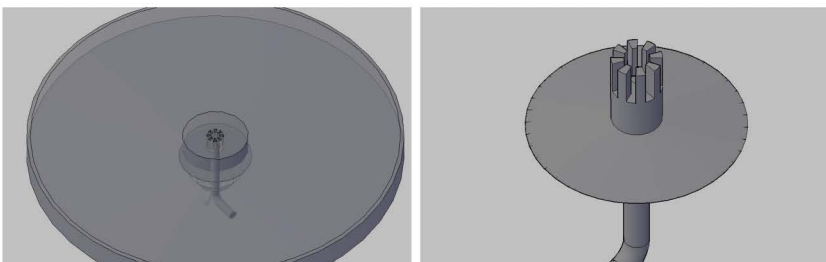


Figure 8.4: Schematic overview of the SST geometry (left) and the inlet structure (right) (Aquafin nv).

Average values of operational parameters under dry and wet weather flow conditions are listed in Table 8.1.

Table 8.1: Summary of operational parameters (average values)

	Dry weather (DW)	Wet weather (WW)
Inlet discharge per SST (m^3/h)		
in summer	345 – 370	870
in winter	420 – 470	870
Q_{RAS} (m^3/h)	± 220	± 270

8.2.2 Acoustic Doppler Current Profiler (ADCP) measurement

To validate the CFD model, a non-invasive Acoustic Doppler Current Profiler (ADCP) Workhorse Rio Grande (Teledyne RD Instruments - Figure 8.5) was used to measure the velocity magnitude and direction of the Suspended Solids (SS) inside the SST.

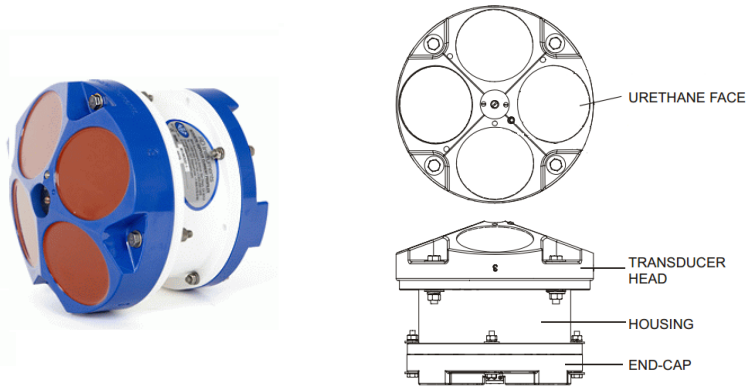


Figure 8.5: The Acoustic Doppler Current Profiler (ADCP).

The working principle of the ADCP is based on the Doppler effect. The device has four transducers which transmit sound signals at a constant frequency (1200 kHz) into the water. These sound waves travel through the water column and are partially scattered back by particles suspended in the moving water. The ADCP records these echoes at precise time intervals corresponding to fixed depths in the water column which can be determined based on the traveling time of the signals. The water column is thus divided in successive vertical elements (called bins) along the axis of the beams (Figure 8.6). The ADCP measures the change in wavelength between the emitted signal and the received signal coming from successive bins (Doppler frequency shift). This allows the determination of the particle velocity over a range of depths (Cobb, 1993; Kinnear and Deines, 2001). The software package WinRiver II[®] (Teledyne RD Instruments) is used for data collection and processing. Measurements in this work were performed

8.2. Materials and methods

with the Rio Grande High Resolution Mode (Mode 12) which is characterised by an acoustic frequency of 1200 kHz, a sampling interval of 1 s, a velocity resolution of 1 mm/s and which allows measurements up to 25 m depth.

It is important to consider that this technique measures the velocity of solid particles, not the liquid velocity itself. These latter two velocities may differ in a SST, e.g. the velocity of large and dense flocs may deviate from the liquid velocity due to settling and drag forces.

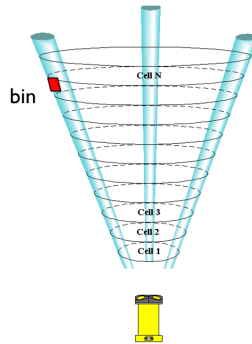


Figure 8.6: Schematic representation of the working principle of the ADCP.

The four transducers are positioned around a horizontal circle every 90 degrees and directed outwards at a certain angle to the vertical. This configuration allows to estimate the 3-dimensional velocity components: a tangential, radial and vertical component. However, only three beams are required to determine these three velocity components. The fourth beam allows to calculate two separate vertical velocities and hence the difference can be considered as an estimate of the measurement error in order to check the homogeneity of the flow field (Kinnear and Deines, 2001).

The larger the beam angle with the vertical, the more sensitive the ADCP becomes to horizontal velocity measurements. However, simultaneously the capacity of the ADCP to measure particle velocities at larger depth decreases. This can be explained by the occurrence of side lobes when an acoustic signal is transmitted by the transducers. If these side lobes reach the bottom or any other internal structures (baffles or the scraper mechanism) before the main signal the transducers will first receive the reflected side-lobe signals (typically stronger than the signals reflected from particles). This may blur the particle return signals and hamper the measurements (Cobb, 1993). Consequently, the ADCP is not able to measure velocities near the wall or other internal structures (for example inside the flocculation well) nor can it record velocity measurements at the bottom region of the tank due to acoustic reflection of the bottom wall. In addition, the ADCP cannot conduct measurements within 0.5 m of its head due to the time needed

to convert the equipment head from transmitter to receiver (the blanking period).

8.3 Integrated model development

8.3.1 CFD model

Geometry

Although the processes occurring in a real-life clarifier are three dimensional in nature, frequently a 2-D modelling approach is used in order to reduce the complexity of the model and the necessary computational time (Ekama et al., 1997). The geometry of the SST under study in this chapter, creates a flow that is approximately evenly distributed in the radial plane. This allows to model the SST along a radial cross-sectional plane in two dimensions (axisymmetric flow). To avoid long computational times, the sludge removal system is not considered in the model.

The inlet structure of the settling tank, including the inlet pipe, was considered in the computational domain in order to describe the flow field in the flocculation well more accurately. This is especially important when modelling the flocculation process in the settling tank. However, only one inlet opening of the inlet structure is considered in 2-D. The model does not consider the full 3-D inlet structure. The resulting geometry (Figure 8.7) is implemented in the commercial software package Fluent[®] (ANSYS, USA).

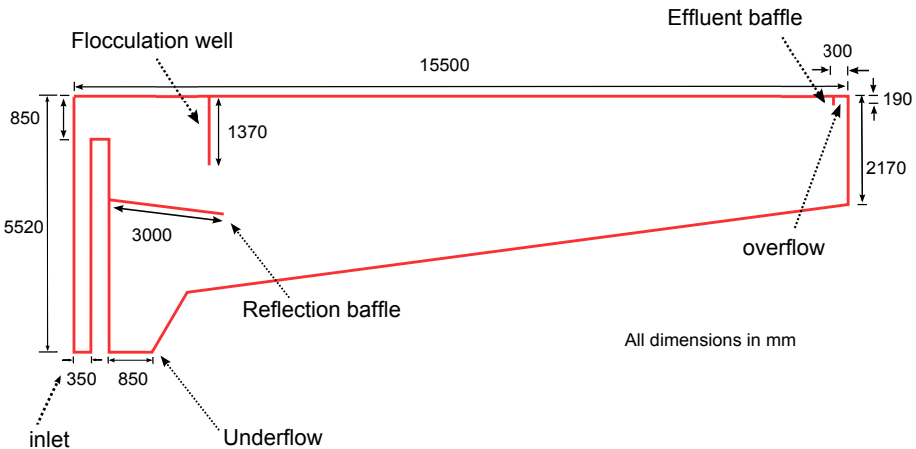


Figure 8.7: The geometry of the SST (in mm).

8.3. Integrated model development

Governing equations

By considering a 2-D axi-symmetric geometry, the continuity and momentum equations described in Chapter 2 can be simplified. Continuity and momentum equations for an axisymmetric, incompressible flow in the 2-D SST are written as follows:

- the **continuity** equation:

$$\frac{\partial u}{\partial x} + \frac{\partial v}{\partial r} = 0 \quad (8.1)$$

- the **momentum equations**

$$\frac{\partial u}{\partial t} + \frac{\partial u^2}{\partial x} + \frac{\partial(uv)}{\partial r} = -\frac{1}{\rho} \frac{\partial p}{\partial x} + \frac{\partial}{\partial x} \left(\nu_{eff} \frac{\partial u}{\partial x} \right) + \frac{\partial}{\partial r} \left(\nu_{eff} \frac{\partial u}{\partial r} \right) - g \quad (8.2)$$

$$\frac{\partial v}{\partial t} + \frac{\partial(uv)}{\partial x} + \frac{\partial v^2}{\partial r} = -\frac{1}{\rho} \frac{\partial p}{\partial r} + \frac{\partial}{\partial x} \left(\nu_{eff} \frac{\partial v}{\partial x} \right) + \frac{\partial}{\partial r} \left(\nu_{eff} \frac{\partial v}{\partial r} \right) \quad (8.3)$$

with x and r , the two dimensions of the system, g the acceleration of gravity, p is the pressure, u and v the fluid bulk velocity components in x and r directions, respectively.

The sludge-water mixture is modelled as a single phase and the solids are accounted for as a User Defined Scalar (UDS) with an additional scalar transport equation. The transport equation is written as follows:

$$\frac{\partial \phi}{\partial t} + \frac{\partial}{\partial x} \phi(u - u_s) + \frac{\partial}{\partial r} \phi v = \frac{\partial}{\partial x} \left(\frac{\nu_{eff}}{\sigma_s} \frac{\partial \phi}{\partial x} \right) + \frac{\partial}{\partial r} \left(\frac{\nu_{eff}}{\sigma_s} \frac{\partial \phi}{\partial r} \right) + S_\phi \quad (8.4)$$

with ϕ the volume fraction of the particles, $u_s = v_s$ the settling velocity in the direction of gravity and S_ϕ a source term.

Sludge viscosity is described by a modified Herschel-Bulkley model (Eq. 2.27) with parameter values as summarised in Table 8.2 (taken from Lakehal and Krebs (1999)). Turbulence is modelled by a standard k- ϵ turbulence model.

Mesh

Next, the computational domain is meshed into a finite number of grid cells (discrete control volumes). According to the Finite Volume Method (FVM) the governing equa-

Table 8.2: Parameters for the modified Herschel-Bulkley model

Parameter	Value
β_1	9.04e-3
β_2	1.12
β_3	2.48e-4
m	163.4
n	0.777

tions are integrated over each control volume (or cell) of the computational mesh such that conversion of mass and momentum is enforced for each control volume. The meshing step is an essential part of the CFD analysis since the selection of the shape and size of the control volumes will determine to a large extent the numerical accuracy and convergence time of the solution (Zikanov, 2010).

The presence of non-parallel walls in the geometry of the SST adds additional complexity to the meshing process. For these reasons, an unstructured grid is selected mainly due to its geometric flexibility. This grid arrangement allows to use a mixture of quadrilateral and triangular cell types, providing a flexible way to introduce non-parallel walls, such as the inclined bottom and the reflection baffle.

The mesh quality can be investigated based on different criteria. Here, the aspect ratio and skewness of the mesh were evaluated (Table 8.3). The aspect ratio of a cell is the ratio of the longest edge length to the shortest edge length. Hence, an optimal aspect ratio has a value of one. Grid cells with large aspect ratios should be avoided since they may cause convergence problems and unacceptable interpolation errors. The skewness is defined as the deviation of a cell to its ideal shape (equilateral or equiangular). For example, the skewness of a quadrilateral element indicates the deviation of its angles from 90° . For good meshing practices, the skewness should be between 0 and 0.5. For the selected mesh, more than 90% of the grid cells has an aspect ratio between 1 and 1.2 and a skewness below 0.07.

Table 8.3: Mesh quality metrics

Quality metric	minimum	maximum	average \pm std. dev.
Aspect ratio	1	3.52	1.10 \pm 0.051
Skewness	0	0.6	0.013 \pm 0.0025

Operational and boundary conditions

The SST is simulated for the prevailing flow conditions at the WWTP on 18/11/2013. The average flow rates used to define the SST in the CFD model are given in Table 8.4.

8.3. Integrated model development

Comparing these conditions to the yearly average values from Table 8.1 shows that the treatment plant was subjected to wet weather conditions during the measurement day.

Table 8.4: Average operating characteristics of the Roeselare WWTP on 18/11/2013

Operating characteristic	Value
Inflow rate	701 m ³ /h
Return flow	266 m ³ /h
Waste flow	331 m ³

Six different boundary types are defined in the CFD model (Figure 8.8): (1) an inflow (2) an underflow, where the thickened sludge is withdrawn from the SST, (3) an outflow at the effluent overflow, (4) a symmetry boundary at the water surface, (5) rigid walls and (6) a symmetry-axis.

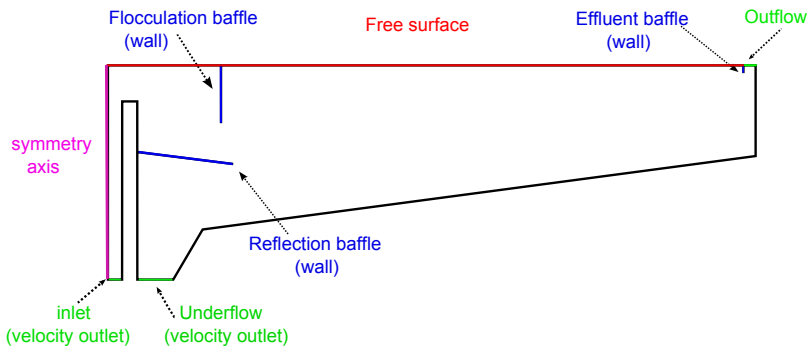


Figure 8.8: Illustration of the different boundary conditions: outer walls (black), interior walls (blue), inlet and outlets (green), free surface (red) and axis (purple).

The free water surface is considered as a symmetry plane or fixed surface, assuming that changes in the water surface positions are negligible. Across the symmetry plane, there is no convective or diffusive flux. As only half of the SST cross-section is modelled, the left side of the inlet pipe can be considered as a symmetry-axis.

A uniform velocity profile is applied at the inlet and underflow boundary. For the inlet, the velocity equals the average inflow rate divided by the cross-section area of the inlet pipe (diameter = 0.70 m). At the underflow boundary a negative velocity is defined since the flow is directed outwards. The velocity magnitude is calculated based on the underflow rate and the hydraulic diameter of the sludge withdrawal surface (0.85 m).

Next to the flow rates also the turbulence quantities need to be specified at the inlet and underflow boundaries. Due to a lack of knowledge about the specific values of

the kinetic energy k and the energy dissipation ϵ at these boundaries, the turbulence quantities are defined in terms of the turbulent intensity and the hydraulic diameter assuming a fully developed upstream flow. The turbulence intensity for the inflow and outflow is calculated as follows:

$$I = 0.16(\text{Re})^{-\frac{1}{8}} \quad (8.5)$$

with Re , the Reynolds number. The Reynolds number for the flow in the inlet pipe and the withdrawal pipe depends on their hydraulic diameters D_h and is determined by:

$$\text{Re} = \frac{D_h \rho v}{\mu} \quad (8.6)$$

where, μ and ρ are the viscosity and the density of the fluid, respectively, and v is the mean velocity of the fluid. Here, the physical properties of water at 20°C are used ($\mu=1.003\text{e-}3$ kg/(m.s) and $\rho=998$ kg/m³).

The calculated variables used to define the boundary conditions for the turbulent quantities are summarised in Table 8.5 for the inflow boundary (left) and the underflow boundary (right).

Table 8.5: Summary of variables used to define the inflow boundary conditions (left) and the underflow boundary conditions (right)

Variable	Value	Variable	Value
Inflow velocity (m/s)	0.51	Inflow velocity (m/s)	-0.013
Hydraulic diameter (m)	0.70	Hydraulic diameter (m)	0.85
Reynolds number (-)	2.82e4	Reynolds number (-)	1.0e4
Turbulent intensity (%)	3.24	Turbulent intensity (%)	4.59

The effluent weir is defined with zero gradient for velocity and atmospheric pressure (pressure outlet BC in Fluent). No conditions need to be defined as all variables are extrapolated from the computed variables in the cells near the outlet.

Obviously, the turbulent flow is influenced by the presence of walls in the computational domain. At the rigid walls (i.e. sides, bottom, interior baffles) of the SST, the no-slip boundary condition is applied. According to Adams and Rodi (1990) walls in the SST can be considered as smooth due to the occurrence of a large viscous layer near the surface where the flow field is almost laminar. This assumption allows to use the k - ϵ turbulence model with standard wall treatments (Launder and Spalding, 1974).

8.3. Integrated model development

With this approach, turbulence modelling is only applied up to a certain distance to the wall whereas semi-empirical wall functions are used to bridge the viscosity-affected region between the wall and the fully-turbulent region.

At the inlet boundary, a uniform SS volume fraction is added to the water flow. This volume fraction is determined by the solids concentration (average measured value on 18/11/2013 = 2.897 g/l) divided by the sludge density (1050 kg/m³). At the underflow boundary, a zero-gradient for turbulent properties and solids concentrations is adopted. In order to avoid solids flowing through the walls, a zero-gradient for the SS is applied at both outer and interior walls.

8.3.2 Sludge settling velocity

The settling behaviour of the SS is modelled in the scalar transport equation as a mass flux of solids in the direction of gravity with a settling velocity v_s (Eq. 8.4). The settling velocity is described by the exponential hindered settling velocity function of Vesilind (1968) (Eq. 2.1). The parameters of the settling function are calibrated based on the linear slopes of batch settling curves collected at the WWTP of Roeselare on 18/11/2013. The calibration procedure is described in Chapter 5. The optimal values and confidence intervals (95% significance level) of the parameters are listed in Table 8.6.

Table 8.6: Optimal value and confidence intervals for the estimated parameters of the settling function of Vesilind (1968)

	Optimal value	Confidence interval
V_0 [m/h]	10.2696	± 0.0958
r_V [l/g]	0.2920	± 0.0040

8.3.3 Flocculation model

Several types of flocculation models are available in literature (Parker et al., 1972; Biggs, 2000; Nopens et al., 2005). These models differ in their degree of complexity defined by the number of classes considered and the level of detail included in their aggregation/breakage rates. In this chapter, the aim is to investigate the feasibility of a coupled flocculation-CFD model to study the settling behaviour in the clarification zone. Therefore, as a proof of concept, the rather simple flocculation model by Parker et al. (1972) is used. This model divides the Activated Sludge (AS) into two classes: primary particles and flocs. Based on these two size classes the flocculation kinetics of turbulent mixing are described assuming that break-up and aggregation processes occur simultaneously. The net rate of change of the volume fraction of primary particles

(Φ_p) and flocs (Φ_f) with respect to time is given by the following set of differential equations:

$$\begin{cases} \frac{d\Phi_p}{dt} = K_b \cdot \rho \cdot \Phi_f \cdot G^m - K_a \cdot \rho \cdot \Phi_f \cdot \Phi_p \cdot G \\ \frac{d\Phi_f}{dt} = -K_b \cdot \rho \cdot \Phi_f \cdot G^m + K_a \cdot \rho \cdot \Phi_f \cdot \Phi_p \cdot G \end{cases} \quad (8.7)$$

with G the mixing intensity or shear rate, m a parameter, ρ the density of the mixture, K_b the breakage rate and K_a the aggregation rate.

The dimensionless exponent m is set to a value of 2 based on analysis by Parker et al. (1972). The aggregation and break-up coefficients are determined experimentally by Griborio and McCorquodale (2006). The applicability of this theoretical model is supported by Wahlberg et al. (1994) who tested this model on batch flocculation data of activated sludge samples from 21 full-scale clarifiers.

The local mixing intensity expressed as velocity gradient G is calculated by the CFD model through the concept of maximal strain rate (Kramer and Clark, 1999). Coupling of the flocculation model with the CFD model allows to calculate the flocculation rates at each location in the SST. This coupling is achieved through the definition of two UDSs (for flocs and primaries resp.). The flocculation model is added as a source term in the transport equations of these scalars (Eq. 2.25). (Note that for simulations without flocculation, the sludge is defined by a single UDS. The number of classes in the coupled flocculation-CFD model can thus easily be extended with additional UDSs and corresponding transport equations.)

The models for flocculation and sludge settling velocity are implemented as separate C-functions and subsequently loaded into the software package Fluent[®] as User Defined Functions (UDFs).

8.4 Results and discussion

In the first part of this section simulation results of the CFD model are shown with a single UDS representing the sludge. The model is initialised, the accuracy of the numerical solution is verified and the results are validated with experimental data. Subsequently, the flocculation model is coupled to the CFD model and the impact of aggregation and breakage on the sludge concentration profile is investigated.

8.4. Results and discussion

8.4.1 CFD model

Grid dependency test

In any CFD study, the accuracy of the approximate numerical solutions with respect to the exact solution of the underlying equations needs to be evaluated. Therefore, it is investigated whether the discretisation of the computational domain (i.e. the mesh) is chosen sufficiently fine. A mesh dependency test is performed to check the extent to which the solution changes by refining and/or coarsening the grid size (McCorquodale and Zhou, 1993; De Clercq, 2003). Although the ideal final mesh refinement should result in an invariable solution, also the required simulation time should be considered. A finer mesh results in a longer simulation time. Hence, the objective is to determine the 'optimal' mesh in terms of accuracy and computational time by making a cost-benefit analysis. To determine the impact of the mesh resolution on the numerical solution, three different mesh sizes were investigated: a **coarse**, **medium** and **fine** mesh (resp. called mesh 1, mesh 2 and mesh 3). The mesh size (i.e. the number of cells) for the different meshes together with the corresponding ESS concentration and RAS concentration at steady-state are given in Table 8.7.

Table 8.7: Results of the mesh dependency test

	mesh 1	mesh 2	mesh 3
Size (nr of cells)	35052	56069	103166
ESS concentration [g/l]	3.905e-3	3.157e-3	3.152e-3
RAS concentration [g/l]	6.161	5.687	5.684

For the medium and fine mesh only small differences between the predicted ESS and RAS concentrations can be observed whereas the results for the coarse grid deviate notably from the two other grids. The simulation time approximately doubled for each mesh refinement. From this it can be concluded that the medium mesh is sufficiently accurate to be used in further simulations.

Preliminary CFD simulation results

The CFD model is first simulated with only water until steady-state. Subsequently the UDS representing the sludge is switched on and a uniform SS volume fraction of 2.897 is added to the incoming flow. Figure 8.9 illustrates how the SST is gradually filled with ML. (Note that the flocculation model is not considered in these simulations.)

The SS enter the SST through the opening of the inlet structure. A recirculation pattern causes an intense mixing of the SS in the flocculation well. The density difference causes the denser incoming ML to fall down to the bottom of the tank. Here, it splits up

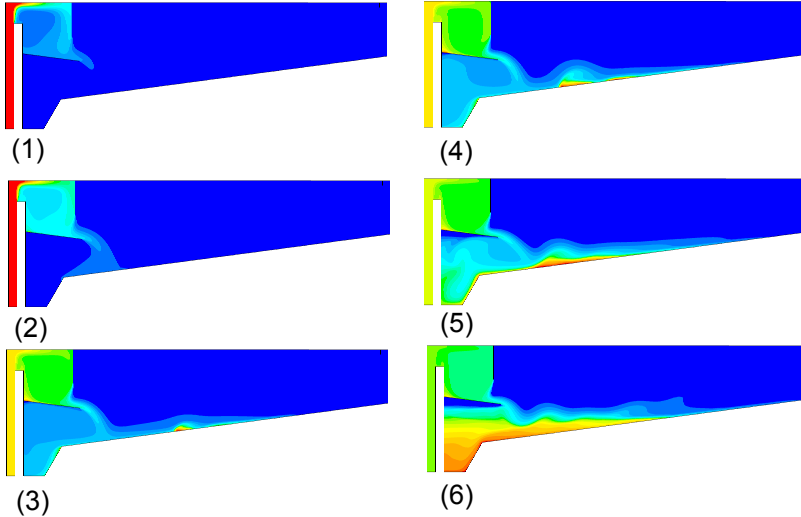


Figure 8.9: Concentration profiles during the filling of the SST with ML. No colorbar is provided as it differs between the different profiles. However, higher concentration are always indicated in red and lower concentrations in blue.

into a current towards the sludge hopper and a bottom current towards the peripheral effluent weir. The sludge blanket develops further until a steady state is reached with a RAS concentration of 5.57 g/l (Figure 8.10). A substantial sludge blanket can be observed which could be expected as the SST is simulated under wet weather conditions.

The predicted velocity vector field at steady-state is shown in Figure 8.11. An important feature of the flow field is found in the central flocculation well where intense mixing is occurring due to a recirculating flow pattern. The recirculation process increases the residence time of sludge in the flocculation well and promotes the contact between the suspended particles. Moreover, it can be seen that the velocities at the outflow of the flocculation well are much smaller compared to the velocities at the inlet indicating that the kinetic energy of the inlet flow has dissipated in the center well. Energy dissipation in the centre well plays a major role in improving the tank hydrodynamics as it decreases the strength of the density jet and avoids high turbulence at the sludge blanket interface which could otherwise cause resuspension of previously settled SS (Griborio, 2004).

Furthermore, a clear multi-layered recirculation pattern is observed. The density difference between the incoming flow and the sludge blanket creates an outward horizontal

8.4. Results and discussion

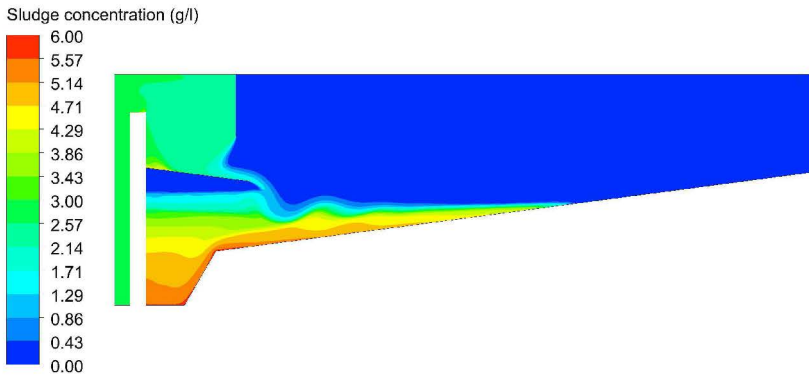


Figure 8.10: Concentration profile in the SST at steady-state.

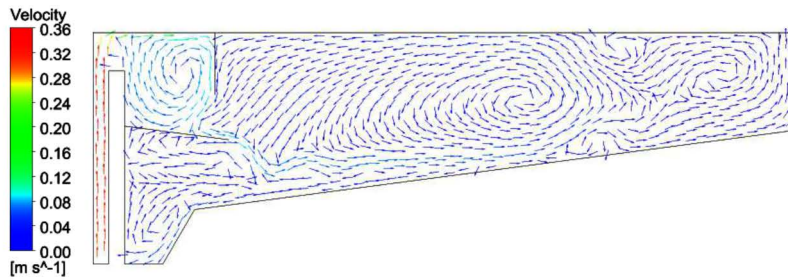


Figure 8.11: Velocity vector field of the mixed liquor in the SST (m/s) at steady-state.

flow at the top of the sludge blanket. When this flow reaches the tilted tank bottom at the end of the sludge blanket, the flow is forced upward and redirected back to the center of the tank, i.e. a counter-current is introduced. This recirculation pattern is advantageous in a SST since it avoids short-circuiting of ML to the effluent weir. The effect of this recirculating pattern on the sludge becomes evident when rescaling the concentration profile to enhance the visibility at low sludge concentrations (Figure 8.12). The upward flow at the edge of the sludge blanket transports particles into the clarification zone. Should this occur near the effluent weir (for example if the Sludge Blanket Height (SBH) would increase further due to increased loading), these particles could be carried over the overflow weir and deteriorate the effluent quality.

Model validation

The simulated hydrodynamic profile is validated with ADCP measurements performed at the full-scale SST. Measurements were conducted at different locations along the ra-

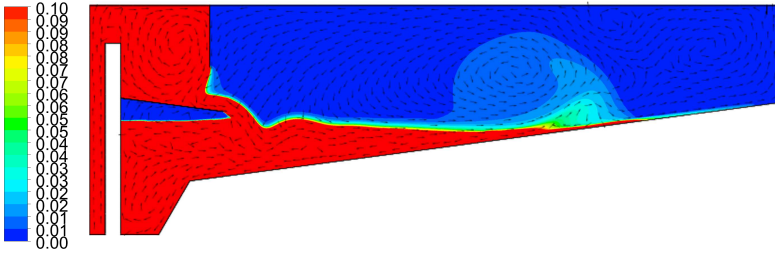


Figure 8.12: Concentration profile in the SST at steady-state. Color scale zoomed in on concentrations below 0.1 g/l

dius of the SST. In order to stabilize the ADCP, the device was mounted on a vertical pole and fixed to the bridge, as illustrated in Figure 8.13. The bridge was turned off during the measurements to avoid interference of the ADCP signal with the sludge removal system under the bridge. The device was used in the down-looking position and submerged 20 cm under the water surface. Each measurement represents an average value over approx. 20 minutes.



Figure 8.13: The experimental set-up of the ADCP

Four measurements were performed at resp. (1) 3.40 m, (2) 6.5 m, (3) 10.1 m and (4) 13.5 m from the center of the tank. The resulting velocity profiles of the ADCP measurements are shown in Figure 8.14. The corresponding measurement errors are

8.4. Results and discussion

plotted in Figure 8.15.

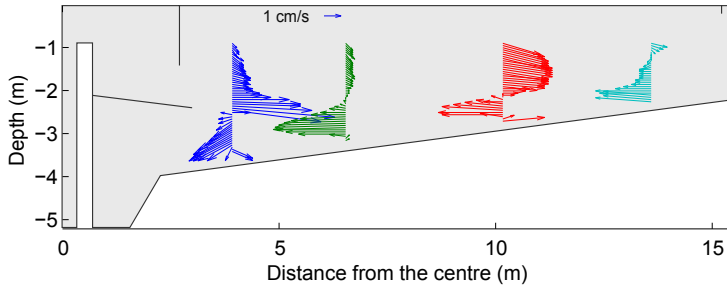


Figure 8.14: Measured velocity profiles with the ADCP at the WWTP of Roeselare.

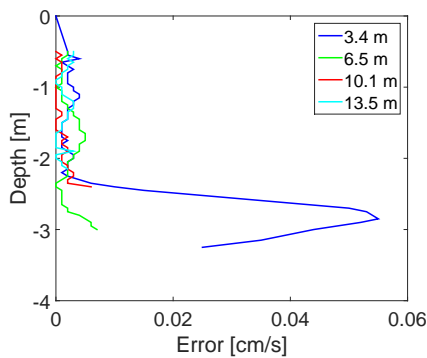


Figure 8.15: Measurement errors (cm/s) for the different measurement locations as a function of depth.

The largest errors in the ADCP measurements are observed close to the outflow of the centre well indicating that these measurements may be influenced by the nearby baffle. The measured velocity profile confirms that the incoming ML follows a circular pattern throughout the lower part of the SST. The density jet flowing outwards from the flocculation well towards the effluent weir can clearly be observed. This horizontal flow is located directly above the sludge blanket. The ADCP measurements can thus be used to predict the location of the sludge blanket. For both the simulated and the predicted velocity profile the position of the sludge blanket is located at the outflow of the flocculation well (in the extension of the reflection baffle). Inside the sludge blanket a horizontal flow towards the sludge hopper is observed. This bottom current in the sludge blanket was also predicted by the simulation results. Although the general features of the flow pattern in the bottom region of the clarifier are similar, the simulation results do not correspond to the measurements in the top region of the SST. In the top region the CFD model predicts a recirculation pattern which cannot be observed in

the measured velocity profiles. These discrepancies may have multiple reasons. First, no ADCP measurement are available for the last meter from the surface. Hence, it is possible that in the real SST the recirculation flow is present in this region. Second, the measurements in the upper region of the tank are less reliable as the ADCP only measures particle velocities and only few particles are present in this region (De Clercq, 2003). An alternative measurement technique should be used to characterise the top part of the SST in terms of velocity profiles. This is still an important bottleneck in the validation of CFD models of SSTs (De Clercq, 2003). Hence, although the general trends are predicted well by the CFD model it is not yet fully validated and its results (especially quantitatively) should be interpreted with care.

8.4.2 Integration of a flocculation model

Subsequently, the flocculation model of Parker et al. (1972) is coupled to the CFD model and the concentration profiles of the flocs and primary particles are investigated. The aggregation and breakage coefficients were taken from Griborio and McCorquodale (2006) who measured the values of $K_a = 7.4e-5 \text{ m}^3/\text{kg}$ and $K_b = 8e-6 \text{ number.s/kg}$ from batch flocculation tests. The concentrations of flocs and primaries in the feed flow to the clarifier were arbitrarily defined as 2.75 g/l and 0.095 g/l, respectively.

Impact of aggregation/breakage

Simulation results are shown in Figure 8.16. Only the concentration profiles of the primary particles are shown here since small particles are known to have a lower settling velocity and will thus have the highest impact on the effluent quality. The left-hand side of Figure 8.16 shows the concentration profiles of the primary particles without flocculation (K_a and K_b equal to 0). The right-hand side shows the resulting distribution when aggregation and breakage of particles is included ($K_a = 7.4e-5 \text{ m}^3/\text{kg}$ and $K_b = 8e-6 \text{ number.s/kg}$). The complete concentration profile between the ESS and RAS concentrations covers a large range of concentrations making local variations difficult to observe. Therefore, the colour scale was adjusted with a maximum of 0.1 g/l to improve the visibility of the flocculation dynamics in regions with lower concentration.

It can be seen that the inclusion of a flocculation model has a profound impact on the prediction of primary particles. The importance of the flocculator well is clearly shown as floc break-up can be observed in this region resulting in a higher concentration of primary particles. No breakage can be observed at other locations in the tank, indicating that the energy in the incoming flow is adequately dissipated in the flocculator well.

These observations do not correspond to the findings of Griborio and McCorquodale (2006) who concluded that aggregation was occurring for the measured parameter val-

8.4. Results and discussion

ues. However, it should be noted that the simulations in Figure 8.16 are performed under wet weather conditions. Increased flow rates will likely induce more shear in the flocculation well thus causing floc break-up. A comparative simulation for dry-weather conditions would be an interesting scenario to assess the impact of different flow rates on the flocculation behaviour. However, this analysis is not performed in the present research.

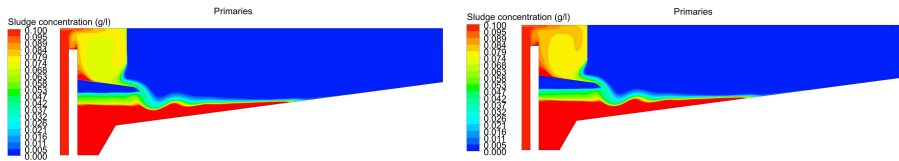


Figure 8.16: Concentration profiles of primary particles in the secondary clarifier without flocculation (left) and with a flocculation model included (right). Colour scale adapted with a maximum of 0.1 g/l.

Subsequently, the qualitative effect of aggregation (for example by addition of polymers) is investigated by increasing K_a with a factor 1000. Figure 8.17 shows the effect of increased aggregation on the concentration profile. The results confirm that a large fraction of the incoming primary particles is now included into flocs which will improve their settling.

These observations are a straightforward result of the flocculation model. However, the coupling of the flocculation model with the CFD model provides important information on the specific locations in the tank where flocculation is taking place. Significant aggregation of primary particles into flocs can be observed in the inlet channel, in the flocculation well and in the sludge blanket itself. The first two regions are of particular importance when predicting the effluent concentration since primary particles that are not captured into flocs here have a high probability of being conveyed towards the overflow weir. Flocculation that occurs inside the sludge blanket is of lesser importance with respect to the effluent concentration but can potentially provide more insight in the compression phenomenon (see Chapter 7). However, compression is not considered in the current CFD model.

Impact on ESS concentration

Next to the concentration profiles, the effect of aggregation and breakage dynamics on the ESS concentration is investigated. Table 8.8 presents ESS and RAS concentrations for the different flocculation scenarios. An increase in aggregation rate K_a causes a decrease in ESS and RAS concentrations of the primary particles as these particles are aggregated into flocs. In general, the simulated ESS concentrations (≈ 0.003 g/l)

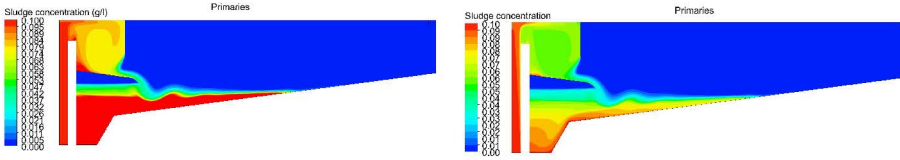


Figure 8.17: Effect of increased aggregation on the concentration profile of primary particles in the SST. Simulation with $K_a = 7.4e-5 \text{ m}^3/\text{kg}$ and $K_b = 8e-6 \text{ number.s/kg}$ (left) and $K_a = 7.4e-2 \text{ m}^3/\text{kg}$ and $K_b = 8e-6 \text{ number.s/kg}$ (right).

are much lower than observed in reality ($\approx 0.02 \text{ g/l}$). The reason for this is the selection of the settling function of Vesilind (1968) which predicts unrealistically high settling velocities at low concentrations. A more realistic range could be obtained with the settling velocity function of Takács et al. (1991). Alternatively, as the developed modelling framework allows to simulate the concentration of different particle classes, the settling behaviour at low concentration can be modelled in a more realistic way by including discrete settling. This would require further extension and calibration of the coupled flocculation-CFD model.

Table 8.8: ESS and RAS concentrations for the different flocculation scenarios.

	Flocs		Primaries	
	ESS [g/l]	RAS [g/l]	ESS [g/l]	RAS [g/l]
$K_a = K_b = 0$	3.21e-3	5.49	4.99e-5	0.19
$K_a = 7.4e-5$ & $K_b = 8e-6$	3.14e-3	5.43	8.21e-5	0.19
$K_a = 7.4e-2$ & $K_b = 8e-6$	3.19e-3	5.51	7.33e-5	0.098

8.4.3 Further model development

The results show that valuable insight in the performance of a secondary settling tank can be obtained from the integration of a flocculation model with a CFD model. By gaining insight into the specific locations where flocculation is taking place, the combination of these models can be used to optimise the design of settling tanks. Nevertheless, the results shown above provide only qualitative information on the ESS concentration. The distribution between primary particles and flocs can be predicted at different locations throughout the tank. Since primary particles are known to have a very low settling velocity, a higher concentration of primary particles will consequently result in a higher ESS concentration. However, if we want to be able to model the quantitative effect of flocculation on the effluent quality, the discrete settling behaviour of the sludge needs to be taken into account.

8.5. Conclusions

This can be achieved by adjusting the settling velocity function to include a different settling regime below a certain threshold ($X_{lim} \approx 500$ mg/l). Above this threshold the settling velocity can still be described by the hindered settling velocity function. In regions where the total sludge concentration is below the threshold value, discrete settling prevails and each particle class will be given a constant individual settling velocity. This approach requires data on the discrete settling velocity of the different size classes.

Hence, for this model to be used in practical applications to improve operational strategies or design features, a number of questions need to be answered. Firstly, the required complexity of the model needs to be defined. The model by Parker et al. (1972) represents a very simplified flocculation model. More complex flocculation models have been developed in literature (Biggs, 2000) which would obviously increase the accuracy of the predictions. However, when choosing the number of size classes one needs to account for the computational effort that this brings along as well as the desired accuracy. Basically, the coupling results in the incorporation of n transport equations in each bin of the mesh (n being the number of size classes considered in the PBM). The number of classes thus needs to be chosen with care. The number of classes required to meet the model's goal can be assessed by collecting experimental data of changes in particle size distribution during settling. Secondly, experimental data is needed to determine the discrete settling velocities of the different size classes. Both these issues will be addressed in Chapter 9 where a novel methodology to perform measurements of discrete settling is developed.

Finally, the aggregation and breakage rates need to be determined. Griborio and McCorquodale (2006) calibrated the parameters K_a and K_b based on batch flocculation tests. However, a more recent analysis by Gong et al. (2011) showed that different values for K_a and K_b are obtained depending on the Mixed Liquor Suspended Solids (MLSS) concentration suggesting that it is not possible to describe the flocculation process with constant values for K_a and K_b . Different functions that aim for a more accurate description of the complex aggregation and breakage processes have been presented in literature (Spicer et al., 1996). However, none of these kernels is able to accurately describe the activated sludge flocculation process (Nopens et al., 2005). Hence, the definition of the aggregation and breakage rates in the flocculation model and their calibration deserves ample attention. A detailed analysis of aggregation dynamics under different conditions is therefore presented in Chapter 10.

8.5 Conclusions

A 2-D axisymmetric CFD model was developed for a circular SST of the WWTP of Roeselare and simulated under wet weather conditions. Preliminary simulation results showed the development of an elevated sludge blanket and a recirculating flow pat-

tern in the SST. Subsequently, the CFD model was coupled with a flocculation model to investigate the effect of aggregation/breakage throughout the SST. The following conclusions could be drawn.

- Through the coupling of a flocculation model with a CFD model a qualitative analysis of the effect of aggregation and breakage on the distribution of flocs and primary particles can be made. Moreover, the integrated model allows to detect specific regions in the SST where flocculation and breakage are taking place. The importance of the flocculator well for proper mixing and energy dissipation was clearly shown by the simulation results.
- Moreover, the integrated model allows the implementation of a more realistic settling behaviour for the clarification zone in future simulation studies. As the concentrations of different particle size classes are tracked by the flocculation model, the discrete settling behaviour could be modelled by providing each size class with its proper settling velocity.
- In order to use this model for the development of improved design or operational strategies, further information is required through experimental data collection and analysis. The number of classes necessary to accurately describe the particle size distribution needs to be determined as well as a discrete settling velocity for each class. This will be addressed in Chapter 9. Furthermore, more insight in the aggregation/breakage dynamic is needed which will be the subject of Chapter 10.

CHAPTER 9

A novel methodology for the calibration of discrete settling behaviour of activated sludge

Redrafted from: Torfs, E., Mahdavi Mazdeh, F., Bellandi, G., and Nopens, I. (2014). A novel methodology for the calibration of discrete settling behaviour of activated sludge. In *Proceedings of the IWA Specialist Conference on Advances in Particle Science and Separation*, Sapporo, Japan, June 15-18.

Abstract

Coupling of CFD with flocculation models can serve as a powerful tool to gain knowledge on the processes affecting clarification and hence, the effluent quality in SSTs. However, the practical application of these models requires the selection of a number of particle size classes as well as a definition of the settling velocity for each class. Therefore, a new measurement device was developed which allows collecting detailed data of changes in PSDs during discrete settling. The results show that the discrete settling behaviour of activated sludge can be described by dividing the sludge into roughly 5 classes. Moreover, by measuring the evolution in PSD along different depths in the settling device, the discrete settling velocities of the different classes can be quantified. This information can subsequently be used in a coupled flocculation-CFD model in order to model the impact of different environmental and operational conditions on the effluent quality.

9.1 Introduction

The previous chapter illustrated how a CFD model can be coupled with a flocculation model in order to study the settling and flocculation processes in the clarification re-

gion of a SST. The flocculation model that was used in this chapter is the very simple flocculation model by Parker et al. (1972) which divides the sludge particles into two classes and assumes constant aggregation and breakage rates. Through the coupling of these models specific regions in the SST where flocculation is taking place could be determined. This approach allows simulating the quantitative effect of varying conditions on the effluent concentration from which appropriate operational and control strategies can be developed.

Although these types of coupled models provide a promising tool to gain system knowledge, additional information on the required complexity of the flocculation model (i.e. selection of a number of representative classes) and the discrete settling velocities for each of the defined classes are needed for their practical application in WWTP modelling. Hence, a measurement technique through which high quality data of the discrete settling process can be collected is needed.

Some experiments to measure discrete settling have been presented in literature (Ramalingam et al., 2012; Chebbo and Gromaire, 2009). These techniques provide measurements of the velocity distribution as a certain mass fraction of particles that settles during a certain time. However, they do not provide any information on the underlying property distribution (size, density, porosity,...) that causes the distributed behaviour of the settling velocity.

Therefore, this work aims to develop a new measuring technique through which detailed information on the dynamics of the PSD both in time and throughout the depth of a settling reservoir can be collected. This information allows to select the required number of particle classes as well as a measurement of the discrete settling velocity for each class.

9.2 Materials and methods

9.2.1 Settling column

A new measurement device was developed to determine discrete settling velocities of different size ranges of activated sludge useful as inputs to a coupled CFD-flocculation model. The device consisted of a settling column of approximately 9 liters with an inner diameter of 150 mm and sampling points at different heights along the column. A total of sixteen sampling holes were located at four different heights. At each height 4 holes were spread equally over the diameter of the settling column. The dimensions and a schematic representation of the settling column are shown in Figure 9.1. This set-up allows taking frequent samples at different heights in the settling column during a batch settling experiment. By alternating the sampling locations at one depth between the 4

9.2. Materials and methods

sampling holes along the diameter, subsequent samples can be taken independently of hydraulic disturbances that might have been caused by previous sampling.

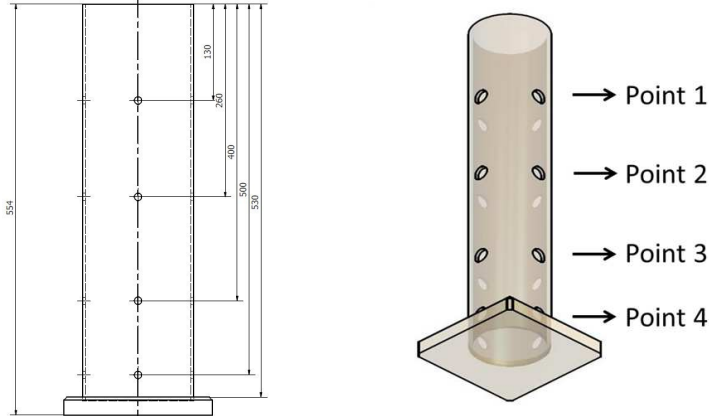


Figure 9.1: Schematic representation of the settling column.

With respect to the choice of sampling technique, care was taken to ensure that the measurements are not biased by wall effects or sample disturbances. Finding the optimal sampling technique is not straightforward. Larger diameters will have less chance of causing interaction between the particles and the wall of the sampling channel but will create larger sample volumes and thus more disturbance in the column. Sampling at a larger distance from the wall entails less risks of wall effects but forces the sample to cross a longer trajectory through the sampling tube which can again disturb the sample. Therefore, a number of sampling strategies (differing in diameter of the sampling tube and the distance of the sampling point from the inner wall of the column) were tested and compared to a reference sample. The reference sample was collected with a pipette of approx. 2 mm in diameter at the same height as the first sampling holes by submerging the pipette from the top of the column. By comparing the different sampling techniques to the reference sample, it was found that the length of the sampling tube should be kept as short as possible and that a diameter of 1 mm is sufficient to obtain a very good correspondence to the reference sample. However, through this rather small sampling tube, large flocs will be excluded from the measurement. The consequences of this choice will be addressed in the results section.

9.2.2 PSD measurements

The set-up above allows taking frequent samples at different heights in the settling column during a settling experiment. To investigate the discrete settling behaviour, PSDs are measured for each sample. Changes in PSDs at one height in time give information on which particle sizes have preferentially settled during a certain time

(i.e. are no longer present in the PSD). Comparing PSDs at different heights allows to determine the velocities of particle classes as the distance between height 1 and 2 divided by the time between the disappearance of size x in the PSD at height 1 and the disappearance of size x from the PSD at height 2.

Several methods are available to analyse particle size: microscopy, laser diffraction, laser obscuration, image analysis (Govoreanu, 2004). Here, PSD were measured with the Eye-Tech particle size analyser (Ankersmid, The Netherlands). Sludge samples to be analysed were placed into 3 ml cuvettes and put into the magnetic stirrer cell of the Eye-Tech where the magnetically driven mixer maintains the particles in suspension during measurement. Subsequently, analysis of the PSD can be performed by two different methods: (1) a laser channel which uses a measurement of Laser Obscuration Time (LOT) and (2) a video channel which uses image analysis. A general overview of the set-up is shown in Figure 9.2.

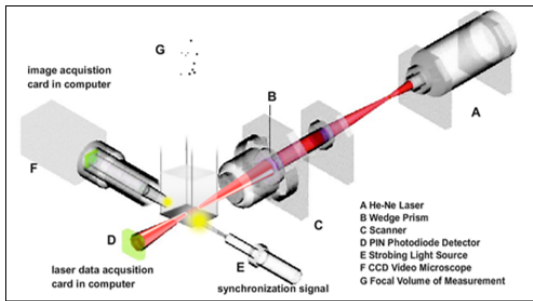


Figure 9.2: Dual measurement channels of the Eye-Tech.

For the laser channel, the measurement set-up consists of a He-Ne laser beam. A single particle in the sample is scanned by a rotating wedge prism (at constant rotating speed: 200 Hz). The size of each particle can be determined from the duration of the beam obscuration signal (= LOT). As LOT represents a direct measurement of particle size, this technique provides a significant advantage compared to laser diffraction. In the latter technique, the size of a particle needs to be determined from the measured refraction profiles by an optical model which is based on some assumptions (e.g. known refractive index, particle sphericity,...). The measurement range of the laser channel is 0.1-2000 μm .

In the second analysis channel (i.e. the video channel) a CCD video camera microscope provides images of the particles which can then be processed through image analysis software. A diverse selection of lenses with different magnifications are available resulting in a measurement range of 1 - 1200 μm . Moreover, this channel allows to include information with respect to the two dimensional shape of a particle whereas the laser channel assumes sphericity of the particles. Information on shape is included

9.3. Results and discussion

through the calculation of the average Feret diameter. Instead of only calculating the diameter in one-dimension, the average Feret diameter determines the diameter along three specified directions and calculates the statistical average. This is illustrated in Figure 9.3.

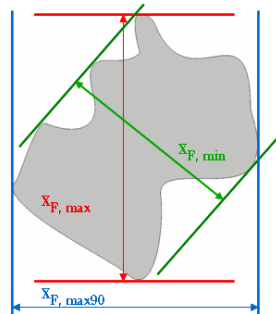


Figure 9.3: Definition of feret diameter.

As sphericity is often a rather harsh assumption for activated sludge flocs, the video channel was selected to measure PSDs in this chapter.

9.2.3 Sludge samples

The settling column tests were performed on activated sludge collected from the WWTP of Roeselare (Belgium). To investigate the discrete settling behaviour, a sludge sample from the aeration tank was diluted with effluent to a concentration of approximately 1 g/l and allowed to settle in the column. The experiments were performed at a concentration of 1 g/l to ensure that the initial settling behaviour is still in the hindered settling regime. In this way both transition from hindered settling to discrete settling and the subsequent dynamics of discrete settling can be studied.

9.3 Results and discussion

Batch settling experiments were performed in the settling column on two different measurement days. On each measurement day, several experiments were conducted during which frequent samples were collected in time and the dynamic evolution of the particle size distribution was measured with the Eye-Tech analyser. The resulting PSDs are shown as absolute number of particles vs. particle size (μm) (i.e. Feret diameter). Presenting the results as number distributions was preferred over volume distributions since the latter are very sensitive to small variations in large particles (the occurrence of only 1 or 2 large particles can cause a severe shift in volume distribution) but much less sensitive to changes in small particles. As small particles typically make up most of

the ESS concentration, the absolute number distribution provides more relevant information than the volume distribution when investigating the discrete settling behaviour.

The measured particles in each sample are divided in the following classes of increasing size (μm):

0-6	31-37	99-116	275-316
6-9	37-44	116-134	316-363
9-12	44-53	134-155	316-363
12-16	53-62	155-180	363-417
16-20	62-73	180-207	417-479
20-25	73-85	207-239	479-549
25-31	85-99	239-275	

9.3.1 Qualitative measurements of discrete settling behaviour

Figures 9.4-9.7 show a detailed evolution of the changes in PSD at the top of the column (sampling point 1) during 2 hours of settling. It should be noted that particles larger than $500 \mu\text{m}$ were not sampled with the current device even though they were visually detected in the settling column. The reason for this lies in the small diameter of the sampling tube and the fact that these larger particles (even though they represent a significant volume) are only present in very low numbers. A possible improvement for this would be to increase the diameter of the sampling tube. However, this would hamper the measurement of smaller particles as significant alterations in the volume of the column would disturb the settling process too much. Moreover, even at larger sample volumes, accurate detection of the larger particles cannot be ensured since the volume for analysis in the Eye-Tech device is only 3 ml making the chance of capturing particles larger than $500 \mu\text{m}$ in this volume rather small. Nevertheless, from visual observations it could be concluded that these large particles settle very fast and will be removed from the system at a very early stage in the experiment. In a coupled flocculation-CFD model, they can thus be classified as a single class of fast settling particles.

From Figure 9.4 it can be seen that during the first 2 minutes of settling, the number of particles in all particle classes decreases simultaneously indicating that the settling process is dominated by the hindered settling regime (i.e. particles settle collectively as a zone independent of size). After this initial period of hindered settling, discrete settling starts with the preferential settling of particles larger than $400 \mu\text{m}$ between 2 and 3 min. after the start of the experiment. These particles together with larger flocs that could only be detected visually can thus be classified as a class of good settling particles.

9.3. Results and discussion

After 10 minutes of settling particles larger than $300\ \mu\text{m}$ are no longer found in the sample (Figure 9.5). This class of particles was thus removed from the top of the settling column between 5 and 10 min. after the start of the experiment. Particles in the range of $220\text{-}300\ \mu\text{m}$ and particles in the range of $150\text{-}220\ \mu\text{m}$ are resp. removed after 20-30 minutes (Figure 9.6) and 1-2 hours of settling (Figure 9.7). Particles smaller than $100\ \mu\text{m}$ do not show any significant decrease in numbers even after 2 hours of settling (Figure 9.7).

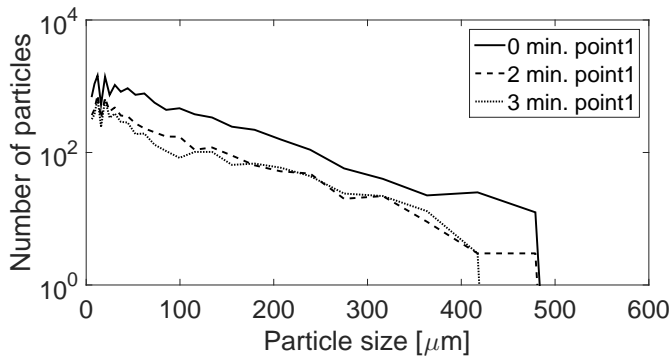


Figure 9.4: Evolution in absolute number distribution at sampling point 1 during the first 3 minutes of settling.

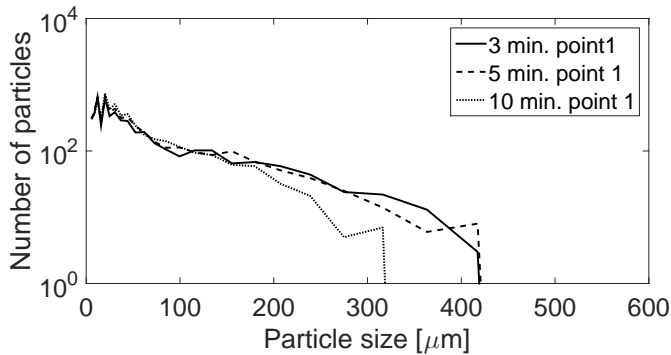


Figure 9.5: Evolution in absolute number distribution at sampling point 1 between 3 and 10 minutes of settling.

These results indicate that the discrete settling behaviour of an activated sludge sample can be described by dividing the sludge in approx. 5 classes going from large flocs ($>400\ \mu\text{m}$) with a high settling velocity to very small particles $<150\ \mu\text{m}$ that hardly show any tendency to settle in the discrete settling regime. In between these two extremes, 3 more classes can be defined ($300\text{-}400\ \mu\text{m}$, $220\text{-}300\ \mu\text{m}$ and $150\text{-}220\ \mu\text{m}$) with decreasing settling velocities. Note that in reality the discrete settling of particles

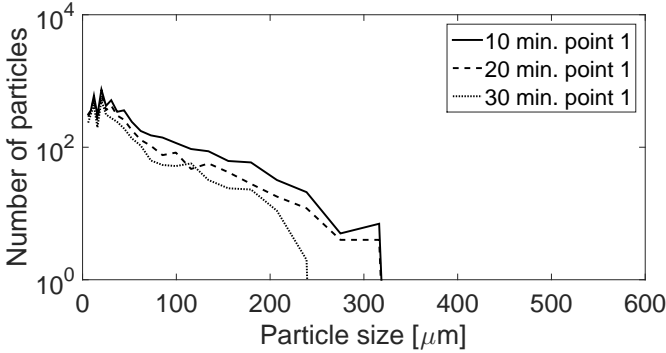


Figure 9.6: Evolution in absolute number distribution at sampling point 1 between 10 and 30 minutes of settling.

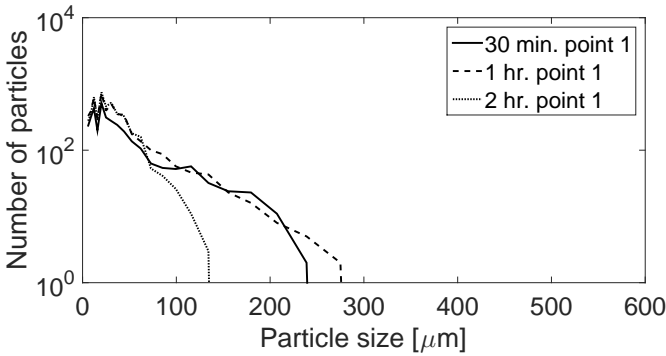


Figure 9.7: Evolution in absolute number distribution at sampling point 1 between 30 minutes and 2 hours of settling.

as a function of size is not as strictly defined. However, the classification of particle sizes with similar settling velocities as defined above provides a good approximation of the true continuous process.

In order to verify these findings, the batch settling experiment was repeated on a second measurement day and the results are shown in Figure 9.8. Similar trends as for the first measuring day can be observed: hindered settling prevails during the first few minutes of settling followed by sequential settling of particles of different sizes during the remainder of the experiment. Particles smaller than 150 μm show very poor settling properties although some reduction in particles between 100 and 150 μm can be observed after 2 hours. Particles between 150 μm (non-settleable fraction) and 500 μm (fast settling particles that could be observed visually) behave somewhat different than for the previous experiment. For example, after 1 hour of settling particles larger than

9.3. Results and discussion

220 μm can still be observed whereas these had all disappeared from the top of the column in the previous experiment. Hence, for a proper definition of the intermediate size classes more repetitions are needed.

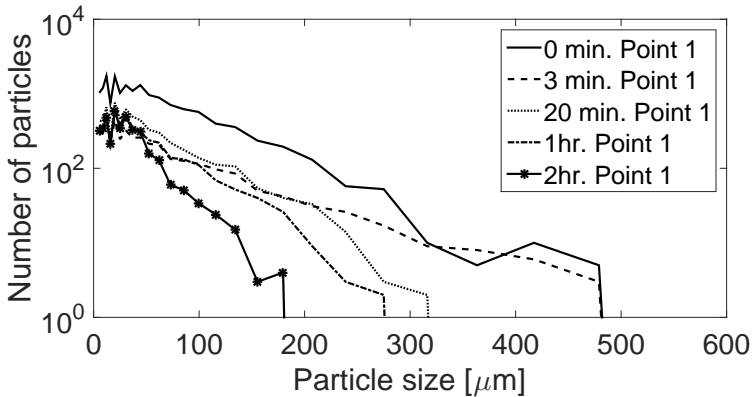


Figure 9.8: Evolution in absolute number distribution at sampling point 1 during 2 hours of settling (on measurement day 2).

Finally, the settling column test was repeated at a lower initial concentration (by diluting the mixed liquor sample to approx. 500 mg/l). With this set-up, the initial concentration is too low for hindered settling and the settling should immediately start in the discrete regime. The resulting PSD distributions (Figure 9.9) indeed do not show a simultaneous initial decrease in all size ranges as could be observed for the previous experiments thus confirming that no hindered settling is taking place. During the first 5 minutes of settling no significant changes in PSD are measured, however, discrete settling of particles $> 500 \mu\text{m}$ could be observed visually during this time. Between 5 and 10 minutes after the start of the experiment, discrete settling of particles between 220 and $500 \mu\text{m}$ can be observed (Figure 9.9). The remainder of the experiment shows similar trends as the experiments at higher initial concentrations.

9.3.2 Comparison to effluent quality

To investigate the quality of the settling process during settling in the batch column, the supernatant PSD after 2 hours of settling was compared to the PSD in the effluent of the WWTP (Figure 9.10). The number distribution after 2 hours of settling shows very good correspondence to the number distribution in the effluent sample for particles smaller than $100 \mu\text{m}$. This confirms that particles smaller than $100 \mu\text{m}$ can be considered as a class of non-settling particles, even in a full-scale settler. Removal of particles smaller than $100 \mu\text{m}$ should thus be accomplished through flocculation of

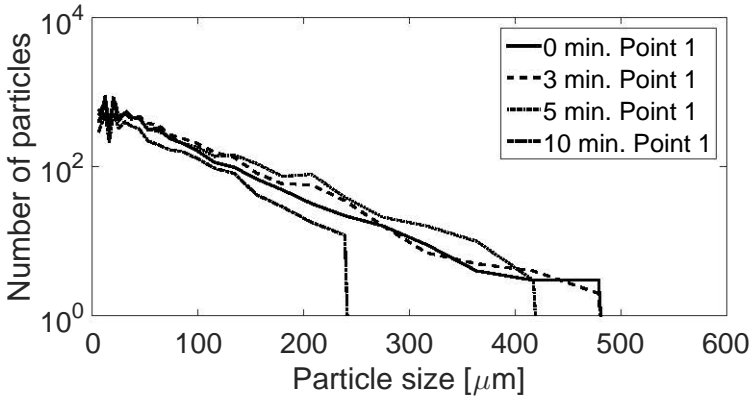


Figure 9.9: Evolution in absolute number distribution at sampling point 1 during the first 10 minutes of settling at an initial concentration of 500 mg/l.

these particles in the flocculation well or by capturing them in the sludge blanket during the hindered settling regime. The effluent sample, however, still shows the presence of particles larger than 150 μm whereas after 2 hours of settling in the settling column all particles in this range were removed. Online measurements of the incoming flow rates during sampling show that the average hydraulic residence time in the SST is approx. 9 hours. However, in a full-scale clarifier, particles are not only subjected to a gravitational settling flux but will undergo an additional upward convective flux (due to the overflow) in the clarification zone. This explains the somewhat worse settling behaviour in the effluent compared to the batch experiments.

9.3.3 Quantitative determination of the discrete settling velocity

The results above (measured at the first sampling point) allow distinguishing different classes of particles depending on their settling velocity. However, in order to quantify their discrete settling velocities, the time it takes for particles of a certain class to travel the distance along the column needs to be measured. This can be accomplished by comparing the changes in PSD at different heights throughout the column. Information from the lowest sampling point cannot be used since this sampling point is located inside the sludge blanket. Therefore, the changes in PSD at sampling point 3 (located 27 cm below sampling point 1) during 2 hours of settling are investigated (Figure 9.11) and compared to the results at sampling point 1 (Figure 9.8).

Similar as to what was observed at the top of the settling column, also in the lower regions of the column a first period of hindered settling can be observed. Approx. 5

9.4. Conclusions

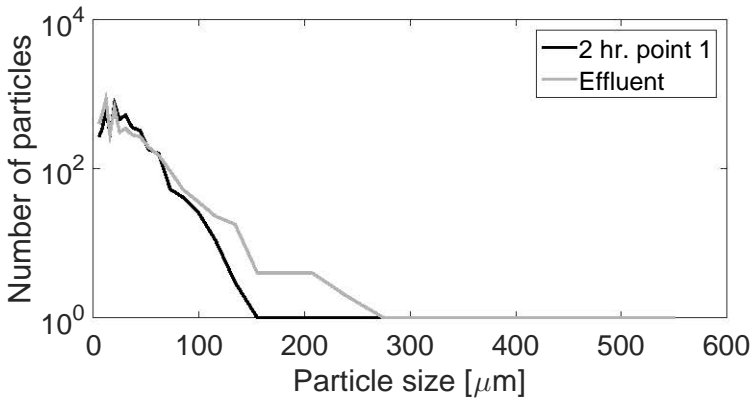


Figure 9.10: Comparison between the absolute number distributions after 2 hours of settling in a settling column and in an effluent sample of the WWTP of Roeselare.

minutes after the start of the experiment, the settling behaviour shifts to the discrete regime. As mentioned earlier, particles larger than $500 \mu\text{m}$ are not recorded in the PSD measurements. However, the removal of these fast settling flocs beyond point 3 could be detected visually after approx. 3 min. thus giving them a settling velocity $> 10 \text{ cm/min}$. As can be seen from Figure 9.11, it takes a long time for particles $< 400 \mu\text{m}$ from the top of the column to settle past point 3. Only after 2 hours of settling particles $> 300 \mu\text{m}$ are no longer detected in the measured PSD. From Figure 9.8 it can be seen that this same group of particles could no longer be detected at the top of the column after 1 hour of settling. Hence, it takes particles between 300 and $500 \mu\text{m}$ about 1 hour or less to travel the 27 cm distance between point 1 and point 3 setting the lower limit of their settling velocity at 0.5 cm/min .

In order to quantify the settling velocities of the smaller size classes, the experiment should be conducted for longer settling times and more frequent data should be collected at later times during the settling process. Moreover, additional repetitions are needed to confirm the presented findings.

9.4 Conclusions

A new measurement device was constructed which allows to measure changes in PSD during settling at low concentrations in a batch settling column. Through measurements of PSDs at different settling times and at different heights of the settling column both quantitative and qualitative information on the discrete settling behaviour of activated sludge was collected.

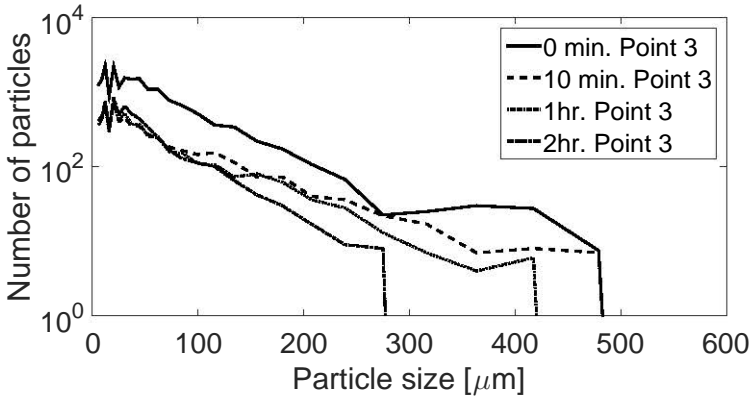


Figure 9.11: Evolution in absolute number distribution at sampling point 3 between 10 minutes and 2 hours of settling (on measurement day 2).

- By comparing PSDs at different settling times at the top of the column, particles could be classified in roughly 5 classes with comparable settling velocities: a class of large flocs ($>500 \mu\text{m}$) that settle rapidly and will be preferentially removed during the first few minutes of settling, a class of non-settling particles $<150 \mu\text{m}$ and 3 intermediate classes ($300\text{-}400 \mu\text{m}$, $220\text{-}300 \mu\text{m}$ and $150\text{-}220 \mu\text{m}$) with settling velocities that are decreasing with size. However, for a reliable definition of the intermediate size classes more repetitions of the experiment are required.
- The PSD after 2 hours of settling in the column was compared to a measurement of the PSD in the effluent of the WWTP. A good correspondence between the number of particles $<150 \mu\text{m}$ confirming that these particles can be classified as a non-settleable fraction. The PSD of the effluent showed an increase in particles $>150 \mu\text{m}$ compared to the batch settling results after 2 hours. This can be explained by the additional convective flux due to the overflow in a full-scale SST.
- Moreover, measuring the evolution in PSDs at different depths throughout the column allows quantifying the discrete settling velocities in the different size classes. Discrete settling velocities were calculated from the difference between the time a certain class is removed from the top of the column and the time that the same class can no longer be detected at a pre-defined distance further down the column. This indicated a settling velocity of 10 cm/min for particles $>500 \mu\text{m}$ and a minimal velocity of 0.5 cm/min for particles between $300 \mu\text{m}$ and $500 \mu\text{m}$. Experiments including longer settling times are needed to determine the settling velocity of smaller size classes.

9.4. Conclusions

- The results in this chapter showed that a simple newly developed measurement device can bring a lot of new insights with respect to activated sludge settling. Detailed information on dynamic PSD can significantly aid in understanding (and modelling) the complex settling and flocculation behaviour of sludge particles at low concentrations which will consequently lead to improved predictions of the effluent concentrations.

CHAPTER 10

Towards mechanistic models for activated sludge flocculation under different conditions based on inverse problems

Redrafted from:

Torfs, E., Dutta, A., and Nopens, I. (2012b). Investigating kernel structures for Ca-induced activated sludge aggregation using an inverse problem methodology. *Chem. Eng. Sci.*, 70:176–187.

Torfs, E., Bellandi, G., and Nopens, I. (2012a). Towards mechanistic models for activated sludge flocculation under different conditions based on inverse problems. *Water Sci. Technol.*, 65(11):1946–1953.

Abstract

The flocculation of AS is a crucial process in SSTs as the PSD will significantly influence the settling behaviour and thus the effluent quality (Chapter 8). However, the mechanisms driving the flocculation processes are not yet fully understood and current kernel structures for collision frequency and efficiency are unable to accurately describe activated sludge flocculation data (chapter 2). Therefore, in this chapter, dynamic PSD data of activated sludge flocculation under different conditions of ionic strength, temperature and dissolved oxygen concentration are analysed with an inverse problem yielding empirical models.

A similarity analysis of the experimental data showed multiple sequential similarity regions for Ca-induced flocculation suggesting different flocculation mechanisms occurring in time. Empirical aggregation kernel structures are recovered from the exper-

imental data and implemented in a PBM to model the aggregation process. The use of multiple kernels for specific similarity regions in the data results in improved model predictions. Furthermore, a methodology is proposed to compare the retrieved kernel with literature kernels in order to identify their flaws. This comparison indicated the need for a fractal dimension that depends on floc size. This chapter shows the useful application of inverse problems to improve the understanding of complex mechanisms such as aggregation.

10.1 Introduction

In Chapter 8 it was shown that a flocculation model integrated with CFD allows to model the influence of local velocity gradients on the flocculation and clarification dynamics. As a proof of concept the simplified flocculation model of Parker et al. (1972) was used in which aggregation and breakage dynamics are described as a constant value. In reality the flocculation of activated sludge is much more complex and the mechanism has neither been thoroughly investigated nor successfully quantified.

PBMs have been developed to model the dynamics of PSDs (Ramkrishna, 2000). In these models, aggregation and breakage dynamics are described by mathematical functions, called kernels. To model the aggregation process, information regarding the frequency of collision between particles and the efficiency of these collisions is required. The frequency of collisions is generally described by a transport equation also called the collision frequency kernel or β kernel. The efficiency of the collisions between flocs is described in the collision efficiency kernel or α kernel. The latter represents a function that incorporates information concerning attachment of the particles (surface properties, short range forces...). Different expressions for both α and β kernels have been presented in literature (Spicer and Pratsinis, 1996a). However, Ducoste (2002) and Nopens et al. (2005) confronted these models with experimental data by numerically solving the PBM (see Figure 10.1 - conventional path) and showed that the kernels from literature are not able to describe the activated sludge flocculation process. Hence, important processes are likely missing in existing kernel structures. Determining the exact cause using a forward simulation (i.e. numerically solving the PBM with a specific kernel function) is difficult as it resembles "finding a needle in a haystack". An alternative approach is to solve the inverse problem based on dynamic experimental data, yielding empirical models (Wright and Ramkrishna, 1992; Nopens et al., 2007b). The concept of the inverse problem methodology is illustrated in Figure 10.1 - inverse path.

It is important to stress that no kernel functions are used in the inverse problem methodology. Experimental data of dynamic particle size distributions are used to extract an empirical kernel. Solving the inverse problem is, hence, an elegant way to retrieve a mathematical function that is able to describe the dynamics in the data. The downside

10.1. Introduction

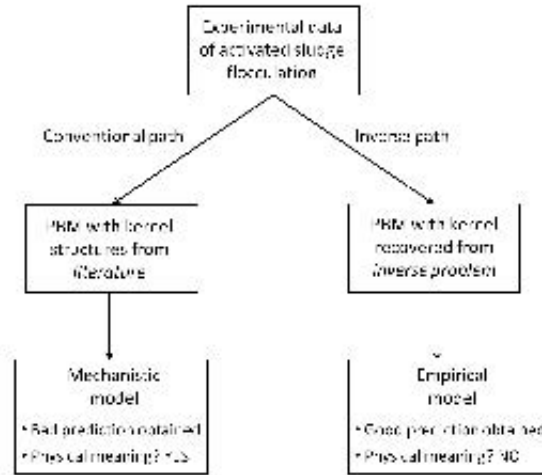


Figure 10.1: Schematic representation of the different routes that can be followed: the conventional path (left) versus the inverse path (right). Note that the bad prediction for mechanistic kernels was only shown for the process studied and should not be generalised.

of this approach lies in the empirical nature of the recovered kernel functions making them unsuited for direct application in system analysis or process optimisation. They can, however, provide valuable insights into the true dynamics of the flocculation mechanism and allow evaluating where conventional kernel structures fail to capture the true dynamics and how they can be improved.

Knowledge related to the flocculation process can be improved only by a careful analysis of the physico-chemical factors affecting it. Both environmental conditions and process parameters will influence the floc properties. A deeper, thorough investigation of these effects will eventually allow understanding the complex processes related to the floc formation. This could improve the activated sludge performance with regard to separation. In this chapter, aggregation dynamics under different conditions of ionic strength (in terms of calcium (Ca^{2+}) concentration), Dissolved Oxygen (DO) and temperature are investigated. Next to these factors, also pH has been reported to have a significant influence on activated sludge structure and properties (Mikkelsen, 2001). However, the effect of the latter is not considered in this chapter.

Sludge concentration and ionic strength affect bioflocculation where an increase in ionic strength can lead to flocculation whereas a decrease can cause deflocculation, since it weakens the floc strength. Govoreanu (2004) found a relationship between increased ionic strength and floc size by showing that the average floc diameter could be increased at high shear (mixing intensity) when Ca^{2+} was added. Addition of calcium

acts as a sludge conditioning agent resulting in larger flocs; although the degree of flocculation is not linearly proportional to the amount of Ca^{2+} added (Biggs et al., 2001).

Moreover, evidence is provided in literature that short-term effects of temperature and DO concentration have a significant influence on the flocculation process of activated sludge (Sürücü and Çetin, 1989; Wilén and Balmér, 1999; Liao et al., 2001). Temperature has a complex influence on the performance of the activated sludge flocculation process. The temperature effect is related to both transport and attachment of the flocs. When temperature increases, the mixed liquor viscosity decreases, improving its mixing behaviour and enhancing Brownian motion of small particles. The latter is, however, only important for relatively small particles ($< 1\mu\text{m}$) and is, therefore, often not considered to be important in activated sludge flocculation compared to the magnitude of other transport mechanisms. Next to the viscosity effect, the separation properties of the activated sludge are also influenced by temperature due to a change in function and charge of the EPS (Sürücü and Çetin, 1989; Wilén, 1999). However, very little is known about the direct impact of the short-term temperature effect on floc size dynamics.

Li and Ganczarzyk (1993) found that the availability of DO is one of the most significant factors which influence the size distribution of activated sludge flocs. Wilén and Balmér (1999) performed an intensive research study regarding the effect of DO concentration on flocculation. Long term effects were mostly governed by growth of filamentous bacteria. From a short-term perspective, oxygen limitation had a pronounced effect on the amount of small flocs in the supernatant after settling and introduced an increase in effluent turbidity, although the size and structure of the larger flocs was not significantly affected.

This chapter applies the inverse problem methodology on experimental data of dynamic PSD under different conditions in order to unravel the effect of physico-chemical factors on aggregation dynamics. Furthermore, a consistent methodology is proposed to compare the recovered kernels to expressions from literature in order to investigate where existing kernel structures fail to capture the true dynamics and how they could potentially be improved.

10.2 Material and methods

10.2.1 Experimental data

Experimental data of dynamically evolving PSDs are borrowed from Biggs et al. (2001) and Govoreanu (2004). Biggs et al. (2001) conducted different flocculation experiments where either shear-induced (lowering the average shear from 113 to 19.4 s^{-1})

10.2. Material and methods

or Ca-induced (addition of resp. 8, 16 and 32 meq $\text{Ca}^{2+} \text{ l}^{-1}$) aggregation was applied. The Ca^{2+} concentrations are chosen in such a way as to represent concentrations that are typically dosed in full-scale wastewater treatment plants to promote sludge flocculation. The behaviour of shear-induced flocculation was investigated in a previous study (Nopens et al., 2007a). In this chapter, the focus will be on Ca-induced flocculation. However, the data on shear-induced flocculation are also employed for the purpose of comparison between shear-induced and Ca-induced flocculation.

Govoreanu (2004) conducted several experiments under different conditions in which flocculation dynamics were measured by on-line monitoring of PSD. This was done by recording the number of particles in 44 particle size classes every 30 seconds by means of laser diffraction (MastersizerS[®]). In this chapter, only the data of PSD under changing conditions of temperature and DO are studied. The DO concentration limits were set between anaerobic conditions (DO=0 mg/l) and an aerobic level at DO=4 mg/l. DO=2 mg/l was chosen as an intermediate reference value. To raise the oxygen in the vessel O_2 -gas was supplied through a permeable silicon tube, from where the gas diffuses into the liquid in a bubble-less manner (avoiding additional shear). To decrease the oxygen level, N_2 -gas is used in a similar way. Temperature experiments were conducted at resp. 5°C, 15°C and 25°C.

The workflow of each experiment of Govoreanu (2004) is shown in Figure 10.2. First, a sludge sample was taken from a SBR breeding reactor and transferred into a flocculation vessel (separate setup). Initial conditions in this vessel were set by diluting the sludge to the desired concentration using SBR effluent (step 1) and controlling the experimental parameters (e.g. DO, T,...) at reference values (step 2), to which the sludge was given time to acclimatize (t_1). This allowed each experiment to start with a similar sludge, acclimatized under identical conditions. PSDs were recorded at these initial conditions during $t_2 = 10$ min (step 3). Subsequently, one or more of the experimental parameters were changed to correspond to the design of the specific experiment (step 4). Once again, the sludge was given time to acclimatize (t_3) after which particle size distributions were measured at the new design point during $t_4 = 10$ min (step 5). Finally, Ca^{2+} was added to promote flocculation (step 6) in order to study the Ca-induced flocculation dynamics for the new experimental conditions (step 7).

Next to these dynamic experiments, Govoreanu (2004) performed a second set of experiments which consisted of consecutive variations of each studied parameter in the reactor vessel without addition of Ca^{2+} . These experiments allow comparing the steady state floc size for different experimental conditions. These experiments will be referred to as the steady state experiments.

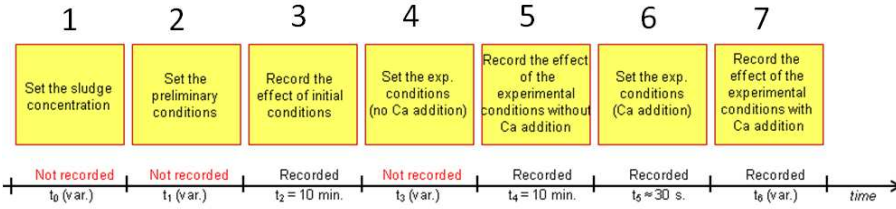


Figure 10.2: Time scale evolution of the flocculation experiments by Govoreanu (2004).

10.2.2 Inverse problem methodology

As the goal of this chapter is to investigate the aggregation dynamics of activated sludge a PBM is adopted which contains only aggregation and whereby breakage is assumed negligible. This can be justified based on Figure 10.4 from which it can be observed that the floc size distribution is evolving in time towards a larger size range, indicating that aggregation is the dominant process for Ca-induced flocculation.

The methodology for solving the inverse problem is adopted from Wright and Ramkrishna (1992). Figure 10.3 provides a schematic representation of the different steps that comprise the solution of an inverse problem and the recovery of a valid kernel. First, similarity analyses are performed on all data sets. Subsequently, the aggregation kernel structures are extracted and used to perform a check with regard to the quality of the inversions. More details of the different steps are given below.

Similarity analysis

The idea behind a similarity analysis (step 1 in Figure 10.3) is to look for a scaling function that can rescale the set of experimental PSDs collected at different time instants, in such a way to make all those separate distributions collapse onto a single distribution (i.e. the similarity distribution). Note that no information is lost during this procedure since no datapoints are omitted from the analysis, only a transformation of the data is accomplished. Transforming the separate PSDs into one collapsing distribution allows to rewrite the Population Balance Equation (PBE) in a simplified form, which considerably enhances the solution of the inverse problem. Practically, this means that for each time instant a scaling function $h(t)$ is computed and used to rescale the particle volume x into the similarity variable η :

$$\eta \equiv \frac{x}{h(t)} \quad (10.1)$$

10.2. Material and methods

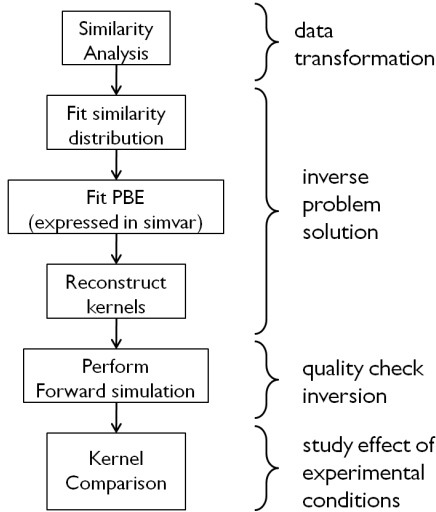


Figure 10.3: Schematic representation of the inverse problem methodology.

In the case of pure aggregation the scaling function is given by the ratio of two successive integral moments μ of the number density function $f(x, t)$ as shown in Eq. 10.2 (Wright and Ramkrishna, 1992). The process of determining k typically proceeds through trial and error.

$$h(t) = \frac{\mu_{k+1}(t)}{\mu_k(t)} = \frac{\int_0^{\infty} x^{k+1} f(x, t) dx}{\int_0^{\infty} x^k f(x, t) dx} \quad (10.2)$$

Figure 10.4 demonstrates the principle behind this similarity analysis. The cumulative PSD measurements of a flocculation experiment are given on the left side of Figure 10.4. After rescaling x for each experimental distribution to the similarity variable η with an optimal k -value Figure 10.4 (right) is obtained. Every measurement of each distribution from the left figure is included in the right figure, the data have merely been transformed to make them collapse onto one single distribution as function of η by eliminating time.

Performing a similarity analysis is a crucial step in solving the inverse problem, for if no similarity can be found, the PBE cannot be written in terms of the similarity variable and consequently finding a solution for the inverse problem becomes more challenging (but is not impossible).

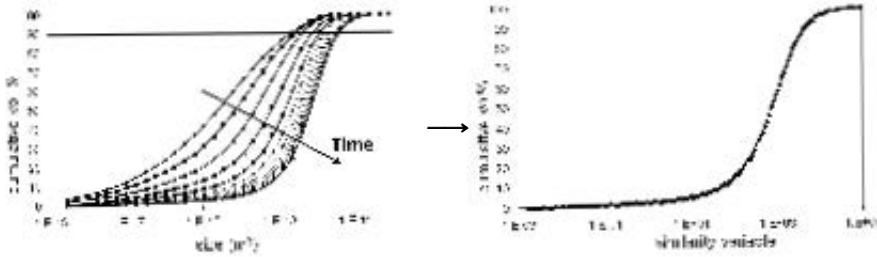


Figure 10.4: Time evolution of the cumulative distribution of an aggregation experiment (left) and its rescaled similarity distribution (right)

Solving the inverse problem

The PBE for pure aggregation as function of the similarity variable η is given by (Wright and Ramkrishna, 1992):

$$\eta\Phi'(\eta) = \int_0^\eta d\eta' \Phi'(\eta') \int_{\eta-\eta'}^\infty d\eta'' \frac{\Phi'(\eta'')}{\eta''} \frac{\alpha(\eta', \eta'')}{\langle\alpha\rangle} \quad (10.3)$$

Here, $\Phi'(\eta)$ is the first derivative of the cumulative similarity function and $\alpha(\eta', \eta'')/\langle\alpha\rangle$ is the unknown function that needs to be reconstructed. It represents the scaled aggregation frequency (in terms of similarity variable) divided by the mean scaled aggregation frequency (Ramkrishna, 2000). After solving the inverse problem, $\alpha(\eta', \eta'')/\langle\alpha\rangle$ can be converted back to the unscaled kernel (in terms of size) which can then be used in a forward simulation. The procedure for solving the PBE in terms of similarity variable (Eq. 10.3) is summarized below.

For each experiment the similarity distribution ($\Phi(\eta)$) is approximated using an expansion of γ -functions (step 2 in Figure 10.3). Note that this leads to the additional advantage of filtering out noise that might possibly be present in the dynamic dataset. The unknown aggregation frequency $\alpha(\eta', \eta'')/\langle\alpha\rangle$ can be represented by linear combinations of basis functions (Laguerre polynomials). As aggregation is a particle-particle interaction process, a linear combination of Laguerre polynomials is defined for each particle axis and the unknown aggregation frequency is calculated as the inner products of the Laguerre polynomials over each axis at all discretised η -values. The number of inner products used in the inversion depends on the number of basis functions n_b used per axis. Here, n_b is chosen to be 2.

The inverse problem can then be solved by fitting the right hand side of Eq. 10.3, which

10.3. Results

can be computed, to the left hand side that can be extracted from the experimental data, resulting in an optimal set of coefficients for the linear combination of Laguerre polynomials (step 3 in Figure 10.3). The optimization method is a constrained one where symmetry is enforced on the kernel. Identifiability was not investigated as such, however it is expected that this would not pose problems. After all, the recovered optimal coefficients have no actual physical meaning and the goal of this chapter is to study the structure of the recovered kernel, which will not be influenced by identifiability in the coefficients. Finally, the recovered kernel can be reconstructed from the linear combination of Laguerre coefficients using the optimal set of coefficients (step 4 in Figure 10.3). The quality of the recovered kernel can be checked by implementing this kernel in the PBM and performing a forward simulation (step 5 in Figure 10.3).

Comparison of inversely recovered kernels and literature kernels

The inversely recovered kernels have the drawback of being empirical, i.e. having no physical meaning. Once a kernel has been recovered successfully, it can be compared to kernels from literature in order to evaluate where the conventional kernels fail (step 6 in Figure 10.3). Aggregation is typically considered to be based on two distinct steps: transport and attachment. The former is described by the collision frequency (β), the latter by the collision efficiency (α). For each process, numerous kernel structures have been suggested in literature. The kernel recovered through the inverse problem actually represents the product of α and β . Comparing this recovered kernel to literature kernels becomes quite challenging in this manner since various combinations of α and β can be made. Therefore, a rigorous methodology for kernel comparison is proposed in Section 10.3.1.

10.3 Results

The inverse problem was solved for experimental data of dynamical PSDs from Biggs et al. (2001) and Govoreanu (2004). First, the effect of ionic strength is investigated based on three datasets of Biggs et al. (2001) which differ in the amount of Ca^{2+} that was added to induce flocculation. Earlier data on shear-induced flocculation are employed for the purpose of comparison. The datasets are referred to as experiment 1 (8 meq Ca^{2+}), experiment 2 (16 meq Ca^{2+}) and experiment 3 (32 meq Ca^{2+}).

Next, PSDs measurements from Govoreanu (2004) are used to study short term effects of dissolved oxygen concentration (experiment 4) and temperature (experiment 5) on the structure of the aggregation kernel.

10.3.1 Experiment 1: 8 meq Ca²⁺

Similarity analysis

Obtaining a feasible solution for the inverse problem depends on the transformation of the experimental PSDs into a self-similar distribution. In order to acquire this transformation, an optimal scaling factor (Eq. 10.2) is required. The original time evolution of the cumulative volume distributions is depicted in Figure 10.5. Figure 10.6 shows the resulting similarity distributions after transformation of the experimental data for different values of the scaling factor k . It is important to note that the first time steps are left out during the similarity analysis since no k -value is found for which similarity can be observed in this region.

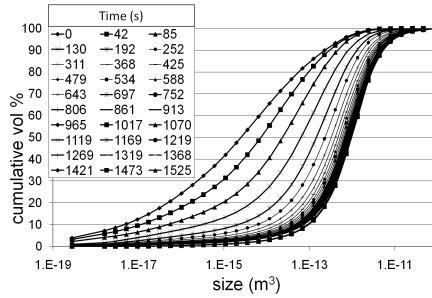


Figure 10.5: Time evolution of the cumulative volume distribution.

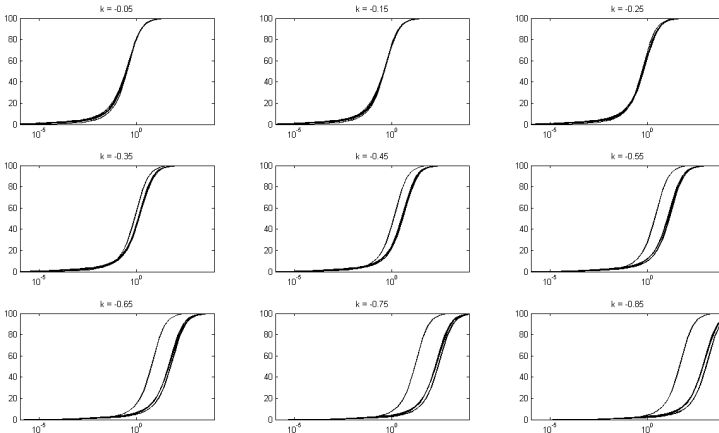


Figure 10.6: Similarity distribution for different values of the scaling factor k .

10.3. Results

From the graphs in Figure 10.6, it seems that the optimal k -value can be found around $-0.15/-0.25$. Here the different PSDs collapse onto one single distribution although some deviation from similarity in the smaller size ranges can be observed. Changing the k -value to more negative values results in the loss of a single similarity distribution. However, not all similarity is lost. The single distribution is simply split into two new similarity distributions whose individual shapes demonstrate a much better similarity than the distribution at $k = -0.15$. Moreover, the experimental PSDs are not randomly distributed amongst these two similarity distributions. Each similarity distribution consists of a well defined time series of consecutive measurements. A further decrease in k introduces a third similarity curve, again formed by a number of consecutive measurements. Hence, three different regions of similarity in time can be observed in the data. For k -values beyond -0.85 , all similarity is slowly lost.

Figure 10.7 (left) gives a more detailed representation of the similarity distributions for a k -value of -0.85 where three separate similarity curves can be observed. This figure clearly shows that each similarity region consists of a well-defined time region of the experimental data. From the time instant similarity is first observed up to 806 s, the measured PSDs collapse onto the first similarity distribution. All PSDs measured at later time instances up to 1368 s form the second similarity region. The last four time instants up to 1525 s form the third similarity region.

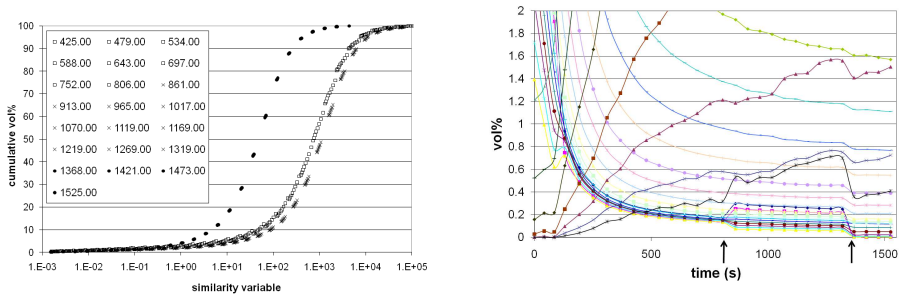


Figure 10.7: Similarity distribution at different time instances for a k -value of -0.85 (left) and the corresponding change in volume percentage for the different classes (right).

The question now arises, what causes these different similarity distributions? Does the loss of similarity always follow a stepwise pattern (this was not the case for the data on shear-induced flocculation investigated by Nopens et al. (2007b)) or is there an underlying phenomenon? To answer these questions, the evolution of the volume fraction for the different size classes in function of time is investigated. Figure 10.7 (right) reveals discontinuities in the evolution of the volume fractions at the exact time instants that the separations of the similarity distributions are found (indicated by the black arrows). Also the directions of the observed discontinuities are opposite for the

two time instants, which can possibly explain why one similarity shift is observed to the left whereas the other one moves to the right. As will be illustrated later, similar observations are made in the other Ca^{2+} addition cases, ruling out the possibility of an experimental artefact. Hence, it is believed that these different similarity regions are caused by the occurrence of different flocculation mechanisms in time, possibly Ca-induced flocculation followed by shear-induced flocculation.

Inverse problem solution

If similarity is observed in the data, the inverse problem can be solved and the aggregation kernel recovered. The observation of different similarity regions in the data indicates that different aggregation kernels may be needed to describe these various regions. To investigate the significance of these similarity regions in predicting aggregation, the inverse problem is solved for three different cases. In the first case ($k=-0.15$) only one similarity curve is considered resulting in one extracted kernel for the entire data interval. For the second ($k=-0.35$) and third case ($k=-0.85$), respectively, two and three inverse problems are solved providing each similarity region with its proper kernel.

For each case, and each time region within one case, an optimisation procedure is applied to find the best fit between the right-hand side and left-hand side of Eq. 10.3. At this stage, the inversion is completed and kernels are recovered for the 3 cases. The quality of the recovered aggregation kernels can now be verified by performing a forward simulation (simply numerically solving the PBE) using the kernel structure found through inversion. If inversion is successful, the model should be able to follow the experimental data from which it was extracted. Since only the dynamic behaviour at time instants where similarity could be observed, is considered, the forward simulation is performed only for these experimental data. The initial distribution is thus set at the time instant where similarity is first observed (i.e 425 s).

The results of the forward simulations for the three defined cases are shown in Figure 10.8. For the first case only one kernel is extracted which is used to describe the entire data range. The resulting forward simulation shows that although the overall trend is captured quite well by the model, an overestimation of the peak values and an underestimation of the upper tail occurs. The overall Sum of Squared Errors (SSE) of the model prediction amounts to 1033.

In the second case ($k=-0.35$), two different regions of similarity are considered and accordingly two different aggregation kernels are extracted. Each similarity region is thus simulated using its proper kernel and with an initial distribution equal to the distribution of the first time instant in the corresponding region. The overall result of these two simulations is depicted in Figure 10.8 (top right). Although for the first region there is still an overprediction in the peak values and an underprediction of the upper

10.3. Results

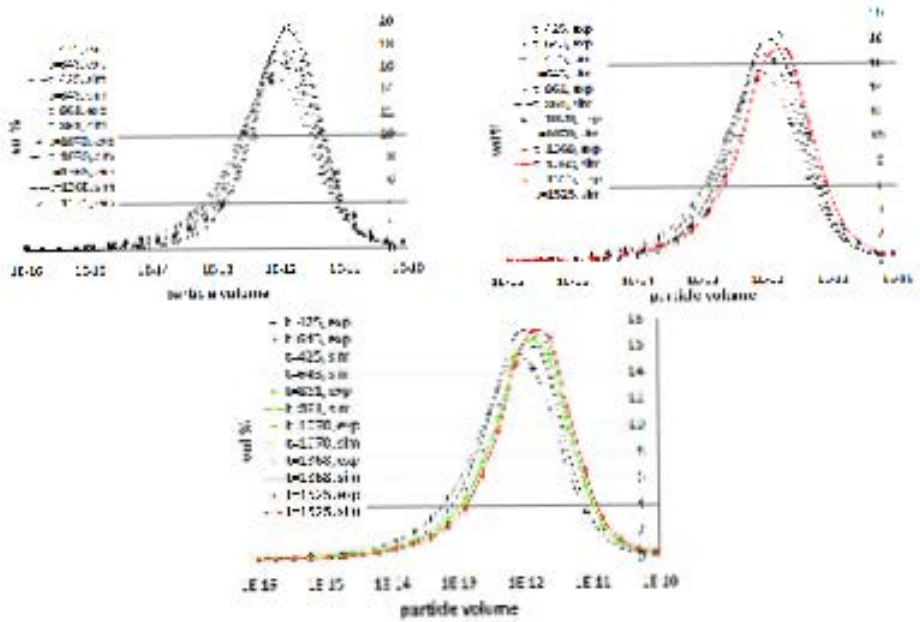


Figure 10.8: Results of the forward simulations for the first (top left), second (top right) and third (bottom) case. The colours indicate the consecutive similarity regions for which different kernels were recovered.

tail, the later time instants (distributions shown in red in Figure 10.8) corresponding to the second region show a much better prediction for peak values as well as the upper tail. The SSE of the model predictions are found to be respectively 274 and 0.35 summing to a total SSE of 274.35 supporting the hypotheses that the overall performance is much better using two different similarity regions. Especially the second region is reproduced very accurately by the model.

The third case ($k=-0.85$) applies three different kernels to the data according to the three similarity regions that are reported. Here, the forward simulations consists of three separate simulations with analogue properties as in the second case. Figure 10.8 (bottom) shows the final results. SSE values of 55, 16 and 0.61 are observed for the different time regions, resulting in an overall SSE of 71.61. Compared to the two previous cases, this represents a significant improvement. These results indicate that performing a thorough similarity analysis provides valuable information on the aggregation dynamics of the data. Accurate predictions of the experimental data are obtained when extracting a separate kernel for each similarity region suggesting that different aggregation dynamics are valid for each similarity region.

Kernel reconstruction

The structure of the different extracted kernels can now be reconstructed (i.e. the scaled recovered kernel should be unscaled by transforming the similarity variables back to original sizes). Subsequently, these kernels can be compared to one another (for the different cases) and, moreover, to the kernel extracted from shear-induced flocculation data (Nopens et al., 2007b). The latter is depicted in Figure 10.9 (left), where the X- and Y-axes represent the floc sizes (in m^3) and the Z-axis shows the aggregation rate ($\alpha_{inv} \times \beta_{inv}$). A monotonic increase in aggregation frequency can be observed for increasing size of both colliding flocs. The increase is, however, most pronounced for homogeneous collisions (i.e. collisions of similar-sized particles).

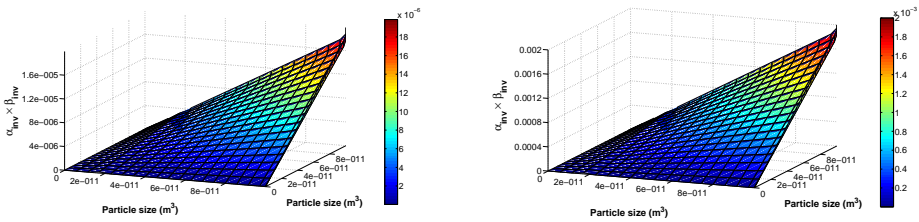


Figure 10.9: Kernels recovered through solving the inverse problem using $nb=2$ for shear-induced flocculation (left) and 8 meq Ca-induced flocculation - case 1 (right)

The recovered kernel for the first case of 8 meq Ca-induced flocculation is represented in Figure 10.9 (right). The general shape for the different kernels is similar. They do, however, differ in absolute value (on Z-axis), i.e. two orders of magnitude higher in the case of Ca^{2+} -addition. This is expected since Ca^{2+} is used as a flocculation promoter.

Kernel evaluation

From the previous sections it has become clear that by solving the inverse problem, a kernel structure can be extracted which is able to accurately describe the activated sludge aggregation dynamics in contrast to conventional kernels which fail in this respect (Nopens et al., 2005). However, the extracted kernel is of a mere empirical nature (Figure 10.1). Consequently, this kernel does not aid in understanding the physical mechanism behind aggregation nor does it provide information on how to optimise the system. Nevertheless, it can be used for comparison with existing mechanistic kernels to find out what is missing in the existing kernel structures and moreover in which direction to focus further research for improvement of the existing kernels.

The kernel recovered through the inverse problem represents the product of both collision frequency and efficiency (i.e. $\alpha_{inv} \times \beta_{inv}$). Comparing this kernel to literature

10.3. Results

kernels becomes quite challenging in this manner since various combinations of α_{lit} and β_{lit} can be made. Therefore, in this section a rigorous methodology for kernel comparison is proposed and applied for the investigation of the recovered kernel structures. The schematic outline of this methodology is shown in Figure 10.10.

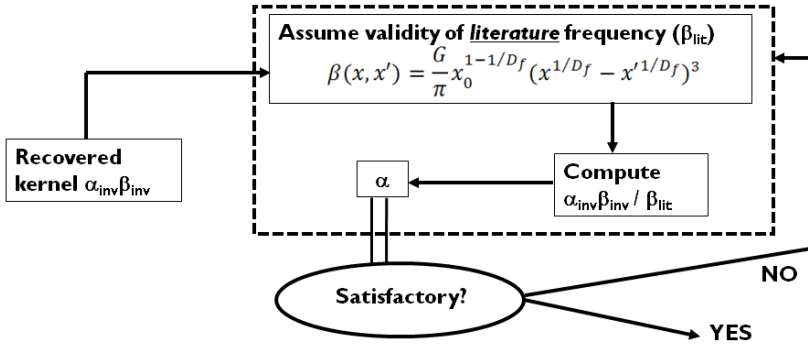


Figure 10.10: Methodology for obtaining expression for α from inverse problem solution.

In order to compare the extracted kernel structure to literature expressions for α and β , a fixed expression for either collision efficiency or collision frequency needs to be chosen from literature. In this way, only one unknown variable remains. It is chosen to fix the collision frequency and focus on the effect of changing physical-chemical factors on the collision efficiency. The reason for this is two-fold. First, given that addition of Ca^{2+} will influence the attachment processes rather than the transport of particles, it is expected that its effect will manifest in the expression for the collision efficiency. Also for DO and temperature this assumption is deemed valid. For the experiments at different DO concentrations, care was taken to supply O_2/N_2 gas in a bubble-less manner so as not to cause additional mixing and shear. The effect of temperature on the transport kernels is limited to very small particles ($<1 \mu\text{m}$) by influencing their Brownian motion. However, the smallest size classes in the available dataset consisted of particles of approximately $4 \mu\text{m}$. Second, more confidence is put into the applicability of literature expressions for β since these are based on studies of hydrodynamics whereas α is governed by a number of short range forces (e.g. electrostatic repulsion, curvilinear vs. rectilinear path) (Thomas et al., 1999) which are much harder to quantify since they are largely pertaining to the nature of the surfaces themselves.

In order to obtain a structure for α from the inverse problem, the recovered kernel needs to be divided by a fixed collision frequency from literature. The methodology is generic and can thus be applied for any choice of β from literature. However, the validity of the chosen β will determine how well the dynamics of collision frequency and efficiency are separated. If the chosen function for β is not valid, a portion of the transport effect will be incorporated in the collision efficiency resulting in an expression for α which is

not satisfactory (e.g. values larger than 1, shape not in correspondence to experimental findings from literature,...). The transport kernel used here (Lee et al., 2000) accounts for shear and incorporates the fractal dimension of the colliding flocs:

$$\beta_{lit}(i, j) = \frac{\bar{G}}{\pi} v_0^{1-\frac{3}{D_f}} \left(v_i^{\frac{1}{D_f}} + v_j^{\frac{1}{D_f}} \right)^3 \quad (10.4)$$

with \bar{G} the average velocity gradient; v_0 , v_i and v_j the volumes of the smallest particle and the two aggregating particles and D_f the fractal dimension. This expression has been successfully used by Ducoste (2002) to model aggregation in a water treatment process (it should be noted that this was a purely chemical flocculation process). Studies have shown D_f values range from 1.4 for fragile flocs and 2.2 for stronger aggregates with an average of about 2 (Dyer and Manning, 1999). Therefore, a fractal dimension of 2 is chosen.

Finally, the validity of the resulting expression for α can be checked by comparing it to observations from literature concerning the collision efficiency process. If discrepancies are found, the expression used for β_{lit} needs to be re-evaluated. If the resulting structure for α is satisfactory, it can be used to evaluate and extend existing literature functions for the collision efficiency.

Figure 10.11 represents the recovered collision efficiency for shear-induced flocculation based on the above described methodology. Collisions between larger particles seem to be more effective than between smaller particles. Values between 0 and 1 are observed which is to be expected since α represents the fraction of collisions that results in the aggregation of particles.

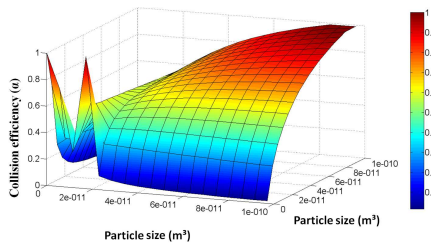


Figure 10.11: Remaining α if literature kernel is valid for shear-induced flocculation.

For 8 meq Ca-induced flocculation the inverse problem is solved for three different cases according to the different similarity distributions that are found. The best performance in the forward simulation is achieved by applying separate kernels for the observed similarity regions. Hence, the recovered kernels for this case are examined here. Dividing the recovered kernel for each similarity region by the expression for β_{lit}

10.3. Results

(Eq. 10.4) provides the corresponding collision efficiencies as depicted in Figure 10.12.

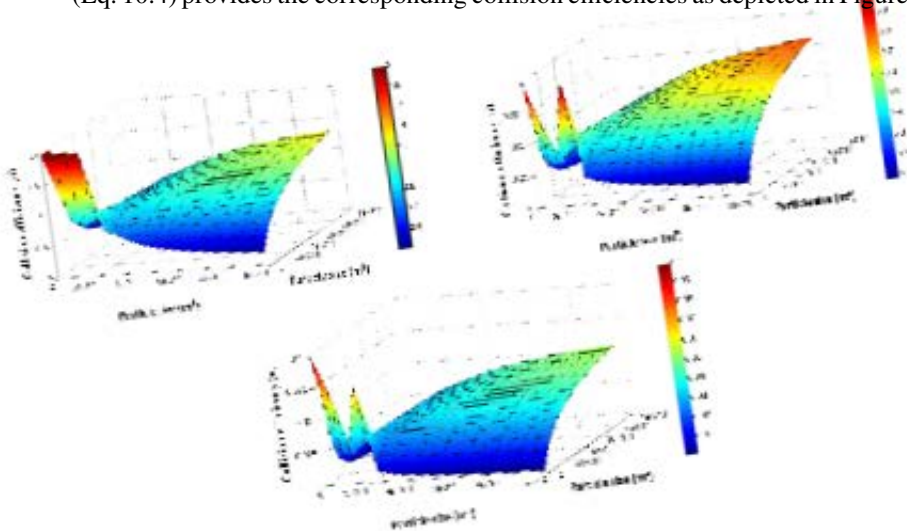


Figure 10.12: Remaining α if literature kernel is valid for the three similarity regions of case 3. Top left: first region, top right: second region, bottom: third region.

For the first similarity region, the collision efficiency is found to be largest for collisions of smaller particles, the lowest values are obtained for intermediate particles. For larger particles, α increases again with particle size. The recovered shapes for the second and third similarity regions compare very well with the one of shear-induced flocculation (Figure 10.11).

When comparing the scaling for the three different similarity regions, it can be observed that generally α decreases from the first to the last similarity region. From this it can be concluded that the effect of Ca^{2+} addition on the collision efficiency varies as a function of time (effect being large at first and then fading out). In the first similarity region, where the effect of Ca^{2+} addition appears to be the most pronounced, values larger than 1 are found whereas α is expected to be between 0 and 1. This could indicate that addition of Ca^{2+} does not only enhance the collision efficiency but also influences the frequency of collisions between particles. If this is the case, Eq. 10.4 needs to be extended to incorporate some effect of Ca^{2+} (this will be discussed later).

10.3.2 Experiment 2: 16 meq Ca^{2+}

The second set of flocculation data only differs from the first in terms of the amount of added Ca^{2+} . In this case, flocculation is induced by adding 16 meq Ca^{2+} . The procedure for solving the inverse problem remains identical. Figure 10.13 shows the distribution of the similarity variable for different values of the scaling factor k . Similar

to the previous case it can be observed that for more negative values of the scaling factor, the similarity distribution splits into a number of distinct similarity regions. When applying a k -value of -0.25 , all time instants collapse onto one single distribution with some deviations in the smaller size ranges. A scaling factor of -0.35 introduces two distributions which show much better overall similarity. The separation occurs between time instants 660 s and 707 s. For more negative k -values (up to -0.85) a third and fourth similarity region become visible. However, a more detailed examination shows that the latter each consist of only one time instant. Thus, only two distinct similarity regions are withheld.

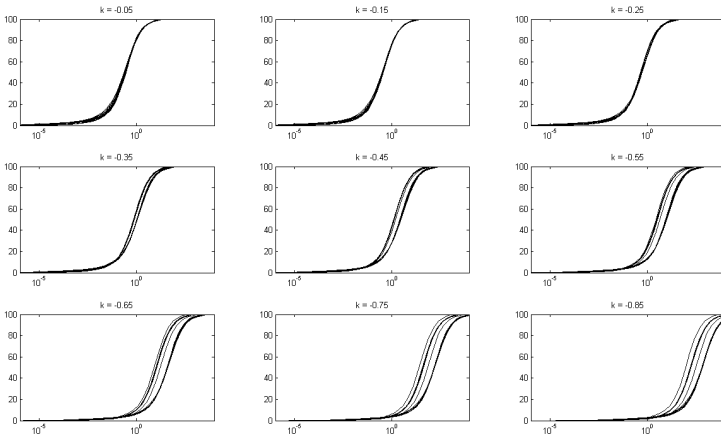


Figure 10.13: Similarity distribution for different values of the scaling factor k .

No similarity can be observed for the first time instants, although similarity is observed at an earlier time instant than for experiment 1 (after 283 s vs. 425 s). Further, the split of the similarity distribution into two separate regions is found to occur at an earlier time instant (707 s vs. 1368 s). Similar as for experiment 1 the observed similarity regions correspond to specific discontinuities in the volume fraction data (figure not shown). This excludes the hypothesis of an experimental flaw since the phenomenon is repeatable.

The inverse problem is solved for two cases, considering respectively 1 (case 1) or 2 (case 2) similarity regions and their corresponding kernels are extracted. Figure 10.14 shows the result of the forward simulations. For the first case, the outcome is similar to 8 meq Ca-induced flocculation: peak values are overestimated and the upper tail is underestimated. The resulting SSE amounts to 2988. As for the second case, the SSE of the model predictions are found to be respectively 167 and 53 summing to a total SSE of 220 confirming earlier observations that the overall prediction improves

10.3. Results

by extracting separate kernels for the two different similarity regions.

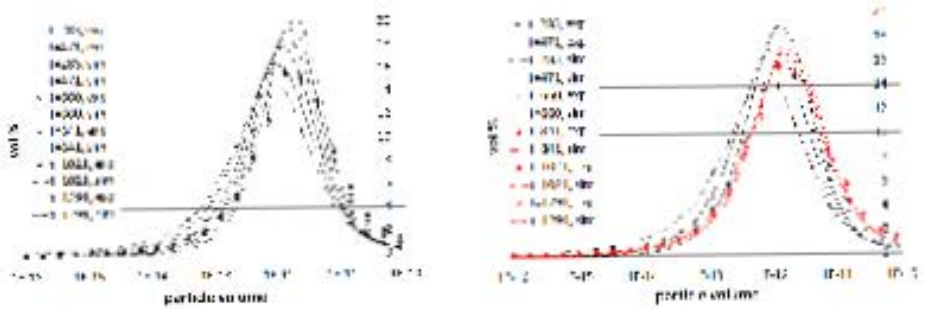


Figure 10.14: Results of the forward simulations for the first case where only one kernel is considered (left) and the second case where the two similarity regions are modelled by their proper kernel (right).

After dividing the recovered kernels by the collision frequency expression according to Eq. 10.4, the collision efficiencies are obtained. Figure 10.15 represents the resulting structures of α for the two similarity regions of case 2. When comparing the collision efficiencies for 16 meq Ca-induced flocculation to the values obtained for 8 meq Ca-induced and shear-induced flocculation, it can be observed that higher α values are retrieved when more Ca^{2+} is added. Once more, α values exceeding the expected maximum value of 1 are encountered, suggesting some unmodelled effect in the expression that was used for β_{lit} .

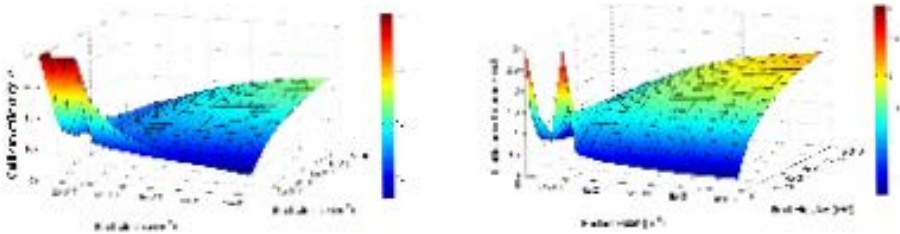


Figure 10.15: Remaining α if literature kernel is valid for the two similarity regions of case 2. Left: first region, right: second region.

The second similarity region shows much lower values for the collision efficiency than the first region confirming that the effect of Ca^{2+} addition is more pronounced during earlier time instants. At later time instants, the collision efficiency will still show elevated values but no longer to the extent as for the first time instants. Not only the magnitude of the Ca^{2+} effect changes in time but also the proportion between different size classes. At earlier time instants, the largest elevation in collision efficiency can

be found for the smaller particles whereas at later time instants, the larger size classes show the highest values for α .

10.3.3 Experiment 3: 32 meq Ca^{2+}

In the third experiment, flocculation is induced by adding 32 meq of Ca^{2+} . Once more the similarity analysis shows different similarity regions depending on the applied scaling factor (figure not shown) with a single similarity distribution at $k=-0.25$ and two distinct regions for $k=-0.35$. In accordance to the previously studied datasets, the time instants of the split between different similarity regions, can be associated to discontinuities in the volume fraction data (figure not shown). Hence, two cases ($k=-0.25$ and $k=-0.35$) are considered for solving the inverse problem.

Forward simulations show SSE values of respectively 1570 and 318 (143 and 175 for the independent similarity regions) for the two cases, resulting in a considerably improved prediction when using separate kernels for the two different similarity regions. The same prediction problems are encountered as with the previous datasets: overprediction of peak values and underprediction of the upper tail.

In general, higher collision efficiencies are found than for the case of 16 meq Ca-induced flocculation. Collision efficiencies up to 35 are found at the earlier time instants, corresponding to the first similarity region. Here, the most prominent effect of Ca^{2+} addition is observed. The second similarity region shows much lower values for α (up to 4.5).

10.3.4 Summary effect of Ca^{2+} addition

Table 10.1 gives an overview of a number of important observations that are made in the analysis of the different experiments of Ca-induced flocculation with the proposed methodology. The results clearly show that the efficiency of collisions between particles increases as more Ca^{2+} is added. Elevated amounts of Ca^{2+} will thus enhance aggregation. However, the observed trend does not exhibit a linear relation. This is in accordance with the findings of Biggs et al. (2001).

Furthermore, it is discovered that for flocculation induced by Ca^{2+} -addition, more than one region of similarity is present and that by applying different flocculation dynamics for each of these regions, model predictions can be enhanced significantly suggesting that different aggregation dynamics are occurring over time.

Each experiment shows at least two different similarity regions where the first region (corresponding to the first time instants) consistently represents much higher α values than the subsequent region. The lower α values found in the second similarity region can indicate a switch back to shear-induced flocculation. This can be due to a saturation

10.3. Results

Table 10.1: Overview of important properties for different Ca^{2+} concentrations

	Ca^{2+2+} concentration (meq)			
	0	8	16	32
Size α_{inv} first similarity region ⁽¹⁾	1	2	20	35
Size α_{inv} second similarity region ⁽¹⁾	n.a. ²	1	2.5	4.5
Time instant similarity shift (s)	n.a. ²	861	707	507
SSE case 1 (1 similarity region)	41	1033	2988	1570
SSE case 2 (2 similarity regions)	n.a.	274	220	318
SSE case 3 (3 similarity regions)	n.a.	72	n.a.	n.a.

¹ Values for collision between the largest particles

² not applicable

effect (i.e. all negative sites on the floc have been bound by a Ca^{2+} ion) since this switch occurs earlier with higher Ca^{2+} concentrations (Table 10.1). Also, at earlier timesteps smaller particles show the largest values for α , whereas for later time steps collisions between larger particles become more dominant. This could be explained by the number of sites available for binding Ca^{2+} . In the experiment with 8 meq Ca^{2+} -addition, a third similarity region is observed which is not present in the experiments with higher Ca^{2+} dosage. The recovered α values for this region show values less than 0.1 implying that almost no aggregation is taking place here and an equilibrium state is reached. Possibly, this third region is not visible for the other experiments because the duration of the experiments was too short.

The high values (> 1) observed for the recovered collision efficiencies indicate that a re-evaluation of the expression used for β_{lit} (Eq. 10.4) is required since α -values are expected to be situated between 0 and 1. However, for shear-induced flocculation, Eq. 10.4 did result in satisfactory values for the collision efficiency kernel suggesting that the collision frequency will somehow be influenced by Ca^{2+} -addition. Since the application of Ca^{2+} will not alter transport in the system, the effect of Ca^{2+} will most probably be of an indirect nature by influencing the structure of the sludge flocs. This structural effect is incorporated in the expression for collision frequency through the fractal dimension.

Any object found in a real physical process has a mass fractal dimension D_f between 1 and 3. High fractal values indicate compact aggregates whereas low values correspond to more ‘loose’ aggregates (Govoreanu, 2004; Li et al., 2006). Jin et al. (2003) found that the fractal dimension of flocs decreases with increasing floc size. Thus, since Ca^{2+} enhances the rate of floc growth, the application of Ca-induced flocculation will reduce the fractal dimension of the sludge flocs. Indeed, by decreasing the fractal dimension in Eq. 10.4 with increasing Ca^{2+} concentration collision efficiencies of $0 < \alpha < 1$ are obtained for all data sets. For example, Figure 10.16 shows the collision frequency

for the case of 16 meq Ca^{2+} -addition (case 2, first similarity region) adjusted with a constant fractal dimension of 1.8 (instead of 2) in order to illustrate the effect of a lower D_f . However, applying a single fractal dimension for the entire size distribution is a crude simplification since the fractal dimension changes with floc size (Vahedi and Gorczyca, 2012). Therefore, a size dependent fractal dimension should be included in the expression for β_{lit} to obtain an accurate collision frequency kernel. Defining the exact relationship between size and D_f requires further investigation.

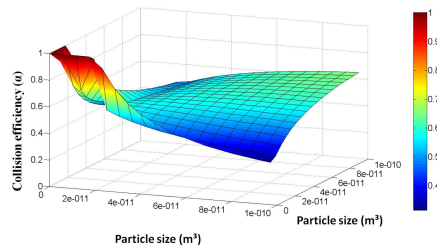


Figure 10.16: Recovered α for 16 meq Ca^{2+} flocculation (case 2, second region) considering a constant fractal dimension of 1.8.

Addition of Ca^{2+} has been shown to enhance flocculation of activated sludge flocs as higher amounts of Ca^{2+} result in an increased collision efficiency. This would indicate that short range aggregation kinetics are altered by the application of Ca^{2+} . Figure 10.17 presents a conceptual hypothesis of the change in aggregation kinetics as more Ca^{2+} is added.

Without Ca^{2+} addition (a), the negative charges on the surfaces of the sludge flocs will repel one another. Collisions can only be efficient if the large energy barrier, created by the electrostatic forces between two sludge flocs, is overcome. When a small amount of Ca^{2+} is added (b), Ca^{2+} -ions will bind on some of the negative sites on the sludge surface each replacing a negative charge with a positive one. The overall charge of the interface between two colliding particles will thus be less negative, resulting in a decrease of the electrostatic repulsion. Since the corresponding energy barrier is lower for this case, the efficiency of collisions will be enhanced.

As more Ca^{2+} is added (c) the introduction of positive charges on the sludge flocs will not only aid in overcoming the electrostatic forces between two particles but the positive Ca^{2+} -ion bound on one floc can react with a negative site on a second floc linking both particles together. The resulting floc will no longer be a merge of the two original flocs but a looser structure where the original particles are simply bridged by the Ca^{2+} -ion. A further increase in Ca^{2+} concentration will cause more and more bridging to occur instead of merging of flocs and will even result in multiple bridging where more than two particles are linked together by several Ca ions (d).

10.3. Results

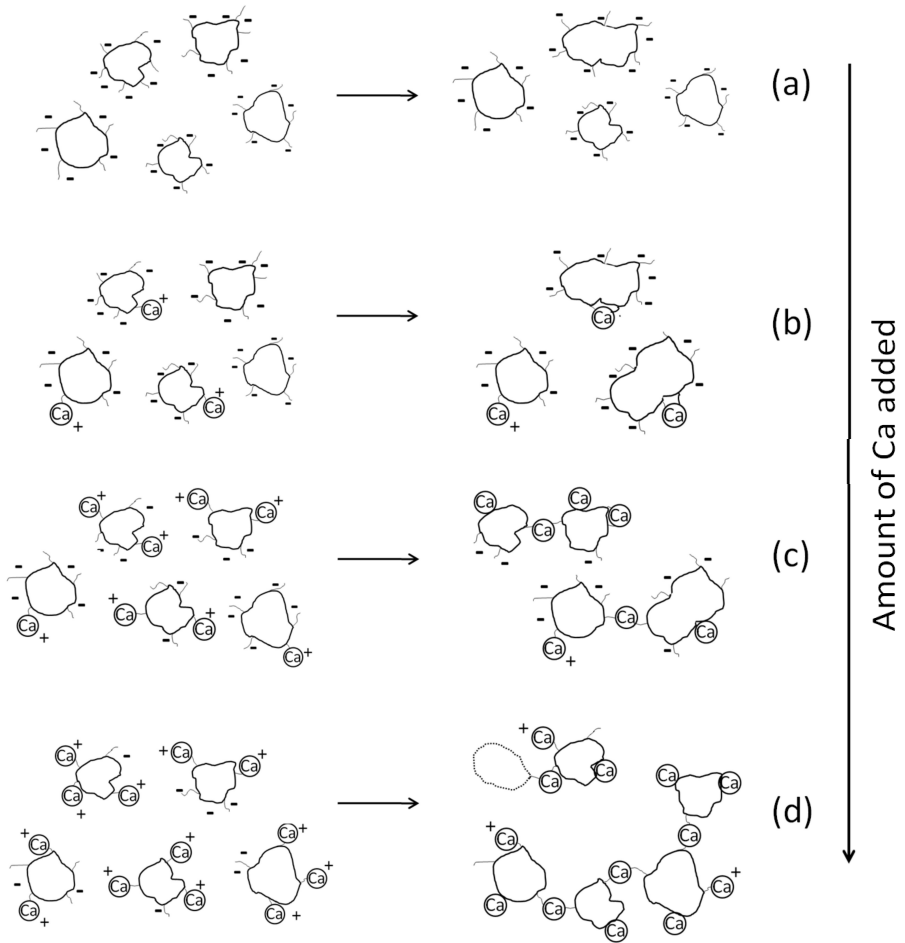


Figure 10.17: Schematic representation of aggregation kinetics as a function of the amount of added Ca^{2+} . (a) electrostatic repulsion, (b) charge neutralisation, (c) charge neutralisation & bridging, (d) bridging & multiple bridging

Although the addition of Ca^{2+} enhances the aggregation rate resulting in the fast formation of large flocs, the resulting flocs will have a structure that is more open and thus less dense than that of merged particles, resulting in a lower fractal dimension of these flocs. The higher the amount of Ca^{2+} added, the lower the fractal dimension and thus the floc density which will have a negative impact on the settling velocity. From this it can be hypothesized that an optimal Ca^{2+} concentration can be determined where the rapid growth of large flocs is enhanced in combination with a minimal formation

of loose aggregates by bridging. However, this hypothesis needs further confirmation through experimental observation.

10.3.5 Experiment 4: impact of DO

In this section, the impact of the DO-concentration on the aggregation dynamics of activated sludge is investigated based on PSDs from experiments at 3 different DO concentrations, resp. 0, 2 and 4 mg/l. Figure 10.18 shows the evolution of the mean floc diameter for both the dynamic and steady state experiments. From both experiments it can be observed that altering the DO concentrations affects the mean floc diameters.

The aggregation dynamics for the entire distribution can be analysed in more detail by solving the inverse problem for each dynamic dataset. The performance of the inverse problem solution relies entirely on the information content of the measurements. This means that the interval at which measurements are taken should be sufficiently small in order to capture the dynamics and allow the inverse problem to accurately recover the corresponding kernels. For the first few minutes after flocculation was induced through Ca^{2+} addition, the inverse problem could not be solved since the aggregation dynamics are too fast in comparison to the measurement interval. Therefore, the inverse problems were solved for the time interval as indicated by the black box in Figure 10.18. In this interval the aggregation dynamics have returned to shear induced aggregation allowing to investigate the DO effect without interaction of Ca^{2+} . Hence, only one similarity region was found for this time interval.

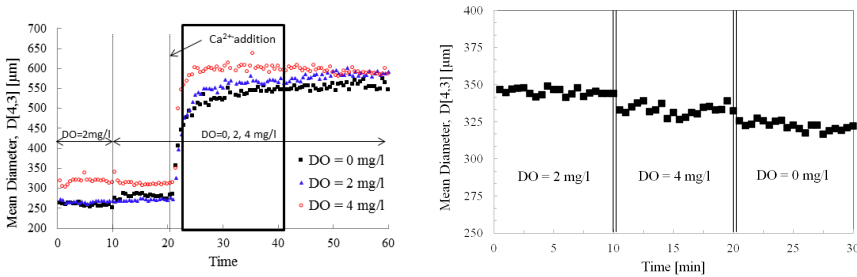


Figure 10.18: Effect of dissolved oxygen concentration on the mean floc diameter. Left: dynamic experiment, right: steady state experiment.

The quality of the recovered aggregation kernel is verified by performing a forward simulation resulting in SSE values of 92, 23 and 68 (for DO concentrations of resp. 0, 2 and 4 mg/l). For reasons of comparison, the data for 0 mg/l DO were also simulated using the frequency kernel by (Lee et al., 2000) (Eq. 10.4) and a constant collision efficiency. The value of the collision efficiency was determined through an optimization

10.3. Results

experiment. The simulation resulted in an SSE of 2443. These results show that the inverse problem was able to extract a valid kernel structure from the experimental data.

To investigate the effect of the DO concentration on the aggregation efficiency for different particle sizes, the recovered kernels are compared amongst the different DO concentrations by calculating the ratios of the aggregation efficiencies with respect to the intermediate DO concentration as shown in Figure 10.19. The highest efficiencies are found for the intermediate concentration of 2 mg/l DO. Both 0 mg/l DO and 4 mg/l DO exhibit less efficient aggregation dynamics compared to a concentration of 2 mg/l. Anaerobic conditions (0 mg/l) appear to be slightly worse than high DO concentrations (4 mg/l). For the anaerobic conditions, the collision efficiency is reduced by a factor of about 5-7. The effect of higher DO concentrations is less severe with a collision efficiency that is about 4 times lower than for the optimal concentration. Furthermore, it can be observed that the impact of a change in DO concentration is more pronounced for the flocculation of larger particles than for smaller flocs.

These results clearly show the importance of the DO concentration with respect to the flocculation behaviour of the sludge. Given the rather rapid nature, the mechanism that drives this phenomenon is thought to be a physico-chemical mechanism. DO is strongly related to activity and production of Soluble Microbial Products (SMP) which act as a glue for the flocs. However, unraveling the exact mechanism behind the influence of DO is outside the scope of this PhD and needs further investigation involving more detailed data collection.

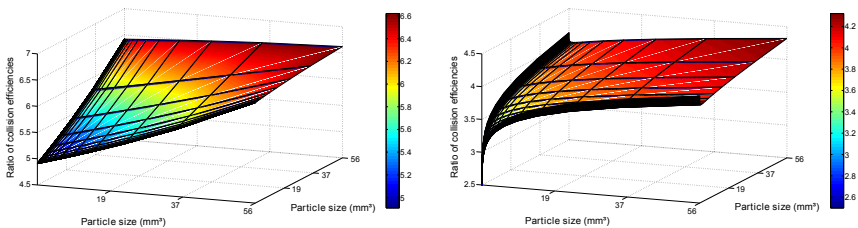


Figure 10.19: Ratio of the recovered collision efficiencies for different DO concentrations. Left: ratio of $\alpha(2 \text{ mg/l})/\alpha(0 \text{ mg/l})$, right: ratio of $\alpha(2 \text{ mg/l})/\alpha(4 \text{ mg/l})$.

10.3.6 Experiment 5: impact of temperature

A similar analysis is performed for sludge flocculation at three different temperatures, resp. 5°C , 15°C and 25°C . The evolutions of the mean floc diameter for both the dynamic and steady state experiments are shown in Figure 10.20. An increase in floc

size can be observed for a decrease in temperature. The observed differences are much more pronounced than was the case for the different DO concentrations.

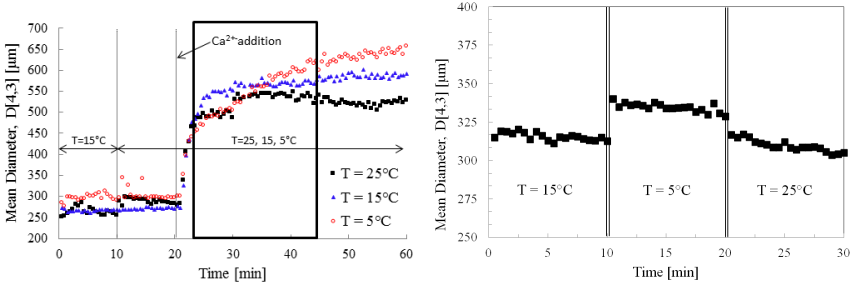


Figure 10.20: Effect of temperature on the mean floc diameter. Left: dynamic experiment, right: steady state experiment.

The black box in Figure 10.20 shows the time interval for which the kernel was recovered. The aggregation dynamics immediately after flocculation was induced by Ca^{2+} addition could not be captured by the inverse problem methodology because flocculation was occurring too fast compared to the measurement interval.

Forward simulations with the recovered kernels resulted in SSE values of 150, 55 and 81 for resp. 5°C, 15°C and 25°C. The effect of temperature variations on the aggregation efficiency is investigated by calculating the ratios of the collision efficiencies (Figure 10.21). A clear impact of temperature can be observed. Lowering the temperature to 5°C induces a remarkable increase in collision efficiency whereas a decrease in α is observed at higher temperature. Moreover, the aggregation of larger particles increases at lower temperature and, in contrast, smaller particles show an improved collision efficiency at higher temperatures.

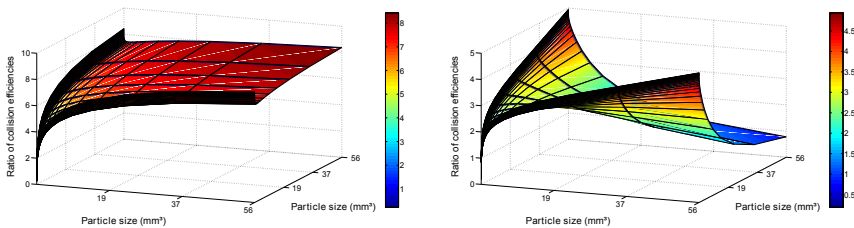


Figure 10.21: Ratio of the recovered collision efficiencies. Left: ratio of $\alpha(5^\circ\text{C})/\alpha(15^\circ\text{C})$, right: ratio of $\alpha(15^\circ\text{C})/\alpha(25^\circ\text{C})$.

However, these results should be interpreted with care. Although several studies revealed larger flocs and better settling at lower temperatures, the exact relation is difficult to quantify since different activated sludge samples respond differently to various

10.4. Conclusions

temperatures depending on the temperature at which they were acclimatized (Wilén, 1999).

10.4 Conclusions

An inverse problem methodology is successfully applied to data of dynamic PSDs to extract information on the influence of different physico-chemical factors (Ca^{2+} -addition, DO and temperature) on the aggregation dynamics of activated sludge.

- A similarity analysis of Ca^{2+} -induced flocculation showed at least two well-defined consecutive similarity regions which require different kernel structures. Simulating each region with its own kernel significantly improved the model predictions indicating that different aggregation kinetics are taking place sequentially. This makes sense as different mechanisms of flocculation are expected to occur: a first one just after Ca^{2+} addition and a second one when all the Ca^{2+} has been bound to the flocs (actually returning to shear-induced flocculation).
- The recovered kernels were compared amongst different Ca^{2+} concentrations. This showed that the addition of Ca^{2+} significantly enhances the aggregation kinetics. Moreover, from the different similarity regions it becomes clear that Ca^{2+} -addition will have its most prominent influence right after the application. After a certain time, the effect will become less severe (i.e. much lower values in the recovered kernel), yet still clearly visible. This time instant occurs earlier with higher Ca^{2+} concentrations, suggesting that saturation takes place.
- A rigorous method to compare the recovered kernel structures to literature kernels has been developed in order to find out where existing kernels fail to capture the true dynamics. This method has been applied to compare the recovered kernels to a literature kernel (i.e. shear-induced flocculation kernel including fractal dimension). Although the effect of Ca^{2+} on the aggregation kinetics occurs mainly by enhancing the collision efficiency, an indirect effect on the transport kernel (through changes in the fractal dimension of the flocs) could be observed. More research concerning the exact relation between fractal dimension and floc size is the first step in improving existing kernel structures.
- A hypothesis is presented concerning the different mechanisms occurring with increased concentrations of Ca^{2+} . Application of Ca^{2+} will enhance the collision efficiency resulting in fast growth of flocs. However, it will also induce bridging causing the formation of less dense structures with a lower fractal dimension. This formation of loose aggregates with low fractal dimensions can have a negative impact on the settling velocity. Hence, an optimal Ca^{2+} concentration should be determined where rapid growth of large flocs is stimulated but the formed structures are sufficiently compact to ensure good settling behaviour.

- By applying the inverse problem methodology to dynamics of PSD data at different DO concentrations, a clear impact of the DO concentration on the flocculation dynamics was found. The most efficient aggregation occurs at a concentration of 2 mg/l. The influence of the DO concentration was more pronounced for larger than for smaller particles. Flocculation data at different temperature showed improved aggregation when temperature decreases with the effect being most pronounced for larger particles.
- For all analysed datasets, the kernels recovered through solving the inverse problem are able to accurately describe activated sludge flocculation dynamics. This makes the inverse problem methodology a powerful tool for system analysis and allows to gain valuable insight in aggregation dynamics and the factors influencing flocculation. A rigorous comparison of the recovered empirical kernels to literature kernels is necessary to translate their information content into actual physical expressions. The latter needs further work, starting with experimental testing of the hypothesis that was put forward in this chapter.
- Finally, the analysis in this chapter has shown that the application of a constant aggregation rate in flocculation models (such as K_a in Chapter 8) is a harsh approximation. Moreover, relating the aggregation dynamics to the MLSS concentration as suggested by Gong et al. (2011) will also not be able to capture the true dynamics as aggregation dynamics are shown to have an increasing relation with particle size and should include information on the fractal dimension of the sludge flocs.

PART IV

Conclusions and perspectives

The work presented in previous parts provided new insights into the different settling regimes in a Secondary Settling Tank (SST) through the combination of experimental analysis and model simulations. The following chapters provide the main conclusions of the presented work as well as a number of suggestions for future research.

CHAPTER 11

General discussion and conclusions

The performance of a SST is characterised by different regimes of settling that occur simultaneously at different locations in the SST. These different settling behaviours each contribute to a separate function of the SST. The settling behaviour at the bottom of the settling tank (i.e. at higher sludge concentrations) is responsible for a proper control of the biomass inventory by recycling a thickened sludge to the bioreactor. At the top of a SST (i.e. at low sludge concentrations), the settling behaviour is responsible for a proper clarification of the sludge from the water to ensure a good effluent quality.

Most simplified 1-D SST models used to date include only one type of settling according to which the sludge will settle as a single mass with a velocity depending on its concentration. However, this is a very harsh approximation. In reality, high concentrations at the bottom of a SST cause flocs and particles to form a network where they undergo a certain solids stress that hampers further settling. This regime is called compressive settling and will play a key role in the formation of the sludge blanket and the final sludge concentration to be recycled. In the diluted top region of a SST on the other hand, particles will not interact and settle at their own velocity depending on individual properties such as size, density,... This regime is called discrete settling and will play an important role with respect to the final effluent quality.

Moreover, more intense rain events caused by climate change, result in Waste Water Treatment Plants (WWTPs) that are increasingly subjected to conditions of high hydraulic and pollutant load. Commonly used SST models loose realism under these conditions as they do not sufficiently account for the different settling dynamics throughout a SST. Proper operation and control of WWTPs under situations that diverge from normal dry weather requires the development of more advanced SST models that explicitly account for the different settling regimes in an SST. In this PhD thesis further insight into the dynamics of the different settling regimes was developed through both experimental work and model-based analysis in order to improve current SST models.

This section provides an overview of the main conclusions drawn.

11.1 Importance of compression settling on operation and control of WWTPs

Comparison of open and closed-loop simulations with the Benchmark Simulation Model No. 1 to online settler data of the WWTP of Eindhoven showed that models that only account for hindered settling overpredict the variations in underflow concentration and underpredict the Sludge Blanket Height (SBH) elevation during storm weather (Chapter 4). By accounting for compression settling much more realistic predictions were obtained for these variables.

As the underflow concentration will directly influence the sludge inventory and related reaction rates, the influence of compression on conversion processes in the bioreactors was investigated. A substantial difference in the predicted nitrification rate was observed indicating that accurate predictions of the recycle concentration will influence the predicted performance of the entire treatment plant. Poor predictions of the recycled biomass due to the lack of compression settling may force modellers to calibrate kinetic parameters for the wrong reasons. These results clearly showed that in order to improve operation and control of WWTPs under wet weather conditions, we need to step away from traditional layer models towards more sophisticated models that explicitly account for compression settling in their model structure.

11.2 Model selection and calibration for hindered and compression settling

In order to model the compression behaviour, a valid mathematical expression to describe the compression dynamics needs to be selected and calibrated. A preliminary attempt to calibrate a 1-D model with both hindered and compression settling based on batch settling data was not successful (Chapter 5). Hence, a more detailed analysis of the different constitutive functions used to describe hindered and compression settling is needed in order to select a combination of functions that is able to describe the true dynamics (Chapters 6 and 7).

First, a critical analysis of hindered settling functions was performed. As compression is typically described by a force working against hindered settling, the two processes are interrelated and an inadequate choice for the hindered settling function can impede the further selection and calibration process of the compression behaviour. Different hindered settling functions (with either an exponential or a power-law nature) were investigated. All functions performed equally well in predicting measured hindered

11.2. Model selection and calibration for hindered and compression settling

settling velocity data. However, these data can only be measured in a limited concentration interval. It was shown that seemingly small differences in the predicted hindered settling velocities between the different functions outside of this range can cause significant differences in 1-D predictions (Chapter 6).

Analysis of 1-D model simulations with different hindered settling functions (no compression considered) on long term batch settling data showed that the commonly used exponential functions underestimate the thickening behaviour of sludge at long settling times indicating that the exponential functions partially lump compression into their model structure. Whereas this behaviour makes exponential settling functions clearly the best choice to be used in simplified 1-D models as it enforces more realism, it makes them unsuitable to be used in next generation 1-D models which aim to explicitly account for each of the different settling behaviours. Hence, in order to model compression settling as an explicit phenomenon in a 1-D SST model, a power-law type function should be used to describe hindered settling (Chapter 6).

Moreover, it was shown that hindered settling velocity functions that include a parameter to model the settling behaviour at low concentrations, cannot be reliably calibrated based on batch settling data. Including an extra term to mimic the settling behaviour in the clarification zone reduces the identifiability and reliability of the parameter estimation. An alternative approach to model discrete settling at low sludge concentrations needs to be developed (Chapter 5 and 6).

Despite this new insight into the modelling of the hindered settling dynamics, a 1-D model with a power-law hindered settling function and a compression function remained unable to simultaneously describe different batch settling curves with a single parameter set. Batch curves for different initial concentrations seem to require different compression dynamics indicating that some unexplained variability still remains in the compression behaviour. Literature findings suggest the existence of a variable critical concentration (i.e. the concentration where compression first occurs). However, no physical explanation for this was presented to date and current implementation strategies rely on specific features of batch settling and are therefore not feasible for dynamic simulations in full-scale SSTs.

In this PhD thesis a hypothesis was formulated relating the observed variability in the critical concentration to changes in the flocculation state and this hypothesis was supported by experimental evidence (Chapter 7). Changes in the flocculation state due to changes in the microbial make-up or application of shear were shown to have a significant influence on the onset of compression settling. Moreover, investigating in-depth settling velocity profiles indicated that segregation of particles along the depth of a settling column is occurring resulting in local variations in floc size distribution. As smaller particles will show different packing properties than larger particles, this segregation influences the build-up of a compressive network and could thus explain the occurrence of a time-varying critical concentration.

11.3 Development of an integrated flocculation-CFD model to model discrete settling

The discrete settling behaviour is often modelled by directly modifying classical hindered settling velocity functions. Unfortunately, this approach is not accurate enough for reliable Effluent Suspended Solids (ESS) predictions since it does not capture the true (distributed) settling behaviour. Moreover, attempting to mimic discrete settling behaviour in a hindered settling function hampers the calibration of these functions (due to parameter identifiability issues) (Chapters 5 and 6).

As discrete settling is not a concentration driven process but dependent on individual particle properties, knowledge on the Particle Size Distribution (PSD) is required to gain further insight into its dynamics. Changes in PSDs in a SST are in turn influenced by shear-driven aggregation and break-up processes. Hence, modelling these processes requires information on the hydrodynamics in the tank. Therefore, a 2-D axisymmetric Computational Fluid Dynamics (CFD) model was developed for a circular SST of the WWTP of Roeselare and coupled to a simple flocculation model with two size classes. The development of these kind of detailed models allows to build knowledge on the true dynamics which may in turn lead to improved next-generation 1-D models (Chapter 8).

The integrated flocculation-CFD model allowed for a qualitative analysis of the effect of aggregation and breakage dynamics on the distribution of particles throughout the SST by detecting specific regions in the SST where flocculation is taking place (Chapter 8). Moreover, by tracking the concentration of different particle size classes throughout the SST, the discrete settling behaviour can be modelled as each size class can be provided with its proper settling velocity. The integrated model thus allows the implementation of a more realistic settling behaviour for the clarification zone in future simulation studies.

11.4 Extension and calibration of an integrated flocculation-CFD model

Application of this model in design or operation studies requires further information on the necessary model complexity, discrete settling velocities and aggregation/breakage dynamics through experimental data collection and analysis (Chapters 9 and 10).

A new measurement device was developed and constructed which allows to measure changes in PSD during settling at low concentrations at different settling times and at different heights in a batch settling column. By comparing PSDs at different settling times at the top of the column it became clear that particles could be classified in roughly five classes: a class of large flocs ($>500 \mu\text{m}$) that settle rapidly and will be

11.5. General conclusions

preferentially removed during the first few minutes of settling, a class of slow-settling particles $<150 \mu\text{m}$ and three intermediate classes. The measurements of the slow-settling particles corresponded remarkably well to measured particles in the effluent of the WWTP indicating that these particles will not settle in a full-scale system either and can thus be classified as a non-settleable fraction (Chapter 9). Moreover, measuring the evolution in PSDs at different depths throughout the column allows quantifying the discrete settling velocities in the different size classes and can thus be used to calibrate the integrated flocculation-CFD model.

An inverse problem methodology was applied to extract information on the influence of different physico-chemical factors on the aggregation dynamics of activated sludge (Chapter 10). The analysis showed that empirical kernel functions describing the aggregation process could be accurately extracted. This makes the inverse problem methodology a powerful tool for system analysis as it allows to gain valuable insight in aggregation dynamics and the factors influencing flocculation. A rigorous method to compare the recovered kernel structures to literature kernels has been developed in order to find out where existing kernels fail to capture the true dynamics. A preliminary analysis showed that the implementation of a size-dependent fractal dimension is the first step in improving existing kernel structures.

11.5 General conclusions

As WWTPs are under increasing pressure through the combination of stringent effluent requirements and increased periods of high hydraulic and pollutant loads, their operation and control require more advanced SST model that account for the different settling regimes in the system. Compression settling and discrete settling should be included in next generation 1-D SST models. However, to accomplish this, existing 1-D models should not simply be extended with new processes. A rigorous analysis of the (empirical) dynamics that are already present should be made in order to allow the inclusion of more realism.

PSDs influenced by flocculation and break-up processes were shown to be a key factor in describing the different settling behaviours. Hence, flocculation processes in SSTs still deserve ample attention. More advanced modelling frameworks such as Population Balance Model (PBM) and CFD should be used to build process knowledge which can in turn be translated into next-generation 1-D SST models.

Chapter 11. General discussion and conclusions

CHAPTER 12

Perspectives and future work

In this PhD thesis compression settling was shown to be an important process to describe the sludge inventory in a WWTP and the development of related control strategies. However, the influence sphere of compression settling is potentially much wider. A rigorous analysis of the effect of compression settling on different processes in a WWTP should be made as this could potentially open up perspectives for a range of advanced operation and control strategies.

- In this respect the SBH can be a crucial operation and control variable. Accurate predictions of SBH (which is highly influenced by compression) would allow to model the influence of imposing higher solids loads than the ones currently being used. This could not only improve operation during storm weather but also allow to assess the feasibility of operating the bioreactors at a higher sludge concentration even during dry weather conditions. Moreover, the effect of new design strategies (for example deepening the SSTs) could be tested.
- Accurate predictions of the sludge concentrations and retention time in the SST can also contribute to improved predictions and control of rising sludge (caused by flotation of solids by nitrogen gas). The most important factor to influence this process in a SST is the biological denitrification rate which is indeed related to the sludge concentration. Reactive settler models are already used to predict biological reactions occurring in SSTs but their performance can be improved by including the effect of compression settling.
- The concentration in the underflow of a SST will not only influence conversion processes in the SSTs and the bioreactors. Processes such as anaerobic digestion and sludge dewatering are highly dependent on the Return Activated Sludge (RAS) as well. For example, a similar analysis as was presented in this PhD thesis could be made with the Benchmark Simulation Model No.2 in order to analyse the impact on anaerobic digestion.

Existing 1-D SST models should be further improved through the following steps:

- Discrete settling can be included by introducing a limited number of particle classes and defining a discrete settling velocity for each class which becomes active once the total sludge concentration drops below a certain threshold value.
- Also the accurate prediction of the compression behaviour requires the inclusion of information on the flocculation state of the sludge. Different modelling frameworks (including different levels of detail) for polydispersed systems undergoing break-up and flocculation are available in literature. The applicability of these models to activated sludge should be tested. An alternative approach would be to define a relation between the critical concentration where compression starts and the concentration in the different size classes that are needed to describe discrete settling. Moreover, including flocculation state as a variable in 1-D SST models would allow to describe the impact of polymer addition on the SST performance.

More information on the optimal approach to extend existing 1-D models can be gathered through the use of advanced modelling frameworks such as PBM and CFD.

- Based on the experimental methodology developed in this PhD thesis, the integrated flocculation-CFD model can be extended with additional classes and corresponding discrete settling velocities.
- Compression settling should be added to the integrated flocculation-CFD model. This would allow to build further knowledge on the variability of the critical concentration with respect to the flocculation state inside the sludge blanket.
- Further calibration of the coupled flocculation-CFD model with velocity measurements in the SST and PSD measurements in the effluent is needed in order to draw more reliable conclusions.
- The implementation of a size dependent aggregation rate (through the inclusion of a size dependent fractal dimension) could include more realism in the flocculation model. Moreover, more insight into the dynamics of breakage needs to be collected (for example by performing flocculation experiments at different shear rates).
- The geometry to which the integrated flocculation-CFD model is applied can be further extended to include the transport system from the bioreactor to the SST. This would allow simulating the impact of breakage during transport of the sludge to the SSTs and assess whether the flocculation well is sufficiently equipped to compensate for this.
- After calibration and validation a coupled flocculation-CFD model can be used to study the behaviour of SSTs under different operational and environmental

conditions. This knowledge can subsequently be translated into so called 'next generation' 1-D SST models. Compartmental models can be an important tool in this respect. From the two dimensional flow pattern predicted by the coupled flocculation-CFD model the geometry can be divided into a number of completely mixed compartments connected by convective and settling fluxes. The decisive difference to the current layer approach is that compartments can also be connected horizontally, thus including 2-D behaviour into a simple SST model.

Chapter 12. Perspectives and future work

Bibliography

- Adams, E. and Rodi, W. (1990). Modeling Flow and Mixing in Sedimentation Tanks. *J. Hydraul. Eng.*, 116(7):895–913.
- Anderson, N. (1945). Design of final settling tanks for activated sludge. *Sewage Works J.*, 17:50–65.
- Ardern, E. and Lockett, W. (1914). Experiments on the oxidation of sewage without the aid of filters. *J. Soc. Chem. Ind.*, 33(10):523–539.
- Armbruster, M., Krebs, P., and Rodi, W. (2001). Numerical modelling of dynamic sludge blanket behaviour in secondary clarifiers. *Water Sci. Technol.*, 43(11):173–80.
- Bachis, G., Maruéjould, T., Tik, S., Amerlinck, Y., Melcer, H., Nopens, I., Lessard, P., and Vanrolleghem, P. (2014). Modelling and characterisation of primary settlers in view of whole plant and resource recovery modelling. In *Proceedings of WWTmod 2014*, Spa, Belgium, March 30–April 2.
- Balemans, S. (2014). Towards improved secondary settling tanks by means of computational fluid dynamics. Master’s thesis, Dept. of Mathematical Modelling, Statistics and Bioinformatics, Ghent University, Ghent, Belgium.
- Betancourt, F., Bürger, D., Diehl, S., and Farás, S. (2014). Modelling and controlling clarifier-thickeners fed by suspensions with time-dependent properties. *Miner. Eng.*, 62:91–101.
- Beven, K. and Binley, A. (1992). The future of distributed models: Model calibration and uncertainty prediction. *Hydrological Processes*, 6(3):279–298.
- Biggs, C. (2000). *Activated sludge flocculation: investigating the effect of shear rate and cation concentration on flocculation dynamics*. PhD thesis, Dept. of Chemical Engineering, University of Queensland, Brisbane, Australia.
- Biggs, C., Ford, A., and Lant, P. (2001). Activated sludge flocculation: Direct determination of the effect of calcium ions. *Water Sci. Technol.*, 43:75–82.
- Biggs, C. and Lant, P. (2002). Modelling activated sludge flocculation using population balances. *Powder Technology*, 124:201–211.
- Bryant, J. (1972). *Continuous Time Simulation of the Conventional Activated Sludge Wastewater Renovation System*. PhD thesis, Clemson University, Clemson, South Carolina, USA.
- Bürger, R. (2000). Phenomenological foundation and mathematical theory of sedimentation-consolidation processes. *Chem. Eng. J.*, 80(1-3):177–188.
- Bürger, R., Diehl, S., Farás, S., Nopens, I., and Torfs, E. (2013). A consistent modelling methodology for secondary settling tanks: a reliable numerical method. *Water Sci. Technol.*, 68(1):192–208.
- Bürger, R., Diehl, S., Farás, S., and Nopens, I. (2012). On reliable and unreliable numerical methods for the simulation of secondary settling tanks in wastewater treatment. *Comput. Chem. Eng.*, 41:93–105.
- Bürger, R., Diehl, S., and Nopens, I. (2011). A consistent modelling methodology for secondary settling tanks in wastewater treatment. *Water Res.*, 45(6):2247–2260.
- Burnham, K. and Anderson, D. (2004). Multimodel inference: Understanding AIC and BIC in model selection. *Sociol. Method. Res.*, 33:261–304.
- Cacossa, K. and Vaccari, D. (1994). Calibration of a compressive gravity thickening model from a single batch settling curve. *Water Sci. Technol.*, 30(8):107–116.
- Chebbou, G. and Gromaire, M.-C. (2009). VICAS - An Operating Protocol to Measure the Distributions of Suspended Solid Settling Velocities Within Urban Drainage Samples. *Journal of environmental engineering*, 135(9):768–775.
- Cho, S., Colin, F., Sardin, M., and Prost, C. (1993). Settling velocity model of activated sludge. *Water Res.*, 27(7):1237–1242.
- Cobb, E. (1993). Broad-band acoustic Doppler current profiler. *Flow Meas. Instrum.*, 4(1):35–37.
- Cole, R. (1968). *Experimental evaluation of the Kynch theory*. PhD thesis, University of North Carolina, Chapel Hill, USA.
- Copp, J. e. (2002). *The COST Simulation Benchmark - Description and Simulator Manual*. Office for Official Publications of the European Communities, Luxembourg.
- Cousin, C. and Ganczarzyk, J. (1999). The Effect of Cationic Salt Addition on the Settling and Dewatering Properties of an Industrial Activated Sludge. *Water Environ. Res.*, 71(2):251–254.
- Das, D., Keinath, T., Parker, D., and Wahlberg, E. (1993). Floc breakup in activated sludge plants. *Water Environ. Res.*, 65(2):138–145.
- De Clercq, B. (2003). *Fluid dynamics of settling tanks: development of experiments and rheological, settling, and scraper submodels*. PhD thesis, Dept. Applied Mathematics, Biometrics and Process Control, Ghent University, Belgium.

Bibliography

- De Clercq, J. (2006). *Batch and continuous settling of activated sludge: In-depth monitoring and 1D compression modell*. PhD thesis, Ghent University.
- De Clercq, J., Jacobs, F., Kinnear, D. J., Nopens, I., Dierckx, R., Defrancq, J., and Vanrolleghem, P. (2005). Detailed spatio-temporal solids concentration profiling during batch settling of activated sludge using a radiotracer. *Water Res.*, 39(10):2125–2135.
- De Clercq, J., Nopens, I., Defrancq, J., and Vanrolleghem, P. (2008). Extending and calibrating a mechanistic hindered and compression settling model for activated sludge using in-depth batch experiments. *Water Res.*, 42(3):781–791.
- Devantier, B. and Larock, B. (1986). Modelling a recirculating density-driven turbulent flow. *Int. J. Num. Meth. Fluids*, 6(4):241–253.
- Dick, R. and Young, K. (1972). Analysis of thickening performance of final settling tanks. In *Proceedings of the 27th Purdue Industrial Waste Conference*, pages 33–54, West Lafayette, Indiana, USA, May 2–4.
- Diehl, S. (2007). Estimation of the batch-settling flux function for an ideal suspension from only two experiments. *Chem. Eng. Sci.*, 62:4589–4601.
- Diehl, S. (2014). Numerical identification of constitutive functions in scalar nonlinear convection - diffusion equations with application to batch sedimentation. *Appl. Numer. Math.*, 1:1–19.
- Diehl, S. and Jeppsson, U. (1998). A model of the settler coupled to the biological reactor. *Water Res.*, 32(2):331–342.
- Ding, A., Hounslow, M., and Biggs, C. (2006). Population balance modelling of activated sludge flocculation: Investigating the size dependence of aggregation and collision efficiency. *Chem. Eng. Sci.*, 61:63–74.
- Dionisi, D., Beccari, M., Di Gregorio, S., Majone, M., Papini, M., and Vallini, G. (2005). Storage of biodegradable polymers by an enriched microbial community in a sequencing batch reactor operated at high organic load rate. *Journal of Chemical Technology and Biotechnology*, 80(11):1306–1318.
- Donckels, B. (2009). *Optimal experimental design to discriminate among rival dynamic mathematical models*. PhD thesis, Dept. Applied Mathematics, Biometrics and Process Control, Ghent University, Belgium.
- Ducoste, J. (2002). A two-scale pbm for modeling turbulent flocculation in water treatment processes. *Chem. Eng. Sci.*, 57(12):2157–2168.
- Dupont, R. and Dahl, C. (1995). A one-dimensional model for a secondary settling tank including density current and short-circuiting. *Water Sci. Technol.*, 31(2):215–224.
- Dupont, R. and Henze, M. (1992). Modeling of the secondary clarifier combined with the activated-sludge model no. 1. *Water Sci. Technol.*, 25(6):285–300.
- Dyer, K. and Manning, A. (1999). Observation of size, settling velocity and effective density of flocs, and their fractal dimensions. *Journal of Sea Research*, 41:87–95.
- Eaton, A., Clesceri, L., and Greenberg, A. (1995). *Standard Methods for Examination of Water & Wastewater, 19th edition*. American Public Health Association, Washington, DC.
- Ekama, G., Barnard, J., Gunthert, F., Krebs, P., McCorquodale, J., and Parker, D. (1997). *Secondary Settling Tanks: Theory, Modelling, Design and Operation*. International Association on Water Quality, London, UK.
- Forster, C. (2002). The rheological and physico-chemical characteristics of sewage sludges. *Enzyme Microb. Tech.*, 30(3):340–345.
- Gernaey, K., Jeppsson, U., Vanrolleghem, P., and Copp, J. (2014). *Benchmarking of Control Strategies for Wastewater Treatment Plants*. IWA Publishing, London, UK.
- Gong, M., Xanthos, S., Ramalingam, K., Fillos, J., Beckmann, K., Deur, A., and McCorquodale, J. (2011). Development of a flocculation sub-model for a 3-D CFD model based on rectangular settling tanks. *Water Sci. Technol.*, 63(2):213–219.
- Govoreanu, R. (2004). *Activated sludge flocculation dynamics: on-line measurement methodology and modelling*. PhD thesis, Ghent University, Belgium.
- Griborio, A. (2004). *Secondary Clarifier Modeling : A Multi-Process Approach*. PhD thesis, University of New Orleans, New Orleans, USA.
- Griborio, A. and McCorquodale, J. (2006). Optimum Design of your Center Well: Use of a CFD Model to Understand the Balance between Flocculation and Improved Hydrodynamics. In *Proceedings of 79th Annual Water Environment Federation Technical Exhibition and Conference (WEFTEC)*, Dallas, Texas, USA, October 21–25.
- Griborio, A., Rohrbacher, J., McGehee, M., Pitt, P., Latimer, R., and Gellner, J. (2010). Combining Stress Testing and Dynamic Linking of Whole Plant Simulators and CFD for the Evaluation of WWTP Wet Weather Capacity. In *Proceedings of 83th Annual Water Environment Federation Technical Exhibition and Conference (WEFTEC)*, New Orleans, Louisiana, USA, October 2–6.
- Guo, J., Peng, Y., Wang, S., Yang, X., and Yuan, Z. (2014). Filamentous and non-filamentous bulking of activated sludge encountered under nutrients limitation or deficiency conditions. *Chem. Eng. Sci.*, 255:453–461.
- Gustavson, K., Ooppelstrup, J., and Eiken, J. (2001). Consolidation of concentrated suspensions - shear and irreversible floc structure rearrangement. *Comput. Visual Sci.*, 4:61–66.
- Guvonvarch, E., Ramin, E., Kulahci, M., and Plósz, B. (2015). iCFD: Interpreted Computational Fluid Dynamics - Degeneration of CFD to one-dimensional advection-dispersion models using statistical experimental design - The secondary clarifier. *Water Res.*
- Hamilton, J., Jain, R., Antoniou, P., Svoronos, S., Koopman, B., and Lybertas, G. (1992). Modeling and pilot-scale experimental-verification for predenitrification process. *J. Environ. Eng.-ASCE*, 118(1):38–55.
- Härtel, L. and Pöpel, H. (1992). A dynamic secondary clarifier model including processes of sludge thickening. *Water Sci.*

Bibliography

- Technol.*, 25(6):267–284.
- He, C., Wood, J., Marsalek, J., and Rochfort, Q. (2008). Using CFD Modeling to Improve the Inlet Hydraulics and Performance of a Storm-Water Clarifier. *J. Environ. Eng.*, 134(9):722–730.
- Henze, M., Van Loosdrecht, M., Ekama, G., and Brdjanovic, D. (2008). *Biological Wastewater Treatment: Principles, Modelling and Design*. IWA Publishing, London, UK.
- Hribersek, M., Zajdela, B., Hribernik, A., and Zadavec, M. (2011). Experimental and numerical investigations of sedimentation of porous wastewater sludge flocs. *Water Res.*, 45:1729–1735.
- <http://www.mikebydhi.com> (Denmark). Modelling and simulation platform WEST.
- Jenkins, D., Richard, M., and Daigger, G. (1993). *Manual on the causes and control of activated sludge bulking and foaming, second edition*. Lewis Publisher, Chelsea, Michigan, USA.
- Jeppsson, U. and Diehl, S. (1996). An evaluation of a dynamic model of the secondary clarifier. *Water Sci. Technol.*, 34(5-6):19–26.
- Jin, B., Wilén, B., and Lant, P. (2003). A comprehensive insight into floc characteristics and their impact on compressibility and settleability of activated sludge. *Chem. Eng. J.*, 95:221–234.
- Jorand, F., Zartarian, F., Thomas, F., Block, J., Bottero, J., Villemin, G., Urbain, V., and Manem, J. (1995). Chemical and structural (2D) linkage between bacteria within activated sludge flocs. *Water Res.*, 29:1639–1647.
- Judd, S. and Judd, C. (2011). *The MBR Book: Principles and Applications of Membrane Bioreactors for Water and Wastewater Treatment*. IWA Publishing, London, UK.
- Kinnear, D. (2002). *Biological Solids Sedimentation: A Model Incorporating Fundamental Settling Parameters*. PhD thesis, University of Utah, Salt Lake City, USA.
- Kinnear, D. and Deines, K. (2001). Acoustic doppler current profiler clarifier velocity measurement. In *Proceedings of 74th Annual Water Environment Federation Technical Exhibition and Conference (WEFTEC)*, Atlanta, USA, October 13-17.
- Koopman, B. and Cadee, K. (1983). Prediction of thickening capacity using diluted sludge volume index. *Water Environ. Res.*, 17(10):1427–1431.
- Kramer, T. and Clark, M. (1999). Incorporation of Aggregate Breakup in the Simulation of Orthokinetic Coagulation. *J. Colloid Interf. Sci.*, 216(1):116–126.
- Krebs, P. (1991). The hydraulics of final settling tanks. *Water Sci. Technol.*, 23(4-6):1037–1046.
- Kynch, G. (1952). A theory of sedimentation. *Transaction of the Faraday society*, 48:166–176.
- Lakehal, D. (2002). On the modelling of multiphase turbulent flows for environmental and hydrodynamic applications. *Int. J. Multiphas. Flow*, 28(5):823–863.
- Lakehal, D. and Krebs, P. (1999). Computing shear flow and sludge blanket in secondary clarifiers. *J. Hydraul. Eng.*
- Larsen, P. (1977). On the hydraulics of rectangular settling basins. Report No. 1001. Technical report, Department of Water Resources Engineering, Lund University, Lund, Sweden.
- Lauder, B. and Spalding, D. (1974). The numerical computation of turbulent flows. *Comput. Method. Appl. M.*, 3(2):269–289.
- Laurent, J., Pierra, M., Casellas, M., Pons, M., and Dagot, C. (2009). Activated sludge properties after ultrasonic and thermal treatments and their potential influence on dewaterability. *J. Residuals Sci. Tech.*, 6(1):159–167.
- Laurent, J., Samstag, R., Ducoste, J., Griborio, A., Nopels, I., Batstone, D., Wicks, J., Saunders, S., and Potier, O. (2014). A protocol for the use of computational fluid dynamics as a supportive tool for wastewater treatment plant modelling. *Water Sci. Technol.*, 70(10):1575–1584.
- Le Clech, P., Chen, V., and Fane, T. (2006). Fouling in membrane bioreactors used in wastewater treatment. *Journal of Membrane Science*, 284(1):17–53.
- Lee, D., Bonner, J., Garton, L., Ernest, A., and Autenrieth, R. (2000). Modeling coagulation kinetics incorporating fractal theories: a fractal rectilinear approach. *Water Res.*, 34(7):1987–2000.
- Li, B. and Stenstrom, M. (2014a). Dynamic one-dimensional modeling of secondary settling tanks and design impacts of sizing decisions. *Water Res.*, 50:160–170.
- Li, B. and Stenstrom, M. (2014b). Dynamic one-dimensional modeling of secondary settling tanks and system robustness evaluation. *Water Sci. Technol.*, 69(11):2339–2349.
- Li, B. and Stenstrom, M. (2014c). Research advances and challenges in one-dimensional modeling of secondary settling Tanks - A critical review. *Water Res.*, 65:40–63.
- Li, D. and Ganczarczyk, J. (1991). Size distribution of activated sludge flocs. *Res. J. Water Poll. C.*, 63(5):806–814.
- Li, D. and Ganczarczyk, J. (1993). Factors affecting dispersion of activated sludge flocs. *Water Environ. Res.*, 65:258–263.
- Li, T., Zhu, Z., Wang, D., Yao, C., and Tang, H. (2006). Characterization of floc size, strength and structure under various coagulation mechanisms. *Powder Technology*, 168:104–110.
- Liao, B., Allen, D., Droppo, I., Leppard, G., and Liss, S. (2001). Surface properties of sludge and their role in bioflocculation and settleability. *Water Res.*, 35(2):339–350.
- Locatelli, F., François, P., Laurent, J., Lawniczak, F., Dufresne, M., Vazquez, J., and Bekkour, K. (2015). Detailed velocity and concentration profiles measurement during activated sludge batch settling using an ultrasonic transducer. *Separ. Sci. Technol.*, 50(7):1059–1065.
- Lu, C. and Spielman, L. (1985). Kinetics of floc breakage and aggregation in agitated liquid suspensions. *J. Colloid Interf. Sci.*, 103(1):95–105.

Bibliography

- Lyn, D., Stamou, A., and Rodi, W. (1992). Density Currents and Shear- Induced Flocculation in Sedimentation Tanks. *J. Hydraul. Eng.*, 118(6):849–867.
- Mancell-Egala, A., Kinnear, D., Murthy, S., and Jones, K. (2012). Settling Transition Concentration Measurement to Quantify Sludge Settling Behavior. In *Proceedings of 85th Annual Water Environment Federation Technical Exhibition and Conference (WEFTEC)*, New Orleans, Louisiana, USA, September 29–October 3.
- Matko, T., Fawcett, N., Sharp, A., and Stephenson, T. (1996). Recent Progress in the Numerical Modelling of Wastewater Sedimentation Tanks. *Process Saf. Environ.*, 74(4):245–258.
- Mazzolani, G., Pirozzi, F., and Dantonoi, G. (1998). A generalized settling approach in the numerical modeling of sedimentation tanks. *Water Sci. Technol.*, 38(3):95–102.
- McCorquodale, J., La Motta, E., Griborio, A., Homes, D., and Georgiou, I. (2004). Development of software for modeling activated sludge clarifier systems. Technical report, Department of Civil and Environmental Engineering, University of New Orleans, New Orleans, USA.
- McCorquodale, J. and Zhou, S. (1993). Effects of hydraulic and solids loading on clarifier performance. *J. Hydraul. Res.*, 31(4):461–478.
- Meerburg, F., Boon, N., Van Winkel, T., Vercamer, J., Nopens, I., and Vlaeminck, S. (2015). Toward energy-neutral wastewater treatment: A high-rate contact stabilization process to maximally recover sewage organics. *Bioresource Technology*, 179:373–381.
- Mikkelsen, L. (2001). The shear sensitivity of activated sludge: relations to filterability, rheology and surface chemistry. *J. Colloid Interf. Sci.*, 182:1–14.
- Mikkelsen, L., Gotfredsen, A., Agerbak, M., Nielsen, P., and Keiding, K. (1996). Effects of colloidal stability on clarification and dewatering of activated sludge. *Water Sci. Technol.*, 34(3-4):449–457.
- Mikkelsen, L. and Nielsen, P. (2001). Quantification of the bond energy of bacteria attached to activated sludge floc surfaces. *Water Sci. Technol.*, 43(6):67–75.
- Nelder, J. and Mead, R. (1965). A simplex-method for function minimization. *Comput. J.*, 7:308–313.
- Nopens, I. (2005). *Modelling the activated sludge flocculation process: a population balance approach*. PhD thesis, Dept. of Applied Mathematics, Biometrics and Process Control, Ghent University, Ghent, Belgium.
- Nopens, I., Biggs, C., De Clercq, B., Govoreanu, R., Wilén, B., Lant, P., and Vanrolleghem, P. (2002). Modelling the activated sludge flocculation process combining laser diffraction particle sizing and population balance modelling (PBM). *Water Sci. Technol.*, 45(6):41–49.
- Nopens, I., Koegst, T., Mahieu, K., and Vanrolleghem, P. (2005). PBM and activated sludge flocculation: From experimental data to calibrated model. *AIChE Journal*, 51(5):1548–1557.
- Nopens, I., Nere, N., Vanrolleghem, P., and Ramkrishna, D. (2007a). Formulation of effective mechanism aggregation kernels for the flocculation process with concurrent mechanisms using inverse problem solution. In *Proceedings of the AIChE Annual Meeting*, Salt Lake City, USA, November 4-9.
- Nopens, I., Nere, N., Vanrolleghem, P., and Ramkrishna, D. (2007b). Solving the inverse problem for aggregation in activated sludge flocculation using a population balance framework. *Water Sci. Technol.*, 56(6):95–103.
- Nopens, I., Torfs, E., Ducoste, J., Vanrolleghem, P., and K.V., G. (2015). Population balance models: a useful complementary modelling framework for future WWTP modelling. *Water Sci. Technol.*, 71(2):159–167.
- Otterpohl, R. and Freund, M. (1992). Dynamic models for clarifiers of activated sludge plants with dry and wet weather flows. *Water Sci. Technol.*, 26(5-6):1391–1400.
- Parker, D., Kaufman, W., and Jenkins, D. (1970). *Characteristics of Biological Flocs in Turbulent Regimes*. Sanitary Engineering Research Laboratory. University of California, Berkeley, California, USA.
- Parker, D., Kaufman, W., and Jenkins, D. (1972). Floc Breakup in Turbulent Flocculation Processes. *Journal of the Sanitary Engineering Division*, 98(1):79–99.
- Patry, G. and Takács, I. (1992). Settling of flocculent suspensions in secondary clarifiers. *Water Res.*, 26:473–479.
- Patziger, M., Kainz, H., Hunze, M., and Józsa, J. (2012). Influence of secondary settling tank performance on suspended solids mass balance in activated sludge systems. *Water Res.*, 46:2415–2424.
- Pitman, A. (1984). Settling of nutrient removal activated sludges. *Water Sci. Technol.*, 17:493–504.
- Plósz, B., De Clercq, J., Nopens, I., Benedetti, L., and Vanrolleghem, P. (2011). Shall we upgrade one-dimensional secondary settler models used in WWTP simulators? - An assessment of model structure uncertainty and its propagation. *Water Sci. Technol.*, 63(8):1726–1738.
- Plósz, B., Weiss, M., Printemps, C., Essemiani, K., and Meinhold, J. (2007). One-dimensional modelling of the secondary clarifier-factors affecting simulation in the clarification zone and the assessment of the thickening flow dependence. *Water Res.*, 41(15):3359–3371.
- Ramalingam, K., Xanthos, S., Gong, M., Fillos, J., Beckmann, K., Deur, A., and McCorquodale, J. (2012). Critical modeling parameters identified for 3D CFD modeling of rectangular final settling tanks for New York City wastewater treatment plants. *Water Sci. Technol.*, 65(6):1087–1094.
- Ramin, E., Flores-Alsina, X., Sin, G., Gernaey, K., Jeppsson, U., Mikkelsen, P., and Plósz, B. (2014a). Influence of selecting secondary settling tank sub-models on the calibration of WWTP models - A global sensitivity analysis using BSM2. *Chem. Eng. J.*, 241:28–34.
- Ramin, E., Wágner, D., Yde, L., Binning, P., Rasmussen, M., Mikkelsen, P., and Plósz, B. (2014b). A new settling velocity model to describe secondary sedimentation. *Water Res.*, 66:447–458.

Bibliography

- Ramkrishna, D. (2000). *Population Balances: theory and applications to particulate systems in engineering*. Academic Press, London, UK.
- Ratkovich, N., Horn, W., Helmus, F., Rosenberger, S., Naessens, W., Nopens, I., and Bentzen, T. (2013). Activated sludge rheology: A critical review on data collection and modelling. *Water Res.*, 47:463–482.
- Richardson, J. and Zaki, W. (1954). The sedimentation of a suspension of uniform spheres under conditions of viscous flow. *Chem. Eng. Sci.*, 3:65.
- Rodi, W. (1980). *Turbulence Models and Their Application in Hydraulics*. Int. Assoc. of Hydro-Environment Engineering and Research, Delft, The Netherlands.
- Rushton, A., Ward, A., and Holdich, R. (2000). *Solid-liquid filtration and separation technology, Second, completely revised edition*. Wiley-Vch Verlag GmbH, Weinheim, Germany.
- Saltelli, A., Ratto, M., Andres, T., Campolongo, F., Cariboni, J., Gatelli, D., Saisana, M., and Tarantola, S. (2008). *Global Sensitivity Analysis: The Primer*. John Wiley & Sons, Ltd, New York, USA.
- Sezgin, M., Jenkins, D., and Palm, J. (1980). Floc size, filament length and settling properties of prototype activated sludge plants. *Progress in Water Technology*, 12(3):171–182.
- Smith, W. (2004). *Foundations of Materials Science and Engineering*. McGraw-Hill, New York, USA.
- Spicer, P., Keller, W., and Pratsinis, S. (1996). The Effect of Impeller Type on Floc Size and Structure during Shear-Induced Flocculation. *J. Colloid Interf. Sci.*, 184(1):112–122.
- Spicer, P. and Pratsinis, S. (1996a). Coagulation and fragmentation: universal steady-state particle size distribution. *AIChE J.*, 42:1612–1620.
- Spicer, P. and Pratsinis, S. (1996b). Shear-induced flocculation: the evolution of floc structure and the shape of the size distribution at steady state. *Water Res.*, 30:1049–1056.
- Stamou, A., Theodoridis, G., and Xanthopoulos, K. (2009). Design of secondary settling tanks using a CFD model. *J. Environ. Eng.*, 135:551–561.
- Stenstrom, M. (1976). *A Dynamic Model and Computer Compatible Control Strategies for Wastewater Treatment Plants*. PhD thesis, Clemson University, Clemson, South Carolina, USA.
- Stricker, E., Takács, I., and Marquot, A. (2007). Hindered and compression settling: parameter measurement and modelling. *Water Sci. Technol.*, 56(12):101–110.
- Sürücü, G. and Çetin, F. (1989). Effect of temperature, pH and DO concentration on filterability and compressibility of activated sludge. *Water Res.*, 23:1389–1395.
- Takács, I., Patry, G., and Nolasco, D. (1991). A dynamic model for the clarification-thickening process. *Water Res.*, 25:1263–1271.
- Takeda, Y. (1995). Velocity Profile Measurement by Ultrasonic Doppler Method. *Experimental Thermal and Fluid Science*, 10:444–453.
- Tamayol, A., Firoozabadi, B., and Ashjari, M. (2010). Hydrodynamics of Secondary Settling Tanks and Increasing Their Performance Using Baffles. *J. Environ. Eng.-ASCE*, 136(1):32–39.
- Tchobanoglous, G., Burton, F., and Stensel, H. (2003). *Wastewater Engineering: Treatment and Reuse, 4th ed. Metcalf and Eddy*. McGraw-Hill Science, New York, USA.
- Thomas, D., Judd, S., and Fawcett, N. (1999). Flocculation modelling: a review. *Water Res.*, 33(7):1579–1592.
- Torfs, E., Balemans, S., Locatelli, F., Bürger, R., Laurent, J., François, P., Diehl, S., and Nopens, I. (2015a). Critical analysis of constitutive functions for hindered settling in 1-D settler models. In *Proceedings of Watermatex2015*, Gold Coast, Australia, June 15-17.
- Torfs, E., Bellandi, G., and Nopens, I. (2012a). Towards mechanistic models for activated sludge flocculation under different conditions based on inverse problems. *Water Sci. Technol.*, 65(11):1946–1953.
- Torfs, E., Dutta, A., and Nopens, I. (2012b). Investigating kernel structures for Ca-induced activated sludge aggregation using an inverse problem methodology. *Chem. Eng. Sci.*, 70:176–187.
- Torfs, E., Locatelli, F., Balemans, S., Diehl, S., Bürger, R., François, P., Laurent, J., and Nopens, I. (2015b). Impact of the flocculation state on hindered and compression settling: experimental evidence and overview of available modelling frameworks. In *Proceedings of Watermatex2015*, Gold Coast, Australia, June 15-17.
- Torfs, E., Maere, T., Bürger, R., Diehl, S., and Nopens, I. (2015c). Impact on sludge inventory and control strategies using the Benchmark Simulation Model no. 1 with the Bürger-Diehl settler model. *Water Sci. Technol.*, 71(10):1524–1535.
- Torfs, E., Mahdavi Mazdeh, F., Bellandi, G., and Nopens, I. (2014). A novel methodology for the calibration of discrete settling behaviour of activated sludge. In *Proceedings of the IWA Specialist Conference on Advances in Particle Science and Separation*, Sapporo, Japan, June 15-18.
- Torfs, E., Vesvikar, M., and Nopens, I. (2013a). Improved Predictions of Effluent Suspended Solids in wastewater treatment plants by integration of a PBM with Computational Fluid Dynamics. In *Proceedings of the 5th Population Balance Modelling Conference*, Bangalore, India, September 11-13.
- Torfs, E., Vlasschaert, P., Amerlinck, Y., Diehl, S., Bürger, R., and Nopens, I. (2013b). Towards improved 1-D settler modelling: calibration of the Bürger model and case study. In *Proceedings of 86th Annual Water Environment Federation Technical Exhibition and Conference (WEFTEC)*, Chicago, Illinois, USA, October 5-9.
- Tracy, K. (1973). *Mathematical modelling of unsteady-state thickening*. PhD thesis, Clemson University, Clemson, South-Carolina, USA.
- Vaerenbergh, E. (1980). Numerical computation of secondary settler area using batch settling data. *Trib. Cep.*, pages

Bibliography

- 369–374.
- Vahedi, A. and Gorczyca, B. (2012). Predicting the settling velocity of flocs formed in water treatment using multiple fractal dimensions. *Water Res.*, 46:4188–4194.
- Vanderhasselt, A. and Vanrolleghem, P. (2000). Estimation of sludge sedimentation parameters from single batch settling curves. *Water Res.*, 34(2):395–406.
- Vanhooren, H., Meirlaen, J., Amerlink, Y., Claeys, F., Vangheluwe, H., and Vanrolleghem, P. (2003). WEST: Modelling biological wastewater treatment. *Journal of Hydroinformatics*, 5:23.
- Vesilind, P. (1968). Design of prototype thickeners from batch settling tests. *Water Sewage Works*, 115(7):302–307.
- Vitasovic, Z. (1986). *An integrated control system for the activated sludge process*. PhD thesis, Rice University, Houston, Texas, USA.
- Von Smoluchowski, M. (1917). Versuch einer mathematischen Theorie der Koagulationskinetik kolloidaler Lösungen. *Zeitschrift für physikalische Chemie*, 92(2):129–168.
- Wahlberg, E., Keinath, T., and Parker, D. (1994). Influence of activated sludge flocculation time on secondary clarification. *Water Environ. Res.*, 66(6):779–786.
- Watts, R., Svoronos, S., and Koopman, B. (1996). One-dimensional modeling of secondary clarifiers using a concentration and feed velocity-dependent dispersion coefficient. *Water Res.*, 30(9):2112–2124.
- Wicklein, E. and Samstag, R. (2009). Comparing Commercial and Transport CFD Models for Secondary Sedimentation. In *Proceedings of 82th Annual Water Environment Federation Technical Exhibition and Conference (WEFTEC)*, Chicago, Illinois, USA, October 17-21.
- Wilén, B. (1999). *Properties of activated sludge flocs*. PhD thesis, Chalmers University of Technology, Göteborg, Sweden.
- Wilén, B. and Balmér, P. (1999). The effect of dissolved oxygen concentration on the structure, size and size distribution of activated sludge flocs. *Water Res.*, 33(2):391–400.
- Wilén, B., Jin, B., and Lant, P. (2003). Impacts of structural characteristics on activated sludge floc stability. *Water Res.*, 37(15):3632–3645.
- Wilén, B. and Nielsen, J. (2000). Influence of microbial activity on the stability of activated sludge flocs. *J. Colloid Interf. Sci.*, 18:145–156.
- Wright, H. and Ramkrishna, D. (1992). Solutions of inverse problems in population balances-I. Aggregation kinetics. *Computers Chem. Eng.*, 16(12):1019–1038.
- Xanthos, S., Gong, M., Ramalingam, K., Fillos, J., Deur, A., Beckmann, K., and McCorquodale, J. (2011). Performance Assessment of Secondary Settling Tanks Using CFD Modeling. *Water Resources Management*, 25(4):1169–1182.
- Xanthos, S., Ramalingam, K., Lipke, S., McKenna, B., and Fillos, J. (2013). Implementation of CFD modeling in the performance assessment and optimization of secondary clarifiers: the PVSC case study. *Water Sci. Technol.*, 68(9):1901–1913.
- Zhang, D., Li, Z., Lu, P., Zhang, T., and Xu, D. (2006). A method for characterizing the complete settling process of activated sludge. *Water Res.*, 40(14):2637–2644.
- Zikanov, O. (2010). *Essential computational fluid dynamics*. Wiley, Hoboken, New Jersey, USA.

Appendices

APPENDIX A

Calibration of hindered settling functions based on batch settling data of the WWTP of Roeselare

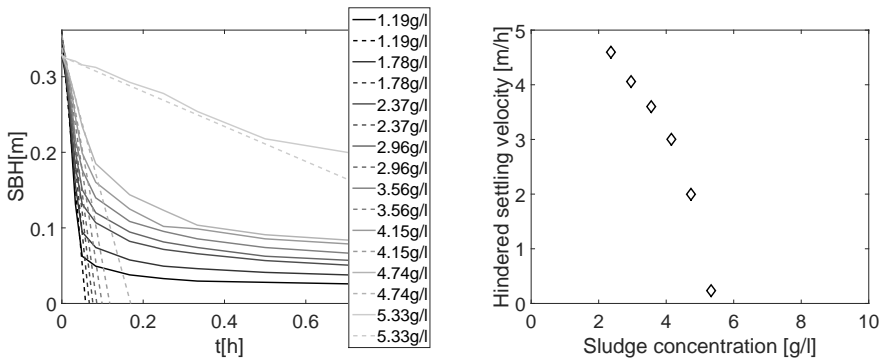


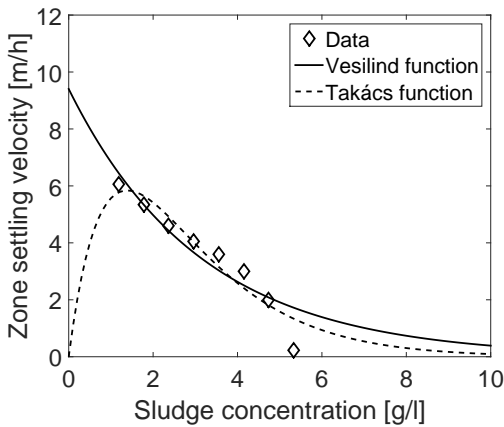
Figure A.1: Batch settling experiments at different initial solids concentrations with indication of the maximum slope for each curve (left). The maximal slope represents a measurement of the hindered settling velocity (right).

Table A.1: Measured hindered settling velocities at different initial concentrations

Concentration (g/l)	v_{hs} (m/h)
1.19	6.06
1.78	5.33
2.37	4.59
2.96	4.06
3.56	3.60
4.15	3.01
4.74	2.00
5.33	0.23

Table A.2: Initial values, optimal values and confidence intervals of the estimated parameters of the settling functions

	Initial value	Optimal value	Confidence interval
Vesilind			
v_0 (m/h)	9.647	9.403	± 1.780
r_V (l/g)	0.488	0.318	± 0.0368
Takács			
v_0 (m/h)	9.647	61.96	± 1049
r_H (l/g)	0.488	0.632	± 1.260
r_P (l/g)	4.88	0.817	± 1.972

**Figure A.2:** Settling velocity as function of the solids concentration. Symbols: measured settling velocities. Lines: calculated settling velocities after calibration of the functions by Vesilind (1968) and Takács et al. (1991).

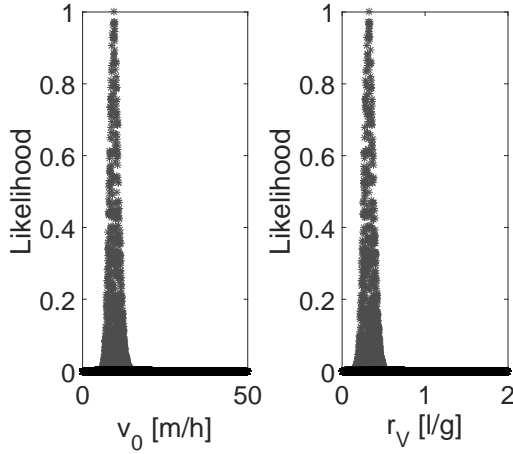


Figure A.3: Plot of the likelihood in function of the parameter values for v_0 (left) and r_V (right) of the settling function of Vesilind (1968). Behavioural runs are indicated in grey, non behavioural runs in black.

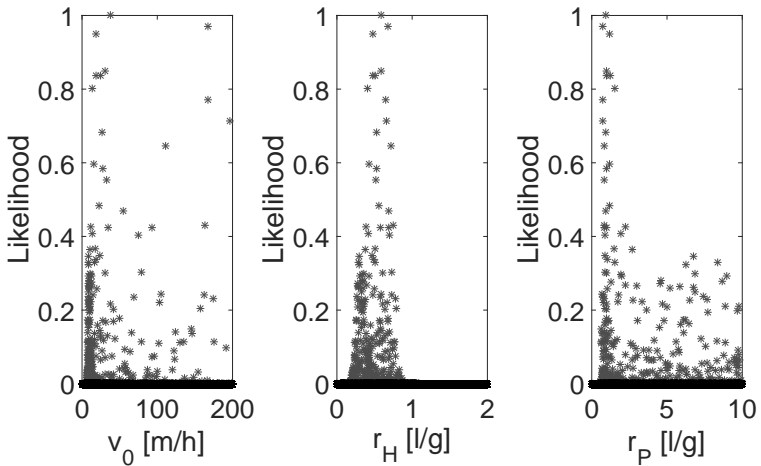


Figure A.4: Plot of the likelihood value in function of the parameter values for v_0 , r_H and r_P . Behavioural runs are indicated in grey, non behavioural runs in black.

APPENDIX B

Calibration of hindered settling functions based on batch settling data of the WWTP of Eindhoven

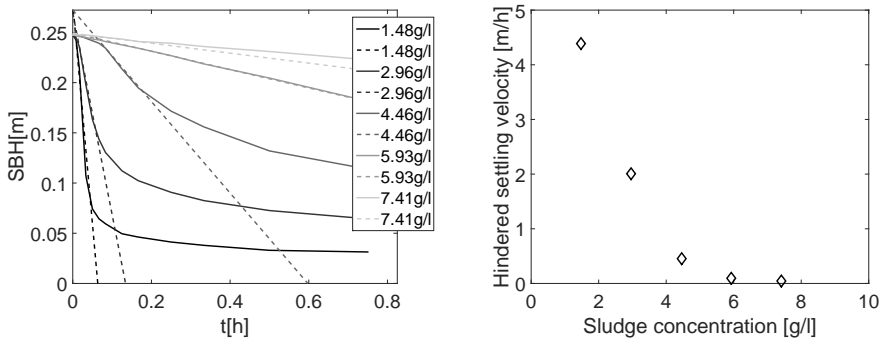


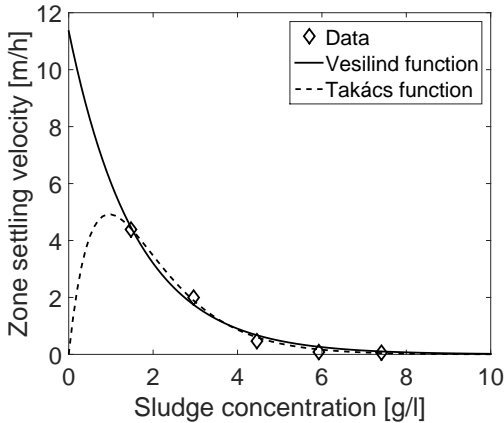
Figure B.1: Batch settling experiments at different initial solids concentrations with indication of the maximum slope for each curve (left). The maximal slope represents a measurement of the hindered settling velocity (right).

Table B.1: Measured hindered settling velocities at different initial concentrations

Concentration (g/l)	v_{hs} (m/h)
1.19	
1.48	4.39
2.96	2.01
4.46	0.46
5.93	0.09
7.41	0.05

Table B.2: Initial values, optimal values and confidence intervals of the estimated parameters of the settling functions

	Initial value	Optimal value	Confidence interval
Vesilind			
v_0 (m/h)	9.647	11.352	± 3.358
r_V (l/g)	0.488	0.633	± 0.0499
Takács			
v_0 (m/h)	9.647	113.00	± 4336
r_H (l/g)	0.488	0.982	± 1.992
r_P (l/g)	4.88	1.105	± 2.838

**Figure B.2:** Settling velocity as function of the solids concentration. Symbols: measured settling velocities. Lines: calculated settling velocities after calibration of the functions by Vesilind (1968) and Takács et al. (1991).

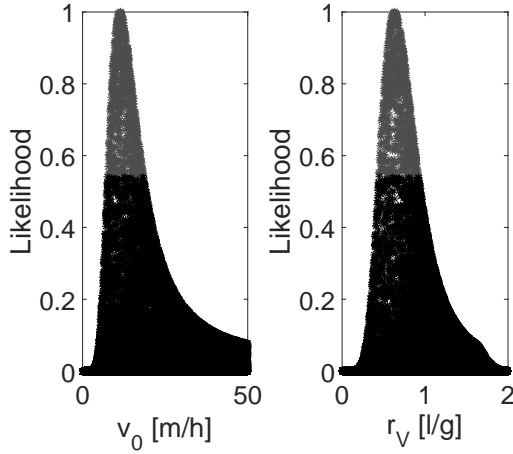


Figure B.3: Plot of the likelihood in function of the parameter values for v_0 (left) and r_V (right) of the settling function of Vesilind (1968). Behavioural runs are indicated in grey, non behavioural runs in black.

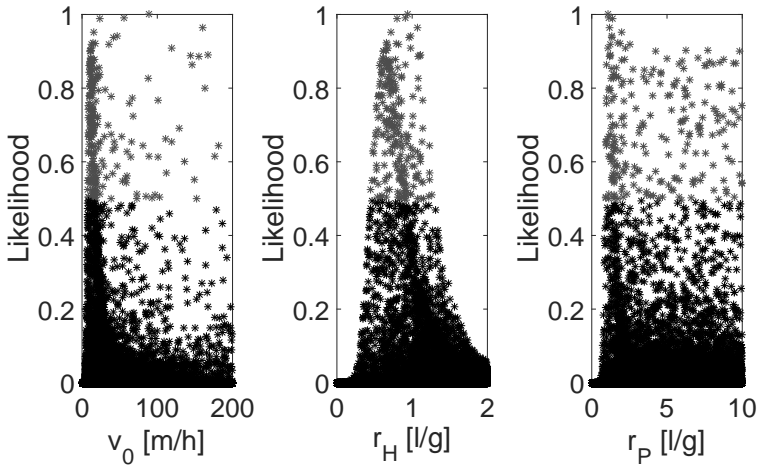


Figure B.4: Plot of the likelihood value in function of the parameter values for v_0 , r_H and r_P . Behavioural runs are indicated in grey, non behavioural runs in black.

Curriculum vitae

Curriculum vitae

Contact and personal information:

Name	Elena Torfs
Address	Loodsenstraat 21a 9000 Gent, Belgium
Cell Phone	+32 498 67 52 10
E-mail	elena.torfs@gmail.com
Date of Birth	October 20, 1986
Place of Birth	Antwerp
Nationality	Belgian

Education:

- 2009 - Currently: Teaching Assistant, Ghent University, Belgium.
PhD title: Different settling regimes in secondary settling tanks: experimental process analysis, model development and calibration
- 2005 - 2010: Master in Bioscience Engineering (Environmental Technology), Ghent University, Belgium.
MSc. Thesis: Chemical stabilisation of cadmium pollution in the regions Kempen by means of phosphorous containing additives. (Chemische stabilisatie van cadmium verontreiniging in de kempen met P-houdende amendementen)

Additional courses without examination:

- Seventh Summer-school on Sensitivity Analysis (JRC, Ispra, Italy - July 3-6, 2012).
- Specialist course: Particle characterization course (Het pand, Gent - February 7 & 19 februari, 2013).
- Specialist course: Computational fluid dynamics (Technicum, Gent - September 17-21, 2012).
- Getting started with High Performance Computing (Sterre S9, Gent - May 30 & June 6, 2011).

- Transferable skills seminar: Authentic Networking (Leszaal De Brug, Gent - December 4 2014).
- Transferable skills seminar: Personal effectiveness (Leszaal De Brug, Gent - January 9, 16 & 23 2013).

MSc. theses supervised:

- 2012-2013: Pieter Vlasschaert: Calibration of a novel 1-D secondary settling model.
- 2012-2013: Faezeh Mahdavi Mazdeh: Investigating flocculation and discrete settling behaviour by means of particle size analysis.
- 2013-2014: Sophie Balemans: Towards improved secondary settling tanks by means of computational fluid dynamics.
- 2014-2015: Veerle De Smedt: The high-rate contact-stabilisation system: combining experiments and modelling to gain system knowledge.

Teaching activities:

- 2009-2014: Modelleren en simuleren van Biosystemen (3rd Ba Bio-ir)
- 2009-2015: Procesregeling (1st master Bio-ir)
- 2009-2015: Bioprocesregeling (1st & 2nd master Bio-ir)
- 2009-2010: Modelling and control of Wastewater treatment plants (1st + 2nd master Bio-ir)
- 2010-2012: Beslissingsondersteunende technieken (MaNaMa Milieusanering)

International Conference - Symposia:

Oral presentation:

1. PBM 2010: 4th international conference on Population Balance Modelling. Berlin, Germany. September 15 - 17, 2010.
Title: Investigating kernel structures for shear and Ca-induced activated sludge aggregation using an inverse problem methodology.
2. Watermatex 2011: 8th IWA Symposium on Systems Analysis and Integrated Assessment. San Sebastian, Spain. June 20-22, 2011.
Title: Construction of mechanistic models for activated sludge flocculation under different conditions based on inverse problems.
3. PBM 2013: 5th International conference on Population Balance Modelling. Bangalore, India. September 11-13, 2013.

Curriculum vitae

Title: Improved predictions of effluent suspended solids in wastewater treatment plants by integration of a PBM with Computational Fluid Dynamics.

4. IWA Specialist Conference on Advances in Particle Science and Separation. Sapporo, Japan. June 15-18, 2014.

Title: A novel methodology for the calibration of discrete settling behaviour of activated sludge.

5. 9th IWA Symposium on System Analysis and Integrated Assessment, 14-17 June 2015, Gold Coast, Australia.

Title: Critical analysis of constitutive functions for hindered settling velocity in 1-D models.

Poster:

1. ICA 2013: 11th IWA conference on Instrumentation, Control and Automation. Narbonne, France. September 18-20, 2013. Awarded best poster presentation.

Title: Towards improved 1-D settler modeling: impact on control strategies using the Benchmark Simulation Model.

2. WEFTEC 2013: Water Environment Federation's Annual Technical Exhibition and Conference. Chicago, USA. October 5-9, 2013.

Title: Towards improved 1-D settler modeling: Calibration of the Bürger model and case-study.

Participant:

WWTmod 2014: 4th IWA/WEF Wastewater Treatment Modeling Seminar. Spa, Belgium. March 30-April 2, 2014. (Member of Scientific Committee)

Peer-reviewed publications: A1:

1. Torfs E., Dutta A. & Nopens I. (2012) Investigating kernel structures for shear and Ca-induced activated sludge aggregation using an inverse problem methodology. *Chem. Eng. Sci.* 70, 176-187.
2. Cierkens K., Nopens I., De Keyser W., Van Hulle S., Plano S., Torfs E., Amerlinck Y., Benedetti L., van Nieuwenhuijzen A., Weijers S. & De Jonge J. (2012). Integrated model-based optimisation of the WWTP of Eindhoven. *Water Practice & Technology*, 7(2).
3. Torfs E., Bellandi G. & Nopens I. (2012). Towards mechanistic models for activated sludge flocculation under different conditions based on inverse problems. *Water Sci. Technol.* 65(11), 1946-1953.

4. Bürger R. , Diehl S., Farås S., Nopens I. & Torfs E. (2013). A consistent modelling methodology for secondary settling tanks: a reliable numerical method. *Water Sci. Technol.* 68(1), 192-208.
5. Nopens I., Torfs E., Ducoste J., Vanrolleghem P.A. & Gernaey K.V. (2015) Population balance models: a useful complementary modelling framework for future WWTP modelling. *Water Sci. Technol.* 71(2), 159-167.
6. Torfs E., Maere T., Bürger R., Diehl S. & Nopens I. (2015). Impact on sludge inventory and control strategies using the Benchmark Simulation Model No. 1 with the Bürger-Diehl settler model. *Water Sci. Technol.* 71(10):1524-1535.